ISBN 978-82-326-4948-8 (printed ver.)
ISBN 978-82-326-4949-5 (electronic ver.)
ISSN 1503-8181

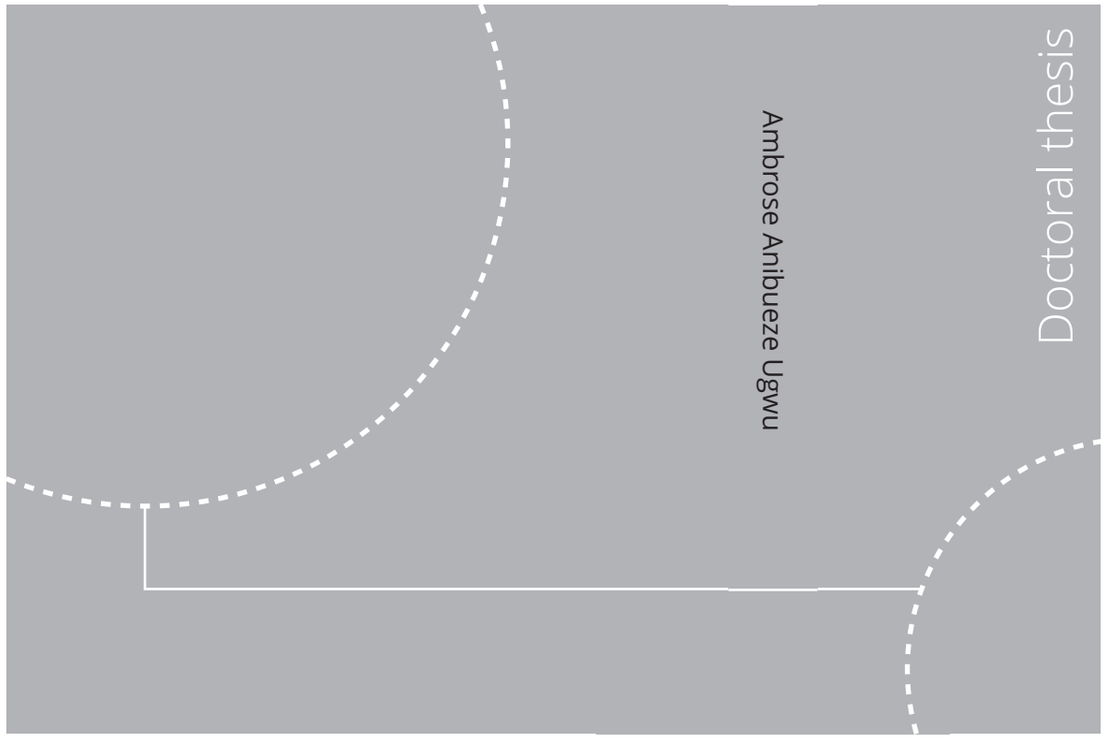

Doctoral theses at NTNU, 2020:300

Ambrose Anibueze Ugwu

Demonstration of Gas Switching Technology for Accelerated Scale-up of Pressurized Chemical Looping Applications

NTNU
Norwegian University of Science and Technology

NTNU
Norwegian University of Science and Technology
Thesis for the degree of Philosophiae Doctor
Faculty of Engineering
Department of Energy and Process Engineering

Doctoral theses at NTNU, 2020:300

NTNU

NTNU
Norwegian University of Science and Technology

Ambrose Anibueze Ugwu

Demonstration of Gas Switching Technology for Accelerated Scale-up of Pressurized Chemical Looping Applications

Thesis for the degree of Philosophiae Doctor

Trondheim, July 2020

Norwegian University of Science and Technology
Faculty of Engineering
Department of Energy and Process Engineering

NTNU
Norwegian University of
Science and Technology

NTNU
Norwegian University of Science and Technology

Thesis for the degree of Philosophiae Doctor

Faculty of Engineering
Department of Energy and Process Engineering

ISBN 978-82-326-4948-8 (printed ver.)
ISBN 978-82-326-4949-5 (electronic ver.)
ISSN 1503-8181

Doctoral theses at NTNU, 2020:300

PRINTED IN NORWAY
NO - 1598

NORDIC SWAN ECOLABEL
Printed matter
2041 0731

Printed by Skipnes Kommunikasjon AS

To my lovely wife Chinazor Monalisa Ugwu, my adorable son Chimbueze Ambrose Ugwu and my wonderful sister Francisca Oyemaechi Ugwu for their love, encouragement and support.

Preface

This thesis is submitted in partial fulfillment of the requirement for the degree of Philosophiae Doctor (Ph.D.) at the Norwegian University of Science and Technology (NTNU). The work was carried out at the Department of Energy and Process Engineering, NTNU with close collaboration with SINTEF Industry under the supervision of Shahriar Amini and Abdelghafour Zaabout. This project (Era-Net GaSTech) was possible due to the funding from The Research Council of Norway and the European Commission under the Horizon 2020 program, ACT Grant Agreement No 691712.

Acknowledgment

I thank God Almighty for His guidance and protection in the three years Ph.D. journey. To my supervisor, Shahriar Amini, thank you for the privilege to work on this project. I acknowledge your support and also thank you for making me feel at home. The wonderful reception and great dinner with your family during my first visit to Trondheim can never be forgotten. A bushel of my gratitude goes to my co-supervisor, Abdelghafour Zaabout for good supervision and involvement in every aspect of this research. You always have a way of making those difficult tasks easy and possible. You are instrumental to every outcome of this work and I owe you more than I can acknowledge. I have learned a lot from you already and I wish to continue learning as we work together in the next project.

This project would not have been possible without the financial support from The Research Council of Norway and the European Commission under the Horizon 2020 program, ACT Grant Agreement No 691712. I also thank the management of Equinor for the 2018 and 2019 publication grants. The VATL Lab technicians at NTNU are equally acknowledged for constructing and maintaining the experimental setup. Thank you Morten Grønli for providing the necessary support and approving my experiments. Paul Svendsen and Martin Bustadmo are more like friends to me; always ready to provide technical assistance. I am also grateful to Aleksander Mosand, Bjørn Volseth, Erik Langørgen, and Reidar Tellebon for their support.

It could be very challenging most times, but the prod and impetus to carry on come from the support and encouragement from the positive people around me to whom I am extremely grateful. My lovely wife Chinazor Monalisa Ugwu has been so supportive. You have shown much understanding and encouragement even with the long working hours making sure that I experience more love and care. I love it when you remind me that I do not have any reason not to deliver. Thank you my love; I will forever be indebted to you. My son Chimbueze Ambrose Ugwu also played a wonderful role; always ready to play with me even when I am not in the mood. Your arrival is a big blessing to our family and I can't love you less. My sister Dr. Francisca Onyemaechi Ugwu has been there for me, providing support, encouragement, and love to make this journey a success. You are a great mentor, confidant, and have been playing a motherly role since I was little. Sister, you will live long to rip the good fruit that you have sown. My Mum Veronica Ovute Ugwu, has proven to be an amazing mother even at old age. Those daily video calls to check how I am doing and the general status of things including the Ph.D. made a great impact; thank you Missy International. To my siblings, umu Edoga and in-laws (Dr. Joseph, Gerald, Bar. Peter, Lebechi, Nkeiruka, Chinasa, Chidiebere & Nonso,

Celestine, Domnic, Dr. Emeka, Uche, Emeka Offor, Ngozi, Amaka & Chidimma), I appreciated you all for the encouragement, love, and support. I also acknowledge my nieces and nephews in Nigeria, Canada and the USA. Thank you my in-laws (Chief Hillary Mbah, Dr. Grace Mbah, Collins, Izu, Ebuka, Ogochukwu, Caleb, and Uche (Ozioko) Onyeke) for your prayer.

My experience at the University of Southeastern Norway has continued to sustain me. One of the greatest things is the opportunity to work with Prof. Britt Moldestad as my supervisor. Britt has continued to keep in touch and play a role as a mentor, and a mother even after all these year and distance. Thank you, Dr. Cornelius Agu for the encouragement, discussions, technical support and the experience working with you on different projects.

Coming to Trondheim brought much progress in my life. Within this short period, I have met wonderful friends that turned more like brothers. Thank you, Chaitanya Dhoke, Mohammed Khan, and Shareq Mohd Nazir. You guys are always ready to help; the support, encouragement, and motivation from you cannot be overemphasized. We had a great time together and I enjoy sharing ideas with you. Mogahid Osman was a great colleague, always ready to assist with my experimental issues. Schalk Cloete has been a great teacher and friend. It was always nice to engage in technical discussions and socialize over some beer. The smile from Jan Hendrik Cloete brings positive energy. Thank you, Henri, for those great pictures and for being a wonderful friend. I would also appreciate Arpit Singhal and Joana Francisco Morgado for the little but memorable time we spent together at Trondheim. Thank you Ama Otabe and Peter Ukoh for the friendship and support. Opeyemi Bamigbeta and Ugochukwu Aronu are equally not forgotten. I also thank Felix Donat, Knuth Albertsen, Bulent Kursun, David Emberson, Dinis Nunes, Petter Røkke, Inge Saanum, Sayed E. Hashemi, and Øyvind Langørgen for the discussions and technical advice. Thank you, Prof. Stein Tore Johansen, for the opportunity to work as a PostDoc under your supervision on natural gas decarbonization/hydrogen production.

I am profoundly grateful to all my friends that have continued to be there even with the communication gap. Thank you Barry Ajokubi (kid Bro) for being a true friend and a brother. You have always been there to support and listen to my issues. I am equally grateful to Christian Ezeagu, Ikenna Ezechukwu, Nnamdi Oleaghara, Courage Asemote, Victoria Agu, Rose Muyiwa, Linda Evbu Øvrebø, Solomon Aromada, Victor Igbokwe, and Kenneth Mozie. Thank you Christine and Nnenna for being wonderful friends to my family; you are so free and we could gist for hours. To my lovely sister Chinyere Vivian Ugwu, I will never forget all your sacrifice and love even with the lack of communication during the Ph.D. struggle. Ezigbo Ada m, just be rest assured that the end is more important and I love you.

Content

Summary

This research focused on the experimental demonstration of Gas Switching Technology as an alternative for pressurized chemical looping. Chemical looping processes usually employ circulation fluidized bed (CFB) arrangement where metal oxides (oxygen carrier) are transported between two or more reactors in contact with different reducing and oxidizing gases. Although chemical looping technologies have enjoyed a great deal of research attention due to the proven capability of CO_2 capture with minimal energy penalty, a high-pressure operation is required to achieve high process efficiency. However, pressurizing the conventional chemical looping with CFB arrangement is always challenging due to the need for precise and reliable circulation of large quantities of oxygen carrier material between interconnected reactors. Aside from the design and operational complexity created by the need to manage the solid circulation so that mass and heat are balanced within the closed-loop, the exchange of solids increases unit costs due to the additional cost of separation systems (cyclones, loop seals, etc.).

To solve these challenges, a novel gas switching Technology has been proposed in this study. Gas switching differs from traditional chemical looping in the sense that the oxygen carrier is maintained in a single bubbling/turbulent fluidized bed reactor where oxidizing and reducing gases are fed alternately without solid circulation. This simple reactor configuration can easily be pressurized and scaled up without facing unforeseen challenges. With this arrangement as well, a wide range of inlet flowrates can be accommodated, with a great reduction in variable loads since the oxygen carrier is confined in one pressurized vessel without circulation.

Four chemical looping applications (combustion, reforming, water splitting, and partial oxidation) were investigated as described below:

- **Combustion:** oxy-combustion of gaseous fuel using the lattice oxygen of metal oxide (oxygen carrier) to produce a pure stream of CO_2 ready for storage/further utilization. The reduced oxygen carrier is regenerated by oxidizing with air with the release N_2 (inherent separation of N_2 from the CO_2 produced during oxidation). The hot stream of N_2 gas that can drive a gas turbine for power generation.
- **Reforming:** Steam/CO_2 reforming of methane to produce syngas (H_2 and CO) with integrated carbon capture. Here, the oxygen carrier does not act only as an oxygen reservoir but also as a catalyst. The overall reaction is endothermic but part of the heat for the process is generated through the oxidation half-reaction.

- **Water splitting:** Partial oxidation of an oxygen carrier with steam to produce pure H_2. The oxygen carrier is first reduced by carbon-rich fuel gases with inherent CO_2 capture. After the partial oxidation of the reduced oxygen carrier with steam, the lattice oxygen is fully restored by complete oxidation with air.
- **Partial oxidation:** Heterogenous partial oxidation of methane using the lattice oxygen of a metal oxide to produce syngas (H_2 and CO) of H_2/CO ratio ~2 for Gas-to-Liquid applications.

Experiments were completed using an existing lab-scale standalone reactor at the Norwegian University of Science and Technology (NTNU) which has been successfully used for demonstration of pressurized gas switching combustion of a previous project.

For the reforming demonstration, the first campaign was completed by co-feeding CH_4 and H_2O (steam methane reforming) in a two (fuel and air) step process for syngas (H_2 and CO) production using three different iron-based oxygen carrier/catalyst (Fe/Al_2O_3, $Fe\text{-}Ce/Al_2O_3$, and $Fe\text{-}Ni/Al_2O_3$) at atmospheric conditions. It was observed that $Fe\text{-}Ni/Al_2O_3$ performed better than the other oxygen carriers in the reforming sub-stage, showing 40% improved methane conversion with about 75 – 80% CH_4 conversion to syngas in the reforming sub-stage. This demonstration shows that CH_4 conversion improves with an increase in temperature and H_2O/C ratio. Autothermal operation of the reactor was also achieved with repeatable performance over several redox cycles. The second reforming demonstration was completed using $Fe\text{-}Ni/Al_2O_3$ at high pressure up to 5bar following the good performance of the oxygen carrier at first atmospheric condition. A four-stage (reduction, partial oxidation, reforming, and oxidation) process was designed to comprehensively test the behavior of the oxygen carrier towards syngas production. CH_4 conversion decreased in the reforming stage as the pressure increases driven by the negative effect of pressure on both carbon gasification by steam and on the steam methane reforming. However, CH_4 conversion was less sensitive to pressure at the partial oxidation stage. Carbon deposition was observed with the mechanism changing from methane cracking at the partial stage to Boudouard reaction at the reforming stage. The third and fourth demonstrations focused on the utilization of CO_2 in dry reforming of methane to produce syngas for GTL applications using Ni-based oxygen. Autothermal and pressurized operations were achieved with the ability to control the syngas ratio (H_2:CO) by adjusting CO_2:CH_4 ratio and addition of steam.

For partial oxidation demonstration, a lanthanum-based oxygen carrier was tested under the Gas Switching Partial Oxidation conditions (GSPOX) for combined syngas production and H_2

production in a three-stage (fuel, steam, and air) process. At the fuel stage, CH_4 is fed in the presence of a fully oxidized oxygen carrier to produce syngas (H_2 and CO) with H_2/CO ratio ~ 2, following the fuel stage is the steam stage where H_2O is supplied to partially oxidize the reduced oxygen carrier to produce pure H_2. The oxygen carrier is regenerated by complete oxidation at the air stage associated with heat generation for the process. Over 70% CH_4 conversion to syngas at the fuel stage while about 30% H_2O conversion to H_2 (above 97% pure) was achieved at the steam stage. Despite the high reactivity and stability of this oxygen carrier, substantial carbon deposition was observed at high CH_4 concentration with a resultant increase in the syngas (H_2/CO) ratio beyond 2. The deposited carbon was gasified completely gasified in the steam stage making carbon deposition not an issue if syngas production is targeted. However, carbon deposition becomes an issue if pure H_2 production is targeted in the steam stage due to the contamination by carbon gasification imposing additional purification measures.

For the water splitting demonstration, an iron-based oxygen carrier with 35 wt% active content was first tested under Gas Switching Water Splitting (GSWS) conditions, with good performance in terms of steam conversion to hydrogen and redox cyclability. However, gas mixing between stages affects H_2 purity, CO_2 purity, and CO_2 capture efficiency negatively. To Maximize gas purity and CO_2 capture, an iron-based oxygen carrier with a high active content ~ 75 wt% active content was manufactured and tested. The high content oxygen carrier exhibited high reactivity, but with a higher tendency to carbon deposition and agglomeration, thus creating operational challenges.

Following the successful standalone GST demonstrations, a $60kW_{th}$ cluster of three reactors was successfully designed and commissioned for continuous operation of the pressurized gas switching concept. The first cluster operation of Gas Switching Combustion (GSC) using $CaMnO_{3-\delta}$-based oxygen carrier is still ongoing. A continuous autothermal pressurized operation is targeted at operating temperatures up to 1000 °C and pressures up to 15 bar. Further GSPOX cluster demonstration is also planned, following the good performance of the first standalone GSPOX demonstration using an optimized La-based oxygen carrier that has been shipped to NTNU. In general, all the cluster demonstrations are aimed to extract important process information to evaluate scale-up and commercialization possibilities.

Thesis outline

The thesis consists of ten chapters with six of the chapters adapted from journal publications of the research outcome. Chapter 1 (introduction) gives an overview of the project, the motivation, the state-of-the-art, collaborations, the objectives, the scope, the method, and the contributions of the research to the future energy ambitions and the scientific community. The technical background is presented in Chapter 2 with a brief review of climate change and energy transition, Carbon Capture, Storage and/Utilization (CCS/CCUS), chemical looping, and the novel gas switching technology under investigation in this study. This chapter also introduces the cluster operation for the continuous operation of the GST operation. A theoretical look at thermodynamics and heat management strategy is presented in Chapter 3 while the demonstrations of Gas Switching Reforming (GSR) are reported in Chapters 4 – 7. Chapter 4 presents the demonstration of steam methane GSR at atmospheric conditions using iron-based oxygen carriers while Chapter 5 demonstrates the pressurized operation. Chapter 6 presents the autothermal Gas Switching Dry Reforming (GSDR) where CO_2 is utilized to reform CH_4 for syngas production for Gas-to-liquid (GTL) processes. Chapter 8 reports the demonstration of a novel Gas Switching Watersplitting (GSWS) process for pure H_2 production through partial oxidation of iron/iron oxide with steam while Chapter 9 presents a concept that combines both syngas and H_2 production in one process through partial oxidation of methane refer to as Gas Switching Partial Oxidation (GSPOX) using the lattice oxygen of a La-based oxygen carrier developed in this project. Finally, a distinct conclusion of the work and recommendations for future work were given in Chapter 10.

1 Introduction

The research is the experimental demonstration part of the Era-Net GaSTech project funded by the Research Council of Norway and the European Commission under the Horizon 2020 program, ACT Grant Agreement No 691712. This research is motivated primarily by the challenges of pressurized chemical looping applications posed by the need for precise and reliable circulation of large quantities of oxygen carrier material between interconnected reactors. Unlike conventional chemical looping, gas switching technology (GST) utilizes a single fluidized bed reactor in bubbling/turbulent flow regime and avoids solid circulation by alternately feeding the oxidizing and reducing gases to achieve redox reactions. This simple reactor configuration can easily be scaled up and pressurized without facing many challenges. Five chemical looping processes: combustion, reforming, water splitting, oxygen uncoupling and partial oxidation of methane were investigated to ascertain their viability with GST. In this way, a business case would be developed for an immediate scale-up and commercialization.

Specialized partners (NTNU, SINTEF Industry, Euro Support Advanced Materials B.V, Universitatea Babeș-Bolyai, Hayat, ETH Zürich, and Universidad Politécnica de Madrid) were responsible for different work packages. ETH was responsible for material selection, characterization, and small-scale pre-testing of the oxygen carrier materials manufactured by Euro Support Advanced Materials B.V for the experimental demonstration at NTNU. The experimental demonstration which is the focus of this thesis was completed using an existing standalone lab-scale reactor at NTNU in close collaboration with SINTEF. SINTEF was also responsible for reactor modeling and provided input to UPM for the process simulations. With the demonstration and modeling outcomes, UBB carried out economic assessments and benchmarked with other similar technologies as published in different journals [1-5]. Finally, HAYAT evaluated the business case based on the main project results.

Experimental demonstrations have been completed under atmospheric and high-pressure conditions showing easy operation and reduced operational risk [6-8]. Gas Switching Technology (GST) has also been proposed for combustion for power generation [3, 9-12], H_2 production through methane reforming [6, 7, 13-16], GHG (CO_2 and CH_4) utilization through dry reforming[17] and provides flexibility in terms of product requirement (H_2 or power) [18]. The process modeling and techno-economic assessment show that this reactor concept can address most of the shortcomings of conventional chemical looping including cost reduction [1-5]. For power production, it has been established that GSC can eliminate the energy penalty of CO_2 capture when combined with an integrated gasification combined cycle (GSC-IGCC)

power plant, achieving around 50% efficiency and with approximately 80% capture rate through natural gas firing [19]. Further research on a simpler configuration using Gas Switching Oxygen Production reactors can improve the efficiency of conventional pre-combustion CO2 capture in IGCC plants by about 7 %-points, with a CO_2 capture ratio above 80% [19]. The economic assessments show that GSC-IGCC can capture CO_2 for as little as 22.4 €/ton. Therefore GSC-IGCC will operate best as baseload power generators, which is not competitive with the rise of variable renewable energy[19]. With this, more focus was given to developing inherently flexible plant configurations (pre-combustion natural gas-fired plant: GSR-CC[3, 18], GSC reactors with a humid air turbine (GSC-HAT) power cycle[20] and GSC membrane-assisted water-gas shift reactor) that integrate well with variable wind and solar power with the goal of maximizing system's flexibility for power/H_2 production. With these configurations, electricity could be produced at an efficiency of 50.3% and H_2 at an efficiency of 67.0% with CO_2 avoidance exceeding 98%. About CO_2 avoidance costs of €20/ton could be achieved for power production better than GSC-IGCC. For pure H_2 production using GSR, an economic assessment has revealed the possibility to produce H_2 at costs below that of conventional steam methane reforming technology [21]. An attractive business case for scale-up was identified where the GSR-H_2 plant is first constructed with no CO_2 capture, resulting in substantially lower costs than benchmarks[21]. Currently, the performance of this plant is being assessed when using an optimized version of the partial oxidation oxygen carrier with the capability of eliminating the thermodynamic restrictions of GSR for power combined power and H_2 production.

Although previous experimentally demonstration for combustion [9-11] and steam methane reforming [13] of this novel reactor concept have been completed at atmospheric conditions in a previous project, this Ph.D. research further demonstrates the gas switching concept for pressurized methane reforming with non-Nickel based catalyst [16, 17, 22], H_2 production through water splitting [23] and partial oxidation of methane[24]. Following the successful demonstrations in the $10kW_{th}$ standalone reactor, a $60kW_{th}$ cluster of three reactors was designed and commissioned for continuous operation of the pressurized gas switching concept. The pre-pilot scale reactor cluster has been successfully commissioned and the demonstration of gas switching combustion using $CaMnO_{3-\delta}$-based oxygen carrier is still ongoing.

1.1 State-of-the-art

Chemical looping has been considered as a promising technology with great potential to reduce the energy penalty, costs associated with the conversion of fossil fuels to cleaner energy carriers. Different Chemical-Looping concepts have been proposed for CO_2 capture including the inherent separation of CO_2 and N_2 [25]. This technology was first applied to combustion for capturing CO_2 [26, 27]. The low energy penalty of technology relative to other CO_2 capture technologies has led to extensions of the chemical looping principle to other CCS and energy-intensive processes such as reforming [28], oxygen production [29] and H_2 production through water splitting [30].

High-pressure operation of these chemical looping concepts is necessary for maximizing energy efficiency and competitiveness with other CO_2 capture technologies. However, the scale-up of pressurized chemical looping processes is difficult due to the mechanical challenges associated with solid circulation between interconnected reactors configuration involving solids circulation between reactors. With these challenges facing the pressurized chemical looping applications, only a few experimental demonstrations of this concept have been recorded [31-34]. This limitation was the basis for research for an alternative pressurized chemical looping concepts such as internal circulating reactor [35, 36], rotating reactor[37], gas switching technology using packed bed reactor [38, 39] and gas switching technology using fluidized bed reactor [9, 14-17, 40] under investigation in this research that can avoid external solid circulation. The GST using a fluidized bed demonstrates advantages over the packed bed option since it avoids material related issues due to uneven solid mixing that leads to excessive coking, sintering, hot spots, and easy deactivation of the metal oxide[1]. The experience from the previous demonstration of GST was utilized in this research with clear objectives defined to ensure a comprehensive investigation of the GST in addressing the aforementioned pressurized chemical looping challenges.

1.2 Objectives

The overall aim of the project is to accelerate the scale-up of pressurized chemical looping applications and contribute to the ongoing CCS/CCUS research through scientific dissemination. A comprehensive investigation of the GST in addressing the aforementioned pressurized chemical looping challenges was achieved with the following realistic objectives:

- Demonstrate pressurized combustion (for power generation), H_2 and syngas production using the existing standalone reactor setup using a non-Nickel based oxygen carrier.
- Develop and commission a pre-pilot scale cluster of three reactors for a continuous GST operation. At least 50 hours of high-pressure operation of each gas switching application will be completed to evaluate oxygen carrier longevity under realistic operating conditions. The results from these tests will give important input to the business case assessment.
- Demonstrate pressurized autothermal chemical looping combustion cluster operation using $CaMnO_{3-\delta}$ based oxygen up to 10bar. This oxygen carrier has been used in previous GSC demonstration [41] but has optimized for better resistance towards carbon deposition.

The use of existing infrastructure saved cost, time, and enable the objectives to be achieved as planned. The assistance and supervision from the SINTEF scientist who designed and previously operated the existing reactor also facilitated the research outcome.

1.3 Method

As mentioned earlier, an existing pressurized 5 cm ID fluidized bed reactor *(Figure **1-1***) was used for the standalone demonstration to the aim to achieve autothermal operation for each GST concept at pressurized conditions. It was also desired to demonstrate the application of non-toxic oxygen carriers for all the GST processes to easy operation and scalability. A proper gas feed system consisting of gas mass flow controllers, stop and multiway valves (controlled through a Labview program) were in place. Temperature and pressure sensors in the reactor setup made it possible to take measurements through the LabView program while the gas composition at the reactor outlet was analyzed using ETG Syngas analyzer. With the successful standalone demonstration, a pre-pilot scale reactor was designed and developed to achieve a continuous GST operation. In summary, the experimental demonstration was flexible enough that different process parameters were studied and evaluate under realistic operating conditions.

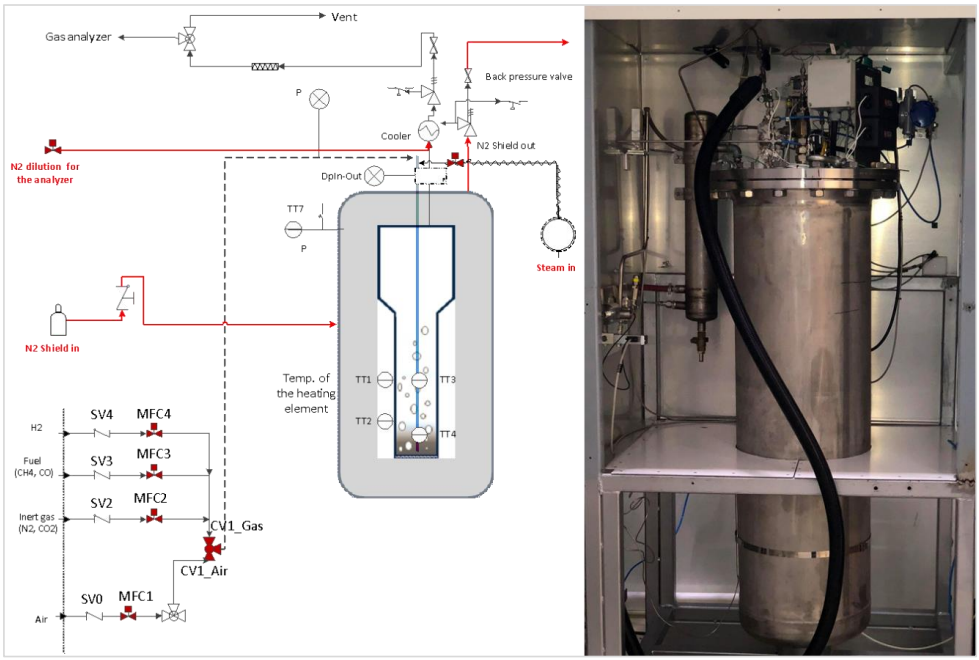

Figure 1-1: Setup of the standalone pressurized fluidized bed reactor used for experimental demonstration

The research activities were ethically executed following in the best practice. There were two independent supervisors to ensure unbiased outcomes and proper adherence to the research scope. The research activities were also discussed and scrutinized in consortium meetings held every six months with other international collaborators. Considering the originality, and proper supervision, this research was completed without ethical issues.

1.4 Contribution

The main contributions of the thesis are summarized below:

- This thesis reports the first demonstration of GSR using a non-Nickel based oxygen carrier and pressurized GST beyond combustion. Autothermal operation and comprehensive sensitivity study of temperature and H_2O:C ratio were achieved. Also, the first demonstration of dry reforming, combined steam and dry reforming and tri reforming of natural gas using GST with the integration to GTL (Methanol) process was completed.
- The first large scale demonstration of GSPOX for combined syngas and H_2/CO production in a single process was achieved with process behavior investigated at different temperatures, CH_4 concentration, flow rate, pressure, and H_2O/CO_2 utilization

were established. A new phenomenon was reported after a prolonged operation (over 12hours) of co-feeding CO_2 and CH_4 in the presence of fully oxidized oxygen with the gas composition suggesting a simultaneous reduction and oxidation at the same rate making the oxygen carrier behave more like a catalyst.

- The first experimental demonstration of Gas switching water splitting (GSWS) for pure H_2 production. The result of the demonstration shows that GSWS could work but requires the development of reactive trivalent oxygen carriers with high active content capable of resisting agglomeration and carbon deposition.
- The first of its kind pressurized 60kW_{th} pre-pilot scale cluster of three reactors for continuous GST operation was successfully developed and commissioned. Currently, the demonstration of gas switching combustion is going on using in the cluster using an optimized Mn-based oxygen carrier. There is also a plan to further to demonstrate continuous GSPOX using the reactor cluster.
- This work has been presented in nine international conferences with six journal articles (four already published and two submitted) in international journals.

1.5 List of articles

Six journal articles (Articles I – VI) have been included in this thesis of which I am the first author of five (Articles II – VI). Four of the articles (I, II, III & V) have been published already while two (IV & VI) have been submitted for publication in international journals. In all the articles, I was responsible for the experimental demonstration, analysis of the results, discussions, and preparation, and submission of the manuscript. Abdelghafour Zaabout participated in the planning, running of the experiments, result analysis, discussion, and preparation of the manuscript in all the studies. Schalk Cloete was involved in result analysis and manuscript preparation for articles I and V, while Paul Inge Dahl and Julian R. Tolchard were responsible for material characterization for articles I and II. Shareq Mohd Nazir was responsible for the process simulation of Article IV. For articles V and VI, Felix Donat and Christoph Müller were responsible for the oxygen carrier selection, chemistry, characterization, small-scale pre-demonstration test, and manuscript review while Knuth Albertsen and Geert van Diest were responsible for the large-scale oxygen carrier development, and also participated in discussions and manuscript review. The entire study was supervised by Abdelghafour Zaabout and Shahriar Amini.

Article I

Zaabout, A., PI. Dahl, A. Ugwu, JR. Tolchard, S. Cloete and S. Amini, *Gas Switching Reforming (GSR) for syngas production with integrated CO_2 capture using iron-based oxygen carriers*. International Journal of Greenhouse Gas Control, 2019. 81: p. 170-180.

Article II

Ugwu, A. Zaabout, JR. Tolchard, PI. Dahl and S. Amini, *Gas Switching reforming for syngas production with iron-based oxygen carrier-the performance under pressurized conditions.* International Journal of Hydrogen Energy, 2020. 45(2): p. 1267-1282.

Article III

Ugwu, A., A. Zaabout, and S. Amini, *An advancement in CO_2 utilization through novel gas switching dry reforming.* International Journal of Greenhouse Gas Control, 2019. 90: p. 102791.

Article IV

Ugwu, A., A. Zaabout, SM. Nazir and S. Amini, Gas-to-liquid process for CO_2 utilization through gas switching dry reforming. *Chemical Engineering Journal*, 2020. Under review.

Article V

Ugwu, A., F. Donat, A. Zaabout, C. Müller, K. Albertsen, S. Cloete, G. van Diest and S. Amini, *Hydrogen Production by Water Splitting using Gas Switching Technology*. Powder Technology, 2020. 370: p. 48 - 63

Article VI

Ugwu, A., A. Zaabout, F. Donat, C. Müller, K. Albertsen, G. van Diest and S. Amini, Combined Syngas and Hydrogen Production using Gas Switching Technology. *Industrial & Engineering Chemistry*, 2020. Under review.

Nomenclature

Abbreviations

CCS	Carbon Capture and Storage
CCUS	Carbon Capture Storage and Utilization
CFB	Circulating Fluidized Bed
CLC	Chemical Looping Combustion
CLR	Chemical Looping Reforming
CLR-H_2	Chemical Looping Reforming Hydrogen
GHG	Greenhouse Gas
GSC	Gas Switching Combustion
GSC-HAT	Gas Switching Combustion Humid Air Turbine
GSC-IGCC	Gas Switching Combustion Integrated Gasification Combined Cycle
GSOP	Gas Switching Oxygen Production
GSPOX	Gas Switching Partial Oxidation
GSR	Gas Switching Reforming
GSR-CC	Gas Switching Reforming Combined Cycle
GSR-H_2	Gas Switching Reforming Hydrogen
GST	Gas Switching Technology
GTL	Gas-to-liquid
HAT	Humid Air Turbine
IGCC	Integrated Gasification Combined Cycle
MFC	Mass Flow Controller
OC	Oxygen Carrier

References

[1] S. Cloete, F. Gallucci, M. van Sint Annaland, and S. Amini, "Gas switching as a practical alternative for scaleup of chemical looping combustion," *Energy Technology,* vol. 4, no. 10, pp. 1286-1298, 2016.

[2] C. A. del Pozo, S. Cloete, J. H. Cloete, Á. J. Álvaro, and S. Amini, "The potential of chemical looping combustion using the gas switching concept to eliminate the energy penalty of CO2 capture," *International Journal of Greenhouse Gas Control,* vol. 83, pp. 265-281, 2019.

[3] S. M. Nazir, S. Cloete, O. Bolland, and S. Amini, "Techno-economic assessment of the novel gas switching reforming (GSR) concept for gas-fired power production with integrated CO2 capture," *International journal of hydrogen energy,* vol. 43, no. 18, pp. 8754-8769, 2018.

[4] S. A. Wassie, S. Cloete, V. Spallina, F. Gallucci, S. Amini, and M. van Sint Annaland, "Techno-economic assessment of membrane-assisted gas switching reforming for pure H2 production with CO2 capture," *International Journal of Greenhouse Gas Control,* vol. 72, pp. 163-174, 2018.

[5] C. A. del Pozo, A. J. Álvaro, J. H. Cloete, S. Cloete, and S. Amini, "Exergy Analysis of Gas Switching Chemical Looping IGCC Plants," *Energies,* vol. 13, no. 3, pp. 1-25, 2020.

[6] S. A. Wassie, F. Gallucci, A. Zaabout, S. Cloete, S. Amini, and M. van Sint Annaland, "Hydrogen production with integrated CO2 capture in a novel gas switching reforming reactor: Proof-of-concept," *International Journal of Hydrogen Energy,* vol. 42, no. 21, pp. 14367-14379, 5/25/ 2017, doi: https://doi.org/10.1016/j.ijhydene.2017.04.227.

[7] S. A. Wassie *et al.*, "Hydrogen production with integrated CO2 capture in a membrane assisted gas switching reforming reactor: Proof-of-Concept," *International Journal of Hydrogen Energy,* vol. 43, no. 12, pp. 6177-6190, 2018/03/22/ 2018, doi: https://doi.org/10.1016/j.ijhydene.2018.02.040.

[8] A. Zaabout, S. Cloete, and S. Amini, "Autothermal operation of a pressurized Gas Switching Combustion with ilmenite ore," *International Journal of Greenhouse Gas Control,* vol. 63, pp. 175-183, 2017/08/01/ 2017, doi: https://doi.org/10.1016/j.ijggc.2017.05.018.

[9] A. Zaabout, S. Cloete, S. T. Johansen, M. van Sint Annaland, F. Gallucci, and S. Amini, "Experimental Demonstration of a Novel Gas Switching Combustion Reactor for Power Production with Integrated CO2 Capture," *Industrial & Engineering Chemistry Research,* vol. 52, no. 39, pp. 14241-14250, 2013/10/02 2013, doi: 10.1021/ie401810n.

[10] A. Zaabout, S. Cloete, M. van Sint Annaland, F. Gallucci, and S. Amini, "A novel gas switching combustion reactor for power production with integrated CO2 capture: Sensitivity to the fuel and oxygen carrier types," *International Journal of Greenhouse Gas Control,* vol. 39, pp. 185-193, 2015.

[11] A. ZAABOUT, S. CLOETE, and S. AMINI, "Autothermal operation of a pressurized gas switching combustion reactor with a Mn-based oxygen carrier."

[12] A. Zaabout, S. Cloete, S. T. Johansen, M. v. S. Annaland, F. Gallucci, and S. Amini, "Experimental Demonstration of a Novel Gas Switching Combustion Reactor for Power Production with Integrated CO2 Capture," *Industrial & Engineering Chemistry Research,* vol. 52, no. 39, pp. 14241-14250, Oct 2 2013, doi: 10.1021/ie401810n.

[13] S. A. Wassie, F. Gallucci, A. Zaabout, S. Cloete, S. Amini, and M. van Sint Annaland, "Hydrogen production with integrated CO2 capture in a novel gas switching reforming reactor: Proof-of-concept," *International Journal of Hydrogen Energy,* vol. 42, no. 21, pp. 14367-14379, 2017.

[14] S. M. Nazir, J. H. Cloete, S. Cloete, and S. Amini, "Efficient hydrogen production with CO2 capture using gas switching reforming," *Energy,* 2019.

[15] A. Ugwu, A. Zaabout, J. R. Tolchard, P. I. Dahl, and S. Amini, "Gas Switching Reforming for syngas production with iron-based oxygen carrier-the performance under pressurized conditions," *International Journal of Hydrogen Energy,* 2019.

[16] A. Zaabout, P. I. Dahl, A. Ugwu, J. R. Tolchard, S. Cloete, and S. Amini, "Gas Switching Reforming (GSR) for syngas production with integrated CO2 capture using iron-based oxygen carriers," *International Journal of Greenhouse Gas Control,* vol. 81, pp. 170-180, 2019.

[17] A. Ugwu, A. Zaabout, and S. Amini, "An advancement in CO2 utilization through novel gas switching dry reforming," *International Journal of Greenhouse Gas Control,* vol. 90, p. 102791, 2019.

[18] S. Szima *et al.*, "Gas switching reforming for flexible power and hydrogen production to balance variable renewables," *Renewable and Sustainable Energy Reviews,* vol. 110, pp. 207-219, 2019.

[19] C. Arnaiz del Pozo, A. Jiménez Álvaro, J. H. Cloete, S. Cloete, and S. Amini, "Exergy analysis of gas switching chemical looping IGCC plants," *Energies,* vol. 13, no. 3, p. 544, 2020.

[20] C. Arnaiz del Pozo, J. H. Cloete, S. Cloete, Á. Jiménez Álvaro, and S. Amini, "Integration of gas switching combustion in a humid air turbine cycle for flexible power production from solid fuels with near-zero emissions of CO2 and other pollutants," *International Journal of Energy Research,* 2020.

[21] S. M. Nazir, J. H. Cloete, S. Cloete, and S. Amini, "Efficient hydrogen production with CO2 capture using gas switching reforming," *Energy,* vol. 185, pp. 372-385, 2019.

[22] A. Ugwu, A. Zaabout, P. I. Dahl, J. R. Tolchard, and S. Amini, "Gas Switching Reforming for syngas production with iron-based oxygen carrier- The performance under pressurized conditions.," PARTEC International Congress on Particle Technology, Germany, 2019.

[23] A. Ugwu *et al.*, "Hydrogen Production by Water Splitting using Gas Switching Technology," *Powder Technology,* vol. Under Review, 2019.

[24] F. Donat, Y. Xu, and C. R. Müller, "Combined Partial Oxidation of Methane to Synthesis Gas and Production of Hydrogen or Carbon Monoxide in a Fluidized Bed using Lattice Oxygen," *Energy Technology,* p. 1900655, 2019.

[25] E. J. Anthony, "Solid looping cycles: a new technology for coal conversion," *Industrial & Engineering Chemistry Research,* vol. 47, no. 6, pp. 1747-1754, 2008.

[26] M. Ishida, D. Zheng, and T. Akehata, "Evaluation of a chemical-looping-combustion power-generation system by graphic exergy analysis," *Energy,* vol. 12, no. 2, pp. 147-154, 1987.

[27] A. Lyngfelt, B. Leckner, and T. Mattisson, "A fluidized-bed combustion process with inherent CO2 separation; application of chemical-looping combustion," *Chemical Engineering Science,* vol. 56, no. 10, pp. 3101-3113, 2001.

[28] M. Rydén, A. Lyngfelt, and T. Mattisson, "Two novel approaches for hydrogen production; chemical-looping reforming and steam reforming with carbon dioxide capture by chemical-looping combustion," in *Proceedings of the 16th world hydrogen energy conference, Lyon, France*, 2006.

[29] B. Moghtaderi, "Application of chemical looping concept for air separation at high temperatures," *Energy & Fuels,* vol. 24, no. 1, pp. 190-198, 2009.

[30] M. Rydén and M. Arjmand, "Continuous hydrogen production via the steam–iron reaction by chemical looping in a circulating fluidized-bed reactor," *International Journal of Hydrogen Energy,* vol. 37, no. 6, pp. 4843-4854, 2012.

[31] R. Xiao, L. Chen, C. Saha, S. Zhang, and S. Bhattacharya, "Pressurized chemical-looping combustion of coal using an iron ore as oxygen carrier in a pilot-scale unit," *International Journal of Greenhouse Gas Control,* vol. 10, pp. 363-373, 2012.

[32] L. Chen, Z. Fan, R. Xiao, and K. Liu, "Pressurized Chemical Looping Combustion for Solid Fuel," *Handbook of Chemical Looping Technology,* pp. 123-158, 2018.

[33] S. Zhang, R. Xiao, and W. Zheng, "Comparative study between fluidized-bed and fixed-bed operation modes in pressurized chemical looping combustion of coal," *Applied energy,* vol. 130, pp. 181-189, 2014.

[34] A. Bischi *et al.*, "Design study of a 150 kWth double loop circulating fluidized bed reactor system for chemical looping combustion with focus on industrial applicability and pressurization," *International Journal of Greenhouse Gas Control,* vol. 5, no. 3, pp. 467-474, 2011.

[35] M. Osman, A. Zaabout, S. Cloete, and S. Amini, "Internally circulating fluidized-bed reactor for syngas production using chemical looping reforming," *Chem. Eng. J.,* 2018/10/04/ 2018, doi: https://doi.org/10.1016/j.cej.2018.10.013.

[36] M. Osman, A. Zaabout, S. Cloete, and S. Amini, "Internally circulating fluidized-bed reactor for syngas production using chemical looping reforming," *Chemical Engineering Journal,* vol. 377, p. 120076, 2019.

[37] S. F. Håkonsen and R. Blom, "Chemical looping combustion in a rotating bed reactor–finding optimal process conditions for prototype reactor," *Environmental science & technology,* vol. 45, no. 22, pp. 9619-9626, 2011.

[38] S. Noorman, M. van Sint Annaland, and H. Kuipers, "Packed bed reactor technology for chemical-looping combustion," *Industrial & Engineering Chemistry Research,* vol. 46, no. 12, pp. 4212-4220, 2007.

[39] H. Hamers, F. Gallucci, P. Cobden, E. Kimball, and M. van Sint Annaland, "A novel reactor configuration for packed bed chemical-looping combustion of syngas," *International Journal of Greenhouse Gas Control,* vol. 16, pp. 1-12, 2013.

[40] S. M. Nazir, J. H. Cloete, S. Cloete, and S. Amini, "Gas switching reforming (GSR) for power generation with CO2 capture: Process efficiency improvement studies," *Energy,* vol. 167, pp. 757-765, 2019.

[41] A. Zaabout, S. Cloete, J. R. Tolchard, and S. Amini, "A pressurized Gas Switching Combustion reactor: Autothermal operation with a CaMnO3− δ-based oxygen carrier," *Chemical Engineering Research and Design,* vol. 137, pp. 20-32, 2018.

2 Technical Background

2.1 Climate change and energy transition

It has not been business as usual as the adverse effects of climate change (such as heatwaves, wildfire, acidic seawater, etc) associated with greenhouse (GHG) emission has already started manifesting. This is in agreement with the 2018 IPCC special report that warns that climate change is already inevitable even without further emission (*Figure **2-1***) and the global temperature rise should be kept below 1.5 to avoid very devastating effects[1]. Meanwhile, if the current anthropogenic warming continues with the current rate, a 1.5°C increase in global temperature relative to the preindustrial level would be attained by 2040[1], thus urgent actions are required to save our planet.

Despite fossil-fuel related GHG emissions being the largest contributor to climate warming, the demand for fossil fuel has continued to increase[1]. As a result, CO_2 emission has also continued to be on the rise with a historic 33.1 gigatons (Gt) CO_2 emission recorded in 2018[2] despite the progress in low/zero-emission technologies (*Figure **2-2***) [3, 4]. The trend indicates that the current low-emission options are not sufficient to meet the rising energy demand and dependency on fossil fuel-driven by the increase in population and higher economic activities[2]. Although the emissions slowed down in the first quarter of 2020 due to the lockdown of COVID 19 which lowered the global energy demand by ~ 3.8% relative to the first quarter of 2019, it is expected that the emissions trend will suffice when the lockdown is relaxed [4].

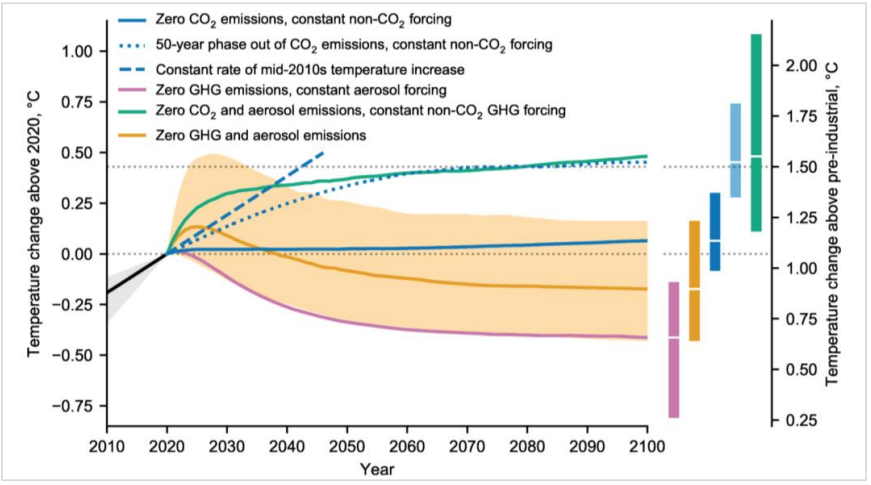

Figure 2-1*: Warming commitment from past emissions of greenhouse gases and aerosols[1]*

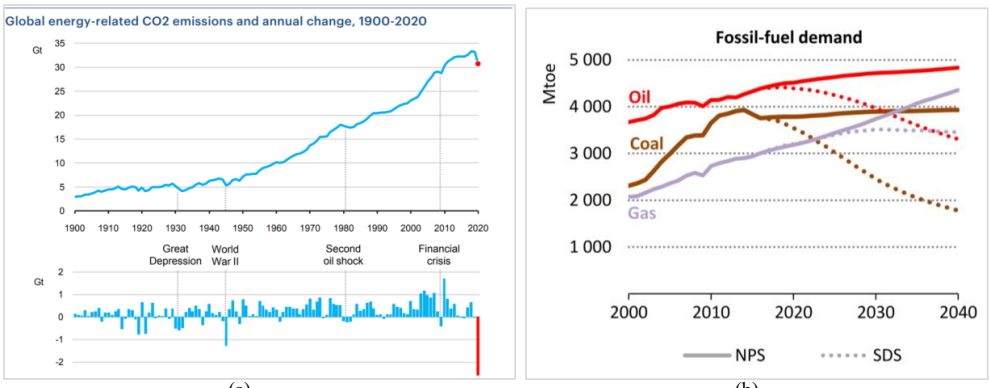

(a) (b)

Figure 2-2: (a) Global CO_2 emission till 2020 [4] and (b) IEA projection of fossil-fuel demand under the Sustainable Development Scenario (SDS) relative to the New Policy Scenario (NPS) showing that demand of natural gas would not decline beyond 2040[3]. Note: The Sustainable Development Scenario maps out a way to meet sustainable energy goals in full, requiring rapid and widespread changes across all parts of the energy system to limit the global temperature rise below 1.5°C while the new policy scenario defines a path to comply with the Paris Agreement by holding the rise in global temperatures below 2°C by 2100.

The reliance on fossil fuel would continue to increase even beyond 2040 according to IEA projection under the new policy scenario [5-8]. Currently, fossil fuel constitutes about 80% of primary energy supply [9] with about 42% of the global fossil CO_2 emission is from coal, 34% from oil, 19% from natural gas, and the remaining 5% from cement and other smaller sources over the past decade[10]. Considering different sectors, about 45% of the global fossil CO_2 emissions is mainly through electricity and heat production, about 23% from the other industrial applications (such as metals production, chemicals, and manufacturing), about 22.5% from transport and 10% from other sources[10].

Among the fossil fuels, only the demand for natural gas has been projected to continue increasing beyond 2030 and even thrive beyond 2040 under the IEA sustainable development scenario (SDS) (*Figure **2-2**b*) [5, 11]. Natural gas is considered a bridge fuel from coal to non-fossil power generation because of its low emission potential of about 40% less CO_2 than coal per unit of energy [10]. With about a 35% global increase in demand in the past decade and about a 44% increase in its use for electricity and heat production without CCS, natural gas has become the fastest-growing source of fossil fuel emissions [10]. This implies that despite the advantages of natural gas in the decarbonization effort, expanding its use without carbon capture and storage (CCS) would lead to enormous CO_2 emission thus hampering the energy transition/ climate ambitions. To ensure that natural gas continues to play the stipulated vital role in the energy-transition roadmap, it is necessary to integrated carbon capture through CCUS to reduce the carbon footprint.

The goal of CCUS is to reduce anthropogenic carbon emissions by capturing, utilizing (carbon circular economy), and/or storing CO_2 in the subsurface geological formations instead of releasing it to the atmosphere. Normally, the energy from fossil fuels is released through combustion (burning) and other conversion processes with CO_2 as a by-product which is usually purified and captured. There are three types of CO_2 capture: pre-combustion, post-combustion, and oxyfuel with post-combustion.

Pre-combustion: pre-combustion CO_2 capture is normally applied to syngas production processes (such as gasification, reforming, partial of methane) from fossil fuel where the CO from the resulting syngas is further reacted with H_2O in water gas shift reaction to produce H_2 and CO_2. The produced H_2 is separated (to be used as fuel) while CO_2 is captured in a relatively pure flue gas stream before the combustion process with separated H_2 to produce only H_2O.

Post-combustion capture: CO_2 is captured after the combustion of the fossil fuel from the flue gases of a point source such as power stations, cement kiln, etc. The technology is well understood and is currently used in other industrial applications, although not on the same scale required for a commercial-scale power station.

Oxyfuel combustion: In oxy-fuel combustion, fossil fuel is burned with pure oxygen instead of air to produce CO_2 and H_2O. H_2O is separated by condensation leaving a pure stream of CO_2 in the flue gas ready for storage or further utilization. The cooled flue gases are usually recirculated to the combustion chamber to control the temperature. Unlike the pre and post-combustion capture, the flue gas stream usually consists of pure CO_2 thus there is no need for additional capture technique to remove CO_2 instead, the flue gas consisting of pure CO_2 is compressed (for non-pressurized systems) and transported for storage or other utilization. The limitation of this capture technique is the high cost associated with the expensive air separation unit required to provide pure O_2 for the process. To this end, chemical looping has demonstrated as a viable alternative since it offers an in-situ air separation using cheap metal oxides that can easily take up oxygen (oxidation) in the presence of air and release it (reduction) in combustion reactions. With the chemical looping approach, the need for the expensive air separation unit is avoided with minimal energy penalty achieved through heat integration of the circulation activities (see section 2.2 for more details).

CCUS is required in all current fossil-fuel infrastructures and has been projected to contribute around 9% of the energy mix in the sustainable development scenario (*Figure **2-3**)* towards a net-zero carbon by 2050 [12]. However, most CCS technologies are still lagging at the small-scale demonstration stage[13]. Besides, the world's largest CCS test facility is located at

Mongstad, Norway, there are currently only five industrial-scale CCS projects that capture CO_2 and store in geological formation are in operation with a combined capture rate of about 6.5 Mt per year. Two of these facilities are in Norway (the Snøhvit and Sleipner projects), one in the USA (the Illinois Industrial CCS project), one in Canada (the Quest CCS project) and one in Australia (the Gorgon project) [14]. There are also six large-scale projects associated with coal-fired power plants, where the captured CO_2 is utilized for CO_2-EOR instead of direct storage. Apart from the Northern Light CCS Project introduced by the Norwegian government to ensure full- scale CCS value chain in Norway by 2024, no new large-scale CCS project is currently in progress, although several projects are in the pre-feasibility stage through the CarbonSAFE program of the US Department of Energy. The main impediment to the deployment of CCS is a lack of incentives [14]. Considering that most operators do not face direct financial burden for emitting CO_2 to the atmosphere, they seem not interested to spend additional money and energy for CCS. These challenges tend to overshadow the importance and hinder CCS investments. It is therefore important to close these gaps now and avoid the pitfall of a technology that has been evolving for over two decades now. One of the possible remedies is Chemical looping technology as explained in the next section.

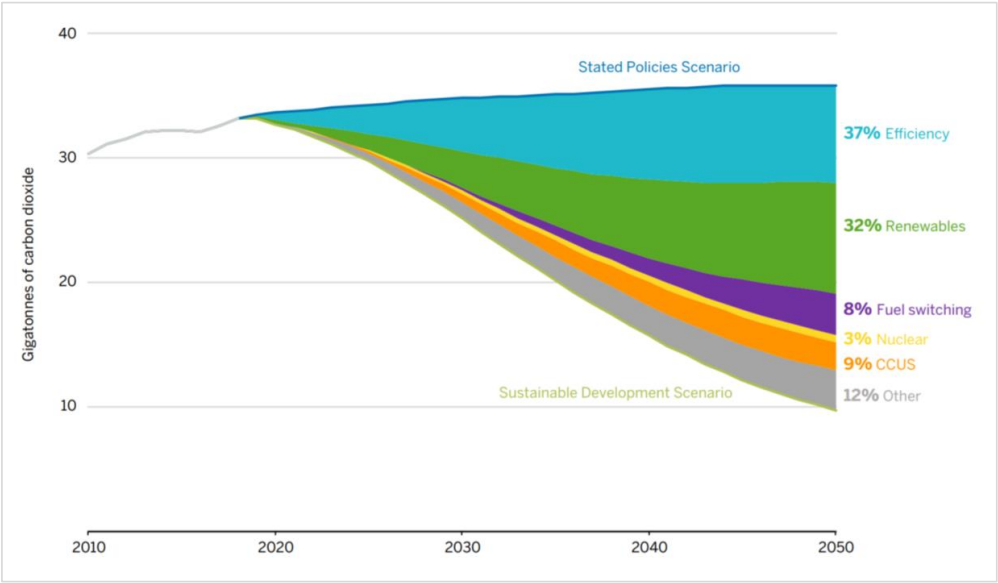

Figure 2-3: The projected contributions from different measures to reduce CO_2 emissions under the Sustainable Development Scenario (SDS) relative to the Stated Policies Scenario (SPS). Note: Reduced thermal losses in power generation account for 15% of efficiency improvements. CCUS = carbon capture, utilization, and storage. The Sustainable Development Scenario maps out a way to meet sustainable energy goals in full, requiring rapid and widespread changes across all parts of the energy system to limit the global temperature rise below 1.5°C while the stated policy scenario defines a path to comply with the Paris Agreement by holding the rise in global temperatures below 2°C by 2100[12].

2.2 Chemical looping technology

Chemical looping typically employs a dual CFB system (*Figure **2-4*** a) where a metal oxide is used as bed material to provide the oxygen/catalysis for the reaction in the fuel reactor. The reduced metal is then transferred to the second reactor (air reactor) where it is re-oxidized before being reintroduced back to the fuel reactor for another cycle of redox reactions. For energy-intensive processes, this technology has been proven to reduce the energy penalty as the heat of reaction could be transferred by metal oxide (oxygen carrier/catalyst) and utilized in the energy-demanding redox step. Another attractiveness of chemical looping is the pure CO_2 stream could be produced in the fuel reactor ready for storage or further utilization without additional CCS cost. Chemical looping technology is mature and demonstrated in several pilot plants under atmospheric conditions [15]. However, a high-pressure operation is required to achieve maximal process efficiency and integration with other downstream processes [16, 17].

Despite the advantages of chemical looping technology, there still many technical and operational challenges associated with the pressurized operation[17] using the interconnected reactor configuration (*Figure **2-4***a). It is always difficult to precisely circulate a large amount of oxygen carrier material to fulfill energy and mass balance within the closed-loop given that each reactor vessel is pressurized independently. Any instantaneous pressure imbalance between the reactors could cause instabilities in solids circulation, resulting in wears, erosion, and leakages through the sealing devices which impacts negatively on gas purity (due to undesired mixing) and CO_2 capture efficiency. This could also lead to an explosion in situations where highly reactive gases mix. Furthermore, the oxygen carrier is always subjected to high stress when transported in between reactors at high pressure which could lead to a change in morphology and a decrease in lifespan through excessive fragmentation. Aside from the design and operational complexity, the exchange of solids itself brings additional costs arising from the need for separation system such as a cyclone. With the aforementioned challenges, only a few experimental demonstrations of this concept have been recorded [18-21]. Attempts have been made in recent years to address these issues through novel reactor concepts that avoid external solid circulation of which Gas Switching Technology (GST) is one of them [22-24].

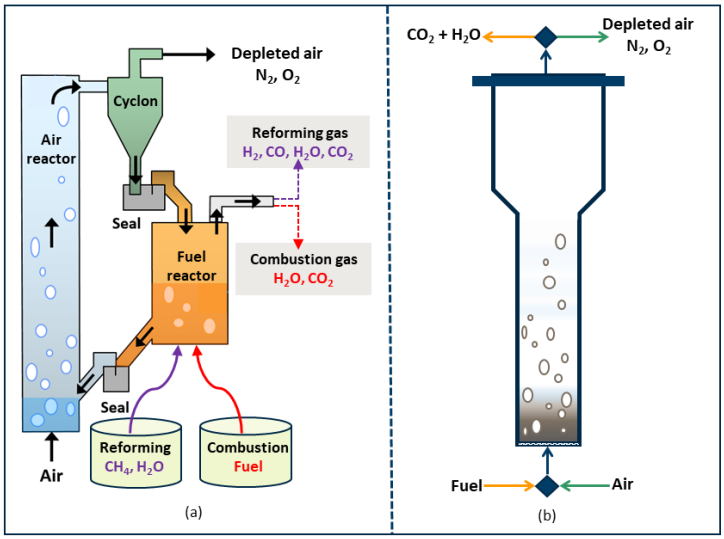

Figure 2-4: Chemical looping and Gas Switching Technology for reforming and combustion applications. (a) represents a scheme of conventional chemical looping reforming and combustion [25] while (b) represents the simplified Gas Switching configuration of Chemical Looping Combustion [26].

2.3 Gas switching technology

Gas Switching Technology (GST) has been proposed as an alternative to the interconnected fluidized bed reactors used in the standard chemical looping processes. Unlike conventional chemical looping, GST utilizes a single fluidized bed reactor where the oxidizing and reducing gases are alternated to achieve a redox reaction avoiding the external circulation of the oxygen carrier (*Figure **2-4***b). With this arrangement, a wide range of inlet flowrates can be accommodated, and load fluctuations would be greatly reduced since the oxygen carrier is confined in one pressurized vessel without external transport. This arrangement also eliminates blower power requirement as the OC is not circulated thereby increasing the process efficiency. The separation systems - cyclones, loop seals, etc are not needed thus avoiding the associated cost, making the process more economical and feasible for commercialization.

Gas Switching Technology (GST) has also been proposed for combustion for power generation [26-30], H_2 production through methane reforming [31-36], and GHG (CO_2 and CH_4) utilization through dry reforming[37]. Process modeling and techno-economic assessment indicate the high competitiveness of this reactor concept in addressing most of the shortcomings of conventional chemical looping including cost reduction [30, 38-41]. In this study, four chemical looping applications (combustion, reforming, water splitting, and partial oxidation of methane) were investigated under gas switching mode as shown in *Figure **2-5***.

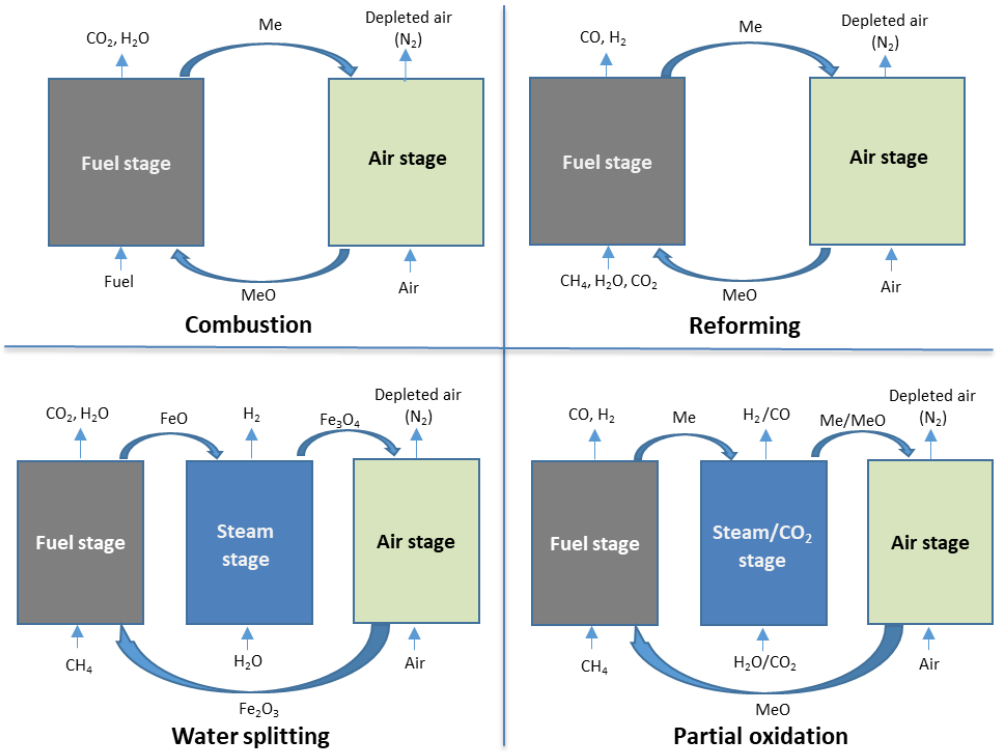

Figure 2-5: The four chemical looping processes under investigation using gas switching technology.

2.3.1 Gas Switching Combustion

Chemical looping is a process where solid or gaseous fuels are combusted using lattice oxygen of metal oxides in a dual (fuel and air reactors) CFB system as illustrated in *Figure **2-6***a. The metal oxide called oxygen carrier (OC) is placed inside the reactor as bed material to provide the oxygen for the reaction in the fuel reactor. Conventionally, the OC is transported between the fuel and the air reactor with the general redox reaction in the fuel and air reactors is presented in (*Reaction **2-1***) and (Reaction **2-2**) respectively [42]. Nitrogen is inherently separated in the air reactor before the combustion in the fuel reactor to produced only of pure stream of CO_2 and H_2O without NOx and other unwanted gases. Thus, this process is highly efficient with a low-energy penalty and eliminates the major cost of CCS as the process produces a pure CO_2 stream ready for utilization and storage [43, 44]. Applying chemical looping combustion to GST as described in section 2.3 is called Gas Switching Combustion (GSC).

GSC Concept has been demonstrated in a single reactor using different oxygens carriers (Ni-based, ilmenite and $CaMnO_{3-\delta}$-based) and fuels, for power generation under atmospheric and pressurized conditions [29, 45, 46] with good performance such as ease of operation and control under pressurized conditions, in addition to sufficiently high CO_2 purity and capture efficiency. GSC-IGCC power plant achieved efficiency as high as 41.9% with 90.5% CO_2 avoidance, relative to 37.7% efficiency, and 87% CO_2 avoidance for an IGCC plant with pre-combustion CO_2 capture and future advanced gas turbine technology. Autothermal operation has also been achieved, using ilmenite and Mn-based oxygen carriers, and CO as fuel without facing major challenges [28]. Although this oxygen carrier has been tested successfully in the standalone reactor, pressurized continuous operation is required to prove the viability of the concept and the feasibility for commercialization.

Fuel stage

$$(2n+m)Me_xO_y + C_nH_{2m} \rightarrow (2n+m)Me_xO_{(y-1)} + nCO_2 + mH_2O \qquad \textit{Reaction 2-1}$$

Air stage

$$Me_xO_{(y-1)} + \alpha Air \rightarrow Me_xO_y + 0.78\alpha N_2 \qquad \textit{Reaction 2-2}$$

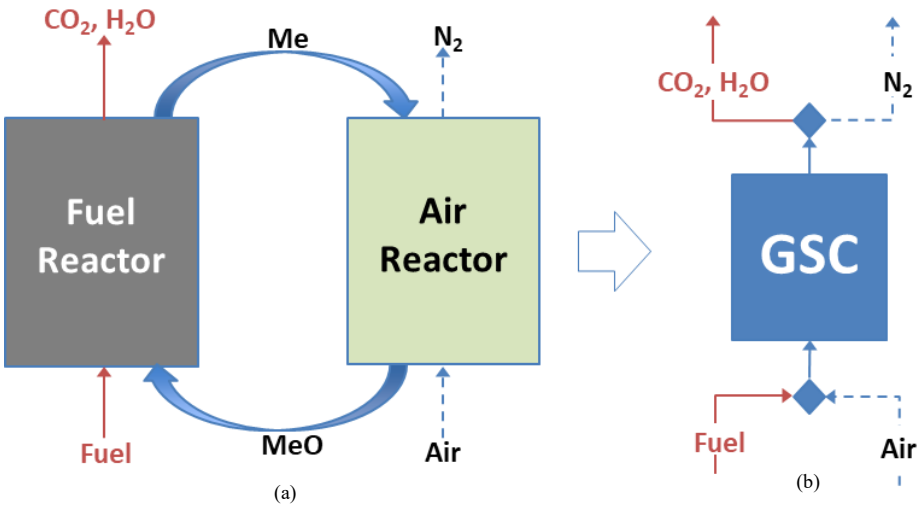

Figure 2-6: Configuration of the (a)convention Chemical Looping Combustion and (b)novel Gas Switching Combustion under investigation in this study.

2.3.2 Gas Switching Reforming

Chemical looping reforming (CLR) is a process for the production of syngas (CO + H_2) with inherent CO_2 capture [47]. In the conventional CLR, the oxygen carrier circulates between two interconnected fluidized-bed reactors (fuel and air reactor) (*Figure* ***2-7***a). The metal oxide acts as both oxygen carrier and catalyst and is first reduced to metallic radical which catalyzes the reforming reaction between CH_4, H_2O, and/or CO_2 to produce syngas. Ni-based metal oxides are commonly used due to their high catalytic activity for methane reforming [48, 49]. The reactions at different CLR stages are given in (*Reaction* ***2-3*** - *Reaction* ***2-7***) [50]. Although reforming reactions in the fuel stage is highly endothermic, CLR process could be integrated to utilize the heat from the exothermic oxidation reaction in the air stage to reduces the energy penalty and achieve autothermal operation[51].

Applying the chemical looping reforming to the GST (single fluidized bed reactor without external solid circulation) as described in section 2.3 is called Gas Switching Reforming (GSR) (*Figure* ***2-7***b). GSR has been experimentally demonstrated using Ni-based catalysts at 1bar[52]. However, there is still a need for further demonstration at pressurized conditions with the possibility of a non-Ni-based oxygen carrier for scale-up and commercialization of this concept.

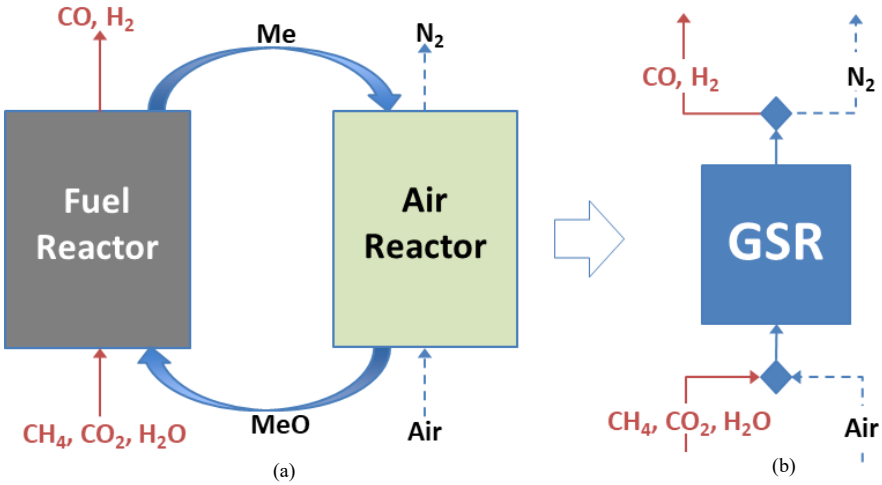

Figure 2-7: Configuration of the convention Chemical Looping Reforming (a) and novel Gas Switching Reforming (b).

Fuel stage

$$CH_4 + MeO \rightarrow 4Me + CO_2 + +H_2O$$ *Reaction 2-3*

$$CH_4 + H_2O \rightarrow CO + 3H_2 \quad (\Delta H_{298K} = +205.9 kJmol^{-1})$$ *Reaction 2-4*

$$CH_4 + CH_2 \rightarrow 2CO + 2H_2 \quad (\Delta H_{298K} = +247.0 kJmol^{-1})$$ *Reaction 2-5*

$$3CH_4 + 2H_2O + CO_2 \rightarrow 4CO + 8H_2 \ (\Delta H_{298K} = 660.9 KJmol^{-1})$$ *Reaction 2-6*

Air stage

$$Me + \alpha Air \rightarrow MeO \ + 0.78\alpha N_2$$ *Reaction 2-7*

2.3.3 Gas Switching Water Splitting

Hydrogen production through water splitting in a chemical looping process (CL-H_2) has been demonstrated as a viable technology [53]. This process produces H_2 through partial oxidation of an oxygen carrier with steam. Subsequently, the oxygen carrier is fully oxidized by air to generate the heat needed to complete the cycle autothermally and reduced by carbon-rich fuel gases with inherent CO_2 capture. Gas Switching Watersplitting (GSWS) is a three-step process utilizing the varying oxidation states of iron to produce H_2 (*Figure **2-8***). In the first stage, Fe_2O_3 is reduced to FeO/Fe by carbon-rich fuel gases with inherent CO_2 capture (*Reaction **2-8***). This is followed by the 2nd stage where FeO/Fe is partially oxidized with steam (slightly exothermic) to produce pure H_2 and Fe_3O_4 (Reaction 2-9). Air is supplied at the 3rd stage to fully oxidize back the oxygen carrier to Fe_2O_3 (Reaction 2-10). The oxygen carrier is then completely oxidized in the third stage to regenerate the oxygen carrier and produce heat for the process. Using the conventional chemical looping approach, this process would be completed in three reactors with the iron-based oxygen carrier circulating between them, a configuration that is indeed difficult to pressurize and scale-up (*Figure **2-8***a). Adapting the process to a single GST reactor (*Figure **2-8***b) that avoids solid circulation provides better utilization of heat of reactions without process integration. A conceptual disadvantage that GSWS has over the three-reactor process, is the mixing of gases when switching from one reaction stage to another, affecting CO_2 capture efficiency, CO_2 purity, and H_2 purity. The extent of the gas mixing depends on the flow rates and volume of the reaction vessel. It is therefore important that the fuel and steam stages are long enough to minimize the extent of the mixing of different gases in the system to achieve an acceptable capture efficiency and product gas purity.

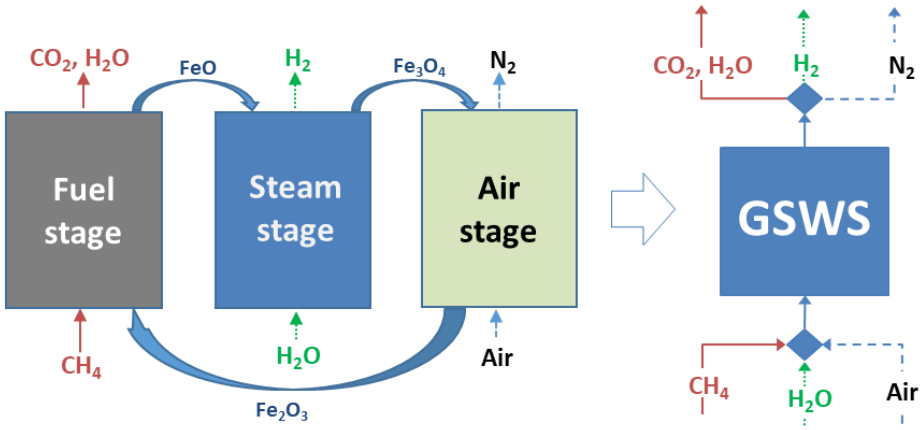

Figure 2-8: (a): Water-splitting process completed following the conventional chemical looping route. (b): Configuration of a simplified Gas Switching Water Splitting, GSWS.

Fuel stage

$$CH_4 + 4Fe_2O_3 \rightarrow CO_2 + 2H_2O + 8FeO$$ *Reaction 2-8*

Steam stage

$$H_2O + 3FeO \rightarrow H_2 + Fe_3O_4$$ *Reaction 2-9*

Air stage

$$2.38Air + 2Fe_3O_4 \rightarrow 3Fe_2O_3 + 1.86N_2$$ *Reaction 2-10*

2.3.4 Gas Switching Partial Oxidation

GSPOX is a three-stage GST process (fuel, steam/CO_2, and air stage) for combined syngas (CO & H_2) and H_2/CO production with integrated CO_2 capture(*Figure* ***2-9***). In the fuel (reduction) stage the oxygen carrier was exposed to CH_4 to produce syngas (CO & H_2), followed by the partial oxidation stage with H_2O/CO_2 to produce H_2 /CO. The reduced oxygen carrier is regenerated by air oxidation. The oxidation stage is also associated with the generation of heat required to sustain the entire redox cycle autothermally. The major reactions of the process are presented (*Reaction* ***2-11*** - *Reaction* 2-14). La-Sr-Fe-perovskite ($La_{0.85}Sr_{0.15}Fe_{0.95}Al_{0.05}O_3$) OC was developed and tested with small-scale setup (at ~10% CH_4 molar concentration under atmospheric conditions) and exhibited excellent performance of about 99% selectivity to syngas production [54]. However, more demonstrations are needed as proof of concept with large-scale setup and high CH_4 concentration and pressure.

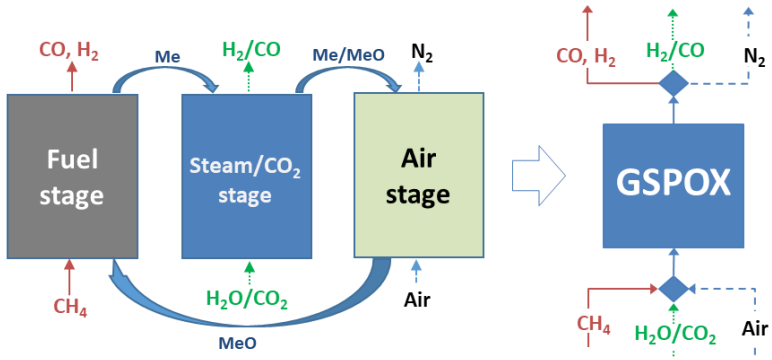

Figure 2-9: Three-stage chemical looping process for combined syngas production with integrated CO_2/steam utilization to produce H_2/CO. (a): Conventional chemical looping arrangement. (b): The simplified Gas Switching Technology under investigation.

Fuel Stage

$$CH_4 + MeO_z \rightarrow CO + 2H_2 + MeO_x \qquad \textit{Reaction 2-11}$$

Steam/CO_2 stage

$$H_2O + MeO_x \rightarrow H_2 + MeO_y \qquad \textit{Reaction 2-12}$$

$$CO_2 + MeO_x \rightarrow CO + MeO_y \qquad \textit{Reaction 2-13}$$

Air Stage

$$MeO_y + \alpha Air \rightarrow MeO_z + 0.78\alpha N_2 \qquad \textit{Reaction 2-14}$$

2.4 Continuous Gas Switching Operation

Following the successful demonstration of the standalone GST processes, a 60KW_{th} pre-pilot cluster of three dynamically identical reactors was designed, developed, and commissioned (*Figure **2-10**a*) to achieve continuous operation of the gas switching technology. Different redox stages are alternated among the three reactors to achieve pseudo-continuous operation (*Figure **2-10**a*). Understanding the interactions between the individual reactors in operation, and implementing the different operational strategies is necessary for commercial deployment of this concept. The setup can withstand up to 1000°C and 20bar. The target is to achieve autothermal operation under combustion (GSC) and reforming modes up to 15bar. Currently, the combustion demonstration using an optimized $CaMnO_{3-\delta}$ based oxygen carrier is ongoing with the preliminary result shown in *Figure **2-11***. It can be seen from the result that over 80% CH_4 conversion was achieved at 800°C at 1bar at the fuel stage indicated in green without carbon deposition and over 97% CO_2 capture efficiency.

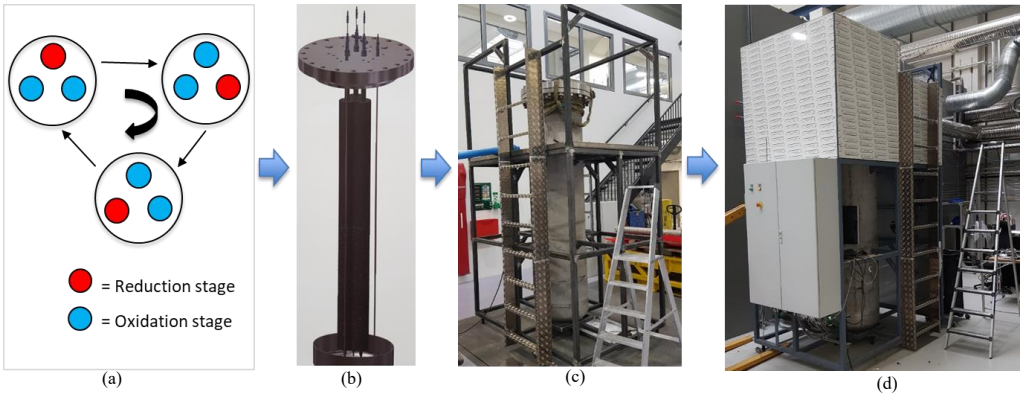

Figure 2-10: The experimental setup of the GST three-reactor cluster designed to achieve continuous operation. (a) the working principle where each circle represents one reactor in different redox stag; (b) the symmetrical arrangement of the three dynamically identical reactor cluster (c)the experimental setup under construction; (d) the commissioned setup.

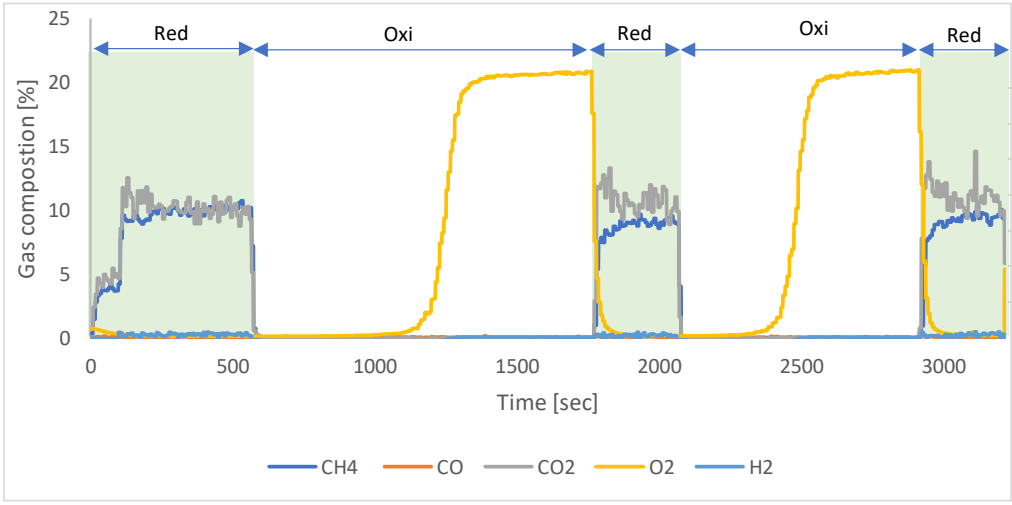

Figure 2-11: Gas composition of Reactor 1 at 800°C and 1bar with the fuel stage indicated as "Red" and the air stage represented as "Oxi". Flowrate at the fuel stage: CH_4 – 5nl/min and N_2 – 15nl/min to the outlet gas stream. Flowrate at the air stage: Air – 30nl/min. NOTE: N_2 composition was not included in the figure accounting for the deficit in gas composition.

Nomenclature

CCS	Carbon Capture and Storage
CCUS	Carbon Capture Storage and Utilization
CFB	Circulating Fluidized Bed
CLC	Chemical Looping Combustion
CLR	Chemical Looping Reforming
CL-H_2	Chemical Looping Hydrogen
CO_2-EOR	CO_2 Enhanced Oil Recovery
GHG	Greenhouse Gas
GSC	Gas Switching Combustion
GSC-IGCC	Gas Switching Combustion Integrated Gasification Combined Cycle
GSPOX	Gas Switching Partial Oxidation
GSR	Gas Switching Reforming
GST	Gas Switching Technology
IEA	International Energy Agency
IGCC	Integrated Gasification Combined Cycle
IPCC	Intergovernmental Panel on Climate Change
Me(MeO)	Metal (Metal Oxide)
NPS	New Policy Scenario
OC	Oxygen Carrier
OXI	Oxidation
POX	Partial Oxidation
RED	Reduction
REF	Reforming
SDS	Sustainable Development Scenario
SPS	Stated Policies Scenario

References

[1] IPCC, *Global Warming of 1.5° C: An IPCC Special Report on t Climate Change.* Intergovernmental Panel on Climate Change, 2018.

[2] IEA, "Global Energy & CO2 Status Report The latest trends in energy and emissions in 2018," 2019. [Online]. Available: https://webstore.iea.org/download/direct/2461?fileName=Global_Energy_and_CO2_Status_Report_2018.pdf

[3] IEA, "World Energy Outlook 2017," 2017. [Online]. Available: https://webstore.iea.org/world-energy-outlook-2017

[4] IEA, "Global Energy Review 2020- The impacts of the Covid-19 crisis on global energy demand and CO2 emissions," 2020. [Online]. Available: https://webstore.iea.org/download/direct/2995?fileName=Global_Energy_Review_2020.pdf

[5] S. Z. Baykara, "Hydrogen: a brief overview on its sources, production and environmental impact," *International Journal of Hydrogen Energy,* vol. 43, no. 23, pp. 10605-10614, 2018.

[6] A. Ersöz *et al.*, "Investigation of a novel & integrated simulation model for hydrogen production from lignocellulosic biomass," *International Journal of Hydrogen Energy,* vol. 43, no. 2, pp. 1081-1093, 2018.

[7] T. Veziroglu, "Ecohealth problems and climate change ii: permanent solution to environmental problems: hydrogen energy system," in *IFSSH World Congress 'Health Challenges of the Third Millenium', Book of Invited Background Papers*, 2005, pp. 21-27.

[8] L. Pérez-Lombard, J. Ortiz, and C. Pout, "A review on buildings energy consumption information," *Energy and buildings,* vol. 40, no. 3, pp. 394-398, 2008.

[9] I. IEA, "International Energy Agency. Key World Energy Statistics," ed, 2015.

[10] G. Peters *et al.*, "Carbon dioxide emissions continue to grow amidst slowly emerging climate policies," *Nature Climate Change,* vol. 10, no. 1, pp. 3-6, 2020.

[11] G. Swanson, "Cost-benefit analysis of Kitima T liquified natural gas project of British Columbia," 2012.

[12] IEA, "World Energy Outlook 2019," 2019. [Online]. Available: https://webstore.iea.org/world-energy-outlook-2019

[13] M. Hurlbert and M. Osazuwa-Peters, "Emerging issues in energy, climate change and sustainability management," *The Central European Review of Economics and Management,* vol. 4, no. 1, pp. 7-12, 2020.

[14] K. W. Bandilla, "Carbon Capture and Storage," in *Future Energy*: Elsevier, 2020, pp. 669-692.

[15] A. Lyngfelt, A. Brink, Ø. Langørgen, T. Mattisson, M. Rydén, and C. Linderholm, "11,000 h of chemical-looping combustion operation—Where are we and where do we want to go?," *International Journal of Greenhouse Gas Control,* vol. 88, pp. 38-56, 2019.

[16] J. Adanez, A. Abad, F. Garcia-Labiano, P. Gayan, and L. F. de Diego, "Progress in Chemical-Looping Combustion and Reforming technologies," *Progress in Energy and Combustion Science,* vol. 38, no. 2, pp. 215-282, Apr 2012, doi: 10.1016/j.pecs.2011.09.001.

[17] H. P. Hamers, M. C. Romano, V. Spallina, P. Chiesa, F. Gallucci, and M. v. S. Annaland, "Comparison on process efficiency for CLC of syngas operated in packed bed and fluidized bed reactors," *International Journal of Greenhouse Gas Control,* vol. 28, no. 0, pp. 65-78, 2014, doi: http://dx.doi.org/10.1016/j.ijggc.2014.06.007.

[18] R. Xiao, L. Chen, C. Saha, S. Zhang, and S. Bhattacharya, "Pressurized chemical-looping combustion of coal using an iron ore as oxygen carrier in a pilot-scale unit," *International Journal of Greenhouse Gas Control,* vol. 10, pp. 363-373, 2012.

[19] L. Chen, Z. Fan, R. Xiao, and K. Liu, "Pressurized Chemical Looping Combustion for Solid Fuel," *Handbook of Chemical Looping Technology,* pp. 123-158, 2018.

[20] S. Zhang, R. Xiao, and W. Zheng, "Comparative study between fluidized-bed and fixed-bed operation modes in pressurized chemical looping combustion of coal," *Applied energy,* vol. 130, pp. 181-189, 2014.

[21] A. Bischi *et al.*, "Design study of a 150 kWth double loop circulating fluidized bed reactor system for chemical looping combustion with focus on industrial applicability and pressurization," *International Journal of Greenhouse Gas Control,* vol. 5, no. 3, pp. 467-474, 2011.

[22] S. Noorman, M. van Sint Annaland, and Kuipers, "Packed Bed Reactor Technology for Chemical-Looping Combustion," *Industrial & Engineering Chemistry Research,* vol. 46, no. 12, pp. 4212-4220, 2007/06/01 2007, doi: 10.1021/ie061178i.

[23] H. P. Hamers, F. Gallucci, P. D. Cobden, E. Kimball, and M. van Sint Annaland, "A novel reactor configuration for packed bed chemical-looping combustion of syngas," *International Journal of Greenhouse Gas Control,* vol. 16, no. 0, pp. 1-12, 2013, doi: http://dx.doi.org/10.1016/j.ijggc.2013.02.021.

[24] A. Zaabout, S. Cloete, and S. Amini, "Hydrodynamic Investigation Into a Novel IC-CLC Reactor Concept For Power Production With Integrated CO2 Capture," in *10th International Conference on Computational Fluid Dynamics In the Oil & Gas, Metallurgical and Process Industries*, Trondheim, Norway, 17-19 June 2014.

[25] N. M. F. Science. "Chemical Looping Combustion." https://mfix.netl.doe.gov/research/chemical-looping-combustion/ (accessed June, 2019).

[26] A. Zaabout, S. Cloete, S. T. Johansen, M. van Sint Annaland, F. Gallucci, and S. Amini, "Experimental Demonstration of a Novel Gas Switching Combustion Reactor for Power Production with Integrated CO2 Capture," *Industrial & Engineering Chemistry Research,* vol. 52, no. 39, pp. 14241-14250, 2013/10/02 2013, doi: 10.1021/ie401810n.

[27] A. Zaabout, S. Cloete, M. van Sint Annaland, F. Gallucci, and S. Amini, "A novel gas switching combustion reactor for power production with integrated CO2 capture: Sensitivity to the fuel and oxygen carrier types," *International Journal of Greenhouse Gas Control,* vol. 39, pp. 185-193, 2015.

[28] A. ZAABOUT, S. CLOETE, and S. AMINI, "Autothermal operation of a pressurized gas switching combustion reactor with a Mn-based oxygen carrier."

[29] A. Zaabout, S. Cloete, S. T. Johansen, M. v. S. Annaland, F. Gallucci, and S. Amini, "Experimental Demonstration of a Novel Gas Switching Combustion Reactor for Power Production with Integrated CO2 Capture," *Industrial & Engineering Chemistry Research,* vol. 52, no. 39, pp. 14241-14250, Oct 2 2013, doi: 10.1021/ie401810n.

[30] S. M. Nazir, S. Cloete, O. Bolland, and S. Amini, "Techno-economic assessment of the novel gas switching reforming (GSR) concept for gas-fired power production with integrated CO2 capture," *International journal of hydrogen energy,* vol. 43, no. 18, pp. 8754-8769, 2018.

[31] S. A. Wassie, F. Gallucci, A. Zaabout, S. Cloete, S. Amini, and M. van Sint Annaland, "Hydrogen production with integrated CO2 capture in a novel gas switching reforming reactor: Proof-of-concept," *International Journal of Hydrogen Energy,* vol. 42, no. 21, pp. 14367-14379, 2017.

[32] S. A. Wassie, F. Gallucci, A. Zaabout, S. Cloete, S. Amini, and M. van Sint Annaland, "Hydrogen production with integrated CO2 capture in a novel gas switching reforming

reactor: Proof-of-concept," *International Journal of Hydrogen Energy,* vol. 42, no. 21, pp. 14367-14379, 5/25/ 2017, doi: https://doi.org/10.1016/j.ijhydene.2017.04.227.

[33] S. A. Wassie *et al.*, "Hydrogen production with integrated CO2 capture in a membrane assisted gas switching reforming reactor: Proof-of-Concept," *International Journal of Hydrogen Energy,* vol. 43, no. 12, pp. 6177-6190, 2018/03/22/ 2018, doi: https://doi.org/10.1016/j.ijhydene.2018.02.040.

[34] S. M. Nazir, J. H. Cloete, S. Cloete, and S. Amini, "Efficient hydrogen production with CO2 capture using gas switching reforming," *Energy,* 2019.

[35] A. Ugwu, A. Zaabout, J. R. Tolchard, P. I. Dahl, and S. Amini, "Gas Switching Reforming for syngas production with iron-based oxygen carrier-the performance under pressurized conditions," *International Journal of Hydrogen Energy,* 2019.

[36] A. Zaabout, P. I. Dahl, A. Ugwu, J. R. Tolchard, S. Cloete, and S. Amini, "Gas Switching Reforming (GSR) for syngas production with integrated CO2 capture using iron-based oxygen carriers," *International Journal of Greenhouse Gas Control,* vol. 81, pp. 170-180, 2019.

[37] A. Ugwu, A. Zaabout, and S. Amini, "An advancement in CO2 utilization through novel gas switching dry reforming," *International Journal of Greenhouse Gas Control,* vol. 90, p. 102791, 2019.

[38] S. Cloete, F. Gallucci, M. van Sint Annaland, and S. Amini, "Gas switching as a practical alternative for scaleup of chemical looping combustion," *Energy Technology,* vol. 4, no. 10, pp. 1286-1298, 2016.

[39] C. A. del Pozo, S. Cloete, J. H. Cloete, Á. J. Álvaro, and S. Amini, "The potential of chemical looping combustion using the gas switching concept to eliminate the energy penalty of CO2 capture," *International Journal of Greenhouse Gas Control,* vol. 83, pp. 265-281, 2019.

[40] S. A. Wassie, S. Cloete, V. Spallina, F. Gallucci, S. Amini, and M. van Sint Annaland, "Techno-economic assessment of membrane-assisted gas switching reforming for pure H2 production with CO2 capture," *International Journal of Greenhouse Gas Control,* vol. 72, pp. 163-174, 2018.

[41] C. A. del Pozo, A. J. Álvaro, J. H. Cloete, S. Cloete, and S. Amini, "Exergy Analysis of Gas Switching Chemical Looping IGCC Plants," *Energies,* vol. 13, no. 3, pp. 1-25, 2020.

[42] T. Mattisson *et al.*, "Chemical-looping technologies using circulating fluidized bed systems: Status of development," *Fuel Processing Technology,* vol. 172, pp. 1-12, 2018.

[43] M. M. Hossain and H. I. de Lasa, "Chemical-looping combustion (CLC) for inherent CO2 separations—a review," *Chemical Engineering Science,* vol. 63, no. 18, pp. 4433-4451, 2008.

[44] A. H. Sahir, J. K. Dansie, A. L. Cadore, and J. S. Lighty, "A comparative process study of chemical-looping combustion (CLC) and chemical-looping with oxygen uncoupling (CLOU) for solid fuels," *International Journal of Greenhouse Gas Control,* vol. 22, pp. 237-243, 2014.

[45] A. Zaabout, S. Cloete, and S. Amini, "Autothermal operation of a pressurized Gas Switching Combustion with ilmenite ore," *International Journal of Greenhouse Gas Control,* vol. 63, pp. 175-183, 2017/08/01/ 2017, doi: https://doi.org/10.1016/j.ijggc.2017.05.018.

[46] A. Zaabout, S. Cloete, J. R. Tolchard, and S. Amini, "A pressurized Gas Switching Combustion reactor: Autothermal operation with a CaMnO3−δ-based oxygen carrier," *Chemical Engineering Research and Design,* vol. 137, pp. 20-32, 2018/09/01/ 2018, doi: https://doi.org/10.1016/j.cherd.2018.06.028.

[47] M. Rydén, A. Lyngfelt, and T. Mattisson, "Chemical-looping combustion and chemical-looping reforming in a circulating fluidized-bed reactor using Ni-based oxygen carriers," *Energy & Fuels,* vol. 22, no. 4, pp. 2585-2597, 2008.

[48] M. Rydén, A. Lyngfelt, and T. Mattisson, "Synthesis gas generation by chemical-looping reforming in a continuously operating laboratory reactor," *Fuel,* vol. 85, no. 12-13, pp. 1631-1641, 2006.

[49] J. Adanez, A. Abad, F. Garcia-Labiano, P. Gayan, and F. Luis, "Progress in chemical-looping combustion and reforming technologies," *Progress in energy and combustion science,* vol. 38, no. 2, pp. 215-282, 2012.

[50] J. Solsvik and H. A. Jakobsen, "Modeling of multicomponent mass diffusion in porous spherical pellets: Application to steam methane reforming and methanol synthesis," *Chemical Engineering Science,* vol. 66, no. 9, pp. 1986-2000, 2011.

[51] M. Ortiz, A. Abad, F. Luis, F. García-Labiano, P. Gayán, and J. Adánez, "Optimization of hydrogen production by chemical-looping auto-thermal reforming working with Ni-based oxygen-carriers," *international journal of hydrogen energy,* vol. 36, no. 16, pp. 9663-9672, 2011.

[52] S. A. Wassie, F. Gallucci, A. Zaabout, S. Cloete, S. Amini, and M. van Sint Annaland, "Hydrogen production with integrated CO 2 capture in a novel gas switching reforming reactor: Proof-of-concept," *International Journal of Hydrogen Energy,* vol. 42, no. 21, pp. 14367-14379, 2017.

[53] D. Sanfilippo, "One-step hydrogen through water splitting with intrinsic CO 2 capture in chemical looping," *Catalysis Today,* vol. 272, pp. 58-68, 2016.

[54] F. Donat, Y. Xu, and C. R. Müller, "Combined Partial Oxidation of Methane to Synthesis Gas and Production of Hydrogen or Carbon Monoxide in a Fluidized Bed using Lattice Oxygen," *Energy Technology,* 2019.

3 Thermodynamics and heat management

3.1 Thermodynamics

A thermodynamic analysis is useful during the planning and the analysis of the GST experimental results. The equilibrium predictions of different possible reaction paths are performed using the non-stoichiometric approach of Gibbs energy function minimization. The equilibrium predictions were compared with experimental results to identify the dominating reaction path at different GSR stages. The equilibrium calculation was implemented using Gibbs reactor of HSC Chemistry by feeding known amounts of the reactants and indicating all the possible products. By minimizing free energy, the equilibrium composition at different temperatures and pressures can be estimated assuming an ideal mixture and the oxygen carrier exist only in the solid phase (activity coefficient of unity - a pure substance in condensed phase). Fuel conversion is an important parameter that determines how much fuel is required across each stage. From the 2nd law of thermodynamics, the expression of the Gibbs free energy at constant temperature and pressure is given as [1].

$$dG|_{T,p} = \sum_{i=1}^{N_{species}} \left[\frac{\partial G}{\partial n_i}\right]_{T,p,n_{j\neq i}} \qquad \textit{Equation 3-1}$$

Assuming ideal gas, for minimum Gibbs free energy, $dG|_{T,p} = 0$ for some n. It is also required that the Hessian matrix ($\partial^2 G/\partial n_i \partial n_j$) is positive. The Gibbs free energy of the reaction is calculated as follows [2]

$$\Delta G_r = \sum G_i(Product) - \sum G_i(reactant) \qquad \textit{Equation 3-2}$$

where $\sum G_i(reactant)$ *is the sum of the Gibbs free energies of the reactants and* $\sum G_i(Product)$ *is the sum of the Gibbs energy of the products.*

The equilibrium constant is calculated as

$$K^0(T) = \exp\left(-\frac{\Delta G_r}{RT}\right) \qquad \textit{Equation 3-3}$$

In terms of the partial pressures and activity coefficient, the equilibrium constant can be expressed as:

$$K^0 = \frac{\prod(\alpha_{\text{product i}})^{s_i}}{\prod(\alpha_{\text{reactant i}})^{s_i}} = \frac{\prod(P_{\text{product i}})^{s_i}}{\prod(P_{\text{reactant i}})^{s_i}} \qquad \textit{Equation 3-4}$$

where α_i is the chemical activity of the compound i, p_i is the partial pressure of the gaseous compound i and s_i the stoichiometric coefficient of the compound i.

3.2 Heat management

Heat management of the GST process is required for the experimental demonstration to ensure minimal energy penalty, achieve autothermal operation, and improve overall process performance. Mass/species and heat balance are computed iteratively by incorporating both thermodynamics and kinetics of the reaction following the algorithm illustrated in *Figure **3-1***. The heat balance expression (*Equation **3-5***) is defined as assuming an isolated system. With this strategy, autothermal operation could be designed where only the heat from the reaction drives the process (no external heat supply) by adjusting various process parameters (such as degree of reduction, temperature, fuel type, etc.) to achieve the same temperature at the start and the end of the cycle.

$$\int_{T_1}^{T_2} n * c_p(T)\, dT \; + \Delta H_r * \xi = 0 \qquad \textit{Equation 3-5}$$

where $\int_{T_1}^{T_2} n * c_p(T)\, dT$ represents the sensible heat while ξ is the reaction extent and ΔH_r the heat of reaction.

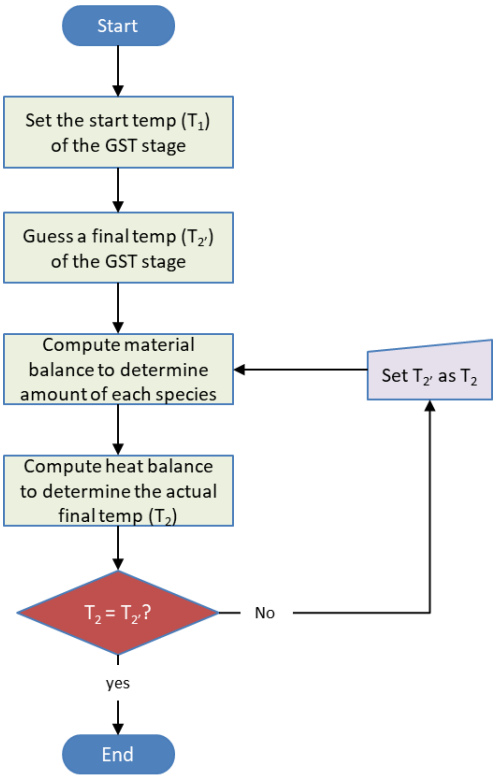

Figure 3-1: GST Heat management algorithm.

3.3 A demonstration of heat management for GSWS

To illustrate the implementation of heat management strategies in gas switching technology, GSWS using Fe_2O_3/Al_2O_3 (35% wt. active content) is used as a case study. As explained in the previous chapter, Gas Switching Watersplitting (GSWS) is a three-step process utilizing the different iron oxide states to produce H_2 with integrated CO_2 capture (*Figure **3-2***). The first procedure is to identify all the possible reactions (*Reaction **3-6*** - *Reaction **3-8***) of each GSWS cycle. Mass/species balance is then computed to determine the actual amount of reaction species considering reaction equilibrium and kinetics. The output of the mass/species balance is utilized in the heat balance (*Equation **3-9*** - *Equation **3-11***) to determine the temperature at the start and end of each stage (temperature profile) as illustrated in *Figure **3-3***.

- T_1 is the temperature at the start of the steam stage
- T_2 is the temperature at the end of the steam stage and the beginning of the air stage
- T_3 is the temperature at the end of the air stage and the beginning at the fuel stage
- T_4 is the temperature at the end of the fuel stage and the beginning of the steam stage

Fuel stage

$$CH_4 + 4Fe_2O_3 \rightarrow CO_2 + 2H_2O + 8FeO \qquad \textit{Reaction 3-6}$$

Steam stage

$$H_2O + 3FeO \rightarrow H_2 + Fe_3O_4 \qquad \textit{Reaction 3-7}$$

Air stage

$$2.38Air + 2Fe_3O_4 \rightarrow 3Fe_2O_3 + 1.86N_2 \qquad \textit{Reaction 3-8}$$

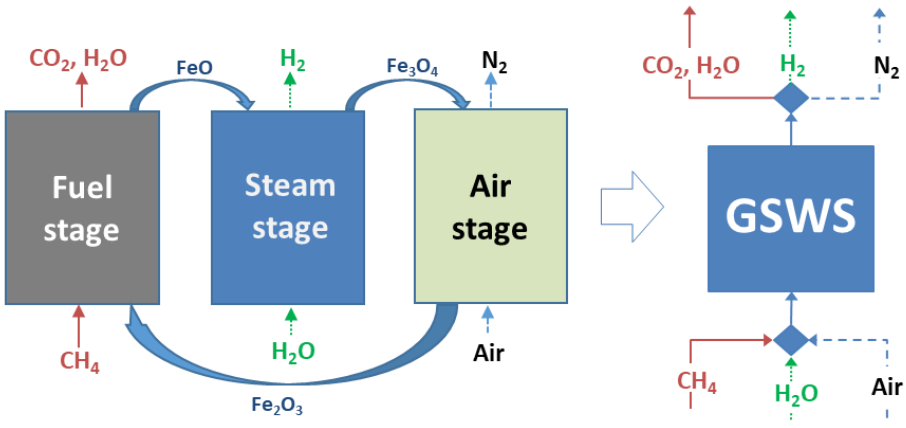

Figure 3-2: (a): Water-splitting process completed following the conventional chemical looping route. (b): Configuration of a simplified Gas Switching Water Splitting, GSWS.

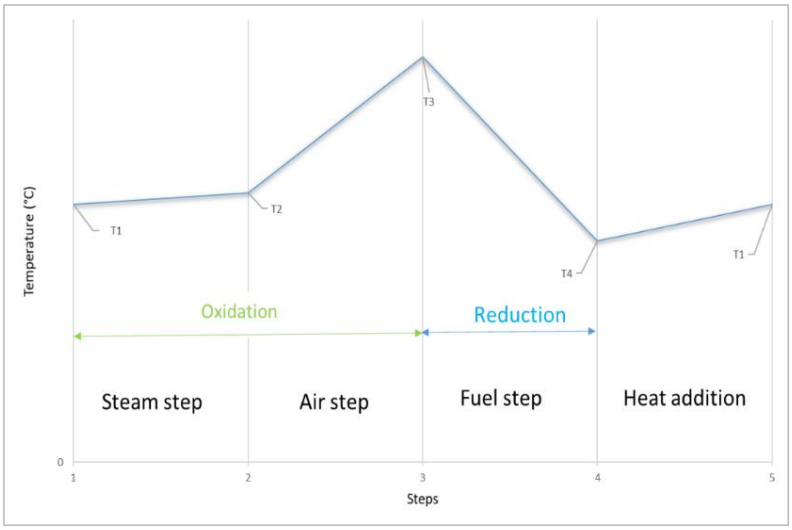

Figure 3-3: A heat management scheme for Gas Switching Water Splitting.

Applying heat balance on the steam stage, a target starts temperature T_1 is fixed and the temperature at the end of the steam stage T_2 was computed. The air stage starts immediately after the steam stage thus it is valid to consider the temperature at the start of the air stage also as T_2 while the temperature at the end of the air stage T_3 is computed. By considering T_3 as the temperature at the start of the fuel stage, the final temperature T_4 at the end of the fuel stage is determined. In the heat management step, autothermal operation could be achieved by applying three heat management strategies of varying the degree of reduction at the fuel stage, the extent of the steam stage, and the use of promoter. Promoters are additional material (usually metal oxides, alloys, etc) add to the oxygen carrier to improve the overall heat capacity.

$$\left\{\begin{array}{c}\int_{T_1}^{T_2} m_{Al_2O_3} Cp_{Al_2O_3}(T)\,dT + \int_{T_1}^{T_2} m_{Fe_3O_4} Cp_{Fe_3O_4}(T)\,dT \\ + \int_{298}^{\frac{T_1+T_2}{2}} m_{H_2} Cp_{H_2}(T)\,dT + \int_{473}^{T_2} m_{steam} Cp_{steam}(T)\,dT = \Delta H^{T}{}_{water\ stage}\end{array}\right\} \qquad \textit{Equation 3-9}$$

$$\left\{\begin{array}{c}\int_{T_2}^{T_3} m_{Al_2O_3} Cp_{Al_2O_3}(T)\,dT + \int_{T_2}^{T_3} m_{Fe_2O_3} Cp_{Fe_2O_3}(T)\,dT \\ + \int_{298}^{\frac{T_2+T_3}{2}} m_{Air} Cp_{air}(T)\,dT = \Delta H^{T}{}_{Air\ stage}\end{array}\right\} \qquad \textit{Equation 3-10}$$

$$\left\{\begin{array}{c}\int_{T_3}^{T_4} m_{Al_2O_3} Cp_{Al_2O_3}(T)\,dT + \int_{T_3}^{T_4} m_{FeO} Cp_{FeO}(T)\,dT + \int_{T_3}^{T_4} m_{CO_2} Cp_{CO_2}(T)\,dT \\ + \int_{T_3}^{T_4} m_{H_2O} Cp_{H_2O}(T)\,dT + \int_{298}^{\frac{T_4+T_3}{2}} m_{CH_4} Cp_{CH_4}(T)\,dT = \Delta H^{T}{}_{Fuel\ stage}\end{array}\right\} \qquad \textit{Equation 3-11}$$

3.3.1 Illustrations and discussion

Figure 3-4a presents the temperature profiles achieved through the proposed heat management strategy for different active content of the oxygen carrier. It is observed that as the active content increases, the temperature at end of the steam and the air stages increases but active content has an opposite effect in the temperature at the fuel (endothermic) stage. However, the temperature at the end of the fuel stage decreases more below the start target temperature. This behavior is due to the combined effect of change in heat of reaction and the heat capacity imposed with the change in the active content. Higher active content implies lower heat capacity due to the reduced proportion of Al_2O_3 but high reaction heat due to the increase of iron content. From

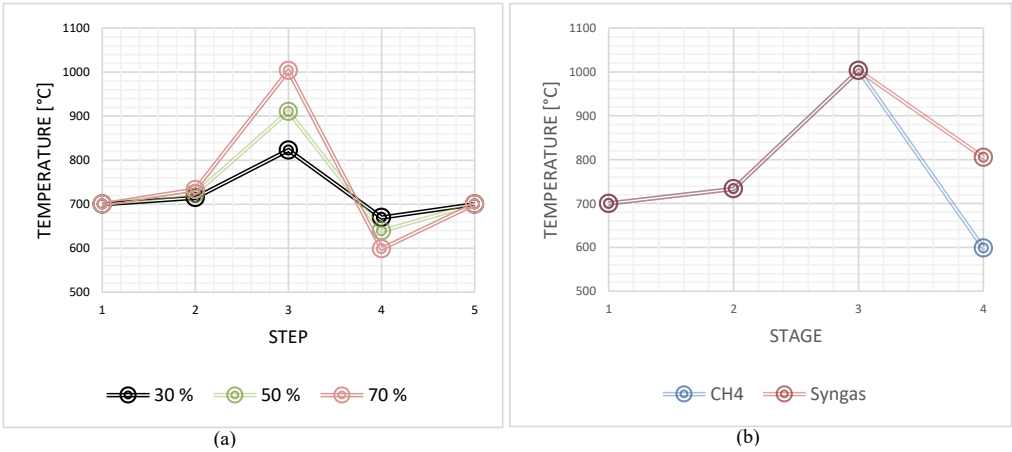

(a) (b)

Figure 3-4: The effect of iron loading on temperature, CH_4 as fuel; and (b): the effect of fuel type for target temperature of 700°C and 70% active content. In general, 80% degree of reduction to FeO was assumed at atmospheric conditions.

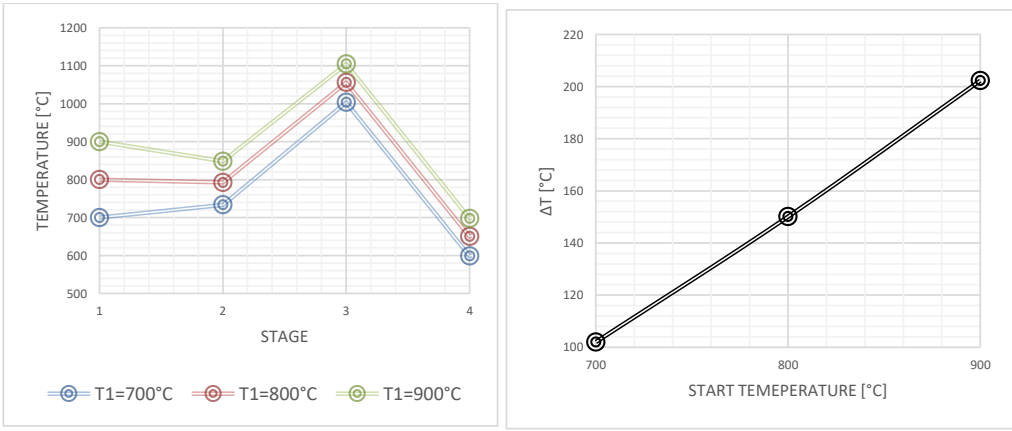

(a) (b)

Figure 3-5: The effect of the target temperature using CH_4 with 70% active content, 80% degree of reduction to FeO at atmospheric conditions.

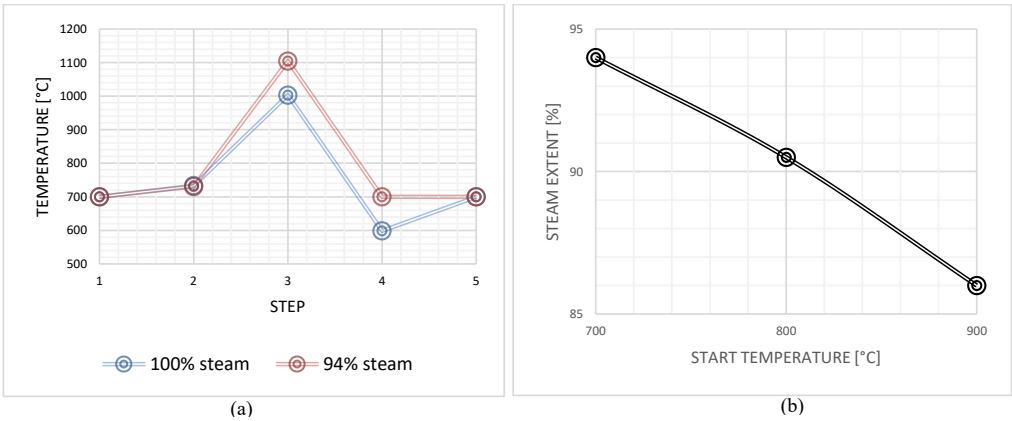

(a) (b)

Figure 3-6: (a): The effect of steam extent for GSWS with CH_4 using Oxygen carrier of 70% active content at 1bar and T1=700C; (b): The effect of starting temperature team extent required to achieve autothemal GSWS operation with CH_4 using Oxygen carrier of 70% active content for different target start temperatures.

material balance, increasing the active content of the oxygen carrier creates room for longer GSWS stages, reduces the effect of gas mixing, and improves CO_2 capture efficiency and H_2 purity. The effect of fuel type could also be studied using the heat management strategy. as illustrated in *Figure **3-4**b* illustrates such a scenario using CH_4 and syngas of H_2/CO molar ratio 1 as fuel types with oxygen carrier of 70% active content at 700°C target temperature at 1bar. The temperature profile shows that the sensitivity of fuel type is more significant in the fuel stage with less drop in temperature achieve with syngas. The effect of the target temperature on the heat behavior of the GSWS process has been investigated using the reference case of 70% active content at atmospheric pressure using CH_4 as fuel (*Figure **3-5***). It can be shown that the higher the target start temperature, the more the temperature decreases at the end of the fuel stage. This could be explained from thermodynamics, as an increase in temperature leads to higher CH_4 conversion and more endothermicity of the *Reaction **3-6***.

*Figure **3-6*** illustrates how the extent of the steam stage could be used to manage the process heat to achieve autothermal operation. As evident from *Figure **3-6***, with less extent of partial oxidation with steam at the stage, less FeO would be partially (*Reaction **3-7***), thus creating more sites for the more exothermic oxidation by air to start the fuel stage at a higher temperature. Through the heat management strategy, the percentage steam extent required to achieve autothermal operation at different starting temperatures is presented in *Figure **3-6***b.

Nomenclature

Abbreviations

GST	Gas Switching Technology
GSWS	Gas Switching Water Splitting

Symbols

α_i	The chemical activity of the compound i
c_p	Heat capacity
ξ	Reaction extent
G	Gibbs free energy
ΔG_r	Change in Gibbs free energy of the reaction
ΔH_r	Heat of reaction
K^0	Equilibrium constant
m	mass
n	mole
p_i	The partial pressure of gaseous compound i
R	The universal gas constant
s_i	The stoichiometric coefficient of the compound i
T	Temperature

Subscripts

i	Species i (compound)
r	Reaction
n_i	Constant species i concentration
p	Constant pressure
T	Constant temperature

Superscripts

$N_{species}$	Number of species

References

[1] J. Solsvik, T. Haug-Warberg, and H. A. Jakobsen, "Implementation of chemical reaction equilibrium by Gibbs and Helmholtz energies in tubular reactor models: application to the steam–methane reforming process," *Chemical Engineering Science,* vol. 140, pp. 261-278, 2016.

[2] I. Barin and G. Platzki, *Thermochemical data of pure substances* (no. 334). Wiley Online Library, 1989.

4 Gas Switching Reforming (GSR) for Syngas Production with Integrated CO_2 Capture Using Iron-Based Oxygen Carriers

This chapter has been adapted from **Article I**

Zaabout, A., PI. Dahl, A. Ugwu, JR. Tolchard, S. Cloete and S. Amini, *Gas Switching Reforming (GSR) for syngas production with integrated CO_2 capture using iron-based oxygen carriers*. International Journal of Greenhouse Gas Control, 2019. 81: p. 170-180.

Abstract

The process behavior of a Gas Switching Reforming (GSR) reactor was studied using three different iron-based oxygen carrier materials: Iron-oxide on Alumina, Iron-Nickel oxide on Alumina and Iron-Ceria on Alumina. It was observed that, for all oxygen carriers, the fuel stage reaction occurs in two distinct sub-stages when feeding methane and steam to a bed of oxidized material, with methane combustion dominating the first and methane reforming dominating the second. This reflects a change in the catalytic activity of the oxygen carrier as it is reduced. The alumina support was observed to play a significant role in the reactions occurring, with the redox-active phases being hematite-structured Fe_2O_3 (oxidized form) and spinel-structured $(FeNiAl)_3O_4$ (reduced form).

The Nickel-containing oxygen carrier outperformed the others in the reforming sub-stage, showing 40% improved methane conversion. The feed of dry methane only during the reforming sub-stage was found to improve methane conversion to syngas in the subsequent reforming sub-stage from 75% to 80% at 800 °C. Results also show that methane conversion improves with the increase in operating temperature and steam/carbon ratio. Autothermal operation of the reactor was also achieved with repeatable performance over several redox cycles. The study therefore successfully demonstrated autothermal N_2-free syngas production with integrated CO_2 capture from the fuel combustion required to supply heat to the endothermic reforming reactions.

4.1 Introduction

According to the latest IPCC report [1], Carbon capture, utilization and storage, CCUS, will play a major role in cost-effective mitigation of climate change caused by anthropogenic CO_2 emissions while meeting the growing global energy demand. Tremendous research efforts have been deployed to applying CCUS to a wide spectrum of industrial applications covering power production [2-4] and CO_2 intensive industries [4-6].

CCUS can have a major impact on the decarbonization of fossil fuel in the form of clean hydrogen production. Natural gas reforming remains the main source for hydrogen [7, 8], but the reforming process involves large CO_2 emissions due to the heat requirement for the highly endothermic methane reforming reaction, being supplied by fossil fuel combustion. The development of environmentally-friendly and cost-effective hydrogen production technologies from natural gas is, therefore, the key to fulfill the expected increasing demand for hydrogen while avoiding the potentially catastrophic consequences of self-strengthening global warming.

Chemical looping reforming (CLR) has emerged as a promising technology with minimal energy penalty for CO_2 capture from natural gas reforming [9, 10]. It is based on the so-called chemical looping combustion technology, CLC, where the difference is the final product being syngas (CO and H_2) for CLR, instead of heat in the case of CLC [9, 10]. The conventional CLR reactor configuration uses two interconnected fluidized bed reactors, namely the air and fuel reactors, where the oxygen carrier circulates between them transferring oxygen from air to the fuel, thereby avoiding any N_2 dilution of the produced syngas [11] (Figure 4-1 shows a simplified scheme of the working principle of the CLR process). The heat from the highly exothermic oxidation reaction that takes place in the air reactor is transported by the oxygen carrier to the fuel reactor to be used mainly by the endothermic reforming reaction. Two main CLR based processes have been investigated in the literature, with the difference being the fuel reactor configuration: i) sCLR process where conventional steam methane reforming takes place in a tubular reactor filled with nickel, inserted in the fuel reactor of a CLC used for providing heat [9], and ii) autothermal CLR (referred to as aCLR) where the oxygen carrier plays the role of a catalyst for methane reforming [10, 12] and reduction and reforming takes place in the same reactor. aCLR (it will be referred to as CLR in the rest of the manuscript) has received the greatest attention due to the better heat integration and process simplification ensured by avoiding the presence of reformer tubes in the fuel reactor [10-12]. This process has also been extended to steam-CLR process for combined syngas and hydrogen production; CH_4

converts to syngas through a gas-solid while pure hydrogen is produced by the steam feed for oxidizing the oxygen carrier [13] .

CLR in the interconnected reactors configuration was successfully demonstrated in lab [9, 10, 14] and pilot scale [11] under atmospheric conditions. To the best of authors' knowledge, no pressurized CLR studies were completed in this configuration to date, despite the predicted benefits of such a technology; a thermodynamic assessment has indeed shown that a 5% increase in energy efficiency could be achieved if CLR is operated under pressurized conditions, mainly gained from the energy saving made in H_2 compression [15]. Scale-up and operation of interconnected pressurized circulating fluidized bed reactors will be challenging. Tightly controlled solids circulation between the two interconnected reactors is critical to fulfill the heat and mass balance of the chemical looping process, but the solids circulation rate is highly dependent on the hydrodynamics in both reactors, presenting an important challenge when scaling up to larger reactor sizes and higher pressures. In addition, each component (reactors, cyclones and loop seals) should be pressurized separately in its own pressure vessel. This will increase cost and complexity and could lead to instantaneous pressure imbalances between the reactors that induce instabilities in solids circulation that could result in large leakages through the sealing devices and upset the reactor mass and energy balances.

This need has prompted research into novel reactor concepts with the ability to operate under pressurized conditions. Alternative reactor configurations proposed in the literature include moving bed [16], internally circulating bed [17], packed bed [18] and gas switching technology [19, 20] (GST). The latter uses a cluster of reactors operating under bubbling/turbulent fluidization where oxidizing and reducing feed gases are alternated to each single reactor in the cluster [21] (*Figure **4-1*** shows the working principle of GST applied to methane reforming). External solids circulation is therefore avoided, thereby greatly simplifying the reactor design and enabling operation under pressurized conditions [22, 23]. GST is based on mature dense fluidized bed technology that is easy to operate and scale-up. It has first been applied to combustion where several oxygen carriers have been tested and shown successful autothermal operation of the concept [21, 23]. It was also successfully extended to methane reforming, through a concept called gas switching reforming (GSR), using a Ni-based oxygen carrier [20] that has good reactive characteristics both in oxidation with air and reduction with methane, in addition to good catalytic activity for methane reforming.

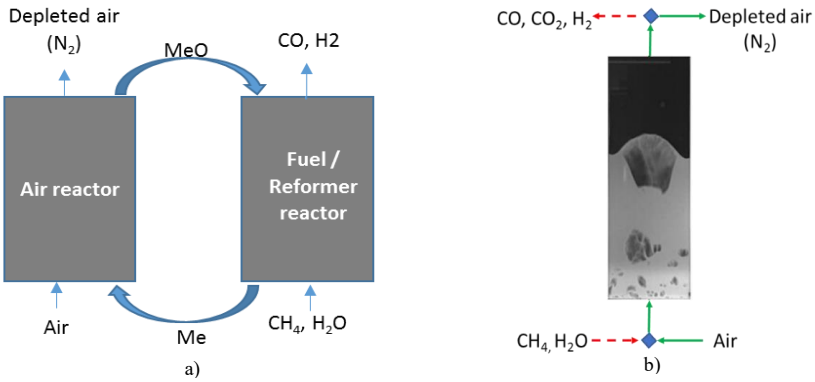

Figure 4-1: Autothermal chemical looping reforming for syngas production with integrated CO_2 capture: a) simplified scheme of CLR process and b) the working principle of the Gas Switching reforming under investigation in this paper

4.2 Oxygen carriers for CLR

Active research activities are ongoing for the development of suitable oxygen carriers for chemical looping reforming. The most successful oxygen carriers to date are Ni-based oxygen carriers, given the high catalytic activity of nickel for methane reforming. Successful experimental operation of the CLR process with Ni-based oxygen carriers covers lab [10, 14] and pilot-scale [11] studies in interconnected fluidized bed reactors, packed bed reactor [18], and GSR configuration under investigation in this study [20]. These oxygen carriers performed well under CLR conditions in atmospheric and pressurized operation (the pressurized study was however completed in a small dense fluidized bed reactor under batch conditions [12]) and have shown high selectivity to CO and H_2.

Attempts have however been made in developing oxygen carriers other than nickel to find cheaper and environmentally sound oxygen carriers with high reactivity and selectivity towards syngas. Fe-, Mn- and Cu-based oxygen carriers were tested in a TGA under CLR conditions but resulted in high methane slippage and low selectivity to syngas [24]. $Fe_2O_3/MgAl_2O_4$ oxygen carriers tested in a gram scale fixed bed reactor have shown good reactivity with methane towards CO_2 and H_2O at the beginning of the reduction stage, but the selectivity shifted to H_2 and CO with advanced reduction level of the oxygen carrier [25]. Authors speculated that the first phase is controlled by combustion where Fe_2O_3 is reduced to Fe_3O_4, before the second period with the selectivity to H_2 and CO begins. In this latter study, the addition of 1 wt.% NiO improved both CH_4 reactivity and selectivity to H_2 and CO. Similar behavior was reported for Fe_2O_3/Al_2O_3 oxygen carriers. Perovskite Fe-based oxygen carriers were tested and have been

shown to be suitable for chemical looping reforming, achieving very high selectivity to H_2 and CO [25]. Several studies have looked at Ce-Fe solid oxides-based oxygen carriers. Oxygen mobility was intensified in these oxygen carriers by the Ce−Fe chemical interaction via the formation of $CeFeO_3$, thereby greatly enhancing their reducibility by CH_4 and syngas selectivity [26, 27]. CeO_2 was also tested under CLR conditions but performed better when doped with Fe [28]. $LaFeO_3$ oxygen carrier performance increased by ~80% when 10% CeO_2 was used as a support and also showed high stability oven the consecutive CLR cycles. The excellent performance was attributed to the formation of Ce^{3+} and Fe^{2+} that maximizes vacant sites for oxygen storage, which also provided good resistance to carbon deposition [29].

To conclude, Fe-based oxygen carriers seem to be promising candidates for the CLR application and have shown good methane conversion and high selectivity to syngas. On this basis, the present study investigates the behavior of the GSR concept with iron-based oxygen carriers. Three Fe_2O_3-based oxygen carriers were prepared by impregnation on Al_2O_3 commercial support and tested in a lab-scale reactor under fluidized bed conditions relevant to the GSR concept. Promising performance has been achieved as it will be shown in the results section. In addition to the introduction and conclusion sections, this paper has two other main sections: i) experimental set-up and GSR operation; ii) results and discussion.

4.3 Experimental setup and operation

4.3.1 Experimental setup

The experimental setup used in this study (*Figure **4-2***) consists of a cylindrical reactor column of, 5 cm in diameter and 50 cm in height. The reactor was also equipped with a freeboard region, that has an expanding conic zone (from 5 cm in the lower end diameter to 10 cm in the top end), followed by a cylindrical part. The total height of the freeboard zone is 40 cm. A porous plate with 20 µm mean pore diameter and 3 mm thickness was used as a gas distributor placed at the bottom of the reactor. Both the reactor body and distributor were made of Inconel 600 to withstand the harsh conditions of high-temperature gas-solids reactive flows (up to 1000 °C). An external electrical heater surrounding the reactor was used to heat up the reactor to the targeted operating temperature. The system heater and reactor were insulated using 25 cm thickness insulation, combining blankets and vermiculate. The hot gases exiting the reactor were cooled down before being sent to the vent, using a heat exchanger installed at the reactor outlet.

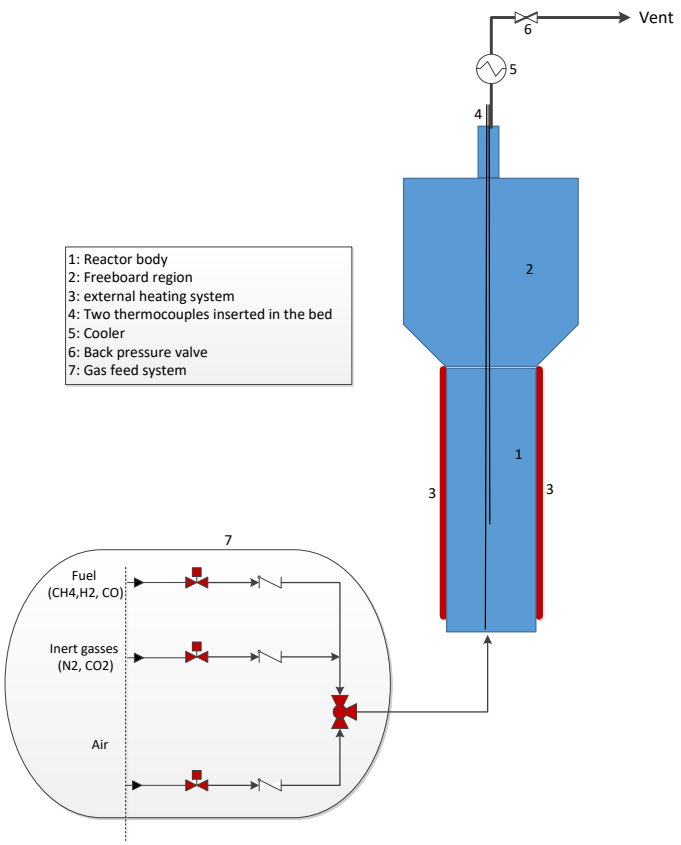

Figure 4-2: A simple sketch of the experimental setup.

Mass flow controllers from Bronkhorst BV were used for feeding the different gases to the reactor. A three-way valve was used to alternate reducing and oxidizing conditions in the reactor. Dry gases were sampled just after the heat exchanger and analyzed with an *ETG MCA 100 Syn* analyzer, to measure the gas composition. The temperature was measured in two positions in the reactor; at 2 and 20 cm above the gas distributor using two thermocouples inserted from the top. A differential pressure sensor was continuously monitoring the pressure difference between the inlet and outlet of the reactor to detect any solid particles loss from the reactor. A steam generator with a high precision water pump was used for controlled steam feed to the reactor. All the measurement instruments and flow controlling devices were controlled through a Labview application. The Labview application was also used for the logging of data.

4.3.2 Oxygen carrier

Spherical gamma-alumina particles from Sasol (Puralox SCCa 150/200) were applied for wet impregnation of concentrated aqueous ammonium iron(I) citrate solution (~50 g/100 g water) aiming to form nanostructured iron oxide inside the mesoporous alumina structure after heat treatment. The iron precursor was partly substituted by nickel(II) nitrate hexahydrate and cerium(III) nitrate hexahydrate to form iron oxide-nickel oxide and iron oxide-cerium oxide composite structures. Homogenous distribution of the active metal oxides throughout the porous particles was obtained by wet impregnation with subsequent drying steps at 120°C after each step up to a theoretical loading of ~10 wt% metal oxide, followed by heat treatment for 5 hours at 500°C (60°C/hour) in ambient air. This procedure was repeated until a theoretical loading of the active elements (Fe, Ni and Ce) was 1:1 by weight compared to Al in the porous alumina structure. The theoretical Fe:Ni and Fe:Ce ratios were 2:1 by weight. After the final impregnation and heat treatment steps, the as produced particles were sieved (100 µm) to remove fines prior to further analysis and testing. Particle size distributions before and after sieving, as measured by light diffraction are presented in *Figure **4-3***.

SEM/EDS analysis on particles after sieving indicated homogenous distribution of the Fe, Ni and Ce throughout the porous alumina structure, as seen in *Figure **4-4***. The measured loading of active elements were slightly lower than aimed for (Fe+Ni+Ce : Al ≈ 0.8 : 1 by weight). This reflects the loss of active material by sieving, in form of fines which are loosely deposited on the surface of the particles. The Fe:Ni and Fe:Ce ratios were found to be ~2:1, as anticipated.

The BET surface areas of the produced Fe-Al_2O_3, Fe-Ni-Al_2O_3 and Fe-Ce-Al_2O_3 impregnated particles were measured to 102.9, 97.2 and 80.9 m^2/g, respectively. In comparison, the bare alumina support particles had a BET surface area of 206.0 m^2/g.

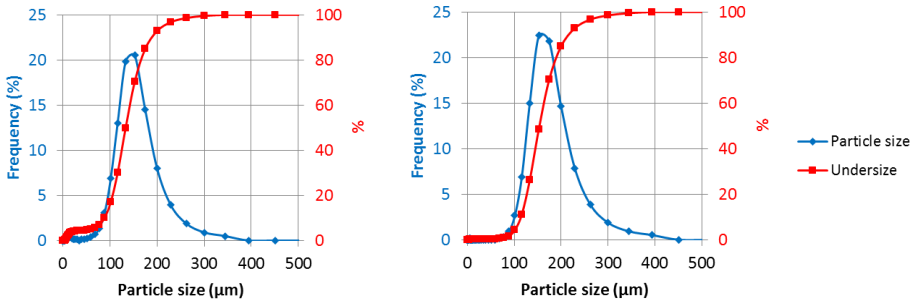

Figure 4-3 Particle size distribution of impregnated supports before (a) and after (b) sieving to remove fines.

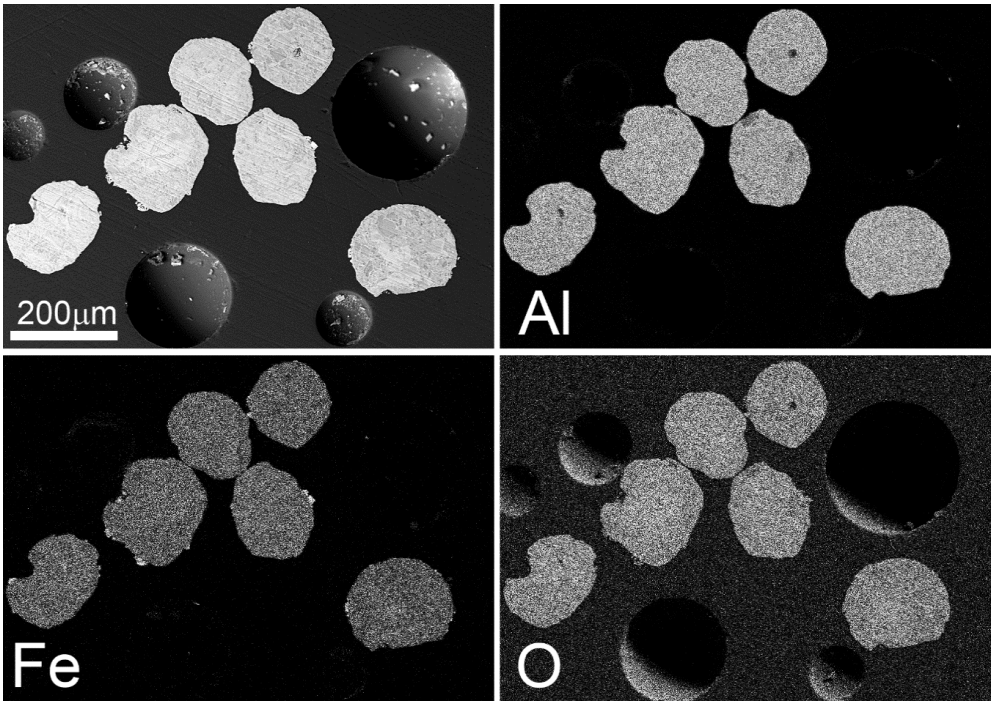

Figure 4-4 SEM/EDS mapping analysis of impregnated alumina particles. The Backscattered electron image is shown in the top left, with corresponding Al, Fe and O maps.

4.4 Reactor operation and performance under the GSR mode

The GSR concept operates in a cyclic mode by alternating air and fuel feeds to the reactor. In GSR autothermal operation, the reactor is first heated up externally to the target temperature before starting gas the switching mode. The heaters are then switched off to complete the autothermal cycling operation, starting with the fuel stage where gaseous fuel is fed for a fixed amount of time called the "fuel time". This stage combines both oxygen carrier reduction and methane reforming to syngas. A feed of air follows to oxidize back the reduced oxygen carrier following an exothermic reaction that builds up heat in the reactor. The generated heat is then being used in the subsequent fuel stage with mainly endothermic reactions (reduction and reforming). Five seconds purging with inert gas is applied between the air and fuel stages to avoid direct contact between them in the feed pipes, thereby eliminating the risk of explosion. The GSR reactor performance was quantified based on CH_4 conversion and selectivity to H_2

and CO calculated following *Equation **4-1**, Equation **4-2***, and *Equation **4-3*** respectively (FCH_4, FH_2 and FCO are the molar flow rates of these species).

300 ml of the oxygen carrier was placed initially in the reactor. In the base case GSR cycle completed in this study, the air was fed at a flow rate of 10 Nl/min while CH_4 was fed at 0.8 Nl/min. Experiments for each operating condition were completed for at least four redox cycles to ensure repeatability. Gas composition at the reactor outlet and reactor temperature was collected continuously and were used to evaluate the GSR performance.

CH_4 Conversion

$$\gamma_{CH_4} = \frac{FCH_{4,in} - FCH_{4,out}}{FCH_{4,in}} \qquad \textit{Equation 4-1}$$

H_2 Selectivity

$$S_{H_2} = \frac{FH_{2,out}}{\gamma_{CH_4} * 3FCH_{4,in}} \qquad \textit{Equation 4-2}$$

CO Selectivity

$$S_{CO} = \frac{FCO_{out}}{\gamma_{CH_4} * FCH_{4,in}} \qquad \textit{Equation 4-3}$$

To operate the system autothermally, it is important to design the length of the stages to meet the heat balance between the different stages, in a way that the temperature in the reactor is cycling around the initial target operating temperature. This is illustrated in *Figure **4-5*** showing a typical GSR reactor temperature behavior under autothermal operation over six GSR cycles (the autothermal behavior is further discussed in *section **4.7***). It could be seen that the temperature in the bed begins at 850 °C at the start of the reduction stage and slightly increases across the stage due to the slightly exothermic reduction between CO and the oxygen carrier. The temperature drops sharply in the reforming stage, due to the endothermic reaction, to end at 810 °C. The exothermic oxidation reaction brings the temperature back to ~855 °C to start a new cycle. 30-50 °C temperature difference was found between the two thermocouples placed at 2 and 20 cm, a result that could be a sign of a low axial mixing in the bed; the fastest response to nature of the reactions in place (endothermic/exothermic) is better seen on the thermocouple at the bottom of the reactor where the reactions mainly take place.

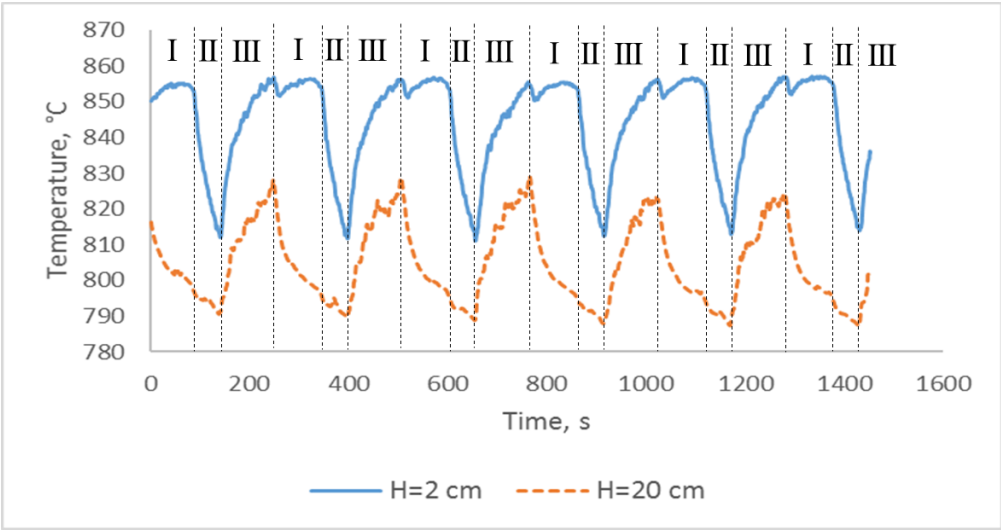

Figure 4-5: A typical transient temperature behavior in two locations in the bed over six cycles of the GSR concept. Target operation temperature was 850 °C. CO was fed in the first 90 s of the fuel stage at 9.6 Nl/min, then followed by CH_4 (2.4 Nl/min) and steam (3.6 g/min). Pure air was fed in the oxidation stage at 15 Nl/min. The GSR stages reduction, reforming and oxidation are numbered respectively I, II and III.

4.5 Results

This section is organized as follows: the GSR behavior with the different iron-based oxygen carriers synthesized in the study is first shown. Afterward, the GSR performance sensitivity to i) steam addition in the reduction stage, ii) the operating temperature, and iii) the steam per methane ratio, referred to as S/C. It should be noted that these experiments were completed with partial heat assistance, using the external heater, to compensate for the large heat losses taking place in the lab-scale reactor over the range of investigated temperatures. This allowed exploring the GSR cycle behavior, with iron-based oxygen carriers, as it would happen in real industrial scale where heat losses will be minimal. Autothermal operation was completed lastly in optimal GSR conditions designed based on the outcome of the sensitivity study completed with external heat assistance.

4.5.1 GSR behaviour with iron-based oxygen carriers

A volume of 300 ml from each oxygen carrier was placed in the reactor where GSR tests were completed on each of them using the same feed conditions at a target temperature of 800 °C and atmospheric pressure. CH_4 and steam were fed in the fuel stage at an S/C=2 (0.8 Nl/min CH_4 and 1.2 g/min water) for 12 min, while pure air was fed in the oxidation stage, at 10 Nl/min,

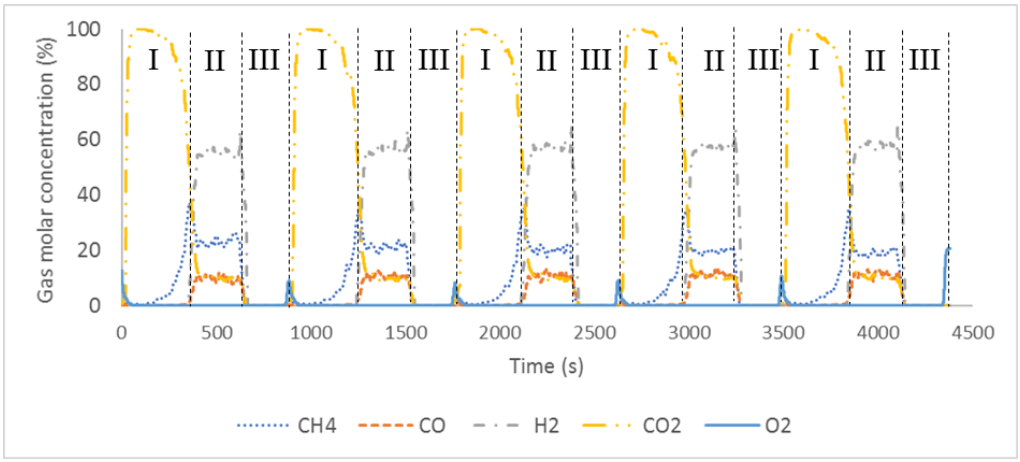

Figure 4-6: Transient gas composition at the reactor outlet for five GSR cycles. Atmospheric pressure operation at 800 °C. The GSR stages reduction, reforming and oxidation are numbered respectively I, II and III.

for 3 min and 40 s (the oxygen carrier is brought back to almost full oxidation as can be seen on *Figure **4-6*** showing a sharp increase of concentration O_2 in the outlet gas stream, just at the end of the oxidation stage).

The transient behaviour of the Fe-Al_2O_3 oxygen carrier over five GSR cycles is shown in *Figure **4-6***. High conversion of CH_4 to CO_2 was achieved in the first half of the fuel stage, but decreases in the second half, showing high selectivity to syngas. Full conversion of oxygen was achieved over the entire oxidation stage, where oxygen comes out sharply only at the end of the oxidation stage. No carbon deposition was observed, as any deposited carbon would have been released in form of CO/CO_2 after being oxidized by the oxygen in the oxidation stage. This GSR cycle behaviour was very repeatable over the cycles as can be seen on *Figure **4-6***.

The Fe-Ce-Al_2O_3 and Fe-Ni-Al_2O_3 have shown similar cycling behaviour as the Fe-Al_2O_3. *Figure **4-7*** compares the achieved CH_4 conversion and selectivity to H_2 and CO for the three oxygen carriers. As found for the Fe-Al_2O_3, two distinct phases could also be identified for Fe-Ce-Al_2O_3 and Fe-Ni-Al_2O_3: complete conversion of methane to CO_2 is achieved in the first phase, while it drops to lower values in the second phase with high selectivity to syngas.

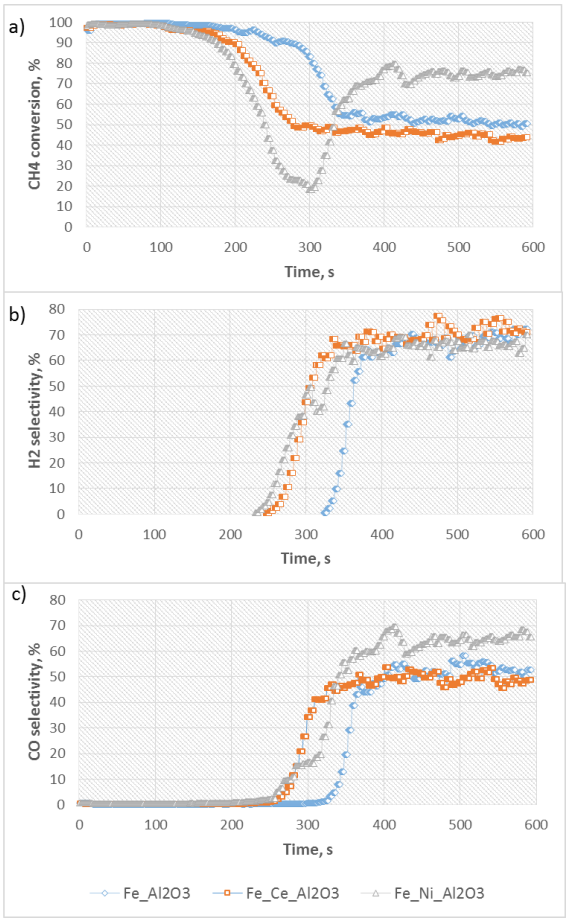

Figure 4-7: Transient GSR performance in the fuel stage with Fe-Al_2O_3, Fe-Ce-Al_2O_3 and Fe-Ni-Al_2O_3 oxygen carriers.

Methane conversion plots (*Figure **4-7**.a*) shows the transition between the two phases to occur similarly for the Fe-Al_2O_3 and Fe-Ce-Al_2O_3 oxygen carriers, although it begins earlier for the latter (this is due to the significant reduction in the oxygen-carrying capacity in the Fe-Ce-Al_2O_3 as CeO_2 did not contribute to the oxygen supply as shown by XRD analysis *Figure **4-9**.a)) . This transition manifests by a drop in CH_4 conversion, but it continues in the combustion mode, where CH_4 converts to CO_2 and H_2O. Reforming of methane to syngas was found to occur only when methane conversion flattens out after the transition to show the very distinct phase 2. Interestingly, in the case of Fe-Ni-Al_2O_3, methane conversion drops substantially in the end of phase 1. This happened jointly with increased selectivity to H_2 and CO before methane conversion inversed to increase sharply and stabilize for the rest of the fuel stage. The different transitional behaviour of the Fe-Ni-Al_2O_3 oxygen carrier could be attributed to the presence of

NiO that has to reduce to metallic Nickel before it starts catalysing the conversion of CH_4 to syngas [30]. It was expected that, at some reduction state of the oxygen carrier, combustion of methane by oxygen from NiO would create enough metallic nickel sites to catalyse significant methane reforming, but the results suggest that reforming activity starts only after the iron compounds in the oxygen carrier are also fully reduced. This could have resulted from the fact that nickel was part of the spinel as shown by the XRD analysis (*Figure **4-9***).

Nevertheless, even though the transition between the two phases is not immediate for the Fe-Ni-Al_2O_3, it could safely be concluded that the fuel stage of the GSR concept, with the three iron-based oxygen carriers, comprises two distinct phases; one is dominated by combustion of methane while the second is dominated by methane reforming to syngas. Mass balance calculation of the reaction of CH_4 with Fe_2O_3 (assuming an ideal scenario where the oxygen carrier transitions between the different iron oxide states which are Fe_2O_3, Fe_3O_4, FeO and Fe) suggests that CH_4 converts well to CO_2 and H_2O over Fe_2O_3 and Fe_3O_4 to FeO. Indeed, for a mass of 286 g of the Fe-Al_2O_3 oxygen carrier, an active content of 35 wt.%, the total moles of Fe_2O_3 available for reaction is 0.35*286/159.7=0.63 mol. For a CH_4 feed rate of 0.8 Nl/min ~288 seconds is needed to fully convert Fe_2O_3 to FeO. It can be seen on *Figure **4-7*** a) that full CH_4 conversion to CO_2 and H_2O occurs only in the first 200 seconds of the fuel stage (before it starts slowing down), corresponding to 70 % of the time needed to fully convert Fe_2O_3 to FeO.

X-ray diffraction data for three samples after final stage reduction is presented in *Figure **4-9***, and an example of material after an oxidation step is presented in *Figure **4-8***. It can be seen that the active oxidised phase in the Fe system is Fe_2O_3, and that at the temperatures of operation of 850 °C, the Al_2O_3 support has changed from a poorly crystalline transition alumina to be a relatively crystalline corundum-type α-alumina (*Figure **4-9***). Some residual spinel phases are also evident (though not fitted), indicating incomplete reaction during the oxidation step.

The phases present after reduction are best understood as being solid solutions of spinel structured oxides of the general form M_3O_4, where M=Ni, Fe, or Al. It is important to note that in all these phases, iron is present as Fe^{2+} or as a mixture of Fe^{2+} and Fe^{3+}. There is no evidence of FeO, NiO or metallic Fe or Ni. For the Fe-Ce sample an additional CeO_2 phase is clearly also present and demonstrates a unit cell parameter in good accordance with literature values (a=5.411Å vs 5.410Å [31]. Data fitting of the spinel component is presented in the form of three overlapping phases, though it is noted that there is complete solid-solubility in the Fe_3O_4-$NiFe_2O_4$-$NiAl_2O_4$-$FeAl_2O_4$ system, so this indicates a level of non-equilibrium.

The majority spinel phase in all samples after reduction (illustrated in red in *Figure **4-9***) exhibits a unit cell parameter in the range 8.10Å to 8.14Å, consistent with an Al-rich Ni-Fe aluminate spinel (see supplementary plot S1). For the Fe-only system, the observed unit cell of a=8.1337(1)Å is in close agreement with that of $FeAl_2O_4$ [32]. The Ni-Fe and Fe-Ce systems exhibit unit cell parameters smaller than those of $FeAl_2O_4$ though (a=8.1131(1)Å and a=8.1060(3)Å respectively). This confirms dissolution of Ni into the spinel phase in the Ni-Fe sample, and suggests a deviation from ideal M_3O_4 spinel stoichiometry towards a defective $Al_{2.66}O_4$ (γ-Al_2O_3 type) composition in the Fe-Ce system, as Ce does not readily form spinel structured solid solutions with Fe and Al.

The minority spinel phases observed are a phase with a unit cell parameter in the range a=8.02 to 8.04Å, and for the Fe and Ni-Fe systems a phase with unit cell parameter in the range a=8.20 to 8.34Å. The former of these is a defective γ-Al_2O_3 type phase, considering the published unit cell parameters for the Fe_3O_4-$NiFe_2O_4$-$NiAl_2O_4$-$FeAl_2O_4$ system [32-35]. The latter is likely a Fe-rich / Alumina poor phase. Similar elements were found for 6 and 12 min fuel time on the Fe-Ni-Al_2O_3 (Figure 4-10) suggesting that no further reduction of the oxygen carrier takes place when the reforming stage begins (it could be observed that the 6 mins data shows an additional phase than the 12 mins, a result that could arise from the fact that the former was sampled after 8 days of operation, causing the sample to deactivate a bit).

Considering the XRD data, a simplified scheme for the redox cycling can be proposed:

Reduction reaction:

$$4Fe_2O_3 + 8Al_2O_3 + CH_4 \rightarrow 8FeAl_2O_4 + CO_2 + 2H_2O \qquad \textit{Equation 4-4}$$

Oxidation reaction:

$$2FeAl_2O_4 + 1/2\,O_2 \rightarrow Fe_2O_3 + 2Al_2O_3 \qquad \textit{Equation 4-5}$$

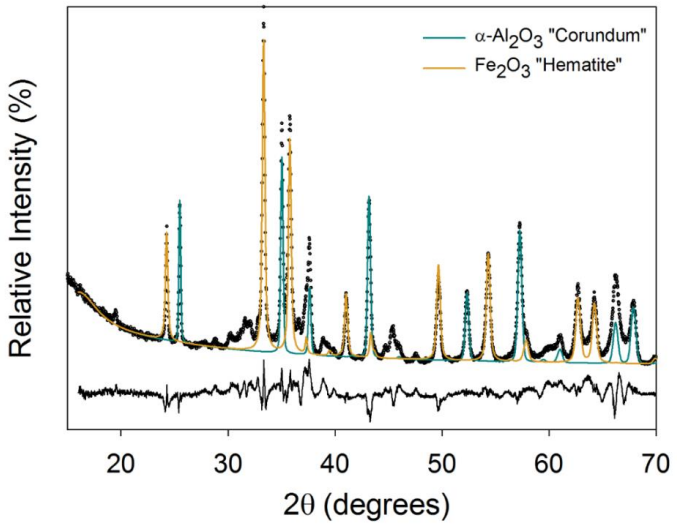

Figure 4-8 - A sample of Fe-Al_2O_3 following GSR cycling and oxidation at 850 °C

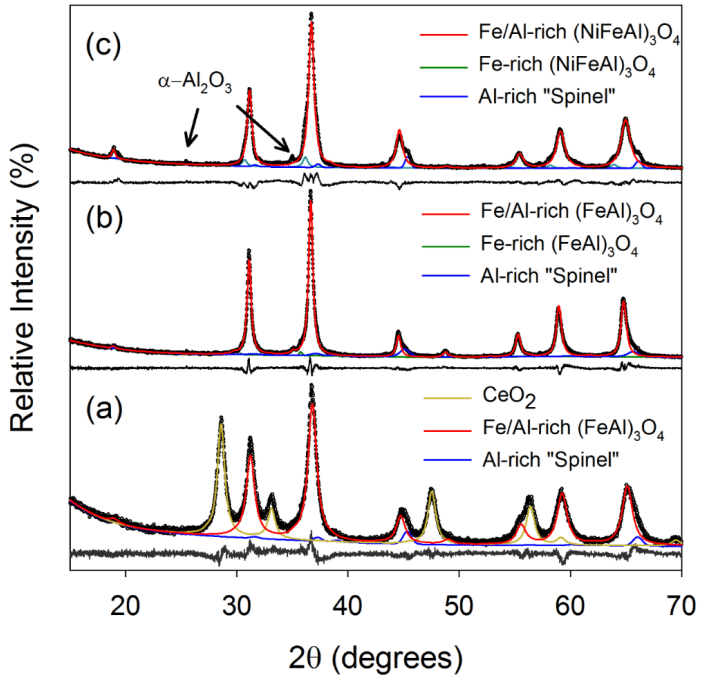

Figure 4-9- Fitted XRD data for (a) A sample of Fe-Ce-Al_2O_3 , after 30 mins final stage reduction at 800°C, (b) a sample of Fe-Al_2O_3, after 30 mins final stage reduction at 800°C, and (c) a sample of Fe-Ni-Al_2O_3, after 30 mins final stage reduction at 800°C.

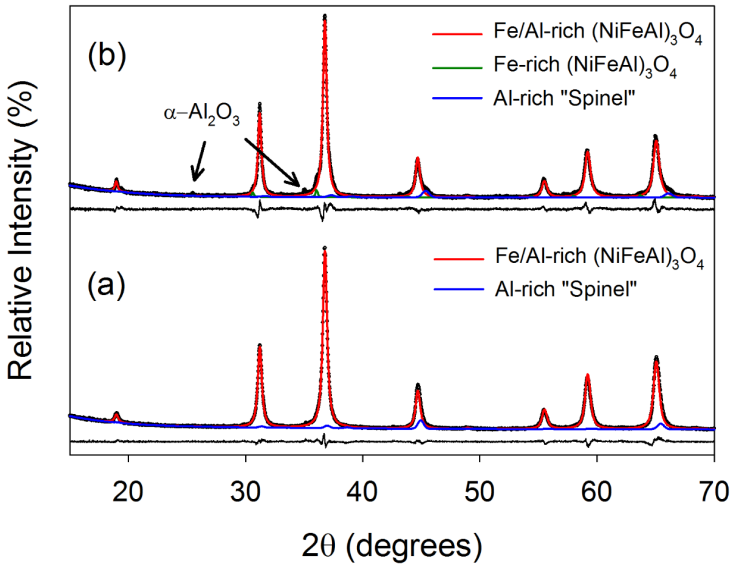

Figure 4-10: Fitted XRD data for (a) A sample of Fe-Ni-Al_2O_3 following 6 mins reforming, and (b) following 12 mins reforming. Both at an operating temperature of 800 °C.

4.5.2 Mechanisms of Fe_2O_3 reduction with methane

On the light of the XRD results, the reduction stage (phase 1) occurs by reducing Fe_2O_3 to $FeAl_2O_4$ following an overall scheme resulting in methane combustion to CO_2. This is different from reaction scheme proposed by Monazam et al. [36] for the reduction of Fe_2O_3 to FeO using methane based on TGA experiments, where the products contain CO_2, CO, H_2O and H_2 (*Equation **4-6***).

$$7CH_4 + 27Fe_2O_3 \rightarrow 10Fe_3O_4 + 24FeO + 4CO_2 + 3CO + 6H_2O + 8H_2 \qquad \textit{Equation 4-6}$$

The reaction showing complete CH_4 conversion (*Equation **4-4***) is expected to occur throughout both the reduction and reforming phases in the oxygen carriers not containing Ni. However, when the Fe_2O_3 reactant becomes depleted, the reaction slows down and significant fuel slip occurs. Once the oxygen carrier becomes highly reduced, it becomes possible to complete oxidization with steam in the water splitting reaction (*Equation **4-7***). It is not clear whether this reaction will produce Fe_2O_3, Fe_3O_4, or some intermediate Fe-Al-oxide, but it has been shown that the water splitting reaction happens when the oxygen carrier is highly reduced. In fact, this reaction has been isolated by feeding only steam to a fully reduced bed to achieve 40% conversion of steam to H_2 at 800 °C (See supplementary plot S2). Although it has not been

explicitly confirmed, conversion of CO_2 to CO may also take place through the same mechanism (*Equation **4-8***).

As shown in the earlier mol balance calculation, the production of H_2 and CO through these reactions become significant only when the oxygen carrier becomes almost completely reduced. Most likely, *Equation **4-7*** starts producing H_2 earlier during the reduction phase, but the produced H_2 is converted back to steam over the excess Fe_2O_3 still present in the reactor. Substantial quantities of H_2 at the reactor outlet are only observed when the presence of Fe_2O_3 becomes very low. In addition, Fe-based materials are known to catalyse the water-gas shift reaction (*Equation **4-9***), which further influences the H_2 to CO ratio in the produced syngas.

Through this mechanism, the Fe-Al_2O_3 and Fe-Ce-Al_2O_3 oxygen carriers behave like catalysts for steam methane reforming, although the reactions are not catalytic, but rather competing heterogeneous gas-solid reactions. The oxygen carrier is continuously reduced by the incoming methane fuel and the highly reduced oxygen carrier particles are oxidized by steam and CO_2 to form H_2 and CO. These reactions can continue indefinitely as long as heat is supplied to drive this endothermic reaction system.

$$2FeAl_2O_4 + H_2O \leftrightarrow Fe_2O_3 + 2Al_2O_3 + H_2 \qquad \textit{Equation 4-7}$$

$$2FeAl_2O_4 + CO_2 \leftrightarrow Fe_2O_3 + 2Al_2O_3 + CO \qquad \textit{Equation 4-8}$$

$$CO + H_2O \leftrightarrow CO_2 + H_2 \qquad \textit{Equation 4-9}$$

$$CH_4 + H_2O \leftrightarrow CO + 3H_2 \qquad \textit{Equation 4-10}$$

The substantial change in oxygen carrier behaviour for the Ni-containing material is signifies a change in mechanism to the catalytic steam-methane reforming reaction (*Equation **4-10***). Even though no free Ni was observed in the XRD analyses, results suggest that the presence of Ni-compounds in the oxygen carrier still facilitates the steam-methane reforming reaction once the oxygen carrier becomes highly reduced.

However, the water splitting (*Equation **4-7***) and CO_2 splitting (*Equation **4-8***) reactions seem to be suppressed by the presence of Ni, as evidenced by the larger drop in methane conversion at the end of the reduction phase compared to the other two oxygen carriers. The operational challenge of this oxygen carrier is therefore to achieve a high degree of reduction to activate the catalytic steam-methane reforming reaction without excessive fuel slip in the reduction phase.

4.6 Sensitivity study

4.6.1 Effect of steam in the reduction stage

Methane is fully converted to CO_2 in phase 1 with all three oxygen carriers despite the presence of steam. Removing steam feed for this phase 1 would therefore allow substantial energy saving, if no negative side effects exist. In this respect, experiments were completed by feeding pure methane in phase 1 (first six minutes of the fuel time) while steam was only fed in phase 2 together with methane. Given the superior performance of the Ni-modified iron-based oxygen carrier in phase 2 dominated by methane reforming, this one was selected for the rest of the study.

As can be seen in *Figure **4-11***. a), removing steam from phase 1 was found to have a very positive impact on methane conversion, leading to further prolonging the period with full methane conversion under the reduction mode in phase 1, and therefore reduces methane slippage in the transition to phase 2. This also delayed appearance of syngas in contrast to the case with steam feed, implying that presence of steam in phase 1 causes an earlier transition to syngas production.

Surprisingly, a large improvement in methane conversion to H_2 and CO occurs in phase 2 (over 90% methane conversion was achieved already at 800 °C), a result that could be attributed to the higher degree of reduction achieved by the pure methane feed. This has also affected the selectivity to hydrogen and CO, suggesting a change in the extents by which the different mechanisms contribute to syngas production.

A negative aspect of these results is that, some carbon deposition was detected in the form of a release of CO_2 in the oxidation stage. This CO_2 can only originate from the combustion of deposited carbon with oxygen in the air feed. Fortunately, this effect was quite small: the total released carbon in the oxidation stage was ~1.1% of the total converted methane in the entire 12 min fuel stage.

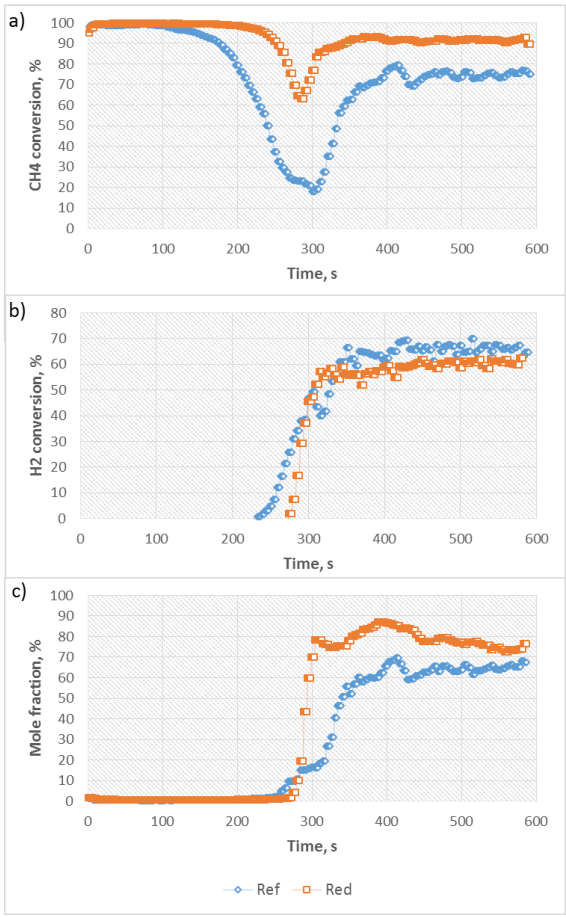

Figure 4-11: Effect of steam in the reduction (phase 1) on the GSR performance in the fuel stage

4.6.2 Effect of temperature

The GSR performance improves in both phase 1 and 2 with the operating temperature, with the largest impact being observed in phase 2 (dominated by the reforming). As can be seen in *Figure* ***4-12***, good methane conversion was achieved at the beginning of phase 1 even at 700 °C. The extent of the complete methane conversion period increases with temperature, to cover more than 90 % of phase 1 time at 850 °C.

In phase 2 dominated by methane reforming, methane conversion to syngas jumps from 20% at 700 °C to close to 100% at 850 °C. A particularly large improvement takes place when increasing the temperature from 750 to 800 °C. This improvement could be attributed to the combined higher reduction degree of the oxygen carrier resulting from the prolonged high CH_4 conversion in phase 1 to CO_2 and H_2O, and the improved reaction kinetics. Appearance of H_2

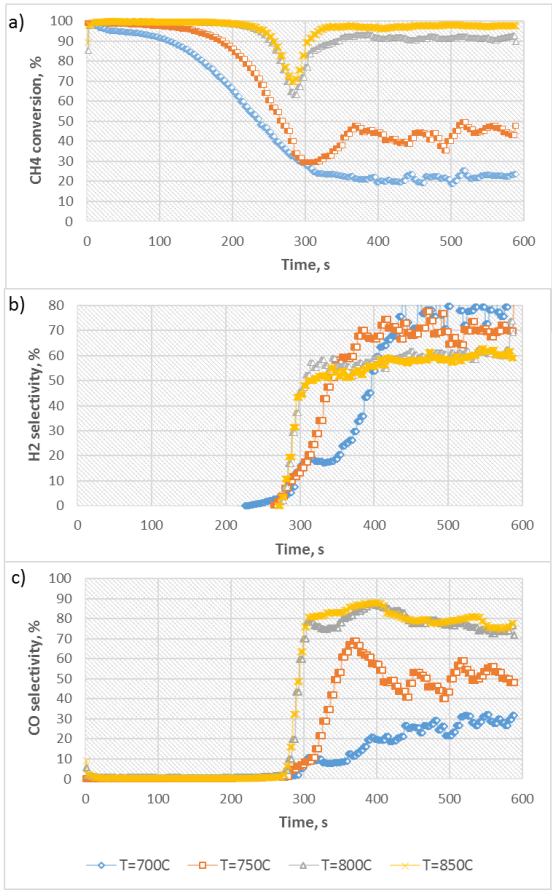

Figure 4-12: Effect of operating temperature on the GSR performance in the fuel stage. Fe-Ni-Al_2O_3 oxygen carrier.

and CO in phase 2 becomes sharper with increased temperature, thereby leading to a faster transition between the combustion and reforming phases. This clear separation between the two phases is very beneficial for designing a GSR cycle with efficient fuel utilization [37]. For the 700 and 750 °C cases, the oxygen carrier is not fully reduced in the start of the reforming phase, thus delaying the onset of steady syngas production.

It could be noticed that increased temperature leads to increased CO selectivity over H_2. A high amount of CO_2 release was detected in the air stage at 700 and 750 °C (~2.3% of converted methane in the entire fuel stage) but reduced to 1.1% at 800 °C and to 0.42% at 850 °C. This explains the high selectivity to H_2 at low temperature, as the carbon from the methane cracking ($CH_4 \leftrightarrow C + 2H_2$) remains on the oxygen carrier while H_2 leaves the reactor (*Figure **4-12***). This tendency was reduced with increasing temperature, thereby demonstrating the positive effect temperature on removing carbon deposition. The selectivity to H_2 and CO was similar

for both 800 and 850 °C, despite the further reduction in carbon deposition. It is therefore recommended to operate the reforming stage at temperatures above 800 °C to maximize methane conversion to syngas at acceptable slippage of carbon to the air stage.

4.6.3 Effect of steam-to-carbon ratio S/C

The effect of steam per carbon ratio, S/C, on the reforming phase performance was studied. Experiments were completed for three S/C, 1, 2 and 3. Pure methane was fed in phase 1 following the improved performance achieved across the whole GSR fuel stage, compared to the case with steam in phase 2, as shown in the previous section.

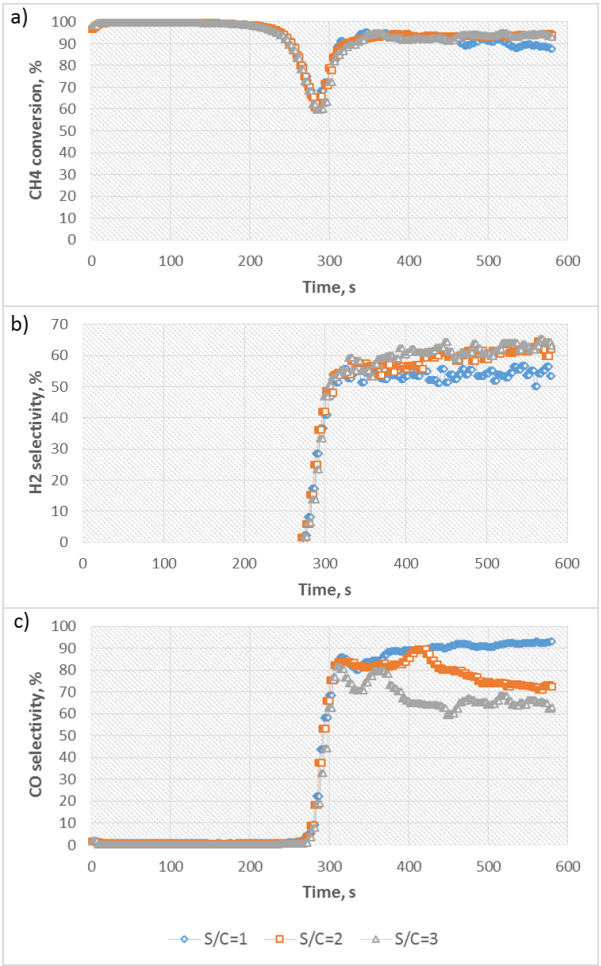

Figure 4-13: Effect of steam per carbon ratio, S/C=1, 2 & 3, on the GSR performance in the fuel stage. Fe-Ni-Al_2O_3 based oxygen carrier was used. Operating temperature of 800 °C.

As can be seen on *Figure **4-13***.a), similar methane conversion in phase 1 was achieved for the three experiments, as pure methane was fed in each one. This means that the oxygen carrier achieves the same level of reduction for the three S/C values before the start of phase 2.

High methane conversion was achieved with no clear effect of S/C in phase 2 (CH_4 conversion for S/C=1 seems to be slightly lower in the second half of phase 2). Obviously, excess of steam enhances selectivity to H_2 while it reduces CO selectivity via the water gas shift reaction that is catalysed by both Ni and Fe compounds. The extent of carbon deposition reduces with the extent of steam excess, from 1.3% at S/C=1 to 0.76% at S/C=3, as excess steam gasifies some of the deposited carbon ($C + H_2O \leftrightarrow CO + H_2$).

4.7 Autothermal operation with Fe_Ni_Al_2O_3

Experience from the prior experiments will now be used to operate the GSR cycle autothermally. In this experiment, no external heat was supplied to the reactor in any stage of the GSR cycle, but rather the cycle was designed in a way that the overall heat requirement (endothermic methane reforming reaction, heat removed by gases, in addition to heat losses from the reactor) is fulfilled by the exothermic reaction (mainly the oxidation of the oxygen carrier, but it could also be in the reduction stage if CO is used).

It is worth reminding that the GSR process with an iron-based oxygen carrier was found to take place following three well-defined stages; oxidation, reduction, and reforming. The transition between the reduction and reforming stages could be completed with minimal fuel slippage if dry gaseous fuel is used in the reduction stage at sufficiently high temperatures (*Figure **4-11***), with steam feed added only in the reforming stage. The three-stage behavior of the GSR process opens the possibility of using gaseous fuels other than methane in the reduction stage. This becomes especially interesting if hydrogen production is the final product, where PSA off-gas could be used as feed to the reduction phase. This GSR configuration has been proposed for H_2 production with integrated CO_2 capture [20, 37, 38]. The presence of a high CO content in the off-PSA gasses gives another advantage to the reforming stage, owing to its exothermic reaction with the iron-based oxygen carrier that releases heat in the reduction, thereby allowing the subsequent reforming stage to start at a higher temperature than the case of methane which has an endothermic reduction reaction.

All combined, the autothermal operation was completed in optimal conditions following the three-stage GSR configuration (to avoid any confusion, the terminology “stage” is used in the

rest of the manuscript instead of “phase”). Pure CO is fed in the reduction stage, steam and methane in the reforming stage, and air in the oxidation stage. The cycle starts with the reduction stage at a reactor temperature of ~850 °C for a reduction time designed to reach the same reduction level achieved in experiments shown in section **4.6.1**. A reforming stage follows where the temperature drops due to the endothermic reaction, then the oxidation stage is applied where heat is built up again in the reactor, thereby bringing the temperature back to 850°C for starting a new GSR cycle.

As can be seen in Figure 4-14, the temperature in the reactor cycles well between 855 °C and ~810 °C by alternating the three GSR stages, demonstrating the ability of the three-stage GSR concept to run autothermally. In the reduction stage, complete conversion of CO was achieved in the two-thirds of the stage, before it starts decreasing gradually towards the end of the stage. The exothermic reaction of CO with the oxygen carrier maintained the temperature high across the stage which allowed starting the reforming stage at a high temperature (855 °C). The reforming stage was stopped at a temperature of 810 °C, to avoid high methane slippage as shown in the previous section **4.6.2**. Gas composition measurements confirm that high conversion of methane to syngas is achieved across the entire reforming stage (*Figure **4-14***). The higher methane slippage compared to the case shown in *Figure **4-11*** and *Figure **4-12***, completed at a similar range of temperature could be attributed to the methane feed rate which is three times higher in this autothermal operation experiment. Full conversion of oxygen was achieved in the entire oxidation stage demonstrating the high reactivity of the oxygen carrier with oxygen. It should also be emphasized that no CO_2 release was observed in the oxidation stage, thereby proving the absence of carbon deposition.

The aforementioned autothermal behaviour of the three-stage GSR configuration was repeatable over cycles, by alternating the gas feeds into the bed of iron-based oxygen carrier, thereby maintaining the bed temperature cycling between 855 and 810 °C.

Due to large heat losses from the lab-scale reactor, the length of the reforming stage was found to be ~2.2 times shorter than the theoretical prediction by heat balance calculation. The total CO feed to the reduction stage was ~0.59 mol, requiring ~1.38 mol of air to oxidize back the oxygen carrier. The total heat generated in the system from the combustion of CO is then equal to ~157.7 kJ (assuming 95% CO conversion). This heat is used for heating up gases from room temperature to the reactor operating temperature for driving the endothermic steam-methane reforming reaction with an enthalpy of 206 kJ/mol. The calculated theoretical time of the reforming stage is ~110 s while the experimental one was only 50 s.

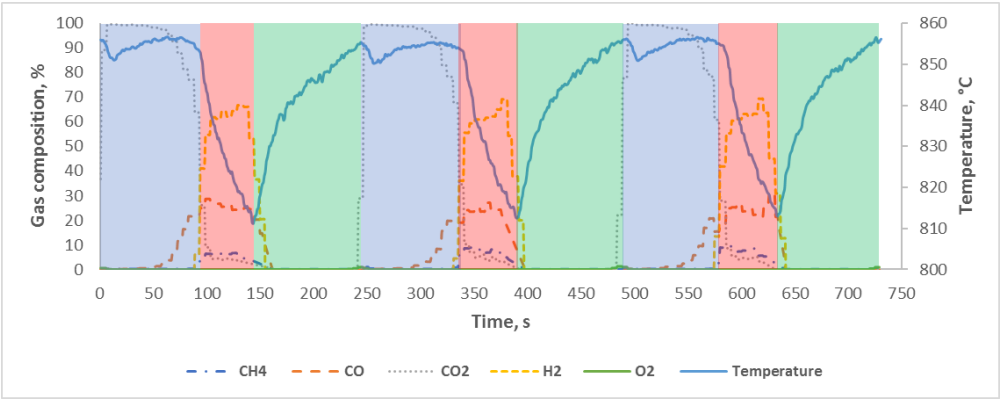

Figure 4-14: Transient temperature and gas composition behavior of autothermal operation of the three-stage GSR process with Fe-Ni-Al_2O_3 based oxygen carrier over three cycles. CO was fed in the reduction stage (9.6 Nl/min for 90 seconds), steam and CH_4 were fed in the reforming stage (2.4 Nl/min with S/C=2, for 50 seconds) and air was fed in the oxidation stage (15 Nl/min for 120 seconds). Reduction stage in blue, reforming stage in red and oxidation stage in green.

4.8 Conclusion

An experimental campaign was completed to investigate the Gas Switching Reforming, GSR, process behaviour with iron-based oxygen carriers, for natural gas conversion to syngas with integrated CO_2 capture. Three iron-based oxygen carriers, prepared using impregnation of active materials on an alumina support, were tested under relevant GSR conditions. The base case oxygen carrier was 35 wt.% hematite on alumina, while 10 wt.% of hematite was replaced by CeO_2 in the second, and by NiO in the third one.

The fuel stage, with CH_4 and steam feed, was found to occur following two separate phases with very distinguished behaviours; methane combustion to CO_2 dominates in sub-stage 1, while high selectivity to syngas dominates in sub-stage 2. The reaction mechanism of the base and CeO_2-doped oxygen carriers during the reforming phase is a combination of Fe_2O_3 reduction with CH_4 to form CO_2 and H_2O and re-oxidation of the oxygen carrier by H_2O and CO_2 to form H_2 and CO. This mechanism only becomes visible when the oxygen carrier becomes highly reduced so that there is almost no Fe_2O_3 left to oxidize the produced H_2 and CO. Due to these simultaneous reactions reducing and oxidizing the oxygen carrier, the overall reaction behaves like a catalytic system even though the oxygen carrier is being altered by the reaction. When NiO is added to the oxygen carrier, however, the reforming stage is dominated by conventional catalytic steam-methane reforming due to the presence of Nickel, which is known to be an excellent catalyst.

Dry methane feed over the Fe-Ni oxygen carrier prolonged the reduction sub-stage 1, implying that greater oxygen carrier reduction is achieved. This led to a substantial improvement of methane conversion to syngas in the reforming sub-stage 2 where CH_4 and steam feed was applied. Carbon deposition (1% from the total converted methane in the entire fuel stage) was however observed in the form of CO_2 release in the beginning of the oxidation stage, originating from carbon oxidation with oxygen in the air feed. Increasing the operating temperature to 850 °C further improved methane conversion in both sub-stages, and also halved carbon deposition. Increasing the steam/carbon ratio from 1 to 3 at 800 °C slightly reduced the extent of carbon deposition and only had a minor effect on methane conversion. Operating the reforming sub-stage at a temperature above 800 °C can therefore ensure both high methane conversion and minimal carbon deposition.

The three distinguished stages (reduction, reforming and oxidation) offer a unique opportunity for maximizing fuel conversion in the GSR process, especially when pure hydrogen production is the final targeted product, where PSA-off gases can be used in the reduction stage. An autothermal operation experiment was then completed in the three-stage GSR configuration, by feeding pure CO in the reduction stage and a mix of CH_4 and steam to the reforming stage. The exothermic reaction of CO with the iron-based oxygen carrier enabled maintaining the bed temperature above 850 °C, which allowed the reforming sub-stage to start at a high temperature to maximize methane conversion. It could therefore be safely concluded that operation of the GSR process with iron-based oxygen carriers is possible at high methane conversion following the three-stage GSR configuration.

Nomenclature

Abbreviations

CCUS	Carbon Capture Storage and Utilization
CFB	Circulating Fluidized Bed
CLC	Chemical Looping Combustion
CLR	Chemical Looping Reforming
EDS	Energy-Dispersive Spectroscopy
GSC	Gas Switching Combustion
GSR	Gas Switching Reforming

GST	Gas Switching Technology
OC	Oxygen Carrier
OXI	Oxidation
POX	Partial Oxidation
PSA	Pressure Swing Adsorption
RED	Reduction
REF	Reforming
S/C	Steam to carbon ratio
SEM	Scanning Electron Microscope
SMR	Steam Methane Reforming
TGA	Thermogravimetric analysis
XRD	X-Ray Diffraction

Symbols:

$FCH_{4,in}$	The molar flow rate of CH_4 into the reactor in the fuel stage
$FCH_{4,out}$	The molar flow rate of CH_4 in the reactor gas outlet at the fuel stage
FCO_{out}	The molar flow rate of CO in the reactor gas outlet at the fuel stage
$FH_{2,out}$	The molar flow rate of H_2 in the reactor gas outlet at the fuel stage
S_{CO}	CO selectivity
$S_{H_2,}$	Hydrogen selectivity
γ_{CH_4}	CH_4 conversion

References

[1] IPCC. Climate change mitigation: Summary for Policymakers

[2] P. Viebahn, D. Vallentin, and S. Holler, "Prospects of carbon capture and storage (CCS) in China's power sector - An integrated assessment," *Applied Energy,* vol. 157, pp. 229-244, Nov 2015, doi: 10.1016/j.apenergy.2015.07.023.

[3] E. S. Rubin, H. Mantripragada, A. Marks, P. Versteeg, and J. Kitchin, "The outlook for improved carbon capture technology," *Progress in Energy and Combustion Science,* vol. 38, no. 5, pp. 630-671, Oct 2012, doi: 10.1016/j.pecs.2012.03.003.

[4] A. M. Cormos, C. Dinca, L. Petrescu, D. A. Chisalita, S. Szima, and C. C. Cormos, "Carbon capture and utilisation technologies applied to energy conversion systems and other energy-intensive industrial applications," *Fuel,* vol. 211, pp. 883-890, Jan 2018, doi: 10.1016/j.fuel.2017.09.104.

[5] D. Leeson, N. Mac Dowell, N. Shah, C. Petit, and P. S. Fennell, "A Techno-economic analysis and systematic review of carbon capture and storage (CCS) applied to the iron and steel, cement, oil refining and pulp and paper industries, as well as other high purity sources," *International Journal of Greenhouse Gas Control,* vol. 61, pp. 71-84, Jun 2017, doi: 10.1016/j.ijggc.2017.03.020.

[6] P. Bains, P. Psarras, and J. Wilcox, "CO2 capture from the industry sector," *Progress in Energy and Combustion Science,* vol. 63, pp. 146-172, Nov 2017, doi: 10.1016/j.pecs.2017.07.001.

[7] L. Barreto, A. Makihira, and K. Riahi, "The hydrogen economy in the 21st century: a sustainable development scenario," *International Journal of Hydrogen Energy,* vol. 28, no. 3, pp. 267-284, 2003, doi: http://dx.doi.org/10.1016/S0360-3199(02)00074-5.

[8] B. Johnston, M. C. Mayo, and A. Khare, "Hydrogen: the energy source for the 21st century," *Technovation,* vol. 25, no. 6, pp. 569-585, Jun 2005, doi: 10.1016/j.technovation.2003.11.005.

[9] M. Ryden and A. Lyngfelt, "Using steam reforming to produce hydrogen with carbon dioxide capture by chemical-looping combustion," *International Journal of Hydrogen Energy,* vol. 31, no. 10, pp. 1271-1283, Aug 2006, doi: 10.1016/j.ijhydene.2005.12.003.

[10] M. Rydén, A. Lyngfelt, and T. Mattisson, "Synthesis gas generation by chemical-looping reforming in a continuously operating laboratory reactor," *Fuel,* vol. 85, no. 12-13, pp. 1631-1641, 2006.

[11] T. Proell, J. Bolhar-Nordenkampf, P. Kolbitsch, and H. Hofbauer, "Syngas and a separate nitrogen/argon stream via chemical looping reforming - A 140 kW pilot plant study," *Fuel,* vol. 89, no. 6, pp. 1249-1256, Jun 2010, doi: 10.1016/j.fuel.2009.09.033.

[12] M. Ortiz, L. F. de Diego, A. Abad, F. Garcia-Labiano, P. Gayan, and J. Adanez, "Hydrogen production by auto-thermal chemical-looping reforming in a pressurized fluidized bed reactor using Ni-based oxygen carriers," *International Journal of Hydrogen Energy,* vol. 35, no. 1, pp. 151-160, Jan 2010, doi: 10.1016/j.ijhydene.2009.10.068.

[13] A. Hafizi, M. R. Rahimpour, and S. Hassanajili, "Hydrogen production via chemical looping steam methane reforming process: Effect of cerium and calcium promoters on the performance of Fe2O3/Al2O3 oxygen carrier," *Applied Energy,* vol. 165, pp. 685-694, Mar 2016, doi: 10.1016/j.apenergy.2015.12.100.

[14] L. F. de Diego, M. Ortiz, F. García-Labiano, J. Adánez, A. Abad, and P. Gayán, "Hydrogen production by chemical-looping reforming in a circulating fluidized bed reactor using Ni-based oxygen carriers," *Journal of Power Sources,* vol. 192, no. 1, pp. 27-34, 2009/07/01/ 2009, doi: https://doi.org/10.1016/j.jpowsour.2008.11.038.

[15] J. Adanez, A. Abad, F. Garcia-Labiano, P. Gayan, and L. F. de Diego, "Progress in Chemical-Looping Combustion and Reforming technologies," *Progress in Energy and Combustion Science,* vol. 38, no. 2, pp. 215-282, Apr 2012, doi: 10.1016/j.pecs.2011.09.001.

[16] A. Tong, L. Zeng, M. V. Kathe, D. Sridhar, and L.-S. Fan, "Application of the Moving-Bed Chemical Looping Process for High Methane Conversion," *Energy & Fuels,* vol. 27, no. 8, pp. 4119-4128, 2013/08/15 2013, doi: 10.1021/ef3020475.

[17] A. Zaabout, S. Cloete, and S. Amini, "A Novel IC-CLC Reactor Concept For Power Production With Integrated CO2 Capture: Hydrodynamic Experimental Study," *Powder Technology (To be Submitted),* 2014.

[18] V. Spallina, B. Marinello, F. Gallucci, M. C. Romano, and M. V. Annaland, "Chemical looping reforming in packed-bed reactors: Modelling, experimental validation and large-scale reactor design," *Fuel Processing Technology,* vol. 156, pp. 156-170, Feb 2017, doi: 10.1016/j.fuproc.2016.10.014.

[19] A. Zaabout, S. Cloete, S. T. Johansen, M. v. S. Annaland, F. Gallucci, and S. Amini, "A Novel Gas Switching Combustion Reactor For Power Production With Integrated CO2 Capture: Sensitivity To The Fuel Type," in *3rd International Conference on Chemical Looping*, Chalmers University of Technology, Gothenburg, Sweden, 9-11 September 2014.

[20] S. A. Wassie, F. Gallucci, A. Zaabout, S. Cloete, S. Amini, and M. van Sint Annaland, "Hydrogen production with integrated CO2 capture in a novel gas switching reforming reactor: Proof-of-concept," *International Journal of Hydrogen Energy,* vol. 42, no. 21, pp. 14367-14379, 5/25/ 2017, doi: https://doi.org/10.1016/j.ijhydene.2017.04.227.

[21] A. Zaabout, S. Cloete, S. T. Johansen, M. v. S. Annaland, F. Gallucci, and S. Amini, "Experimental Demonstration of a Novel Gas Switching Combustion Reactor for Power Production with Integrated CO2 Capture," *Industrial & Engineering Chemistry Research,* vol. 52, no. 39, pp. 14241-14250, Oct 2 2013, doi: 10.1021/ie401810n.

[22] S. A. Wassie *et al.*, "Hydrogen production with integrated CO2 capture in a membrane assisted gas switching reforming reactor: Proof-of-Concept," *International Journal of Hydrogen Energy,* vol. 43, no. 12, pp. 6177-6190, 2018/03/22/ 2018, doi: https://doi.org/10.1016/j.ijhydene.2018.02.040.

[23] A. Zaabout, S. Cloete, and S. Amini, "Autothermal operation of a pressurized Gas Switching Combustion with ilmenite ore," *International Journal of Greenhouse Gas Control,* vol. 63, pp. 175-183, 2017/08/01/ 2017, doi: https://doi.org/10.1016/j.ijggc.2017.05.018.

[24] Q. Zafar, T. Mattisson, and B. Gevert, "Redox investigation of some oxides of transition-state metals Ni, Cu, Fe, and Mn supported on SiO2 and MgAl2O4," *Energy & Fuels,* vol. 20, no. 1, pp. 34-44, Jan-Feb 2006, doi: 10.1021/ef0501389.

[25] M. Rydén, A. Lyngfelt, T. Mattisson, D. Chen, A. Holmen, and E. Bjørgum, "Novel oxygen-carrier materials for chemical-looping combustion and chemical-looping reforming; LaxSr1−xFeyCo1−yO3−δ perovskites and mixed-metal oxides of NiO, Fe2O3 and Mn3O4," *International Journal of Greenhouse Gas Control,* vol. 2, no. 1, pp. 21-36, 2008/01/01/ 2008, doi: https://doi.org/10.1016/S1750-5836(07)00107-7.

[26] K. Z. Li, H. Wang, Y. G. Wei, and D. X. Yan, "Transformation of methane into synthesis gas using the redox property of Ce-Fe mixed oxides: Effect of calcination temperature," *International Journal of Hydrogen Energy,* vol. 36, no. 5, pp. 3471-3482, Mar 2011, doi: 10.1016/j.ijhydene.2010.12.038.

[27] X. Zhu, K. Z. Li, Y. G. Wei, H. Wang, and L. Y. Sun, "Chemical-Looping Steam Methane Reforming over a CeO2-Fe2O3 Oxygen Carrier: Evolution of Its Structure and Reducibility," *Energy & Fuels,* vol. 28, no. 2, pp. 754-760, Feb 2014, doi: 10.1021/ef402203a.

[28] F. He, Y. G. Wei, H. B. Li, and H. Wang, "Synthesis Gas Generation by Chemical-Looping Reforming Using Ce-Based Oxygen Carriers Modified with Fe, Cu, and Mn Oxides," *Energy & Fuels,* vol. 23, no. 3-4, pp. 2095-2102, Mar-Apr 2009, doi: 10.1021/ef800922m.

[29] Y. Zheng *et al.*, "Designed oxygen carriers from macroporous LaFeO3 supported CeO2 for chemical-looping reforming of methane," *Applied Catalysis B: Environmental,* vol. 202, pp. 51-63, 2017.

[30] Z. Zhou, L. Han, and G. M. Bollas, "Model-based analysis of bench-scale fixed-bed units for chemical-looping combustion," *Chemical Engineering Journal,* vol. 233, pp. 331-348, 2013/11/01/ 2013, doi: https://doi.org/10.1016/j.cej.2013.08.025.

[31] S. F. Pal'guev, S. I. Alyamovskii, and Z. S. Volchenkova., *Russian Journal of Inorganic Chemistry,* vol. 4, pp. 1185-1188, 1959.

[32] R. J. Harrison, S. A. T. Redfern, and H. S. C. O'Neill, *American Mineralogist,* vol. 83, pp. 1092-1099, 1998.

[33] J. N. Roelofsen, R. C. Peterson, and M. Raudsepp, *American Mineralogist,* vol. 77, pp. 522-528, 1992.

[34] C. Quintanar, V. Fuentes, M. P. Jiménez, S. Aburto, and R. Valenzuela, *J. Magn. Magn. Mat. ,* vol. 54/57 pp. 1339-1340, 1986.

[35] B. A. Wechsler, D. H. Lindsley, and C. T. Prewitt, *American Mineralogist,* vol. 69, pp. 754-770, 1984.

[36] E. R. Monazam, R. W. Breault, R. Siriwardane, G. Richards, and S. Carpenter, "Kinetics of the reduction of hematite (Fe2O3) by methane (CH4) during chemical looping combustion: A global mechanism," *Chemical Engineering Journal,* vol. 232, pp. 478-487, 2013/10/01/ 2013, doi: https://doi.org/10.1016/j.cej.2013.07.091.

[37] S. M. Nazir, S. Cloete, O. Bolland, and S. Amini, "Techno-economic assessment of the novel gas switching reforming (GSR) concept for gas-fired power production with integrated CO2 capture," *International Journal of Hydrogen Energy,* 2018/04/10/ 2018, doi: https://doi.org/10.1016/j.ijhydene.2018.02.076.

[38] J. Francisco Morgado, S. Cloete, J. Morud, T. Gurker, and S. Amini, "Modelling study of two chemical looping reforming reactor configurations: looping vs. switching," *Powder Technology,* vol. 316, pp. 599-613, 2017/07/01/ 2017, doi: https://doi.org/10.1016/j.powtec.2016.11.059.

5 Gas Switching Reforming for syngas production with iron-based oxygen carrier- The performance under pressurized conditions

This chapter has been adapted from **Article II**

Ugwu, A. Zaabout, JR. Tolchard, PI. Dahl and S. Amini, *Gas Switching reforming for syngas production with iron-based oxygen carrier-the performance under pressurized conditions.* International Journal of Hydrogen Energy, 2020. 45(2): p. 1267-1282.

Abstract

A four-stage Gas Switching Reforming for syngas production with integrated CO_2 capture using an iron-based oxygen carrier was investigated in this study. The oxygen carrier was first reduced using dry methane, where a high methane conversion rate was achieved producing CO_2 and steam. Following the reduction, stage is a transition to syngas production in an intermediate stage that begins with partial oxidation of methane while methane cracking dominates the rest of the stage. This results in substantial carbon deposition that gasifies in a subsequent reforming stage by co-feeding steam and methane, contributing to more syngas yield. Some of the deposited carbon that could not gasify during the reforming stage slip to the oxidation stage and get combusted by oxygen in the air feed to release CO_2, thereby reducing the CO_2 capture efficiency of the process. It is in this oxidation stage that heat is being generated for the whole cycle given the high exothermicity nature of this reaction. Methane conversion was found to drop substantially in the reforming stage as the pressure increases driven by the negative effect of pressure on both carbon gasification by steam and on the steam methane reforming. The intermediate stage (after reduction) was found less sensitive to the pressure in terms of methane conversion, but the mechanism of carbon deposition tends to change from methane cracking in the POX stage to Boudouard reaction in the reforming stage. However, methane cracking shows a tendency to reduce substantially at higher pressures. This is a very interesting result reflecting that high-pressure operation would remove the need for a reforming stage with co-feeding of steam as no carbon would have been deposited in the POX stage.

Keywords: Chemical looping; gas switching reforming; Iron-based oxygen carrier; Hydrogen and syngas production; Natural gas reforming; Carbon capture.

5.1 Introduction

Fossil energy consumption has steadily increased in recent decades, due to a continuous increase in global energy demand, leading to a rise in CO_2 emission[1]. With the rising concerns of global warming and associated climate change [2], the development of affordable, clean, and reliable energy sources is of high priority. Natural gas conversion into cleaner energy carriers, such as hydrogen, is seen as one of the most sustainable options, given its projected 45% increase in global production and demand by 2040 [1]. Steam methane reforming (SMR) process is widely used for industrial conversion of natural gas to syngas (CO + H_2), but it is associated with high CO_2 emissions, due to its highly endothermic reaction (R1 and R5) requiring heat supply by fossil fuel combustion. Chemical looping reforming (CLR) has been demonstrated as a promising technology integrating the combustion (for heat supply) and reforming steps into a single process, thereby facilitating CO_2 capture at minimal energy penalty [3-5]. This technology was first applied to combustion for capturing CO_2 [6, 7] where the typical configuration consists of two interconnected fluidized bed reactors with a metal oxide (oxygen carrier) circulating between them to transport oxygen from air to the fuel reactor for oxy-combustion. In this way, a pure CO_2 stream is produced (free of N_2) ready for compression and storage [8, 9] (*Figure* ***5-1***). The low energy penalty of chemical looping relative to other CCS technologies has led to the extension of the principle to other energy-intensive processes such as reforming, through the so-called CLR [3, 4]. This process has successfully been demonstrated at lab and pilot scales under atmospheric conditions [10-18].

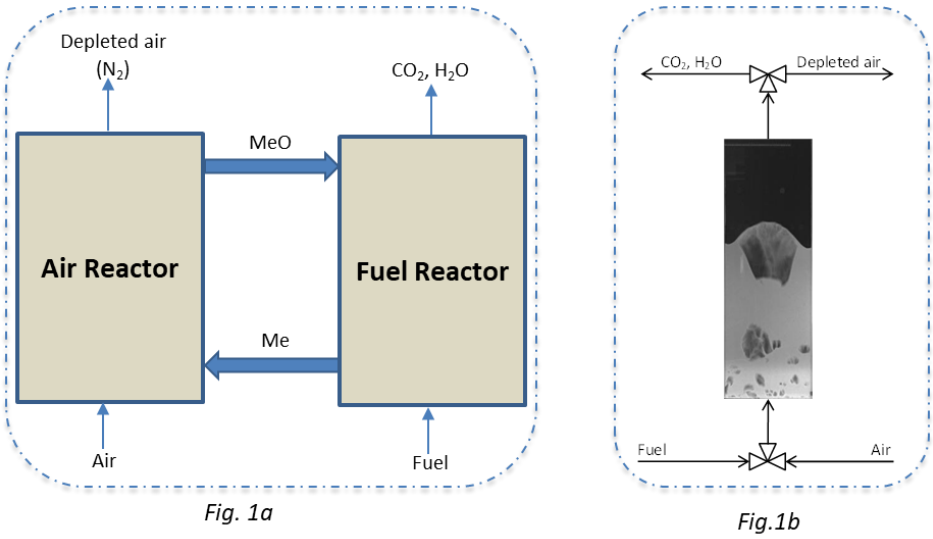

Figure 5-1: Chemical looping combustion. (Fig. 1a: Conventional CLC scheme. Fig. 1b: Simplified GSC scheme).

Traditionally, research on CLR has focused on developing suitable oxygen carriers. It is not surprising that Ni-based oxygen carriers were identified as the best performing, owing to the high catalytic activity of metallic nickel for methane reforming [16-18]. The suitability of other environmentally friendly oxygen carriers, such as Fe-, Mn- and Cu-based was also investigated [19-28]. Fe-based oxygen carriers have shown acceptable performance, with good selectivity to syngas when reducing Fe_3O_4 to FeO [19]. Further improvement in reactivity and selectivity to syngas was achieved by doping the Fe-based oxygen carrier (OC) with promotors such as NiO [19]. Fe-based solids oxides such as Ce-Fe and La-Fe have also been reported to exhibit high selectivity of methane conversion to syngas, resulting from the intensification of oxygen mobility occurring in the Fe-based solid oxides [29-31].

As for the contacting system, given the necessity of high-pressure operation for maximizing energy efficiency and competitiveness with other CO_2 capture technologies [32], the circulating fluidized bed (CFB) configuration is unlikely to be suitable. Stable solids circulation between the two interconnected reactors would be difficult to achieve under pressurized conditions given that each reactor should be pressurized independently, while it is essential to fulfilling the heat and mass balance of the chemical looping process. Any instantaneous pressure imbalance between the reactors may induce instabilities in solids circulation and result in large leakages through the sealing devices, thereby increasing explosion risks. To date, only one pilot-scale experimental study on pressurized chemical looping combustion (CLC) in an interconnected fluidized bed configuration has been completed [33], despite the predicted benefits of such technology in terms of increased energy efficiency [34]. Apart from these operational challenges, there is additional cost and complexity associated with separation systems like cyclone and loop seals.

Attempts have been made in recent years to address these issues where several reactor configurations with no external solid circulation have been proposed and tested [35-39]. Among these, the “Gas Switching Technology (GST)” has a high potential in minimizing the scale-up challenges of pressurized chemical looping. This technology employs a single dense fluidized bed reactor operating under bubbling/turbulent regimes and avoids the circulation of solid oxygen carrier by alternating the feeds of the oxidizing and reducing gases to complete the different reactions involved in the chemical looping process while ensuring inherent CO_2 capture (*Figure **5-1b***). The GST technology has been proposed for heat [40, 41] and hydrogen production with integrated CO_2 capture [8, 9]. Experimental studies have proved ease of operation of this technology under atmospheric and pressurized conditions [8, 9, 42].

5.2 Gas Switching Reforming

The GST technology was extended to methane reforming for syngas production with integrated CO_2 capture, the so-called Gas Switching Reforming (GSR) process, as an alternative to the CLR process that uses the interconnected fluidized bed reactors [8, 9]. Similar to CLR (*Figure **5-2a***), the typical GSR cycle consists of an air stage where heat for the endothermic reforming reaction is generated through the exothermic oxidation reaction. The heated oxygen carrier is then exposed to a feed of CH_4 in the fuel stage where a simultaneous reduction of the oxygen carrier and methane reforming to syngas take place (*Figure **5-2b***). In this case, the oxygen carrier should also play the role of a catalyst for methane reforming. The major advantage of the GSR process is the efficient use of the reaction heat produced during the oxidation stage for the endothermic reforming stage since the reactions occur in a single reactor vessel facilitating autothermal operation of the process [43]. GSR was first demonstrated using a Ni-based oxygen carrier that has shown a very good performance both in the oxidation and reduction stages [8]. This oxygen carrier exhibited an interesting behaviour in the fuel stage showing two distinct sub-stages, where pure combustion of methane takes place in the first one (oxygen carrier reduction), while pure selectivity to syngas takes place in the second. This behaviour opens the possibility for feeding PSA-off gases to the reduction sub-stage, thereby maximizing fuel

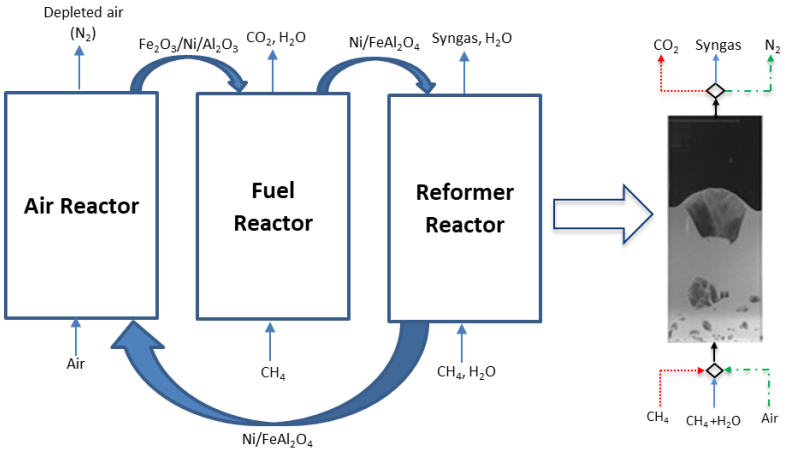

Figure 5-2: Conceptual scheme for autothermal syngas production with integrated CO_2 capture using the three-stages chemical looping reforming technology. Fig. 2a: Conventional CLR process arrangement and Fig. 2b: the simplified Gas Switching reforming, GSR, under investigation in this paper.

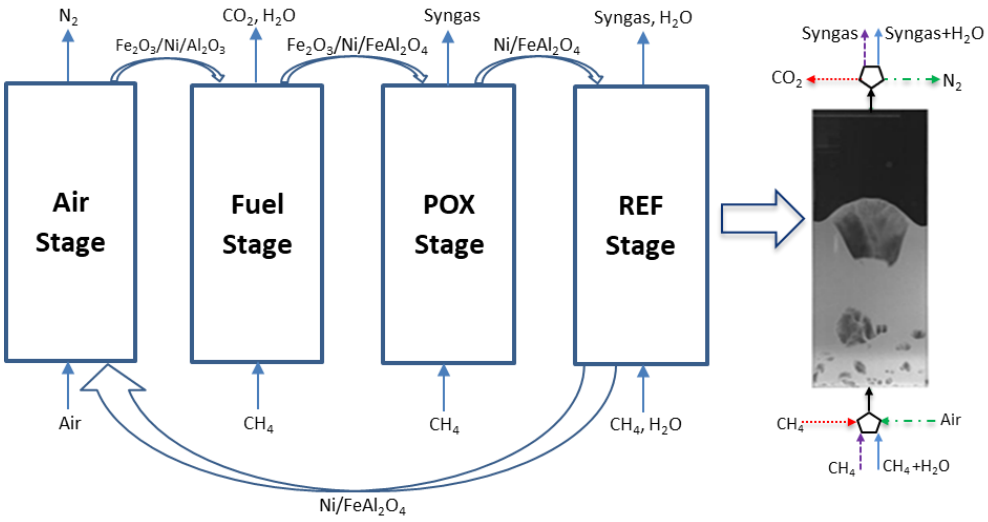

Fig. 3a *Fig. 3b*

Figure 5-3: Proposed 4-stage configuration of autothermal syngas production with integrated CO_2 capture using a four-stages chemical looping reforming technology. Fig. 3a: Conventional CLR process arrangement and Fig. 3b: The simplified Gas Switching Reforming, GSR, under investigation.

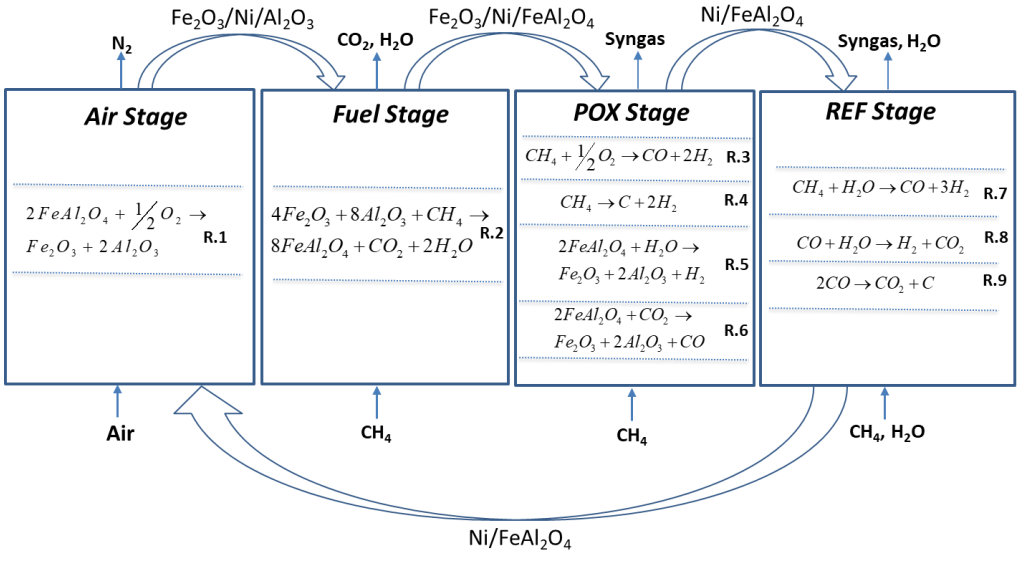

Figure 5-4: The major reactions at different stages of a four-stage chemical looping reforming technology under investigation.

conversion in the GSR process [44]. Another benefit of the use of PSA-off gases in the reduction sub-stage of GSR is the exothermicity of H_2 and CO reactions with the oxygen carrier, that reduces the temperature variation in the GSR cycle, thereby resulting in improved fuel conversion [8]. The three-stage GSR configuration, using CO in the reduction stage, CH_4 in the reforming and air in the oxidation stage was also demonstrated experimentally [8]. GSR process through a four-stages configuration has also been proposed (*Figure **5-3***) with the major reactions at different stages shown in *Figure **5-4***. Like other gas switching concepts, GSR faces a challenge from undesired mixing when switching the inlet feed gases, which causes some N_2 to leak into the fuel stage and some CO_2 to escape to the atmosphere with the depleted air. This leakage is small for reforming concepts though; for example, reactor modeling in a previous study on GSR showed that 97% CO_2 capture could be achieved despite this undesired mixing [44].

The behaviour of GSR using three Fe-based oxygen carriers, supported on commercial alumina (Fe-Al_2O_3, Fe-Ce-Al_2O_3 and Fe-Ni-Al_2O_3), has recently been investigated [45]. The three of them have shown very distinct reduction and reforming stages, similar to the pure Ni-based oxygen carrier tested previously [8], with high conversion of methane to CO_2 in the reduction. As expected, the Fe-Ni-Al_2O_3 outperformed in the reforming showing methane conversion to syngas close to equilibrium at 800-850 °C. The oxidation and reduction mechanisms of the oxygen carrier with Fe-Al_2O_3 have been found to follow ***R.1*** and ***R.2*** (*Figure **5-4***) as revealed by XRD analysis [45]. The phases present after reduction are solid solutions of spinel structured oxides of the general form M_3O_4, where M=Fe, Ni, or Al, wherein all these phases, iron was present as Fe^{2+} or as a mixture of Fe^{2+} and Fe^{3+} with no evidence of the presence of FeO, NiO or metallic Fe or Ni.

For the Ni-free Fe-based oxygen carrier, steam methane reforming occurs following heterogeneous gas-solid reactions. The highly reduced oxygen carrier particles are oxidized by steam and CO_2 to form H_2 and CO (***R.5*** to ***R.9***) as shown in *Figure **5-4***; the oxidized sites immediately reduces with the incoming CH_4 to result in a steady-state steam reforming that can continue indefinitely as long as heat is supplied to drive the overall endothermic reaction system [45]. As for Fe-Ni-Al_2O_3 it is likely that steam methane reforming mainly occurs following reactions ***R.6*** and ***R.7*** (*Figure **5-4***), due to the presence of nickel [45] after the oxygen carrier is sufficiently reduced to $NiFeAl_2O_4$ (the XRD data of the reduced Fe-Ni-Al_2O_3 is shown in *Figure **5-5***.

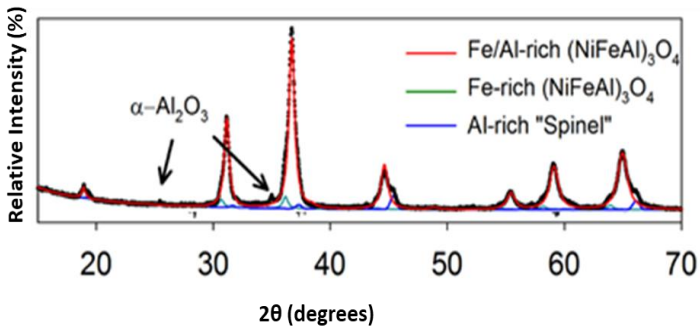

Figure 5-5: Fitted XRD data of the sample (Fe-Ni-Al_2O_3) after 30 minutes final stage reduction at 800°C [46].

This study further investigates the GSR with the NiO promoted oxygen carrier, Fe-Ni-Al_2O_3, developed and tested in Zaabout et al. 2018 [45], where the focus falls on the effect of the operating pressure. The prospects of exploiting methane cracking mechanism ***R.4*** (*Figure* ***5-4***), in hydrogen production with integrated CO_2 capture through GSR is also explored in this study through a four-stages GSR process (*Figure* ***5-3***). In addition to the introduction and conclusion sections, this paper has two other main sections: i) experimental set-up ii) results and discussion.

5.3 Experiment and methods

5.3.1 Experimental Setup

A fluidized bed reactor used for the GSR experiment consists of a cylindrical column (5 cm in inner diameter and 50cm in height) and a freeboard zone as shown in *Figure* ***5-6***. A fluidized bed is desired to achieve good mixing and temperature distribution [47-49]. The freeboard zone consists of an expanding conic zone (from 5cm in the lower end diameter to 10 cm at the top end) followed by a cylindrical part to minimize particle entrainment. The total height of the reactor, including the body and the freeboard, is 90cm. The reactor vessel was made of Inconel 600 to withstand high-temperature gas-solids reactive flows (up to 1000°C). A porous plate with 20μm mean pore size and 3mm thickness, made from Inconel 600, was used as a gas distributor. Heating was done externally through electrically heating elements wound around the reactor vessel to heat up the reactor to a target temperature before starting autothermal GSR process. 25cm thick insulation was applied to the reactor, combining blankets and vermiculate.

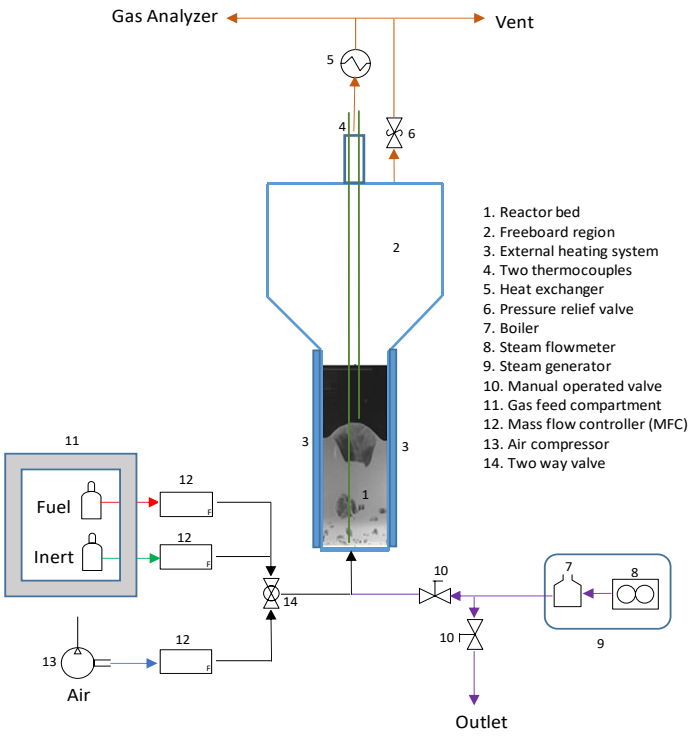

Figure 5-6: GSR Experimental setup.

The reactor was designed to operate at elevated pressures (up to 10bar) and was pressurized using a backpressure valve. Mass flow controllers from Bronkhorst BV were used for feeding gases to the reactor. A three-way electrical valve was used to separate the air and fuel feeds, and to switch between them for cycling reducing and oxidizing conditions in the reactor. A cooler was installed at the outlet of the reactor to cool down the stream of hot gases before sending it to the vent. The gas composition was measured using ETG syngas analyzer connected to the outlet gas stream. The analyzer can sample gases only under atmospheric pressure, which means that in our case the gas had to be sampled after the back-pressure valve. It is necessary to mention that the setup does not allow direct measure steam due to condensation in the heat exchanger. However, the quantity of steam could be quantified through H_2 balance. The temperature was measured at two positions in the reactor, 2cm and 20cm above the gas distributor using two thermocouples inserted through the middle axis of the reactor. All the measurement instruments and flow controlling devices were controlled through a LabVIEW application. The LabVIEW application was also used for data acquisition and storage.

5.3.2 Oxygen carrier

Spherical gamma-alumina particles from Sasol (Puralox SCCa 150/200) were applied for wet impregnation of concentrated aqueous ammonium iron(I) citrate solution (~50 g/100 g water) aiming to form nanostructured iron oxide inside the mesoporous alumina structure after heat treatment. The iron precursor was partly substituted by nickel (II) nitrate hexahydrate to form iron oxide-nickel oxide composite structure. Homogenous distribution of the active metal oxides throughout the porous particles was obtained by wet impregnation with subsequent drying steps at 120°C after each step up to a theoretical loading of ~10 wt% metal oxide, followed by heat treatment for 5 hours at 500°C (60°C/hour) in ambient air. This procedure was repeated until a theoretical loading of the active elements (Fe and Ni) was 1:1 by weight compared to Al in the porous alumina structure. The theoretical Fe:Ni ratio were 2:1 by weight. After the final impregnation and heat treatment steps, the as produced particles were sieved (100 µm) to remove fines before further analysis and testing. The particle size distribution range was 100-450 µm. SEM/EDS analysis on particles after sieving indicated homogenous distribution of the Fe and Ni throughout the porous alumina structure, as seen in *Figure* ***5-7*** respectively. The measured loading of active elements (Fe+Ni): Al ≈ 0.8:1 by weight which is slightly lower than the aimed value of 1:1. This reflects the loss of active material by sieving, in form of fines which are loosely deposited on the surface of the particles. The Fe:Ni ratio was

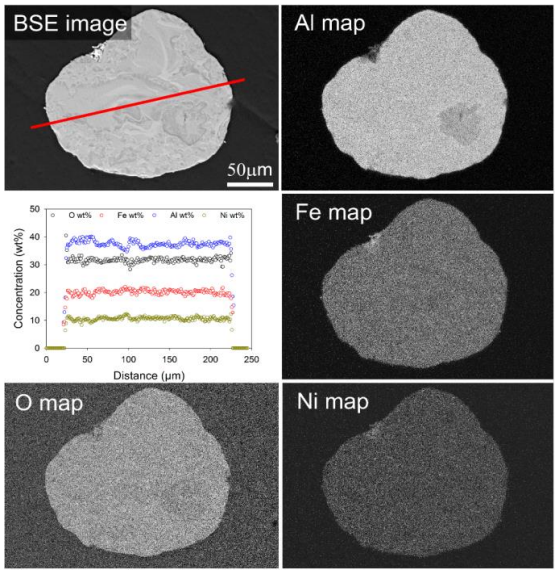

Figure 5-7: Backscattered Electron (BSE) image of a catalyst carrier cross section with corresponding X-ray element maps and quantitative line scan data. The linescan data was collected along the red line indicated on the BSE image.

found to be ~2:1, as anticipated. The BET surface areas of the produced Fe-Al_2O_3 and Fe-Ni-Al_2O_3 impregnated particles were measured to 102.9 and 97.2m^2/g, respectively. In comparison, the bare alumina support particles had a BET surface area of 206.0 m^2/g.

5.3.3 Methodology

The GSR concept operates in a cyclic mode by alternating air and fuel feeds to the reactor. During the experiment, various gas was fed to carry out reduction, reforming and oxidation reactions in a bubbling fluidized bed of solid oxygen carrier to produce syngas and pure CO_2 ready for storage or further utilization at the fuel stage. A fluidized bed was used to ensure good heat transfer and manage thermodynamic equilibria constraints[50]. About 300 ml of the oxygen carrier was placed initially in the reactor.

The GSR experiments were performed at different operating pressures ranging from 1 – 5bar at 800°C. Three-stage process (reduction, reforming and oxidation stage) was designed as explained in section 5.2 to complete a redox cycle. The cycle starts with the reduction stage where 0.8 - 4nl/min of CH_4 was fed into the reactor between 12 – 2.4min to reduce the Fe_2O_3/Ni/Al_2O_3 oxygen carrier for the catalysis of the steam methane reforming and other competing reactions as shown in ***R.5*** to ***R.9*** (*Figure* ***5-4***). After the reduction stage, the reforming stage starts through a combination of catalytic reforming and other heterogeneous reduction reactions to produce syngas (CO and H_2). A feed of air follows to oxidize back the reduced oxygen carrier following an exothermic reaction that builds up heat in the reactor. The generated heat is then being used in the subsequent fuel stage with mainly endothermic reactions (reduction and reforming). Five seconds purging with inert gas is applied between the air and fuel stages to avoid direct contact between them in the feed pipes, thereby eliminating the risk of explosion. Experiments for each operating condition were completed for at least ten redox cycles to ensure repeatability.

As mentioned earlier, real-time temperature and pressure measurements were collected using a Labview application while the online gas composition was measured using an ETG Syngas analyzer. The reactor performance at different temperatures was evaluated using the following measures: fuel conversion, CO and H_2 selectivity (expressed as H_2/CO and H_2/C ratios), degree of carbon deposition, as described in the next section. These performance measures are defined as specified in *Equation* ***5-1*** to *Equation* ***5-5***. The experimental results were compared with equilibrium predictions.

5.4 Reactor performance measures

The objective of the GSR process is to convert a hydrocarbon fuel (CH_4 in this study) to syngas (H_2 and CO). Therefore, it is desired to maximize the fuel conversion in the reduction stage, maximize CH_4 conversion at all stages. Thus, fuel conversion is an important measure to evaluate the performance of the GSR process. This can be quantified as follows:

$$\gamma_{fuel} = 1 - \frac{n_{fuel,out}}{n_{fuel,in}} \qquad \textit{Equation 5-1}$$

CO and H_2 are the major constituents of syngas that determine the quality and possible usage of syngas. It is therefore important to determine the syngas (H_2:CO) ratio as:

$$\frac{H_2}{CO} = \frac{n_{H_2,out}}{n_{CO,out}} \qquad \textit{Equation 5-2}$$

Significant carbon deposition could block the active sites of the oxygen carrier thereby leading to drop in activity. The deposited carbon would be released in the oxidation stage in form of CO_2. Carbon deposition is therefore and important performance measure and can be quantified as:

$$C_{deposition} = \frac{n_{C\_deposited}}{n_{fuel,converted}} = \frac{n_{C,in} - n_{C,out}}{\gamma_{fuel} * n_{fuel,in}} \qquad \textit{Equation 5-3}$$

Knowing the mechanism (methane cracking or Boudouard reaction) responsible for carbon deposition is important for process improvement. These mechanisms could be identified using H_2/C ratio. A high H_2/C ratio (>2.5) indicates that carbon deposition is mainly through methane cracking and vice versa.

$$\frac{H_2}{C} = \frac{n_{H_2,out}}{n_{CO_2,out} + n_{CO,out}} \qquad \textit{Equation 5-4}$$

The deposited carbon in the previous stage would gasify in presence of steam thus increasing syngas yield. This phenomenon was quantified using carbon deviation as described in *Equation*

5-5. The parameter is deduced from carbon balance with negative values indicating gasification phenomenon while positive values indicate no gasification.

$$Carbon\_dev = \frac{n_{C,in} - n_{C,out}}{n_{C,out}} = \frac{n_{C,in}}{n_{C,out}} - 1 \qquad \textit{Equation 5-5}$$

5.5 Result and Discussion

5.5.1 The behavior of the GSR concept

A three-stages (reduction, reforming and oxidation) cycle was designed to demonstrate the GSR using Fe-Ni/Al_2O_3 oxygen carrier at 1bar and 800°C as shown in *Figure* ***5-8***. The cycle starts with the reduction stage where dry CH_4 is fed to reduce the oxygen carrier, showing high CH_4 conversion (~97.61% close to equilibrium prediction) with a significant yield of CO_2 over several repeatable cycles. As CH_4 conversion starts to drop at the end of the reduction stage, steam is co-fed with CH_4 to start the reforming stage, showing an immediate positive effect by increasing back CH_4 conversion (beyond 90%) to syngas (H_2 and CO) instead of CO_2 as was happening in the reduction stage. CO_2 yield in this stage indicates the presence of water-gas shift reaction. Given that the reactions in both the reduction and reforming stages are

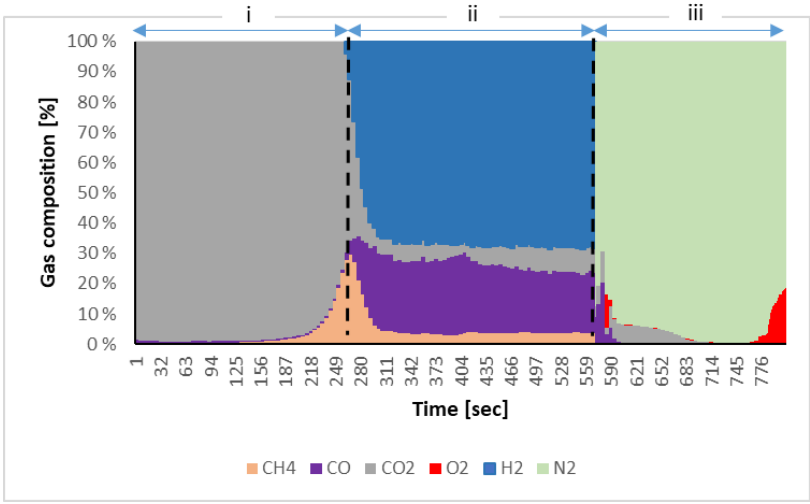

Figure 5-8: The transient dry gas composition at the reactor outlet and H_2/C ratio for a GSR cycle without partial oxidation stage at atmospheric pressure and 800°C. The GSR stages (reduction, reforming and oxidation) are numbered i, ii and iii respectively.

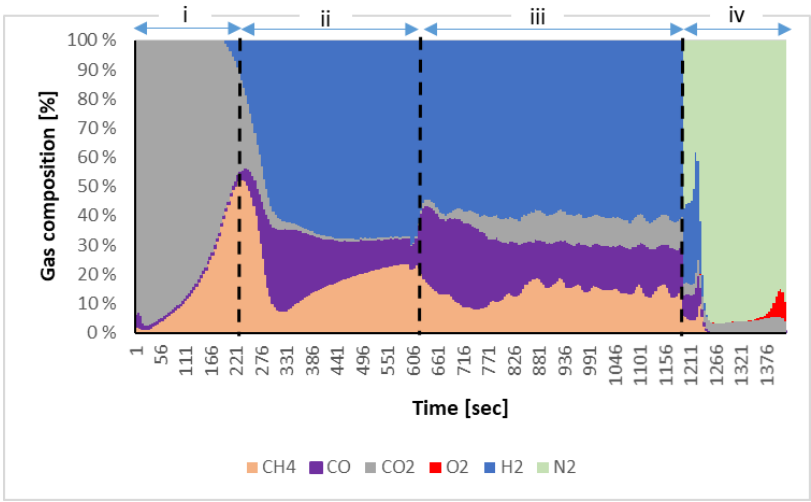

Figure 5-9: The transient dry gas composition at the reactor outlet of a GSR cycles with partial oxidation stage at atmospheric pressure and 800°C. The GSR stages (reduction, partial oxidation, reforming and oxidation) are numbered i, ii, iii and iv respectively.

endothermic and limited by equilibrium, it is necessary that the reforming stage is followed by an exothermic oxygen carrier oxidation stage with air feed, to provide the heat required for CH_4 conversion in the consecutive stages. The oxygen conversion is complete almost in the entire oxidation stage. A switch to the consecutive reduction stage is applied just after O_2 breakthrough (indicating complete oxidation of the oxygen carrier) to ensure maximizing heat usage by the endothermic reforming and reduction reactions (any further feed of air after O_2 breakthroughs leads to heat removal from the system).

It could, however, be observed that CO_2 is generated in the air stage, indicating the presence of deposited carbon from the precedents stages that combust with O_2 in this stage producing CO_2 The estimated total carbon deposition that leaks to the atmosphere in the air stage is ~1.1% of the total converted methane in the entire fuel stage (both reduction and reforming stages). Note that no carbon deposition has been detected when steam was co-fed with CH_4 in the reduction stage as well [45]. Carbon deposition through methane cracking was identified as one of the main mechanisms involved in both Fe_2O_3 and Fe_3O_4 reduction with methane, leading to high hydrogen yield [51]. To explore the prospects of exploiting the methane cracking mechanism in producing hydrogen, the feed of dry methane in the reduction stages has been prolonged, before co-feeding steam. Interestingly, an additional distinct stage appears between the reduction and reforming stages (*Figure **5-9***) where methane conversion improves back after it slows down at the end of the reduction stage, but towards syngas in this intermediate stage,

rather than CO_2. In this stage, the H_2/C ratio starts at values close to 2, indicating that syngas production begins through partial oxidation of methane ***R.3*** (*Figure **5-4***), but it rapidly increases to reach seven at the end of the stage, indicating that the syngas production mechanism quickly shifts to methane cracking. This is also confirmed by the transient carbon deposition showing a sharp increase in this intermediate stage. Note that methane conversion gradually decreases when methane cracking starts taking over but it remains much higher than the level obtained at the end of the reduction stage.

Mass balance calculation was completed for the reaction of CH_4 with Fe_2O_3/NiO to CH_4 and H_2O (assuming an ideal scenario where NiO reduces to Ni while Fe_2O_3 reduces to $FeAl_2O_4$ as shown by XRD analysis depicted in *Figure **5-5***). For a mass of 296 g of the Fe-Ni-Al_2O_3 oxygen carrier, with an active content of 35 wt.% (11.5 wt. NiO and 23.5 w. Fe_2O_3), the total moles of Fe_2O_3 available for the reaction is ~0.44 mol and for NiO is ~0.46 mol. For a CH_4 feed rate of 0.8 Nl/min ~410 seconds is needed to fully convert Fe_2O_3 to FeO (when full CH_4 conversion is assumed). It can however be seen in *Figure **5-9*** that the reduction stage with full selectivity to CO_2 is finished after only 205 s of reduction time, then syngas starts been produced. With the achieved 90% methane conversion rate in the reduction stage, only ~45% of available active content was consumed in the reduction stage, while the rest remains available for the subsequent partial oxidation (POX) and reforming stages. So, in principle, enough oxygen remains available for fully converting the fed methane in the POX stage through the partial oxidation of methane, but the results show that methane cracking overtakes instead. It is likely that the 50% reduced sites on the oxygen carrier were enough to ignite methane cracking.

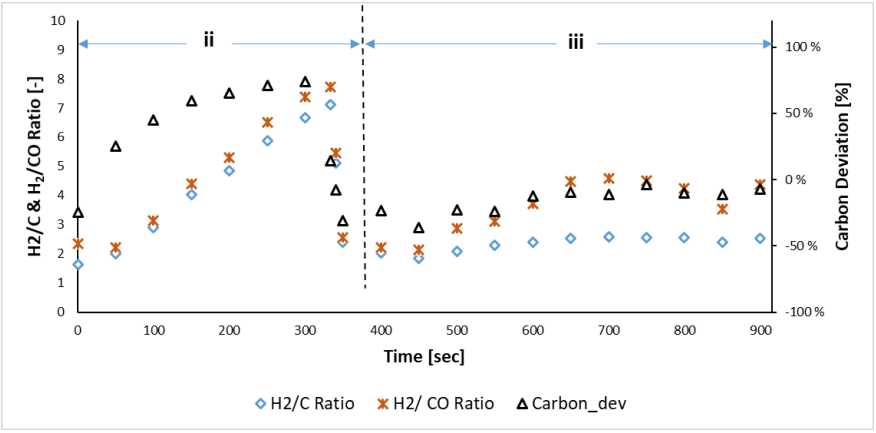

Figure 5-10: The transient H_2/C ratio, H_2/CO syngas ratio and Carbon deviation during the POX and Reforming stage of a GSR cycles at atmospheric pressure and 800°C. The GSR stages (partial oxidation and reforming) are numbered ii and iii respectively.

An immediate sharp drop in the H_2/C ratio occurs (reaching values close to 2) when steam is co-fed with CH_4 after the intermediate stage, combined with a large improvement in methane conversion (*Figure* ***5-10***). Interestingly, the transient carbon imbalance (*Equation* ***5-5***) is negative in this reforming stage, indicating the existence of a second source of syngas production, which is the gasification of carbon that has deposited in the previous stage, by the steam co-fed with methane. This carbon imbalance shows above 30% contribution of carbon gasification in the first third of reforming time but reduces to below 10% after, reflecting that steam methane reforming is becoming the dominating mechanism in syngas production. This is confirmed by the H_2/CO ratio that follows the same trend as the carbon imbalance, showing values ~2 in the first third of reforming time (high contribution of carbon gasification by steam) but increases gradually to stagnate at ~4 in the rest of the stage (methane reforming domination). CO_2 concentration starts very low in the reforming stage showing a gradual increase then plateaus as carbon gasification slows down, likely originating from the water-gas-shift reaction between the feed steam and the produced CO. The overall CH_4 conversion in this reforming stage was however lower than the case without the intermediate POX stage (*Figure* ***5-11***). It could be speculated that the high amount of carbon deposition on the oxygen carrier surface increases the resistance to gas diffusion to the catalytic sites of the oxygen carrier, leading to a reduced methane conversion.

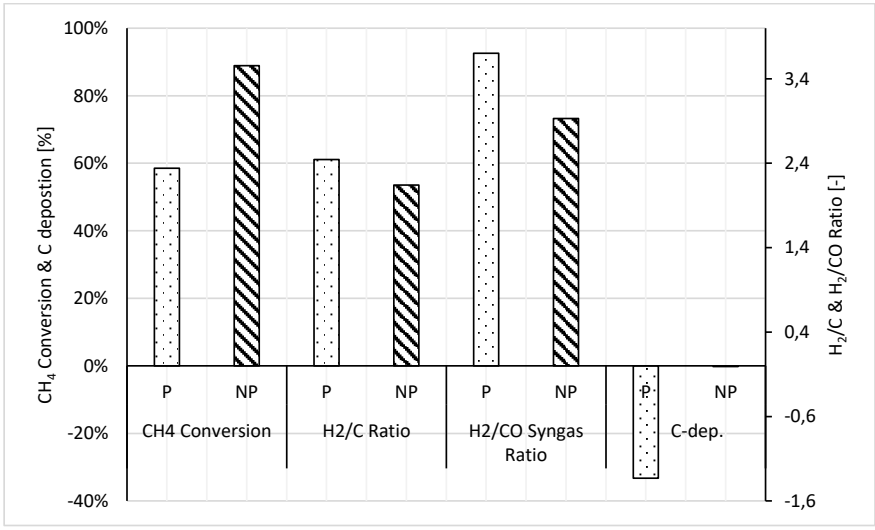

Figure 5-11: Comparison of the performance in the reforming stage (when steam is cofed with methane) between the case with and without POX at 1bar and 800°C. P and NP represents the case with Partial oxidation and without partial oxidation respectively.

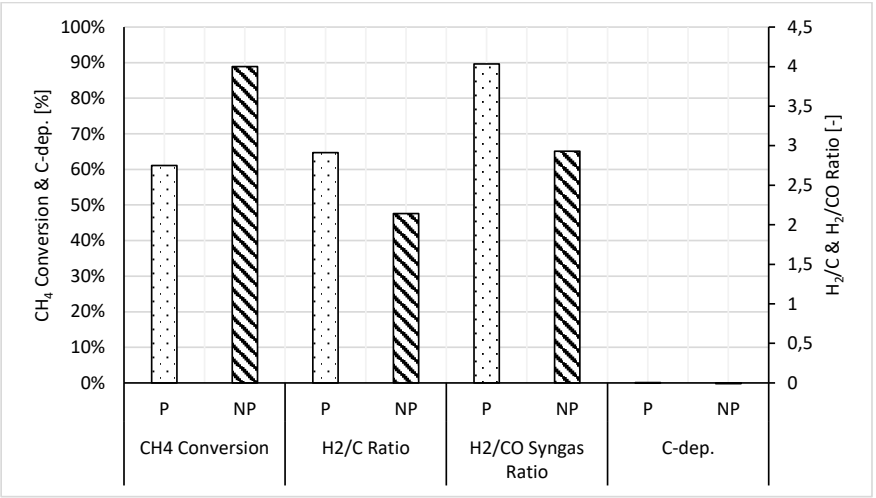

Figure 5-12: Comparison of the performance in the syngas production stage (POX + Ref) between the case with and without POX at 1bar and 800°C. P and NP represents the case with Partial oxidation and without partial oxidation respectively.

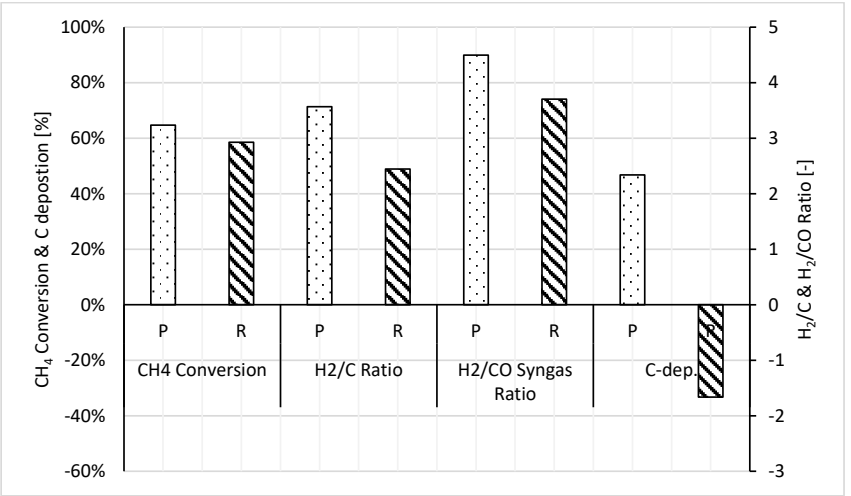

Figure 5-13: Comparison of the performance between the POX and reforming stage for the four-stages GSR cycle (with the intermediate POX case) at 1bar and 800°C. P and R represent the POX and the Reforming stages respectively.

In short, a large contribution of carbon gasification to syngas production occurs first when steam is co-fed with methane, then steam methane reforming dominates. The integral of the carbon balance shows that almost 100% of the total carbon deposited in the POX intermediate stage gasifies with steam in the reforming stage (*Figure **5-12***). Some of the deposited carbon is found to combust in the oxidation stage. This implies that some carbon deposition has happened

already in the reduction stage with dry methane. A longer reforming stage or an additional separate stage with only steam feed could be applied to fully remove the carbon before the air stage if high CO_2 capture efficiency is targeted. The heat balance is however an important factor to take in consideration when designing such a cycle targeting autothermal operation.

Overall, better total methane conversion was achieved in GSR configuration with only the reduction and reforming stage, with a lower H_2/CO ratio and minimal carbon deposition (*Figure **5-11***). However, given that the different mechanisms involved in syngas production through methane (SMR, POX, methane cracking) are affected differently by the operating pressure, the sensitivity study to the pressure was completed on the four-stages GSR cycle. This is especially important, given the well-known negative effect of pressure on steam methane reforming reaction (***R.7*** as shown in *Figure **5-4***) limited by equilibrium. As shown in Appendix , very high operating temperatures will be needed with the three-stages GSR process when high-pressure operation is targeted. Some fundamental differences in the performance between the POX and reforming stages could already be seen at atmospheric pressure with higher methane conversion and higher H_2/CO during the POX stage (*Figure **5-13***).

5.5.2 The effect of pressure

Experiments were completed for operating pressures up to 5 bar. The feed flow rates were increased proportionally to the pressure to maintain the gas superficial velocity in the reactor constant, while the stage time was decreased similarly to maintain the oxygen carrier utilization constant. All experiments were completed at a temperature of 800 °C. In general, methane conversion has a decreasing trend with increased pressure as shown in *Figure **5-14***. This behavior is consistent with thermodynamics since the overall reaction during the partial oxidation stage, and reforming is endothermic. Equilibrium predicts almost complete conversion for all stages up to 5bar. However, fuel conversion was below equilibrium prediction showing that the process is limited by kinetics. The highest conversion was achieved during the reduction stage, with almost no sensitivity to the pressure, followed by the POX stage and least during the reforming stage (*Figure **5-14***). This could be explained with the increasing endothermicity of the reaction from the reduction to the reforming stage. Pressure increase will thus result in more moles (molecules) per area within the system blocking active sites for reaction (*Figure **5-14***). The effect of pressure is more pronounced for the reforming stage with conversion dropping by approximately 57% by increasing the pressure from 1bar to 5bar (*Figure **5-14***).

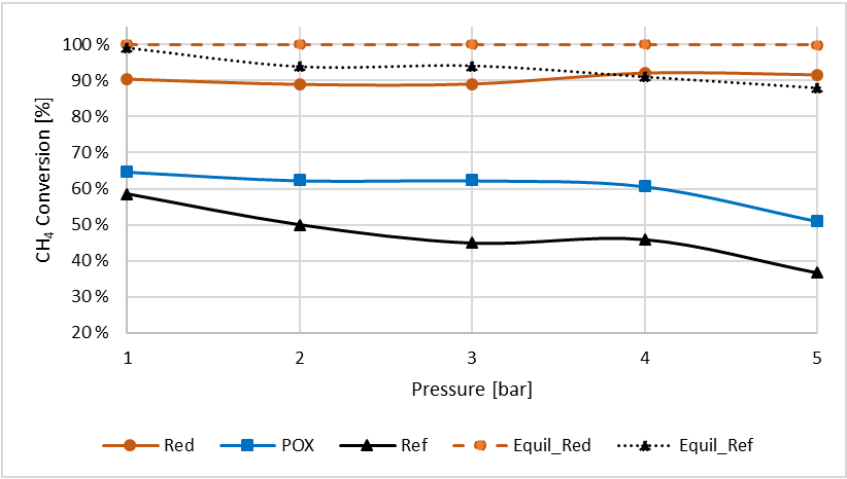

Figure 5-14: Methane conversion at different stages as a function of pressure at 800°C. Red represents the reduction stage, POX, partial oxidation and Ref, the reforming stage.

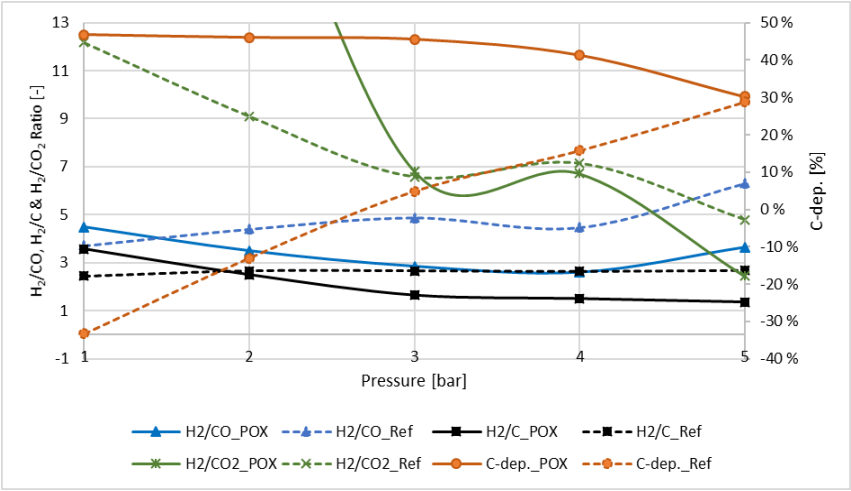

Figure 5-15: Performance (H_2/C ratio, H_2/CO syngas ratio and carbon deposition) at different stages as a function of pressure at 800°C. Red represents the reduction stage, POX, partial oxidation and Ref, the reforming stage.

The H_2/C and H_2/CO ratios reduce with pressure during the POX stage, conforming to thermodynamics as methane cracking reduces with pressure (*Figure* ***5-15***). The results show however that carbon deposition does not follow the sharp trend shown on the H_2/C and H_2/CO ratios, implying a change in the dominating carbon deposition mechanism from methane cracking to Boudouard. This can be clearly seen on the H_2/CO_2 ratio that decreases sharply from 42 at 1 bar to 6.7 at 3 bar and further down to ~4.8 at 5 bar (*Figure* ***5-15***). This means that the selectivity to CO_2 rapidly increases at higher pressure driven by the boudouard reaction (***R.9*** as shown in *Figure* ***5-4***).

As for the reforming stage, it was mentioned earlier that at 1 bar the carbon deposited in the POX stage was gasified by the co-fed steam in the subsequent reforming stage, leading to more than 30% excess of syngas production than would have originated from converted methane (*Figure **5-13***). This is concluded from the calculated negative carbon deposition in the reforming stage, interestingly showing gasification of high percentage of deposited carbon from the previous stage (a slightly longer reforming stage would have led to total gasification of the deposited carbon). The contribution of carbon gasification to syngas production in the reforming stage reduces systematically as the pressure is increased despite the high deposition rate in the previous stage (*Figure **5-15***). This is well in line with the thermodynamic predictions confirming the negative effect of pressure on steam gasification of carbon [52]. The carbon deposition in the reforming stage becomes positive above 3 bar reflecting the overtaking of the boudouard mechanism over steam carbon gasification as the pressure is further increased. As for the H_2/CO ratio, it has increased with pressure driven by the positive effect of pressure on Boudouard and Water-Gas-Shift reactions (*Figure **5-15***). Values beyond 6 were achieved at 5 bar, which could be interesting when hydrogen production is targeted.

The low conversion of methane in this reforming stage combined with the reducing ability in steam gasification of deposited carbon questions the usefulness of combining the POX and reforming stages for syngas production, with integrated CO_2 capture, when a high-pressure operation is targeted. Interestingly, the reducing carbon deposition in the POX, which accentuates at higher pressures, would remove the need for co-feeding steam in the subsequent stage, making the GSR process even simpler, easier to control and more energy-efficient, as steam generation won't be needed. Co-feeding of CO_2 with methane in the POX would also help in further suppressing carbon deposition by reversing the equilibrium Boudouard reaction. In this case, the contribution of methane dry reforming to syngas production should be expected due to the presence of CO_2 with methane on reduced Ni. The low H_2/CO ratio achieved in the POX makes the process better suitable to Fischer-Tropsh applications; this would be even lower if dry reforming is contributing to syngas production if CO_2 is co-fed in the POX. A shift and PSA steps could be applied if H_2 production is targeted.

Future research should focus on investigating the GSR with only the POX stage at higher pressures to confirm the trend of decreased carbon deposition at higher pressures and study the effect of CO_2 co-feeding on the performance in terms of methane conversion, carbon deposition, selectivity to hydrogen and CO and H_2/CO ratio. It is worth mentioning, that a recent study has shown that with a nonstoichiometric CH_4-CO_2 mixture feed (CO_2/CH_4 ratio=0.38) to

a 1 wt% Ni-entrapped Fe_2O_3/Al_2O_3 oxygen carrier at 900 °C, an H_2/CO ratio of 2.09 and high CO selectivity of 96.76% were achieved with minimized carbon deposition [53]. This study was completed at atmospheric pressure.

5.6 Conclusion

The performance of a four-stages GSR process for syngas production with integrated CO_2 capture was tested using an iron-based oxygen carrier. The cycle comprises a reduction stage with dry methane (PSA-off gas could also be used), followed by partial oxidation of methane stage (POX), then a reforming stage where steam is co-fed with methane, and finally the oxidation stage for heat production for the whole cycle by the exothermic oxidation reaction. Experiments were completed at 800°C and a pressure range of 1bar – 5bar. The oxygen carrier consisted of a Fe-Ni/Al_2O_3 prepared following impregnation routes. The effective active content of the oxygen carrier was 35 wt.% with a third of it being NiO and the other two-thirds are Fe_3O_4.

A high methane combustion rate was achieved in the reduction stage to drop at the end of the stage but increases back transitioning to syngas production instead of CO_2 in the reduction stage. At the beginning of the POX stage syngas was produced through partial oxidation of methane, but it shifted gradually to methane cracking, with a high H_2/CO ratio reaching 7 at the end of the stage. This resulted in substantial carbon deposition that gasified in the subsequent reforming stage by the co-fed steam, resulting in additional syngas production than estimated by the converted methane. Some deposited carbon slipped to the oxidation stage to combust with oxygen in the air feed, thereby reducing the overall CO_2 capture efficiency of the process.

Increased pressure has changed the carbon deposition mechanism in the POX stage from methane cracking to Boudouard, but it had a limited impact on the overall methane conversion in this stage. In parallel, increased pressure reduced the ability of co-fed steam in the reforming stage for gasifying the deposited carbon which consequently magnified the negative effect of pressure on overall methane conversion in this stage, leading to a substantial drop in methane conversion. Interestingly, the noticed overall reduction of carbon deposition in the POX stage with increased pressure suggests the possibility of removing the need for any feed of steam in a subsequent reforming stage, thereby maximizing the energy efficiency of the process as no expensive steam raise will be needed. It is therefore concluded that when high-pressure operation is targeted, a GSR process with only three stages (RED+POX+OXI) could be best

suited for syngas production with integrated CO_2 capture. Future research will explore further opportunities for optimizing the three-stages GSR process at even higher pressures.

Acknowledgment

ACT GaSTech project. Project No 271511.

This project has received funding from The Research Council of Norway and is cofounded by the European Commission under the Horizon 2020 program, ACT Grant Agreement No 691712. VATL Lab technicians at the Norwegian University of Science and Technology are equally acknowledged for constructing and maintaining the experimental setup.

Nomenclature

Abbreviations

BET	Brunauer–Emmett–Teller
BSE	Backscattered Electron
CCS	Carbon Capture and Storage
CFB	Circulating Fluidized Bed
CLC	Chemical Looping Combustion
CLR	Chemical Looping Reforming
EDS	Energy-Dispersive Spectroscopy
GSC	Gas Switching Combustion
GSR	Gas Switching Reforming
GST	Gas Switching Technology
OC	Oxygen Carrier
OXI	Oxidation
POX	Partial Oxidation
PSA	Pressure Swing Adsorption

RED	Reduction
REF	Reforming
SEM	Scanning Electron Microscope
SMR	Steam Methane Reforming
XRD	X-Ray Diffraction

Symbols

$C_{deposition}$	Carbon deposition
$Carbon\_dev$	Carbon deviation
$n_{C\_deposited}$	Mole of C deposited
$n_{C,in}$	Total mole of C fed
$n_{C,out}$	Mole of C at the gas outlet
$n_{CO,out}$	Mole of CO at the gas outlet
$n_{CO_2,out}$	Mole of CO_2 at the gas outlet
$n_{fuel,out}$	Mole of fuel at the gas outlet
$n_{fuel,in}$	Mole of fuel fed
$n_{fuel,converted}$	Mole of fuel converted
$n_{H_2,out}$	Mole of H_2 at the gas outlet
γ_{fuel}	Fuel conversion

References

[1] P. Nejat, F. Jomehzadeh, M. M. Taheri, M. Gohari, and M. Z. A. Majid, "A global review of energy consumption, CO2 emissions and policy in the residential sector (with an overview of the top ten CO2 emitting countries)," *Renewable and sustainable energy reviews,* vol. 43, pp. 843-862, 2015.

[2] J. Cook *et al.*, "Quantifying the consensus on anthropogenic global warming in the scientific literature," *Environmental research letters,* vol. 8, no. 2, p. 024024, 2013.

[3] E. J. Anthony, "Solid looping cycles: a new technology for coal conversion," *Industrial & Engineering Chemistry Research,* vol. 47, no. 6, pp. 1747-1754, 2008.

[4] M. Rydén and M. Arjmand, "Continuous hydrogen production via the steam–iron reaction by chemical looping in a circulating fluidized-bed reactor," *International Journal of Hydrogen Energy,* vol. 37, no. 6, pp. 4843-4854, 2012.

[5] J. Adanez, A. Abad, F. Garcia-Labiano, P. Gayan, and F. Luis, "Progress in chemical-looping combustion and reforming technologies," *Progress in energy and combustion science,* vol. 38, no. 2, pp. 215-282, 2012.

[6] M. Ishida, D. Zheng, and T. Akehata, "Evaluation of a chemical-looping-combustion power-generation system by graphic exergy analysis," *Energy,* vol. 12, no. 2, pp. 147-154, 1987.

[7] A. Lyngfelt, B. Leckner, and T. Mattisson, "A fluidized-bed combustion process with inherent CO2 separation; application of chemical-looping combustion," *Chemical Engineering Science,* vol. 56, no. 10, pp. 3101-3113, 2001.

[8] S. A. Wassie, F. Gallucci, A. Zaabout, S. Cloete, S. Amini, and M. van Sint Annaland, "Hydrogen production with integrated CO2 capture in a novel gas switching reforming reactor: Proof-of-concept," *International Journal of Hydrogen Energy,* vol. 42, no. 21, pp. 14367-14379, 2017/05/25/ 2017, doi: https://doi.org/10.1016/j.ijhydene.2017.04.227.

[9] S. A. Wassie *et al.*, "Hydrogen production with integrated CO2 capture in a membrane assisted gas switching reforming reactor: Proof-of-Concept," *International Journal of Hydrogen Energy,* vol. 43, no. 12, pp. 6177-6190, 2018/03/22/ 2018, doi: https://doi.org/10.1016/j.ijhydene.2018.02.040.

[10] B. Kronberger, E. Johansson, G. Loffler, T. Mattisson, A. Lyngfelt, and H. Hofbauer, "A two-compartment fluidized bed reactor for CO2 capture by chemical-looping combustion," *Chemical Engineering & Technology,* vol. 27, no. 12, pp. 1318-1326, Dec 2004, doi: 10.1002/ceat.200402137.

[11] C. Linderholm, A. Abad, T. Mattisson, and A. Lynyfelt, "160 h of chemical-looping combustion in a 10 kW reactor system with a NiO-based oxygen carrier," *International Journal of Greenhouse Gas Control,* vol. 2, no. 4, pp. 520-530, Oct 2008, doi: 10.1016/j.ijggc.2008.02.006.

[12] E. Johansson, T. Mattisson, A. Lyngfelt, and H. Thunman, "A 300 W laboratory reactor system for chemical-looping combustion with particle circulation," *Fuel,* vol. 85, no. 10-11, pp. 1428-1438, Jul-Aug 2006, doi: 10.1016/j.fuel.2006.01.010.

[13] N. Ding, W. R. Wang, Y. Zheng, C. Luo, P. F. Fu, and C. G. Zheng, "Development and Testing of an Interconnected Fluidized-Bed System for Chemical Looping Combustion," *Chemical Engineering & Technology,* vol. 35, no. 3, pp. 532-538, Mar 2012, doi: 10.1002/ceat.201100560.

[14] P. Kolbitsch, J. Bolhar-Nordenkampf, T. Proll, and H. Hofbauer, "Operating experience with chemical looping combustion in a 120 kW dual circulating fluidized bed (DCFB) unit,"

International Journal of Greenhouse Gas Control, vol. 4, no. 2, pp. 180-185, Mar 2010, doi: 10.1016/j.ijggc.2009.09.014.

[15] M. Ryden and A. Lyngfelt, "Using steam reforming to produce hydrogen with carbon dioxide capture by chemical-looping combustion," *International Journal of Hydrogen Energy,* vol. 31, no. 10, pp. 1271-1283, Aug 2006, doi: 10.1016/j.ijhydene.2005.12.003.

[16] M. Rydén, A. Lyngfelt, and T. Mattisson, "Synthesis gas generation by chemical-looping reforming in a continuously operating laboratory reactor," *Fuel,* vol. 85, no. 12-13, pp. 1631-1641, 2006.

[17] L. F. de Diego, M. Ortiz, F. García-Labiano, J. Adánez, A. Abad, and P. Gayán, "Hydrogen production by chemical-looping reforming in a circulating fluidized bed reactor using Ni-based oxygen carriers," *Journal of Power Sources,* vol. 192, no. 1, pp. 27-34, 2009/07/01/ 2009, doi: https://doi.org/10.1016/j.jpowsour.2008.11.038.

[18] T. Proell, J. Bolhar-Nordenkampf, P. Kolbitsch, and H. Hofbauer, "Syngas and a separate nitrogen/argon stream via chemical looping reforming - A 140 kW pilot plant study," *Fuel,* vol. 89, no. 6, pp. 1249-1256, Jun 2010, doi: 10.1016/j.fuel.2009.09.033.

[19] Q. Zafar, T. Mattisson, and B. Gevert, "Redox investigation of some oxides of transition-state metals Ni, Cu, Fe, and Mn supported on SiO2 and MgAl2O4," *Energy & Fuels,* vol. 20, no. 1, pp. 34-44, Jan-Feb 2006, doi: 10.1021/ef0501389.

[20] M. N. Khan and T. J. A. e. Shamim, "Investigation of hydrogen generation in a three reactor chemical looping reforming process," vol. 162, pp. 1186-1194, 2016.

[21] M. N. Khan and T. J. I. J. o. H. E. Shamim, "Techno-economic assessment of a plant based on a three reactor chemical looping reforming system," vol. 41, no. 48, pp. 22677-22688, 2016.

[22] M. N. Khan and T. J. I. J. o. H. E. Shamim, "Exergoeconomic analysis of a chemical looping reforming plant for hydrogen production," vol. 42, no. 8, pp. 4951-4965, 2017.

[23] M. N. Khan and T. J. I. J. o. H. E. Shamim, "Thermodynamic screening of suitable oxygen carriers for a three reactor chemical looping reforming system," vol. 42, no. 24, pp. 15745-15760, 2017.

[24] S. Cloete, M. N. Khan, and S. J. I. J. o. H. E. Amini, "Economic assessment of membrane-assisted autothermal reforming for cost effective hydrogen production with CO2 capture," vol. 44, no. 7, pp. 3492-3510, 2019.

[25] S. M. Nazir, J. H. Cloete, S. Cloete, and S. J. E. Amini, "Gas switching reforming (GSR) for power generation with CO2 capture: Process efficiency improvement studies," vol. 167, pp. 757-765, 2019.

[26] S. M. Nazir, S. Cloete, O. Bolland, and S. J. I. J. o. H. E. Amini, "Techno-economic assessment of the novel gas switching reforming (GSR) concept for gas-fired power production with integrated CO2 capture," vol. 43, no. 18, pp. 8754-8769, 2018.

[27] S. Nazir, O. Bolland, and S. J. E. Amini, "Analysis of combined cycle power plants with chemical looping reforming of natural gas and pre-combustion CO2 capture," vol. 11, no. 1, p. 147, 2018.

[28] S. M. Nazir, O. Bolland, and S. J. E. P. Amini, "Full plant scale analysis of natural gas fired power plants with pre-combustion CO2 capture and Chemical Looping Reforming (CLR)," vol. 114, pp. 2146-2155, 2017.

[29] K. Z. Li, H. Wang, Y. G. Wei, and D. X. Yan, "Transformation of methane into synthesis gas using the redox property of Ce-Fe mixed oxides: Effect of calcination temperature," *International Journal of Hydrogen Energy,* vol. 36, no. 5, pp. 3471-3482, Mar 2011, doi: 10.1016/j.ijhydene.2010.12.038.

[30] X. Zhu, K. Z. Li, Y. G. Wei, H. Wang, and L. Y. Sun, "Chemical-Looping Steam Methane Reforming over a CeO2-Fe2O3 Oxygen Carrier: Evolution of Its Structure and Reducibility," *Energy & Fuels,* vol. 28, no. 2, pp. 754-760, Feb 2014, doi: 10.1021/ef402203a.

[31] Y. Zheng *et al.*, "Designed oxygen carriers from macroporous LaFeO3 supported CeO2 for chemical-looping reforming of methane," *Applied Catalysis B: Environmental,* vol. 202, pp. 51-63, 2017.

[32] H. P. Hamers, M. C. Romano, V. Spallina, P. Chiesa, F. Gallucci, and M. v. S. Annaland, "Comparison on process efficiency for CLC of syngas operated in packed bed and fluidized bed reactors," *International Journal of Greenhouse Gas Control,* vol. 28, no. 0, pp. 65-78, 2014, doi: http://dx.doi.org/10.1016/j.ijggc.2014.06.007.

[33] R. Xiao, L. Chen, C. Saha, S. Zhang, and S. Bhattacharya, "Pressurized chemical-looping combustion of coal using an iron ore as oxygen carrier in a pilot-scale unit," *International Journal of Greenhouse Gas Control,* vol. 10, pp. 363-373, 2012.

[34] J. Adanez, A. Abad, F. Garcia-Labiano, P. Gayan, and L. F. de Diego, "Progress in Chemical-Looping Combustion and Reforming technologies," *Progress in Energy and Combustion Science,* vol. 38, no. 2, pp. 215-282, Apr 2012, doi: 10.1016/j.pecs.2011.09.001.

[35] A. Zaabout, S. Cloete, S. T. Johansen, M. van Sint Annaland, F. Gallucci, and S. Amini, "Experimental demonstration of a novel gas switching combustion reactor for power production with integrated CO2 capture," *Industrial & Engineering Chemistry Research,* vol. 52, no. 39, pp. 14241-14250, 2013.

[36] S. Noorman, M. van Sint Annaland, and Kuipers, "Packed Bed Reactor Technology for Chemical-Looping Combustion," *Industrial & Engineering Chemistry Research,* vol. 46, no. 12, pp. 4212-4220, 2007/06/01 2007, doi: 10.1021/ie061178i.

[37] H. P. Hamers, F. Gallucci, P. D. Cobden, E. Kimball, and M. van Sint Annaland, "A novel reactor configuration for packed bed chemical-looping combustion of syngas," *International Journal of Greenhouse Gas Control,* vol. 16, no. 0, pp. 1-12, 2013, doi: http://dx.doi.org/10.1016/j.ijggc.2013.02.021.

[38] A. Zaabout, S. Cloete, and S. Amini, "Hydrodynamic Investigation Into a Novel IC-CLC Reactor Concept For Power Production With Integrated CO2 Capture," in *10th International Conference on Computational Fluid Dynamics In the Oil & Gas, Metallurgical and Process Industries*, Trondheim, Norway, 17-19 June 2014.

[39] M. Osman, A. Zaabout, S. Cloete, and S. Amini, "Internally circulating fluidized-bed reactor for syngas production using chemical looping reforming," *Chemical Engineering Journal,* 2018/10/04/ 2018, doi: https://doi.org/10.1016/j.cej.2018.10.013.

[40] A. Zaabout, S. Cloete, S. T. Johansen, M. v. S. Annaland, F. Gallucci, and S. Amini, "Experimental Demonstration of a Novel Gas Switching Combustion Reactor for Power Production with Integrated CO2 Capture," *Industrial & Engineering Chemistry Research,* vol. 52, no. 39, pp. 14241-14250, Oct 2 2013, doi: 10.1021/ie401810n.

[41] S. M. Nazir, J. H. Cloete, S. Cloete, and S. J. E. Amini, "Gas switching reforming (GSR) for power generation with CO2 capture: Process efficiency improvement studies," 2018.

[42] A. Zaabout, S. Cloete, and S. Amini, "Autothermal operation of a pressurized Gas Switching Combustion with ilmenite ore," *International Journal of Greenhouse Gas Control,* vol. 63, pp. 175-183, 2017/08/01/ 2017, doi: https://doi.org/10.1016/j.ijggc.2017.05.018.

[43] M. Ortiz, A. Abad, F. Luis, F. García-Labiano, P. Gayán, and J. Adánez, "Optimization of hydrogen production by chemical-looping auto-thermal reforming working with Ni-based oxygen-carriers," *international journal of hydrogen energy,* vol. 36, no. 16, pp. 9663-9672, 2011.

[44] S. M. Nazir, S. Cloete, O. Bolland, and S. Amini, "Techno-economic assessment of the novel gas switching reforming (GSR) concept for gas-fired power production with integrated CO2 capture," *International Journal of Hydrogen Energy,* vol. 43, no. 18, pp. 8754-8769, 2018.

[45] A. Zaabout, P. I. Dahl, A. Ugwu, J. R. Tolchard, S. Cloete, and S. Amini, "Gas Switching Reforming (GSR) for Syngas Production with Integrated CO2 Capture Using Iron-Based Oxygen Carriers," *International Journal of Greenhouse Gas Control* vol. Submitted, 2018.

[46] A. Zaabout, P. I. Dahl, A. Ugwu, J. R. Tolchard, S. Cloete, and S. J. I. J. o. G. G. C. Amini, "Gas Switching Reforming (GSR) for syngas production with integrated CO2 capture using iron-based oxygen carriers," vol. 81, pp. 170-180, 2019.

[47] C. E. Agu *et al.*, "Investigation of Bubbling Behaviour in Deep Fluidized Beds at Different Gas Velocities using Electrical Capacitance Tomography," 2019.

[48] C. E. Agu, L.-A. Tokheim, M. Eikeland, and B. M. J. C. E. J. Moldestad, "Determination of onset of bubbling and slugging in a fluidized bed using a dual-plane electrical capacitance tomography system," vol. 328, pp. 997-1008, 2017.

[49] J. C. Abanades, E. J. Anthony, J. Wang, J. E. J. E. S. Oakey, and Technology, "Fluidized bed combustion systems integrating CO2 capture with CaO," vol. 39, no. 8, pp. 2861-2866, 2005.

[50] K. Svoboda, G. Slowinski, J. Rogut, D. J. E. C. Baxter, and Management, "Thermodynamic possibilities and constraints for pure hydrogen production by iron based chemical looping process at lower temperatures," vol. 48, no. 12, pp. 3063-3073, 2007.

[51] E. R. Monazam, R. W. Breault, R. Siriwardane, G. Richards, and S. Carpenter, "Kinetics of the reduction of hematite (Fe2O3) by methane (CH4) during chemical looping combustion: A global mechanism," *Chemical Engineering Journal,* vol. 232, pp. 478-487, 2013/10/01/ 2013, doi: https://doi.org/10.1016/j.cej.2013.07.091.

[52] D. Roberts, D. J. E. Harris, and Fuels, "Char gasification with O2, CO2, and H2O: Effects of pressure on intrinsic reaction kinetics," vol. 14, no. 2, pp. 483-489, 2000.

[53] D. Kang, H. S. Lim, M. Lee, and J. W. J. A. E. Lee, "Syngas production on a Ni-enhanced Fe 2 O 3/Al 2 O 3 oxygen carrier via chemical looping partial oxidation with dry reforming of methane," vol. 211, pp. 174-186, 2018.

[54] K. Svoboda, G. Slowinski, J. Rogut, and D. Baxter, "Thermodynamic possibilities and constraints for pure hydrogen production by iron based chemical looping process at lower temperatures," *Energy conversion and management,* vol. 48, no. 12, pp. 3063-3073, 2007.

[55] J. Solsvik, T. Haug-Warberg, and H. A. Jakobsen, "Implementation of chemical reaction equilibrium by Gibbs and Helmholtz energies in tubular reactor models: application to the steam–methane reforming process," *Chemical Engineering Science,* vol. 140, pp. 261-278, 2016.

[56] I. Barin and G. Platzki, *Thermochemical data of pure substances* (no. 334). Wiley Online Library, 1989.

Appendix

Thermodynamic analysis

The equilibrium prediction of different possible reaction paths was performed by minimizing the Gibbs energy function through material balance using non-stoichiometric approach. Fifteen possible reactions have been identified and analysed. The equilibrium predictions were compared with experimental results to identify the dominating reaction path at different GSR stages. The equilibrium calculation was implemented using HSC Chemistry by feeding stoichiometric amounts of the reactants and indicating all the possible products. By minimizing free energy, the equilibrium composition at 800°C and pressure between 1-5bar were estimated. Ideal mixture was assumed and the oxygen carrier only in solid phase with the activity coefficient of unity (pure substance in condensed phase). Fuel conversion is an important parameter that determines how much fuel required across each stage. Therefore, fuel conversion was estimated following the same assumptions proposed in the article of Svoboda, et al. [54].

From the 2nd law of thermodynamics, the expression of the Gibbs free energy at constant temperature and pressure is given as: [55].

$$dG|_{T,p} = \sum_{i=1}^{N_{species}} \left[\frac{\partial G}{\partial n_i}\right]_{T,p,n_{j\neq i}} \qquad \textit{Equation 6}$$

Assuming ideal gas, for minimum Gibbs free energy, $dG|_{T,p} = 0$ for some n. It is also required that the Hessian matrix ($\partial^2 G/\partial n_i \partial n_j$) is positive.The Gibbs free energy of the reaction is calculated as follows [56]:

$$\Delta G_r = \sum G_i(final) - \sum G_i(initial) \qquad \textit{Equation 7}$$

where $\sum G_i(final)$ is the sum of the Gibbs free energies of the product and $\sum G_i(initial)$ is the total Gibbs energy of the reactants. The equilibrium constant is then calculated:

$$K^0(T) = \exp\left(-\frac{\Delta G_r}{RT}\right)$$ *Equation 8*

In terms of the partial pressures and activity coefficient, equilibrium constant can be expressed as:

$$K^0 = \frac{\prod(\alpha_{\text{product i}})^{s_i}}{\prod(\alpha_{\text{reactant i}})^{s_i}} = \frac{\prod(P_{\text{product i}})^{s_i}}{\prod(P_{\text{reactant i}})^{s_i}}$$ *Equation 9*

where α_i is the chemical activity of the compound i, p_i is the partial pressure of the gaseous compound i and s_i the stoichiometric coefficient of the compound i.

Reaction 1

$2CO \rightarrow CO_2 + C$

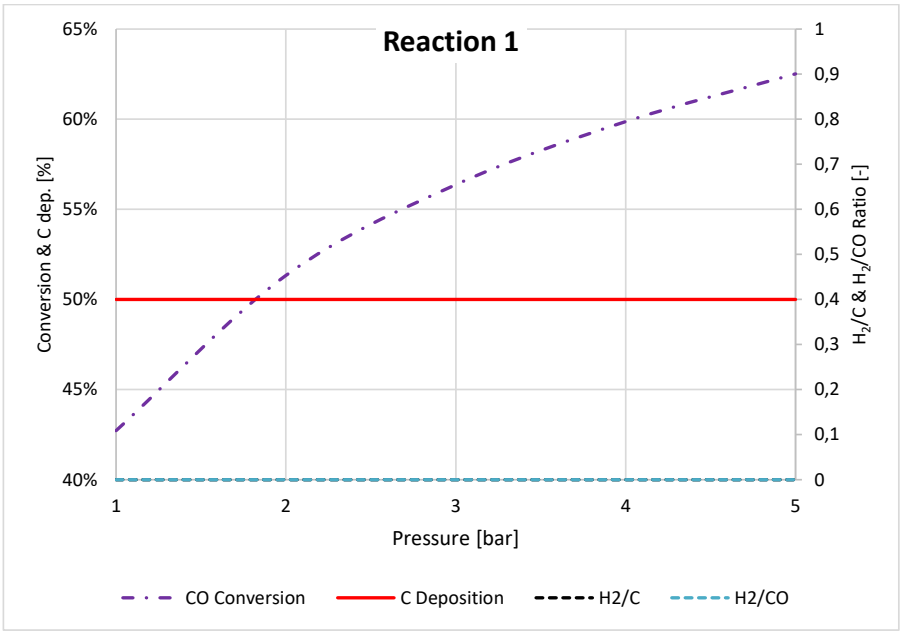

Reaction 2:

Cracking $CH_4 \rightarrow C + 2H_2$

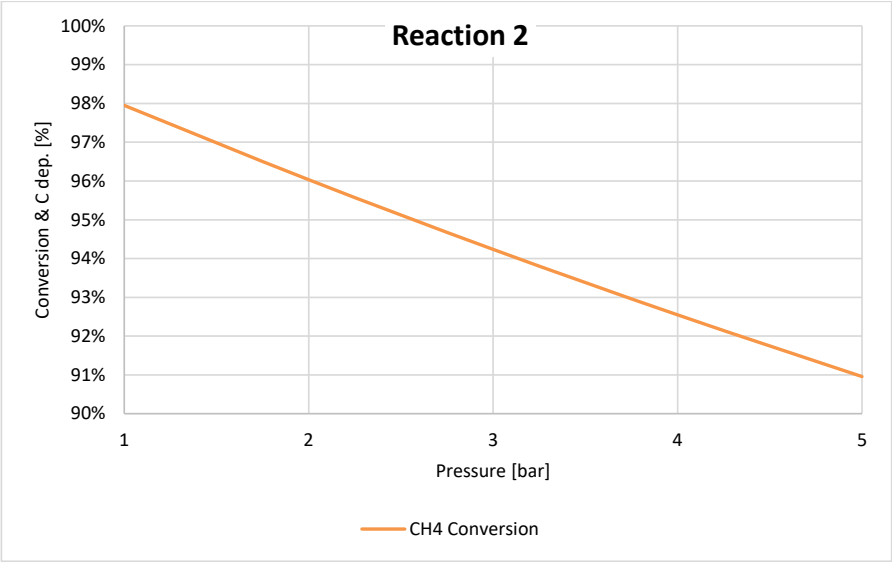

Reaction 3:

Shift reaction $CO + H_2O \rightarrow H_2 + CO_2$

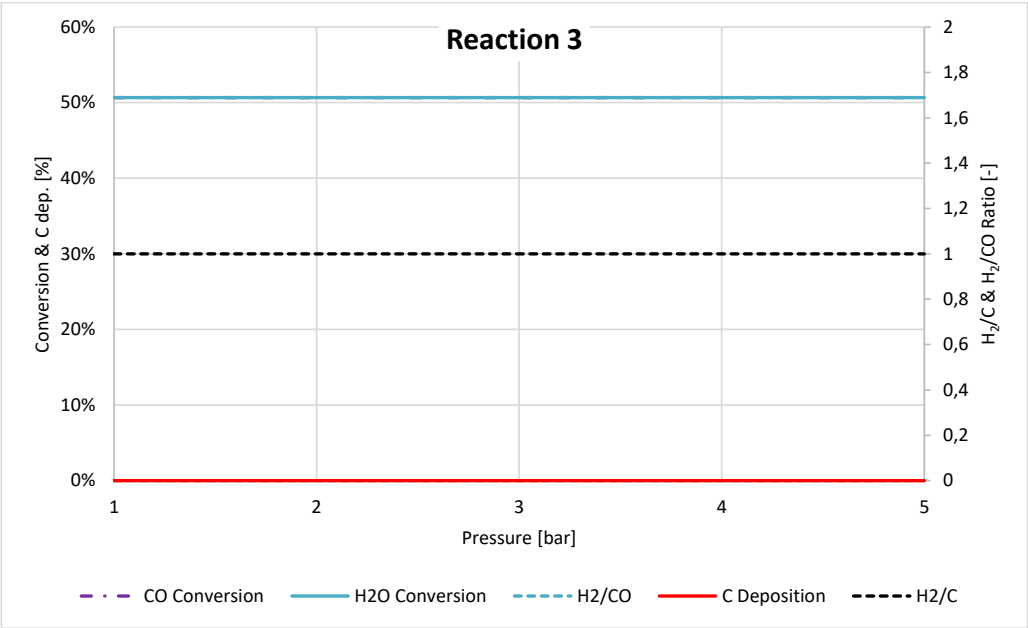

Reaction 4:

SMR $CH_4 + H_2O \rightarrow CO + 3H_2$

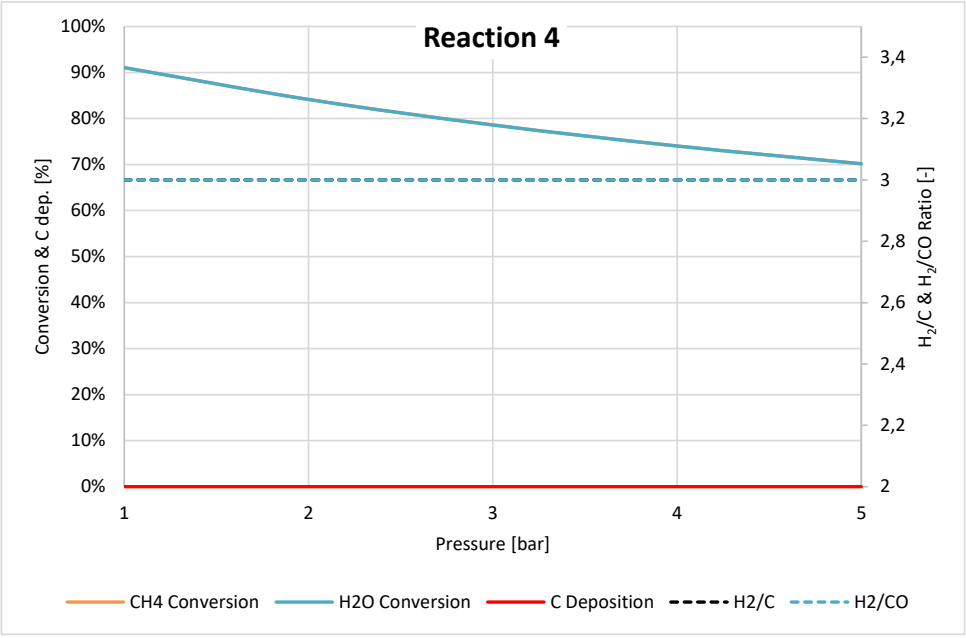

6 An Advancement in CO_2 Utilization through Novel Gas Switching Dry Reforming.

This chapter has been adapted from **Article III**

Ugwu, A., A. Zaabout, and S. Amini, *An advancement in CO_2 utilization through novel gas switching dry reforming.* International Journal of Greenhouse Gas Control, 2019. 90: p. 102791.

Abstract

This study is the first experimental demonstration of CO_2 capture and utilization for dry methane reforming using a novel chemical looping concept, "Gas Switching Dry Reforming" (GSDR) to produce syngas. This new reactor concept utilizes a single fluidized bed reactor to complete redox (reactions) cycles by alternating air and gaseous fuel feeds, generating heat and near pure CO_2 for usage in a consecutive dry reforming stage. Autothermal operation of GSDR was achieved using NiO/Al_2O_3 oxygen carrier, in a three-stages GSDR configuration where pure CO is used in the reduction stage while methane and CO_2 are fed only in the reforming stage. Most of the heat duties of the process is generated by the exothermic oxidation reaction. The reforming stage is very sensitive to temperature with very good methane and CO_2 conversion achieved at 850°C but dropped rapidly at lower temperatures. Carbon deposition is a major issue affecting the performance of the GSDR process although this was found to be minimized by a combination of high operating temperature and a larger CO_2/CH_4 ratio, but also led to low H_2/CO molar ratio driven by the reversed water gas shift reaction. By reducing the utilization of the oxygen carrier by 50% also proved to decrease carbon deposition by 62% due to the presence of latent oxygen on the oxygen carrier. However, CH_4 and CO_2 conversion are affected negatively resulting in a drop of ~22%. An excellent opportunity for maximizing the energy efficiency of the GSDR is by integration with a Gas-To-Liquid (GTL) Fisher Tropsch to use outlet gas stream from the reforming as feedstock to GTL while the unconverted hot gasses from GTL process is fed to the reduction stage of GSDR.

Keywords: Chemical looping; Dry reforming, CO_2 capture, and utilization, Gas switching technology; Hydrogen and syngas production; Natural gas reforming.

6.1 Introduction

CO_2 and CH_4 are the two major primary greenhouse gases (GHG) that pose a threat to the world today through global warming and climate change. As global energy demand and consumption of fossil fuel continue to increase, CCS remains a viable and cost-effective technology to combat greenhouse gas emission and achieve the Paris Climate Accord goals of maintaining the global temperature increase within 1.5 °C [1]. With the projection that natural gas would be the fastest-growing fossil fuel in the coming decades [2, 3], CO_2 methane reforming (dry reforming) would therefore be an attractive technology that can sustainably utilize CO_2 and the abundant natural gas (CH_4) not only to reduce GHG emission but also produce valuable products (syngas) for various applications [4-6].

The particularity of syngas produced from the dry reforming process is the H_2/CO ratio which is close to unity (*Reaction **6-1***), being especially suitable for the synthesis of liquid hydrocarbons, (through the Fisher Tropsch process), oxygenates, and other industrially relevant chemicals[7]. Although the working principle of dry reforming has been experimentally tested, where tens of studies were published for this process mainly about catalyst development [8-13], there are various factors that are still limiting its industrial deployment. Firstly, the reaction is highly endothermic making the process energy intensive requiring an operating temperature above 800°C in order to achieve high conversion [14]. This involves large CO_2 emissions as fossil fuel is used for supplying heat to the endothermic dry reforming reactions. Another major drawback that hampers the commercialization of the process is the high degree of carbon deposition through different mechanisms (*Reaction **6-3*** and *Reaction **6-4***), leading to fast catalyst deactivation [15]. Several studies attempted to tackle the carbon deposition issue through catalyst development [16-18]. Alternatively, it has been shown that a CO_2/CH_4 molar ratio higher than stoichiometry (unity) could improve the reaction kinetics and lead to high syngas yield [14]. Consequently, this leads to low syngas purity due to the presence of excess CO_2 in the produced syngas. Another side effect of feeding excess CO_2 is the low H_2 yield resulting from the reverse water-gas shift reaction. It is, therefore, crucial to develop new technologies that can address the aforementioned issues of dry reforming to make the process environmentally and economically viable for commercial deployment.

$$CH_4 + CO_2 \rightarrow 2CO + 2H_2 \qquad (\Delta H_{298K} = +247 KJmol^{-1}) \qquad \textit{Reaction 6-1}$$

$$CO_2 + H_2 \leftrightarrow CO + H_2O \qquad (\Delta H_{298K} = +41 KJmol^{-1}) \qquad \textit{Reaction 6-2}$$

$$CH_4 \rightarrow C + 2H_2 \qquad (\Delta H_{298K} = +74.9 KJmol^{-1}) \qquad \textit{Reaction 6-3}$$

$$2CO \leftrightarrow C + CO_2 \qquad (\Delta H_{298K} = -172.4 KJmol^{-1}) \qquad \textit{Reaction 6-4}$$

This paper demonstrates a novel chemical looping technology "Gas Switching Dry Reforming (GSDR)" which combines carbon capture and utilization in a single process to produce syngas (H_2 + CO). The aim is to use a novel chemical looping reactor design that can be easily pressurized and scaled up to minimize CO_2 emissions in dry reforming processes by integrating carbon capture in one step and possible utilization of the captured CO_2 as a feedstock for *Reaction **6-1*** in another step as explained in *section **6.2***. If successfully demonstrated and scaled up, this technology can offer a sustainable solution for the costly CO_2 transport and storage issue hindering the implementation of CCS technology. This paper also explores and maps out the opportunities offered by the proposed technology for minimizing carbon deposition on the catalyst/oxygen carrier and maximizing the fuel conversion.

6.2 Gas Switching Dry Reforming

Chemical looping technology is an emerging low-carbon technology which typically employs an interconnected fluidized bed reactor system that circulates a metal oxide (oxygen carrier) to transfer oxygen from the air reactor to the fuel reactor for combusting fuel gases in a N_2-free environment, producing a pure CO_2 stream ready for storage or further utilization (*Figure **6-1*** a) [19, 20]. The low energy penalty of this technology relative to other CCS technologies has led to the extension to other energy-intensive processes such as steam-iron process, low

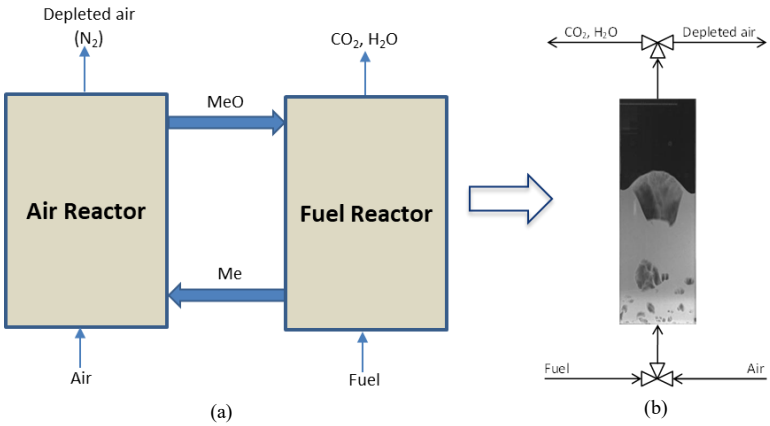

Figure 6-1: (a): Conventional Chemical Looping Combustion Reactor Concept. (b): Simplified Gas Switching Reactor Concept for fuel combustion with integrated CO_2 capture.

emission coal conversion, methane reforming, etc. [21, 22]. The major drawback of the traditional chemical looping systems using CFB configuration is the operational challenges associated with high-pressure processes reflecting why most of the experimental demonstrations were carried out under atmospheric conditions [23-31]. Solid circulation between interconnected reactors would be difficult to achieve under pressurized conditions given that each reactor is pressurized independently while fulfilling the essential need for heat and mass balance. Any instantaneous pressure imbalance between the reactors would induce instabilities and could result in leakages through the sealing devices, thereby increasing the risk of explosion. Even with these limitations, high-pressure operation is however prerequisite in order to maximize the overall process efficiency.

To address the challenges facing pressurized chemical looping applications, recent research has focused on the development of alternative reactor designs with the ability to operate under pressurized conditions [32-36]. One of the promising reactor designs is the Gas Switching Technology (GST) that utilizes only one fluidized bed reactor and avoids solid circulation by alternating the feeds of the oxidizing and reducing gases to depict different redox stages as shown in *Figure **6-1** b*. The reactor choice for a fluidized bed is driven by the previous study that fluidized bed reactors exhibited the highest activity, catalyst stability, lower carbon deposition, and higher conversion compared to a fixed-bed counterpart [37]. Since solid circulation is avoided, GST does not require separation systems like cyclone and loop seals making it less expensive and simpler compared with traditional chemical looping systems. The GST reactor concept has been applied for power production through combustion [38-40] and syngas production through steam methane reforming with integrated CO_2 capture [41-44]. Experimental demonstration studies have also proved the ease of autothermal operation for both combustion and reforming [39, 41, 42]. To capitalize on this success, this study extends the GST concept to dry reforming process for syngas production referred to as Gas Switching Dry Reforming (GSDR).

The working principle of Gas Switching Dry Reforming (GSDR) is very similar to the Gas Switching Reforming (GSR) demonstrated earlier for syngas production with integrated CO_2 capture [41, 43]. It is a three-stage process as illustrated in *Figure **6-2*** comprising of a **fuel stage** where the oxygen carrier is reduced to metallic radical to catalyze the endothermic dry reforming reaction at the consecutive **reforming stage**. The third stage is the **air stage** where the oxygen carrier is reoxidized to generate the heat needed for the highly endothermic dry reforming reaction. In this process, the solid particle plays simultaneous roles of oxygen carrier

and catalyst for dry methane reforming. To demonstrate autothermal operation of the GSDR process, part of the CO produced during the reforming stage is used as fuel in the reduction stage to sustain the bed temperature since the reduction reaction of NiO with CO is slightly exothermic. The separate reduction stage of GSDR will especially be beneficial if the GSDR is integrated with a Gas-To-Liquid (GTL) process, allowing the unconverted GTL outlet gases to be fed to the reduction stage of GSDR (*Figure **6-3***), thereby maximizing fuel usage and overall process efficiency. However, if a similar GSDR process should be implemented with the conventional chemical looping concept using the circulating fluidized bed (CFB) configuration, three interconnected reactors would be required as shown in *Figure **6-2***a, thus increasing the difficulties in controlling the solids circulation rate to meet the tight heat and mass balance of the three separate reactors. A two-reactor CFB configuration could work if the fuel reactor is fed with methane for simultaneous reduction of oxygen carrier and reforming. In this case, the oxidation degree and circulation rate of the oxygen carrier should be well controlled for maximizing the selectivity to syngas instead of CO_2 (if excess of oxygen is available on the oxygen carrier) while accurately supplying the heat needed for the endothermic dry reforming reaction. The two-reactor CFB configuration would also make it difficult to feed GTL unconverted gasses, thereby reducing the process flexibility and its potential for maximizing its energy efficiency. A major advantage of GSDR process is the efficient use of the reaction heat produced during the oxidation stage for the endothermic reforming stage, since the reactions occur in a single reactor vessel, thus facilitating its autothermal operation [45]. The redox reactions involved when a Ni-based oxygen carrier is used are specified in (*Reaction **6-5*** and *Reaction **6-6***) [38, 46], while *Reaction **6-1*** to *Reaction **6-4*** takes place in the reforming stage.

Fuel stage

$$CO + NiO \rightarrow Ni + CO_2 \qquad (\Delta H_{298K} = -43.3 KJmol^{-1}) \qquad \textit{Reaction 6-5}$$

Air Stage

$$Ni + O_2 \rightarrow 2NiO \qquad (\Delta H_{298K} = -479.4 KJmol^{-1}) \qquad \textit{Reaction 6-6}$$

Like other gas switching concepts, GSDR faces the challenge of undesired mixing when switching the inlet feed gases. In the case of GSDR, undesired mixing will cause some N_2 to leak into the syngas and some CO_2 to escape to the atmosphere with the depleted air. This leakage is small for reforming concepts though. For example, reactor modeling in a previous study on GSR showed that 97% CO_2 capture could be achieved despite this undesired mixing [47].

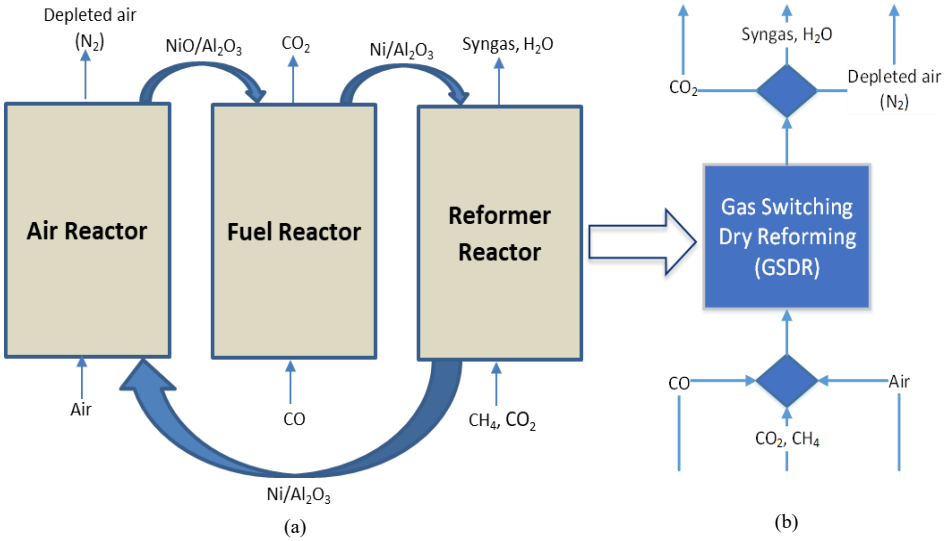

Figure 6-2: Conceptual schemes of dry reforming process. (a): completed following the chemical looping route. (b): Gas Switching Dry Reforming, GSDR.

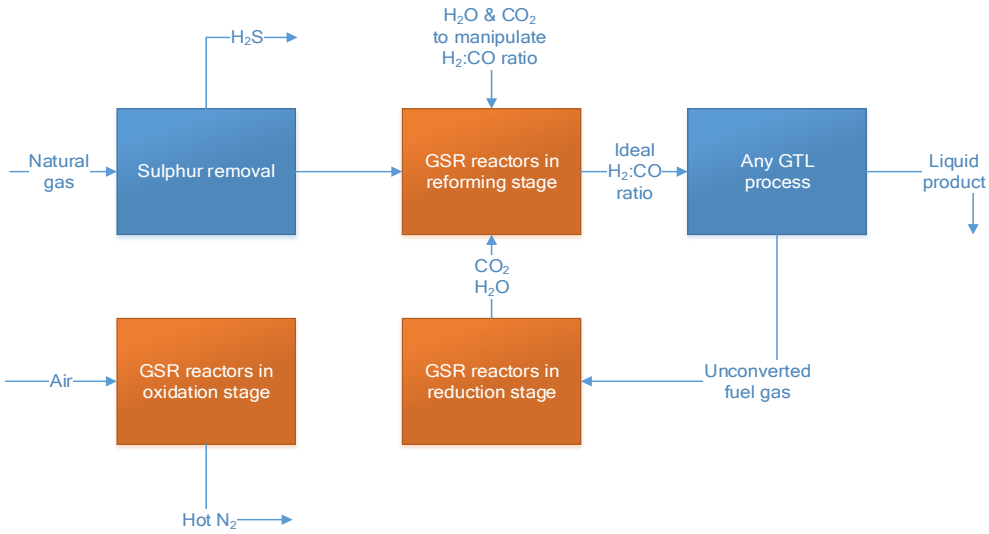

Figure 6-3: Possible integration of GSDR with gas-to-liquids (GTL) processes.

6.3 Experiment and methods

6.3.1 Experimental setup

The core of the experimental set up used for the demonstration of the GSDR concept consists of a fluidized bed reactor with a cylindrical column (5 cm in inner diameter and 50 cm in height) and a freeboard zone (*Figure **6-4***). The freeboard is an expanding conic zone (from 5cm in the lower end diameter to 10 cm at the top end) followed by a cylindrical part to minimize particles elutriation. The total height of the reactor, including the body and the freeboard, is 90cm. The reactor vessel was made of Inconel 600 to withstand high-temperature gas-solids reactive flows (up to 1000°C). A porous plate with 20µm mean pore size and 3mm thickness, made from Inconel 600, was used as a gas distributor placed at the bottom of the reactor. External electrical heating elements wound around the reactor vessel was used to heat up the reactor to a target temperature before starting autothermal GSDR process. A 25cm thickness insulation was installed around the reactor, combining blankets and vermiculate. Mass flow controllers from Bronkhorst BV were used for feeding gases to the reactor. A three-way electrical valve was used to separate the air and fuel feeds when cycling the process stages. A cooler was installed

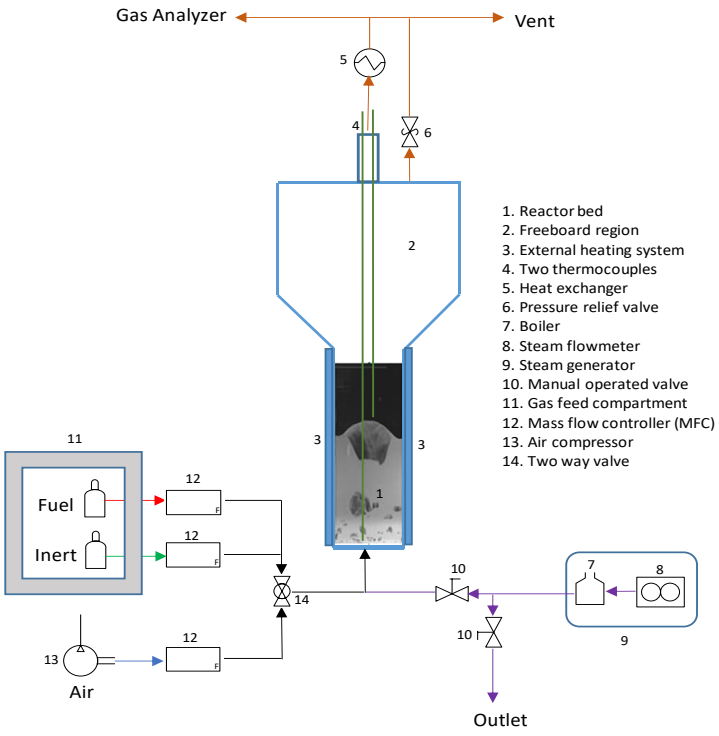

Figure 6-4: GSDR Experimental setup.

at the outlet of the reactor to cool down the stream of hot gases before being sent to the vent. The gas composition was measured using an ETG syngas analyzer sampling the gas on the outlet gas stream. The temperature was measured at two positions in the reactor, 2cm and 20cm above the gas distributor using two thermocouples inserted through the middle axis of the reactor. All the measurement instruments and flow controlling devices were controlled through a LabVIEW application. The LabVIEW application was also used for data acquisition and logging.

6.3.2 Methodology

The GSDR was demonstrated using a highly active NiO/Al_2O_3 oxygen carrier manufactured by VITO through spray drying was used for the GSDR demonstration. The total mass of the oxygen carrier used in this study is 623 g corresponding to a 0.3m static bed height. The oxygen carrier has particle size cut-offs D_{10}, D_{50} and D_{90} of 117.4, 161.7 and 231.3µm respectively. About 33% weight of active NiO is available for reaction. The powder has a loosely packed density of 1950kg/m^3 and a tapped density of 2166 kg/m^3. This oxygen carrier has been used in different chemical looping studies including combustion [38, 48-50] and reforming [42, 51] where it has been excellent stability and catalytic activity for reforming.

In the present study, typical GSDR cycles were completed starting with the reduction stage by feeding CO to react with NiO to produce Ni to catalyze the dry reforming reaction. CO is preferred in the reduction stage because of its high reactivity and the slightly exothermic reaction with NiO allowing sustaining high temperature in the reactor before the start of the dry reforming stage. The reduction stage is followed immediately by the reforming stage where the reduced Ni-based oxygen carrier serves as a catalyst for the dry reforming to produce syngas (CO and H_2). The energy-demanding reforming stage is followed by an air stage where pure air is fed to oxidize Ni back to NiO while producing the heat required to bring back the process to the same temperature at the start of the cycle.

Experiments were performed under different target operating temperatures from 850 - 750°C (the temperature at the start of the reduction stage) at atmospheric pressure. The reactor was first heated up using an external electric heating element up to the target temperature, followed by the autothermal GSDR experiments while the heaters are turned off. Following the three-stages process (reduction, reforming and oxidation) configuration.12.8nl/min CO was fed into the reactor for 5min, 3.2nl/min CH_4 (and CO_2 at various CH_4/CO_2 ratios) in the reforming stage

and 15nl/min feed of pure air in the oxidation stage. The feed rates used ensured operating the reactor at velocities way beyond the minimal fluidization velocity of the powder.

As mentioned earlier, real-time temperature and pressure measurements were logged using a Labview application while the online gas composition was measured using an ETG Syngas analyzer. The reactor performance at different temperatures was evaluated using the following measures: fuel conversion, CO_2 conversion, CO and H_2 selectivity, degree of carbon deposition, syngas purity. The experimental results were compared with equilibrium predictions.

6.4 Reactor performance indicators

The objective of the GSDR process is to convert a hydrocarbon fuel (CH_4 in this study) and CO_2 to syngas (H_2 and CO). Therefore, it is desired to maximize the fuel conversion in the reduction stage and CH_4 and CO_2 conversion in the reforming stage in order to maximize syngas production and CO_2 capture and utilization. The following performance indicators have been defined to evaluate reactor performance.

Firstly, the CO conversion in the reduction stage is quantified as follows:

$$\gamma_{CO} = 1 - \frac{n_{CO,out\_red}}{n_{CO,in\_red}} \qquad \textit{Equation 6-7}$$

Syngas ratio is an important parameter that determines the quality and application of the product syngas. This parameter is defined as:

$$\frac{H_2}{CO} = \frac{n_{H_2,out\_ref}}{n_{CO,out\_ref}} \qquad \textit{Equation 6-8}$$

The methane conversion in the reforming stage is quantified as follows:

$$\gamma_{CH_4} = 1 - \frac{n_{CH4,out\_ref}}{n_{CH_4,in\_ref}} \qquad \textit{Equation 6-9}$$

The carbon present in methane converts to solids carbon that deposits on the oxygen carrier and CO. Thus, the selectivity of converted methane to CO is quantified as follows:

$$s_{CO} = \frac{n_{CO,out\_ref}}{n_{CO,out\_ref} + n_{C,out\_ref}} \qquad \textit{Equation 6-10}$$

The selectivity of converted methane to H_2 is also quantified as:

$$S_{H2} = \frac{n_{H2,out\_ref}}{2\left(\gamma_{CH_4} * n_{CH_4,in\_ref}\right)} \quad \textit{Equation 6-11}$$

The degree of CO_2 conversion in the reforming stage is:

$$\gamma_{CO_2} = 1 - \frac{n_{CO_2,out\_ref}}{n_{CO_2,in\_ref}} \quad \textit{Equation 6-12}$$

Significant carbon deposition also took place during the reforming and fuel stage and this deposited carbon was released in the oxidation stage. The fraction of carbon deposition is therefore quantified as follows based on the oxidation stage outlet and the total methane entering the fuel stage:

$$C_{dep} = \frac{n_{CO,out\_oxi} + n_{CO_2,out\_oxi}}{\gamma_{CH_4} * n_{CH_4,in\_ref} + \gamma_{CO_2} * n_{CO_2,in\_ref} + \gamma_{CO} * n_{CO,in\_red}} \quad \textit{Equation 6-13}$$

Finally, the overall syngas selectivity produced during the reforming stage is quantified as follows:

$$\emptyset_{syngas} = \frac{n_{CO,out\_ref} + n_{H_2,out\_ref}}{n_{H_2,out\_ref} + n_{CO,in\_ref} + n_{C,out\_ref} + n_{H_2O,out\_ref}} \quad \textit{Equation 6-14}$$

6.5 Result and Discussion

6.5.1 Demonstration of GSDR Concept

In order to achieve autothermal operation, a three-stages GSDR process (reduction, reforming and oxidation) was designed where CO was used in a separate reduction stage due to the slightly exothermic reaction between CO and NiO enabling maintaining a high temperature in the reactor before starting the consecutive reforming stage. Using CO in the reduction stage will also implicitly demonstrate the ability to integrate GSDR with a GTL process as discussed in *section* ***6.2***, where CO is the main component in the GTL off-gasses together with H_2 that was shown to convert well with NiO [41, 46]. CH_4 and CO_2 (CH_4:CO_2 =1:2) were fed in the dry reforming reaction to produce syngas while pure air was fed in the oxidation. A typical GSDR behavior is shown through the transient gas species composition and temperature over two

cycles as depicted in *Figure **6-5*** (a larger number of cycles were completed demonstrating the stable repeatability of GSDR autothermal operation; only two are shown for illustration).

During the reduction stage, CO reacts with NiO to produce Ni and pure CO_2 stream ready for usage as feedstock in the reforming stage (otherwise it can be transported for storage in case of no-use). As can be seen in *Figure **6-5***, almost complete conversion of CO (~99%) was achieved in the entire reduction period. It is worth mentioning that the reduction time was selected based on preliminary experiments showing that beyond 6 min a sharp drop in CO conversion occurs indicating depletion of oxygen on the oxygen carrier. Although this reduction reaction is slightly exothermic, the temperature slightly dropped across the stage due to substantial heat loss to the surrounding, but it remained beyond 800 °C before the start of the reforming stage. During this stage, CO_2 reacts with CH_4 producing syngas (CO and H_2). This reaction is catalyzed by the Ni sites of the oxygen carrier generated from the precedent reduction stage. Due to the high endothermic dry reforming reaction, the temperature drop at this stage intensifies, which is evident from the steepness of the temperature profile (*Figure **6-5)***. As the reforming proceeds, the reactor gets colder and CH_4 conversion drops leading to increased CH_4 slippage with an adverse effect on performance. It is, therefore, necessary to stop the reforming stage at a relatively high temperature to maintain high process performance. Alternatively, the GSDR cycle should be designed to start the reforming stage at a temperature higher than 850°C to accommodate the inherent transient drop of temperature in the reforming stage. It is, however, worth mentioning that heat losses from the reactor contribute with the large extent in the sharp temperature drop that occurs in the reforming stage. Heat balance calculations of the present GSDR cycle plotted in *Figure **6-5*** has shown that the achieved length of the reforming stage is only 50% of the theoretically predicted ones. Indeed, for a total CO feed of ~2.6 mol to the reduction stage, ~6.15 mol of air would be required to oxidize back the oxygen carrier. The total heat generated in the system from the combustion of CO is then equal to ~700.9 kJ (assuming 95% CO conversion in the reduction stage). This heat is used for heating up the different feed gases from room temperature to the reactor operating temperature and the rest is utilized for driving the endothermic methane dry reforming reaction with an enthalpy of +247 kJ/mol. The calculated theoretical time of the reforming stage is ~543 s while the experimental one was only 280 s. Nevertheless, heat losses will be negligible in the industrial scale reactor.

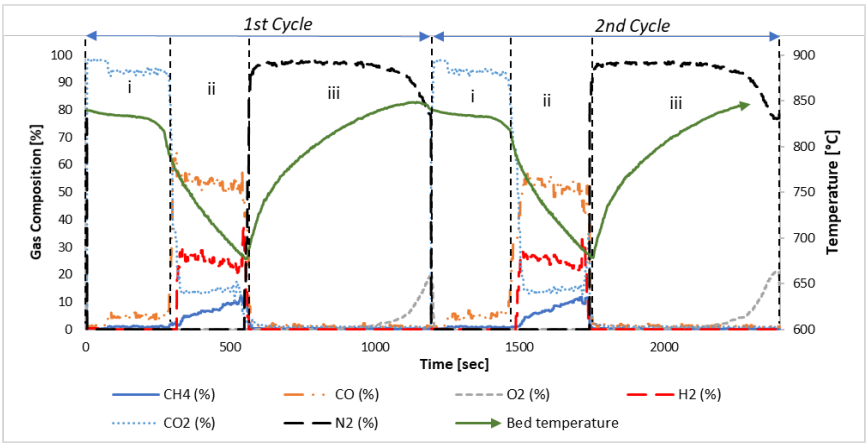

Figure 6-5: Two autothermal GSDR cycles showing transient gas composition and temperature profile. The reduction starts at a temperature of 850°C (target temperature). 1bar operating pressure, CO_2/CH_4 molar ratio of 2 and gas flowrate as follows: CO- 12.8nl/min, CH_4- 3.2nl/min, CO_2-6.4nl/min, Air- 10nl/min. i, ii and iii represent the reduction, reforming and oxidation stages respectively.

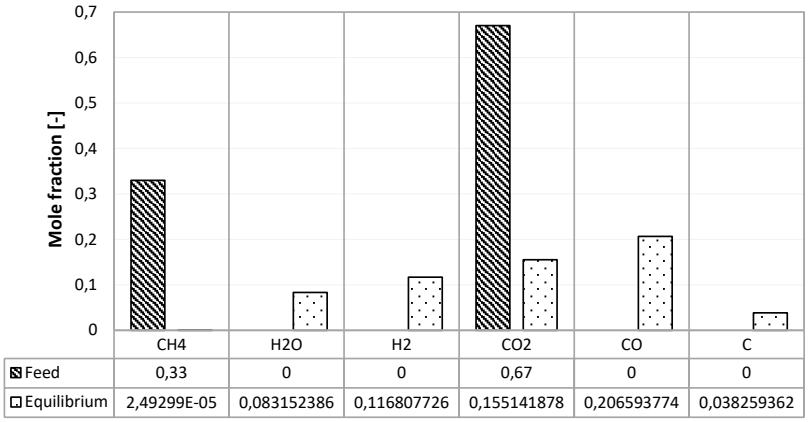

	CH4	H2O	H2	CO2	CO	C
Feed	0,33	0	0	0,67	0	0
Equilibrium	2,49299E-05	0,083152386	0,116807726	0,155141878	0,206593774	0,038259362

Figure 6-6: Equilibrium dry reforming composition at 800°C, 1bar and CO_2/CH_4 molar ratio of 2.

The GSDR cycle is finished by an oxidation stage by feeding air to oxidize back Ni to NiO with inherent separation of N_2 (depleted air) while serving as a main heat source for the GSDR cycle due to the highly exothermic oxidation reaction. This is clearly reflected in the temperature rise in the oxidation stage bringing it back to the initial target temperature for starting a new GSDR cycle. The oxygen carrier was completely oxidized back as reflected by the oxygen breakthrough from the gas composition plot (*Figure **6-5***), where any longer air feed leads to heat removal from the system reducing. Therefore, to ensure optimal heat usage in the GSDR cycle, it is crucial to switch to the next reduction stage at the point where maximum oxidation temperature is attained which occurs just before oxygen breakthroughs in the oxidation stage.

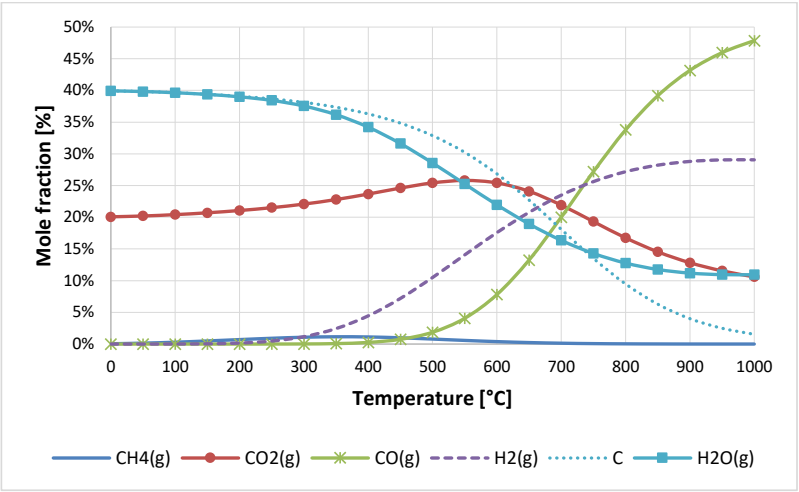

Figure 6-7: Equilibrium gas composition of dry reforming composition from 0 - 1000°C, at 1bar, CO_2/CH_4 molar ratio of 2 and Ni/CH_4 molar ratio of 4.

6.5.2 The effect of temperature

The effect of temperature on the reactor performance at atmospheric pressure and CO_2/CH_4 molar ratio of 2 was investigated by varying the target start temperature from 750°C – 850°C. Equilibrium predictions were computed from HSC Chemistry using the assumptions and parameters similar to Snoeck et al [52-54] for comparison with the experimental results. An example of GSDR equilibrium composition at 1bar, 800°C and CO_2/CH_4 ratio of 2 is shown in *Figure* ***6-6.*** In addition, the equilibrium mole fractions from 0°C – 1000°C at 1bar, CO_2/CH_4 molar ratio of 2 and Ni/CH_4 molar ratio of 4 is shown in *Figure* ***6-7.***

CO conversion in the reduction stage was sensitive to the operating temperature where the overall reduction stage CO conversion has moved from 86 % at 750 °C to 98% at 850 °C (*Figure* ***6-8***). The reforming stage was found to be more sensitive to temperature than the reduction stage. *Figure* ***6-9*** shows the transient conversion of CH_4 and CO_2 across the reforming stage and the corresponding reactor temperature. It could be seen that for the three operating target temperatures that the reactor temperature drops gradually as the reforming stage proceeds. This arises from the heat losses and the high endothermicity of the reactions taking place in the reforming stage. Consequently, a very high difference in the CH_4 and CO_2 conversion is found between the start and the end of the reforming stage showing the large effect temperature has on the stage performance (*Figure* ***6-9***). For example, methane conversion beyond 95% was achieved at the start of the reforming stage at a temperature of ~825 °C but

dropped to 75% at the end of the stage where the reactor temperature reached ~700°C (CO_2 conversion has shown a similar trend). This transient behavior of GSDR makes the overall reforming stage performance relatively low in comparison to what would be achieved with the interconnected fluidized bed reactor configuration where the fuel reactor where both oxygen carrier reduction and methane dry reforming occurs simultaneously under a steady-state [55]. However, integration of the GSDR concept with a GTL process as proposed in *section **6.2 c***ould allow tolerating some unconverted methane in the reforming stage to feed directly to a GTL process. Then all the unconverted gases from GTL (a mixture of syngas, methane, CO_2, and steam) are to be recycled back to be converted at the reduction stage of GSDR, thereby maximizing fuel utilization and overall process efficiency. This potential of integration with a GLT process is not feasible with the interconnected fluidized bed reactor configuration unless a third reactor is added to complete a separate reduction and reforming stages, thus involving additional complexities to the process. Other alternatives to minimize the impact of the transient nature of the GSDR concept is the use of a shorter reforming stage (shorter GSDR cycle), combined with operating the process at the higher target operating temperature, to complete the entire reforming stage at temperatures above 800°C, in order to maximize fuel conversion. However, this will be compromised by lower CO_2 capture efficiency and purity that were shown earlier to be negatively affected when shortening the process cycle due to the unavoidable mixing of gasses that occurs when switching between the stages [50].

The large effect of temperature on the reforming stage performance could clearly be seen on the averaged conversion of CH_4 and CO_2 found to be well below equilibrium predictions at low operating temperature (especially for CH_4) but rapidly increases towards equilibrium at higher temperatures (see *Figure **6-7*** and *Figure **6-10***). This is consistent with thermodynamics since CH_4 and CO_2 are very stable molecules with high dissociation energy thus requires a high temperature to achieve equilibrium conversion [56]. The transient nature of the GSDR process contributes to its low performance; with about $0.010 mol_{CH4}/g_{catalyst}$ is converted at 750°C (average temperature of the reforming stage) which is slightly lower than the conversion $0.012 mol_{CH4}/g_{catalyst}$ achieved by Hao, et. al at 800°C using a micro-fluidized bed reactor [57]. The low conversion below equilibrium predictions at low temperatures could be attributed to the substantial carbon deposition that could result from competing mechanisms; Boudouard (*Reaction **6-4***) and methane cracking (*Reaction **6-3***) reactions (with the former being more favored at low temperature), driven by the well-known high catalytic activity of metallic nickel (the reduced Ni-based oxygen carrier) for carbon deposition [4, 58, 59]. As shown in *Figure*

6-12, beyond 700°C carbon deposition becomes insignificant. This is because Boudouard reaction is not favoured at such high temperatures. This is in line with thermodynamics where the dry reforming reaction being more spontaneous and is favoured more than the methane cracking reaction leading to a decrease in carbon deposition. This is a promising result, showing that operation at industrially relevant temperatures (~1000°C) will most likely not face noticeable carbon deposition problems, thereby GSDR contributes to solving one of the major issues affecting the commercialization of DMR [56, 58, 60]. Carbon deposition also affects CO conversion at the reduction stage.

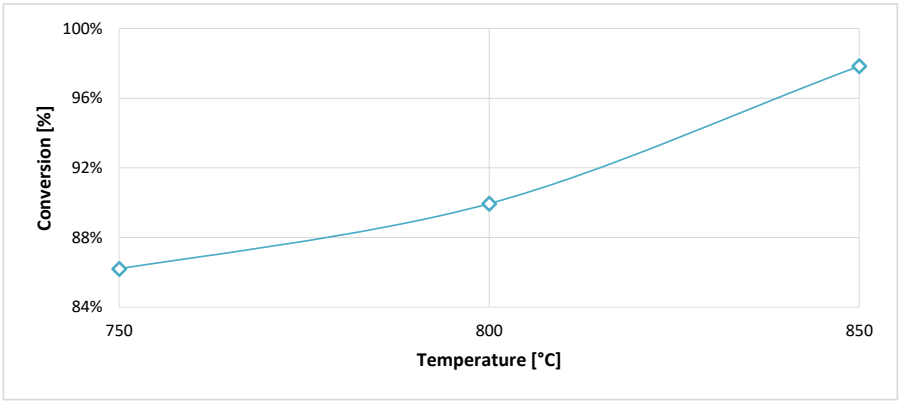

Figure 6-8: Overall CO Conversion in the reduction stage plotted against the target operating temperature.

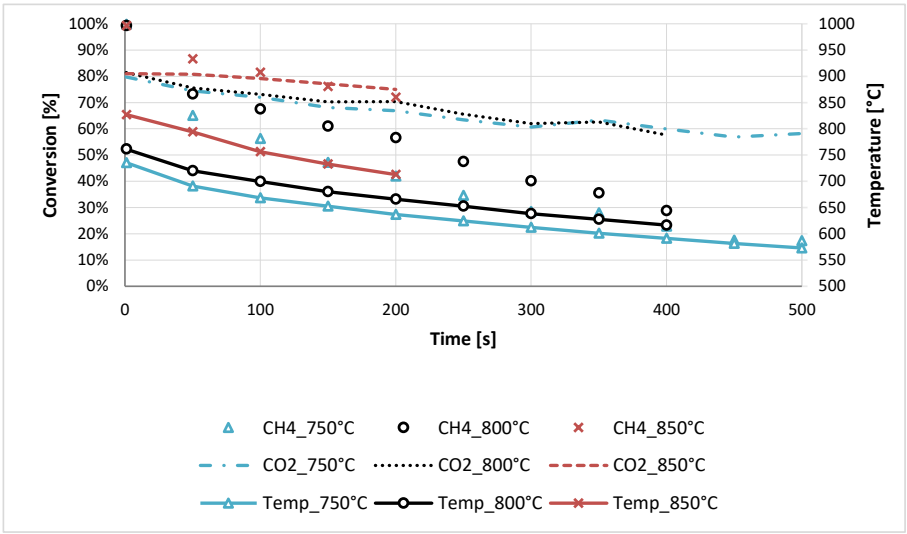

Figure 6-9: Transient CH_4 and CO_2 conversion superposed with temperature profiles during the reforming stage for various target temperatures. 1bar operating pressure, CO_2/CH_4 molar ratio of 2 and gas flowrate as follows: CO - 12.8nl/min, CH_4 - 3.2nl/min, CO_2 - 6.4nl/min, Air - 10nl/min.

Although temperature plays a major role, it is difficult to generalize gas conversion by thermodynamics because it is also dependent on kinetics and the catalyst [8-13, 37, 56, 61]. It is likely that due to kinetic limitation, the dry reforming reaction was slow at low temperature favoring the production of solid carbon on the catalyst and hydrogen from the converted methane. The synthesis method of the catalyst, active content, support and the number of

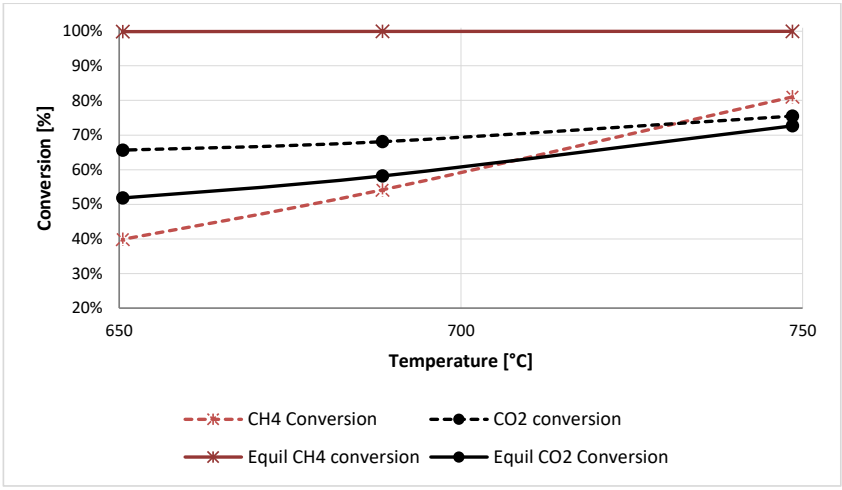

Figure 6-10: Overall CH_4 and CO_2 conversion in the reforming stage plotted against the stage average temperature. 1bar operating pressure, CO_2/CH_4 molar ratio of 2 and gas flowrate as follows: CO - 12.8nl/min, CH_4 - 3.2nl/min, CO_2 - 6.4nl/min, Air - 10nl/min.

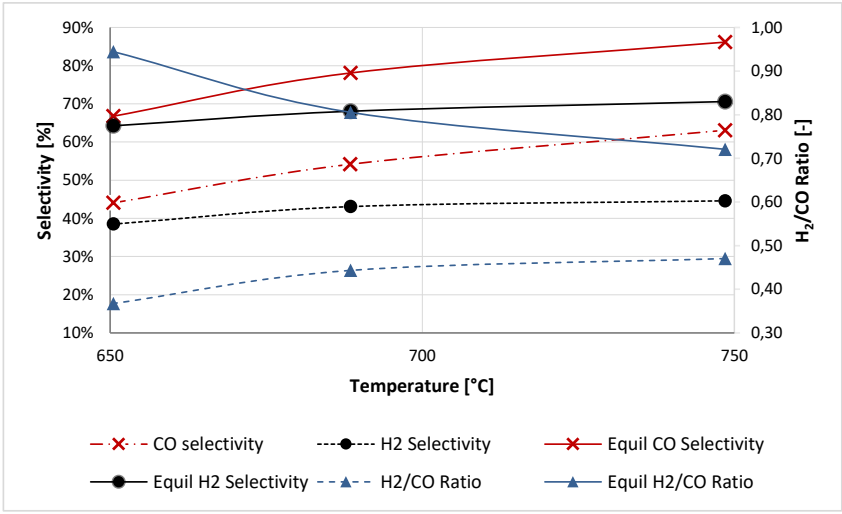

Figure 6-11: Overall Selectivity and syngas ratio in the reforming stage plotted against the stage average temperature. 1bar operating pressure, CO_2/CH_4 molar ratio of 2 and gas flowrate as follows: CO - 12.8nl/min, CH_4 - 3.2nl/min, CO_2 - 6.4nl/min, Air - 10nl/min.

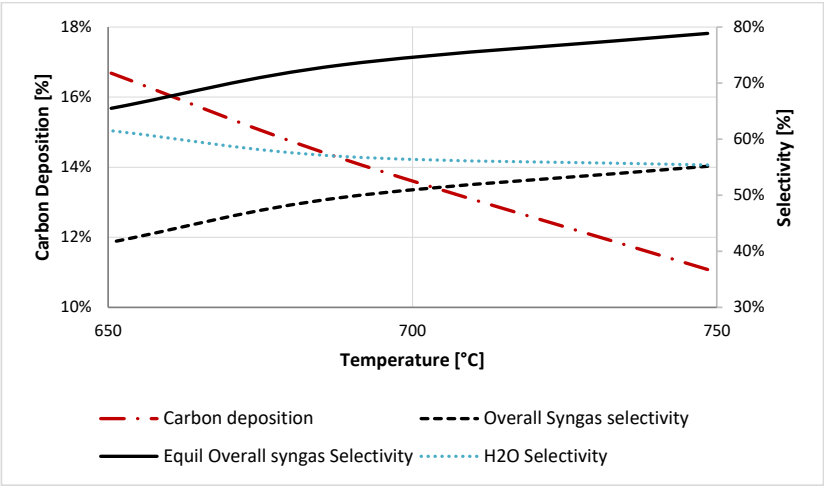

Figure 6-12: Overall carbon deposition, steam selectivity and syngas selectivity in the reforming stage plotted against the stage average temperature. 1bar operating pressure, CO_2/CH_4 molar ratio of 2 and gas flowrate as follows: CO - 12.8nl/min, CH_4 - 3.2nl/min, CO_2 - 6.4nl/min, Air - 10nl/min.

active sites of catalyst also affect conversion and degree of reduction [37, 56]. Too strong interaction of active metals and supports causes the poor reducibility and fuel conversion [56]. Interestingly, despite the tens of GSDR cycles completed at a different temperature that caused carbon deposition at different extents, no deactivation of the oxygen carrier/catalyst was observed demonstrating the robustness of the gas switching concept in prolonging the catalyst lifetime through cyclic gasification of the deposited carbon in the oxidation stage although on the expense of a reduced CO_2 capture and utilization efficiency. Note that the Ni-based oxygen carrier used in this study is a standard Ni/Al_2O_3 oxygen carrier that was tested under chemical looping combustion [38], reforming [41, 42, 62] and no under dry reforming. Promoters would have been needed in the case of conventional DRM, without the redox reaction involved in the chemical looping, to reduce the extent of carbon deposition and extend the catalyst lifetime (e.g. K promoted support was used to improve the reducibility and reduce carbon deposition by creating weak interaction between the NiO/Ni and the support [63, 64]).

Result also indicates low selectivity to H_2 as shown in *Figure **6-11***. This could be explained by the RWGS (*Reaction **6-2***) that uses the excess of CO_2 feed and depletes the hydrogen produced from methane conversion to produce CO and H_2O, while the Boudouard reaction converts that CO back to more solid carbon. The continuous process combining the carbon deposition and RWSG mechanisms, explains the high conversion of CO_2 above the equilibrium prediction despite the low methane conversion. This phenomenon has also favored carbon deposition rather than CO production with a CO selectivity way below equilibrium.

Table 6-1: Thermodynamic data of reactions 1-4: DMR, RWGS, Methane Cracking and Boudouard reactions respectively (source: HSC Chemistry)

T [°C]	ΔG [kJ]				ΔH [kJ]			
	Reaction 1	Reaction 2	Reaction 3	Reaction 4	Reaction 1	Reaction 2	Reaction 3	Reaction 4
750	-30.57	2.056	-21.715	8,854	259.478	34.633	89.078	-170,399
800	-44.741	0.477	-27.139	17,602	259.339	34.12	89.449	-169,890
850	-58.904	-1.079	-32.578	26,326	259.115	33.617	89.75	-169,365

The change of Gibbs free energy can be used to determine which reaction route is favoured most at a particular temperature. The more the change in Gibbs energy tends towards negative the more favoured the reaction indicating that the free energy of the reactants is greater than that of the products, the entropy of the universe will increase in the reaction direction, thus the reaction will have more tendency to occur[65]. Consequently, the resulting overall syngas selectivity (*Figure **6-12***) and H_2/CO ratio (*Figure **6-11***) were relatively low similar to previous results of chemical looping dry reforming [66-68]. This conforms with thermodynamics as DMR is favoured more than RWGS at higher temperatures considering the Gibbs-free energy value of, *Table **6-1***, resulting in lower CO yield similar to the previous experimental results of Khalesi et al. [69, 70]. The performance below the equilibrium prediction supports the previous results of Arora et al. stating that the DMR process is not only affected by thermodynamics but also kinetics [58]. If higher H_2/CO ratios are desired, reactant gas feed of lower C:H ratio should be maintained by reducing the CO_2/CH_4 ratio, co-feeding CO_2 with steam in tri-reforming or possible integration with WGS [37, 56, 71].

However, *Figure **6-12*** also shows that the overall syngas selectivity increases with temperature. This could be attributed to the increase in gas conversion to syngas with reduced carbon formation. In general, higher temperatures will both minimize carbon deposition and maximize the syngas yield (CO and H_2). The GSDR process should, therefore, be operated at the highest achievable temperature.

6.5.3 The effect of CO_2/CH_4 Ratio

Additional experiments were completed investigating the CO_2/CH_4 at 750°C and 1bar. *Figure **6-13*** shows that CH_4 conversion increases with the CO_2/CH_4 ratio, which is in line with the findings of Arora and Prasad that CO_2 gas as an oxidant has a positive effect on CH_4 conversion[58]. The improvement in CH_4 conversion (*Figure **6-13***) was however marginal with an excess of CO_2 at 750°C, confirming the large effect that temperature has on overall reforming

stage performance. Previous studies show that the initial step of dry reforming is methane decomposition (*Reaction* ***6-3***) to produce solid carbon and H_2 followed by the gasification of the solid C (*Reaction* ***6-15***) with CO_2 to produce CO [37, 72]. It could also be inferred from *Figure* ***6-15*** that increasing CO_2/CH_4 has resulted in reduced carbon deposition. This agrees with the result of Nakagawa and Tomishige suggesting that the higher tendency towards carbon deposition will be observed in lower O/C[72]. As a matter of fact, carbon deposition arises mainly from CH_4 cracking and intensive CO_2 dissociation on the surface of the catalyst [61]. With insufficient reducible oxides (CO_2), the rate of methane decomposition will surpass CO_2 dissociation leading to carbon deposition[37]. It could also be speculated that the excess CO_2 has enhanced the RWGS (*Reaction* ***6-4***) that has consumed more H_2 for producing CO and H_2O (*Figure* ***6-15***). These phenomena affect H_2/CO ratio as it decreases with the increase in CO_2/CH_4 ratio since a shift towards RWGS leads to more CO and less H_2 yield while a decrease in methane cracking as the partial pressure of CH_4 decrease also deteriorates H_2 yield (*Figure* ***6-14*** and *Figure* ***6-15***).

$$C + CO_2 \rightarrow 2CO \qquad (\Delta H_{298K} = +172.4 KJmol^{-1}) \qquad \textit{Reaction 6-15}$$

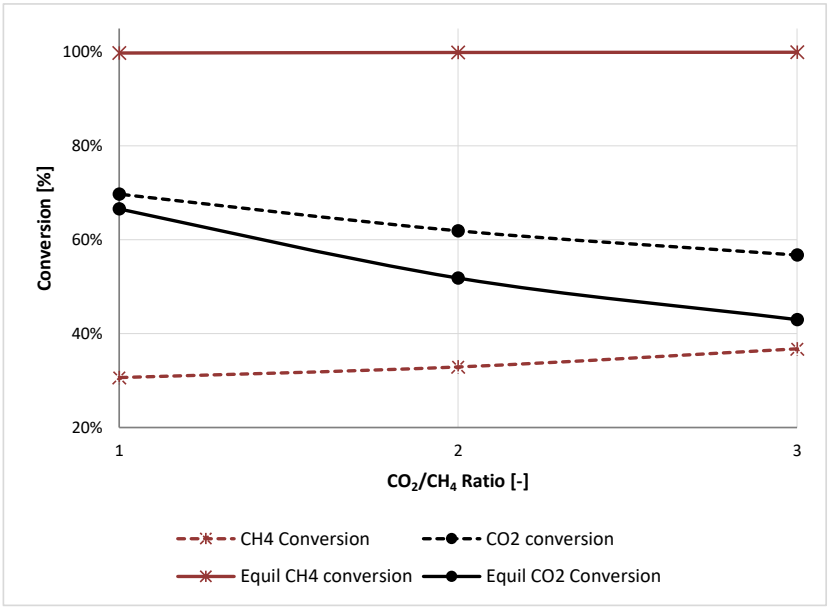

Figure 6-13: Overall gas conversion in the reforming stage plotted against CO_2/CH_4 molar ratio. 1bar operating pressure, 750°C and gas flowrate as follows: CO - 12.8nl/min, CH_4 - 3.2nl/min, Air- 10nl/min.

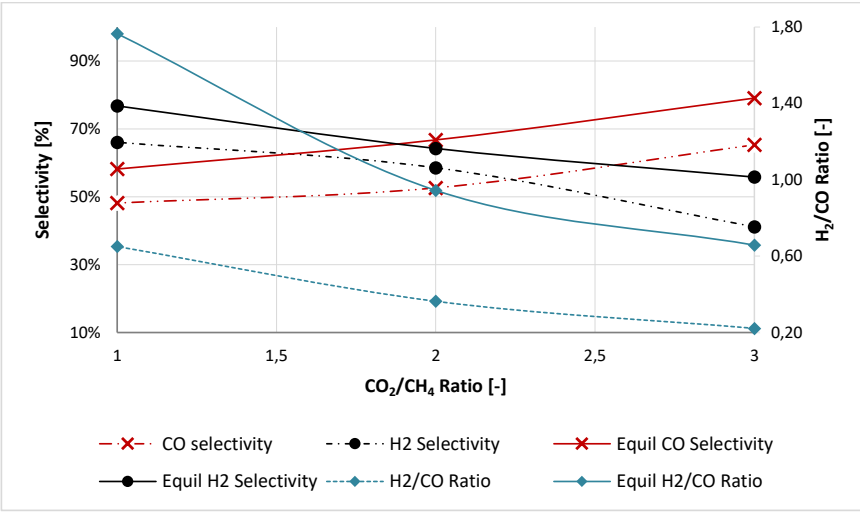

Figure 6-14: Overall Selectivity and H_2/CO molar ratio in the reforming stage plotted against CO_2/CH_4 molar ratio. 1bar operating pressure, 750°C and gas flowrate as follows: CO - 12.8nl/min, CH_4 - 3.2nl/min, Air - 10nl/min.

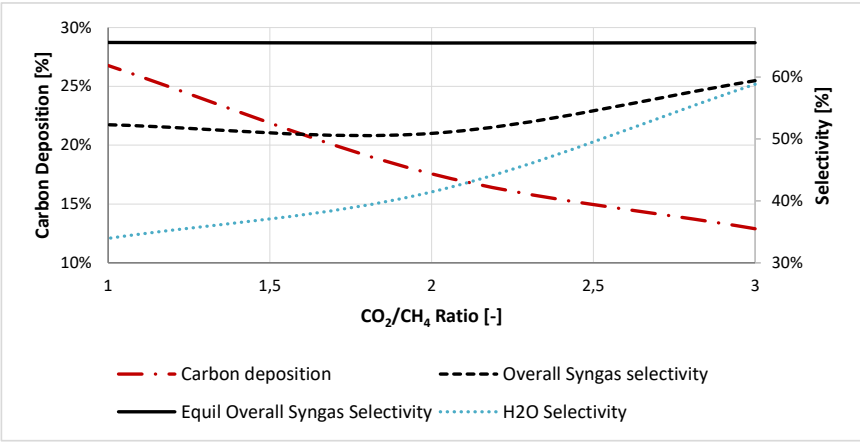

Figure 6-15: Overall carbon deposition, steam selectivity and syngas selectivity in the reforming stage plotted against CO_2/CH_4 molar ratio. 1bar operating pressure, 750°C and gas flowrate as follows: CO- 12.8nl/min, CH_4 - 3.2nl/min, Air - 10nl/min.

6.5.4 The effect of oxygen carrier utilization

The oxygen carrier utilization was changed by varying the degree of reduction of the oxygen carrier before starting the reforming stage. In other words, 50% oxygen carrier utilization means that the oxygen carrier was 50% reduced (starting from a fully oxidized state), while 50% of the active content remains as NiO, before the start of the reforming stage. In this sensitivity study, 50% and 100% oxygen carrier utilizations were tested (the oxygen carrier is fully reduced

to metallic nickel in the last case). 62% carbon deposition reduction in the case of 50% oxygen carrier utilization compared to 100% case (*Figure **6-17***), reflecting the immediate positive impact of the presence of latent oxygen on the catalyst, in the form of NiO, during the reforming stage hindering carbon deposition likely through enabling oxy-gasification of the carbon. This has largely affected the mechanisms by which syngas is produced in the reforming stage. The oxy-gasification of carbon by latent oxygen on the catalyst favored CO production that in turn reduced the extent of the RWGS reaction, leading to improved H_2 selectivity and consequently higher H_2/CO ratio and overall syngas selectivity. This also means that CO_2 conversion through the RWGS would reduce resulting in poorer overall CO_2 conversion in the reforming stage which was confirmed by the experimental results. Additionally, the 50% oxygen carrier utilization has also affected methane conversion that has shown a 22% reduction compared to the fully reduced catalyst (*Figure **6-16***). The main reason for this could be the smaller availability of metallic Nickel sites to catalyze the dry reforming reaction, as 50% of nickel on the oxygen carrier is present in oxidized form; NiO. This is in agreement with the finding from a previous study with the same oxygen carrier that has shown that steam methane reforming begins only when a good reduction level is reached on the oxygen carrier [51].

Another positive impact of smaller oxygen carrier utilization is the improved CO conversion in the reduction stage facilitated by the easily accessible latent oxygen in this case (*Figure **6-16***). This further strengthens the business potential of integrating the GSDR with a GTL process, which will maximize the use of unconverted outlet stream gasses from GTL in the reduction stage of GSDR. As mentioned in the introduction section, such integration with GTL will not be efficient if an interconnected fluidized configuration is used for the chemical looping dry reforming [55]. In this case, the unconverted fuel gases in a GTL upstream will have to be fed jointly with methane to the fuel reactor of the interconnected fluidized bed configuration resulting in a methane-rich stream that leads to simultaneous oxygen carrier reduction and dry methane reforming reactions. This will have two negative impacts on the fuel reactor performance: i) lower fuel conversion will be achieved due to the low reactivity of methane with the oxidized oxygen carrier [51] and ii) the simultaneous DMR and reduction reactions will make it difficult to control the oxygen carrier utilization, thereby reducing the ability to achieve a high methane conversion, to control carbon deposition and to counteract the RWGS, and thus failing to solve the low H_2/CO ratio issue encountered in conventional dry reforming [56, 58, 60, 73].

To summarize, the insights brought by the chemical looping process in general and particularly the gas switching to the dry reforming process, will largely reduce the issues raised in the introduction section that hinder dry reforming commercialization: i) reduce CO_2 emissions from energy-intensive conventional dry reforming; instead, it is used as a feedstock to produce valuable value chemical ii) prolong the catalyst lifetime by gasifying the deposited carbon on the catalyst in the redox cycle and iii) solve the low H_2/CO ratio by partial oxygen carrier utilization. Clearly, the optimal operation of GSDR should consider tuning the three sensitivity parameters investigated in this section (temperature, CO_2/CH_4 ratio, and oxygen carrier utilization), in addition to considering the requirements of the downstream GTL process to integrate with GSDR. Further measures could be taken for approaching the H_2/CO ratio to unity such as using a proper oxygen carrier that both reduces carbon deposition and minimizes the extent of CO_2 and H_2 conversion through the RWGS. Co-feeding of steam would also minimize these issues, but it will reduce the extent of CO_2 use in GSDR[43]. Alternatively, the GSDR system demonstrated in this work with the current oxygen carrier offers great opportunities for using renewable hydrogen from electrolysis to further improve CO_2 conversion in the reforming stage, but through the RWGS. Further research is needed both on the experimental and process integration aspects for better highlighting the full potential of GSDR in capturing and utilization of CO_2 for producing high-value chemicals and fuel at the highest possible efficiency.

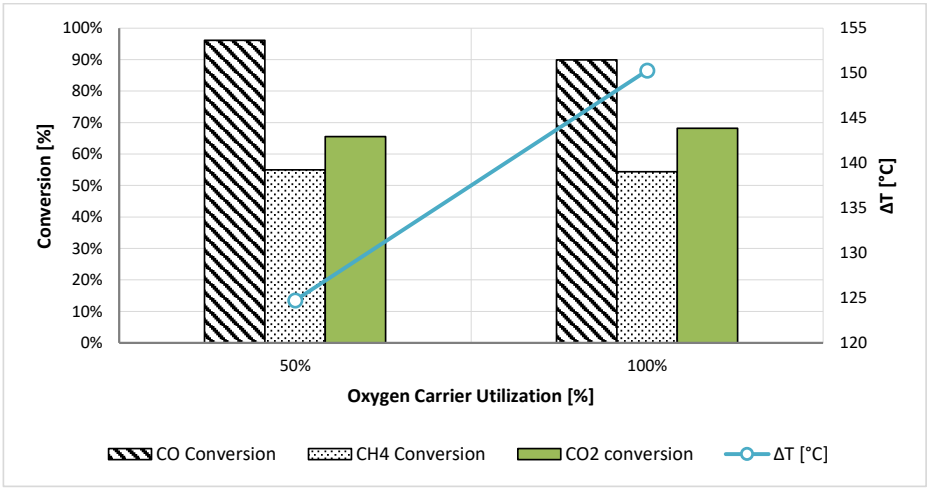

Figure 6-16: Overall gas conversion and temperature change in the reforming stage plotted against Oxygen carrier utilization. . 1bar operating pressure, CO_2/CH_4 molar ratio of 2 and gas flowrate as follows: CO - 12.8nl/min, CH_4 - 3.2nl/min, CO_2 - 6.4nl/min, Air - 10nl/min.

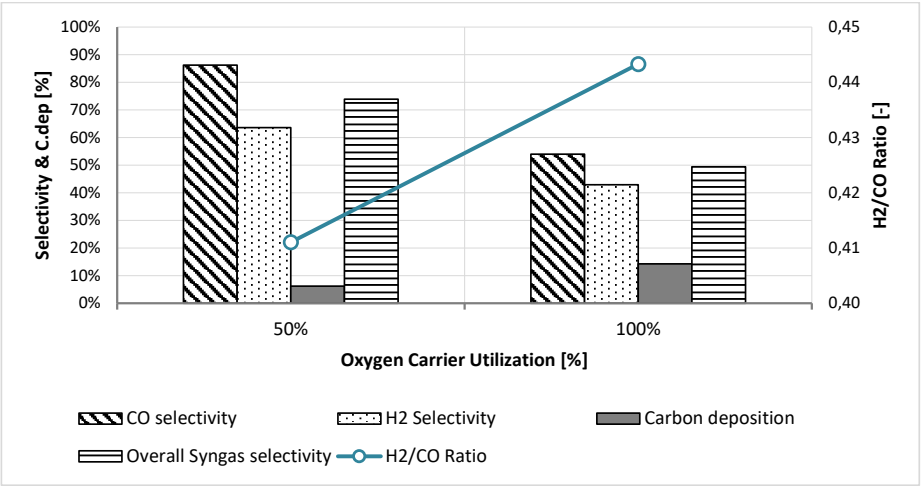

Figure 6-17: Overall selectivity, carbon deposition and H_2/CO molar ratio in the reforming stage plotted against Oxygen carrier utilization. 1bar operating pressure, CO_2/CH_4 molar ratio of 2 and gas flowrate as follows: CO - 12.8nl/min, CH_4 - 3.2nl/min, CO_2 - 6.4nl/min, Air - 10nl/.

6.6 Summary and conclusion

This paper extended the Gas Switching technology to dry methane reforming, GSDR, for capturing and utilization of CO_2 in syngas production. This technology uses a single fluidized bed reactor cycling redox and reforming conditions into a bed of oxygen carrier, thereby greatly simplifying the operating and scale-up challenges encountered in conventional chemical looping configuration.

Autothermal operation was experimentally demonstrated using the three-stages GSDR process (Reduction, Reforming and Oxidation) owing to the excellent heat integration between the different stages. The use of CO in the reduction stage was beneficial due to its slightly exothermic reaction with the Ni-based oxygen carrier allowing starting the reforming stage at a temperature high enough that ensured high CH_4 and CO_2 to syngas. However, the transient nature of the GSDR resulted in a continuous drop in temperature across the reforming stage causing a rapid deterioration of CH_4 and CO_2 conversions. In this respect, short GSDR cycles combined with elevated operation temperature would maximize GSDR performance in the reforming stage.

Carbon deposition was a major issue that results in reduced carbon capture efficiency, as the deposited carbon gasifies and combusts in the oxidation stage where the exhaust gases are vented to the atmosphere. Increasing the operating temperature and the CO_2/CH_4 proved to

minimize carbon deposition, likely due to the overtake of the dry reforming reaction over methane cracking, but on the expenses of lower H_2/CO ratio of the produced syngas, driven by the reverse water gas shift reaction favored at higher temperature and excess of CO_2. Smaller oxygen carrier utilization (lower reduction degree) has also proved to reduce carbon deposition while increasing the H_2/CO ratio but caused lower CH_4 and CO_2 conversion. The remaining latent oxygen on the catalyst (when the oxygen carrier is 50% reduced) has likely reduced the catalytic activity of the three reactions taking place in the reforming stage (*Reaction* ***6-1***, *Reaction* ***6-2*** and *Reaction* ***6-3***). Additional benefits of smaller oxygen carrier utilization are the smaller temperature variation in the cycle that improves GSDR performance in the reforming stage and the better CO conversion in the reduction stage. It should also be emphasized that no deactivation was observed showing the robustness of the gas switching concept in prolonging the catalyst lifetime through cyclic gasification of the deposited carbon in the oxidation stage although at the expense of a reduced CO_2 capture and utilization efficiency.

Clearly, the key for GSDR performance optimization lays in the proper tuning of the process parameters investigated in this study, but also by using a more appropriate oxygen carrier/catalyst. Finally, integration of GSDR with a Gas-To-Liquid process (outlet stream from GSDR to GTL while unconverted hot gasses from GTL are to feed to the reduction stage of GSDR) has a great potential for maximizing fuel conversion and energy efficiency of the overall process.

Acknowledgment

ACT GaSTech project. Project No 271511.

This project has received funding from The Research Council of Norway and is cofounded by the European Commission under the Horizon 2020 programme, ACT Grant Agreement No 691712. It also received the 2018 Equinor Publication Grant. VATL Lab technicians at the Norwegian University of Science and Technology are equally acknowledged for constructing and maintaining the experimental setup.

Nomenclature

Abbreviations

CCS	Carbon capture and storage
CLDR	Chemical Looping Dry Reforming
CLR	Chemical Looping Reforming
GSDR	Gas Switching Dry Reforming
GSR	Gas Switching Reforming
GST	Gas Switching Technology
GTL	Gas-To-Liquid
RWGS	Reverse Water Gas Shift

Symbols

C_{dep}	Carbon deposition.
D_{10}	Diameter of the catalyst which 10% of a sample mass is smaller than
D_{50}	Diameter of the catalyst which 50% of a sample mass is smaller than
D_{90}	Diameter of the catalyst which 90% of a sample mass is smaller than
n_{C,out_ref}	Mole of C at the gas outlet during reforming stage
n_{CH_4,in_ref}	Mole of CH_4 fed during reforming stage
n_{CH4,out_ref}	Mole of CH_4 at the gas outlet during reforming stage
n_{CO,out_oxi}	Mole of CO at the gas outlet during oxidation stage
n_{CO_2,out_oxi}	Mole of CO_2 at the gas outlet during oxidation stage
n_{CO,out_red}	Mole of CO at the gas outlet during reduction stage
n_{CO,in_red}	Mole of CO fed during reduction stage
n_{CO,out_ref}	Mole of CO at the gas outlet during reforming stage
n_{CO_2,in_ref}	Mole of CO_2 fed during reforming stage
n_{CO_2,out_ref}	Mole of CO_2 at the gas outlet during reforming stage

n_{H_2,out_ref}	Mole of H_2 at the gas outlet during reforming stage
n_{H_2O,out_ref}	Mole of H_2O at the gas outlet during reforming stage
s_{CO}	CO selectivity
s_{H2}	H_2 selectivity
$\emptyset_{syngas}$	Overall syngas selectivity
γ_{CH_4}	CH_4 conversion
γ_{CO}	CO conversion
γ_{CO_2}	CO_2 conversion

References

[1] IPCC, "Global Warming of 1.5C- An IPCC Special Report on the impacts of global warming of 1.5C above pre-industrial levels and related global greenhouse gas emission pathways, in the context of strengthening the global response to the threat of climate change, sustainable development, and efforts to eradicate poverty. Summary for Policymakers," IPCC, Switzerland, 2018. [Online]. Available: https://report.ipcc.ch/sr15/pdf/sr15_spm_final.pdf

[2] P. Nejat, F. Jomehzadeh, M. M. Taheri, M. Gohari, and M. Z. A. Majid, "A global review of energy consumption, CO2 emissions and policy in the residential sector (with an overview of the top ten CO2 emitting countries)," *Renewable and sustainable energy reviews,* vol. 43, pp. 843-862, 2015.

[3] B. H. Baltagi, G. Bresson, and A. Pirotte, "Comparison of forecast performance for homogeneous, heterogeneous and shrinkage estimators: Some empirical evidence from US electricity and natural-gas consumption," *Economics Letters,* vol. 76, no. 3, pp. 375-382, 2002.

[4] O. Muraza and A. Galadima, "A review on coke management during dry reforming of methane," *International Journal of Energy Research,* vol. 39, no. 9, pp. 1196-1216, 2015.

[5] A. Sternberg, C. M. Jens, and A. J. G. C. Bardow, "Life cycle assessment of CO 2-based C1-chemicals," vol. 19, no. 9, pp. 2244-2259, 2017.

[6] J. L. Ewbank, L. Kovarik, C. C. Kenvin, and C. J. G. C. Sievers, "Effect of preparation methods on the performance of Co/Al 2 O 3 catalysts for dry reforming of methane," vol. 16, no. 2, pp. 885-896, 2014.

[7] M. Usman, W. W. Daud, and H. F. Abbas, "Dry reforming of methane: Influence of process parameters—A review," *Renewable and Sustainable Energy Reviews,* vol. 45, pp. 710-744, 2015.

[8] J. Wei and E. Iglesia, "Isotopic and kinetic assessment of the mechanism of reactions of CH4 with CO2 or H2O to form synthesis gas and carbon on nickel catalysts," *Journal of Catalysis,* vol. 224, no. 2, pp. 370-383, 2004.

[9] J. Wei and E. Iglesia, "Structural and mechanistic requirements for methane activation and chemical conversion on supported iridium clusters," *Angewandte Chemie International Edition,* vol. 43, no. 28, pp. 3685-3688, 2004.

[10] J. Wei and E. Iglesia, "Mechanism and site requirements for activation and chemical conversion of methane on supported Pt clusters and turnover rate comparisons among noble metals," *The Journal of Physical Chemistry B,* vol. 108, no. 13, pp. 4094-4103, 2004.

[11] J. Wei and E. Iglesia, "Isotopic and kinetic assessment of the mechanism of methane reforming and decomposition reactions on supported iridium catalysts," *Angewandte Chemie International Edition,* vol. 6, no. 13, pp. 3754-3759, 2004.

[12] J. Wei and E. Iglesia, "Structural requirements and reaction pathways in methane activation and chemical conversion catalyzed by rhodium," *Journal of Catalysis,* vol. 225, no. 1, pp. 116-127, 2004.

[13] J. Wei and E. Iglesia, "Reaction pathways and site requirements for the activation and chemical conversion of methane on Ru− based catalysts," *The Journal of Physical Chemistry B,* vol. 108, no. 22, pp. 7253-7262, 2004.

[14] N. A. K. Aramouni, J. G. Touma, B. A. Tarboush, J. Zeaiter, and M. N. Ahmad, "Catalyst design for dry reforming of methane: Analysis review," *Renewable and Sustainable Energy Reviews,* 2017.

[15] S. T. Oyama, P. Hacarlioglu, Y. Gu, and D. Lee, "Dry reforming of methane has no future for hydrogen production: comparison with steam reforming at high pressure in standard and membrane reactors," *International journal of hydrogen energy,* vol. 37, no. 13, pp. 10444-10450, 2012.

[16] Z. Hou, P. Chen, H. Fang, X. Zheng, and T. Yashima, "Production of synthesis gas via methane reforming with CO2 on noble metals and small amount of noble-(Rh-) promoted Ni catalysts," *International journal of hydrogen energy,* vol. 31, no. 5, pp. 555-561, 2006.

[17] C. Carrara, J. Munera, E. A. Lombardo, and L. M. Cornaglia, "Kinetic and stability studies of Ru/La 2 O 3 used in the dry reforming of methane," *Topics in Catalysis,* vol. 51, no. 1-4, pp. 98-106, 2008.

[18] P. Chen, H.-B. Zhang, G.-D. Lin, and K.-R. Tsai, "Development of coking-resistant Ni-based catalyst for partial oxidation and CO2-reforming of methane to syngas," *Applied Catalysis A: General,* vol. 166, no. 2, pp. 343-350, 1998.

[19] M. Ishida, D. Zheng, and T. Akehata, "Evaluation of a chemical-looping-combustion power-generation system by graphic exergy analysis," *Energy,* vol. 12, no. 2, pp. 147-154, 1987.

[20] A. Lyngfelt, B. Leckner, and T. Mattisson, "A fluidized-bed combustion process with inherent CO2 separation; application of chemical-looping combustion," *Chemical Engineering Science,* vol. 56, no. 10, pp. 3101-3113, 2001.

[21] E. J. Anthony, "Solid looping cycles: a new technology for coal conversion," *Industrial & Engineering Chemistry Research,* vol. 47, no. 6, pp. 1747-1754, 2008.

[22] M. Rydén and M. Arjmand, "Continuous hydrogen production via the steam–iron reaction by chemical looping in a circulating fluidized-bed reactor," *International Journal of Hydrogen Energy,* vol. 37, no. 6, pp. 4843-4854, 2012.

[23] T. Proell, J. Bolhar-Nordenkampf, P. Kolbitsch, and H. Hofbauer, "Syngas and a separate nitrogen/argon stream via chemical looping reforming - A 140 kW pilot plant study," *Fuel,* vol. 89, no. 6, pp. 1249-1256, Jun 2010, doi: 10.1016/j.fuel.2009.09.033.

[24] B. Kronberger, E. Johansson, G. Loffler, T. Mattisson, A. Lyngfelt, and H. Hofbauer, "A two-compartment fluidized bed reactor for CO2 capture by chemical-looping combustion," *Chemical Engineering & Technology,* vol. 27, no. 12, pp. 1318-1326, Dec 2004, doi: 10.1002/ceat.200402137.

[25] C. Linderholm, A. Abad, T. Mattisson, and A. Lynyfelt, "160 h of chemical-looping combustion in a 10 kW reactor system with a NiO-based oxygen carrier," *International*

Journal of Greenhouse Gas Control, vol. 2, no. 4, pp. 520-530, Oct 2008, doi: 10.1016/j.ijggc.2008.02.006.

[26] E. Johansson, T. Mattisson, A. Lyngfelt, and H. Thunman, "A 300 W laboratory reactor system for chemical-looping combustion with particle circulation," *Fuel,* vol. 85, no. 10-11, pp. 1428-1438, Jul-Aug 2006, doi: 10.1016/j.fuel.2006.01.010.

[27] N. Ding, W. R. Wang, Y. Zheng, C. Luo, P. F. Fu, and C. G. Zheng, "Development and Testing of an Interconnected Fluidized-Bed System for Chemical Looping Combustion," *Chemical Engineering & Technology,* vol. 35, no. 3, pp. 532-538, Mar 2012, doi: 10.1002/ceat.201100560.

[28] P. Kolbitsch, J. Bolhar-Nordenkampf, T. Proll, and H. Hofbauer, "Operating experience with chemical looping combustion in a 120 kW dual circulating fluidized bed (DCFB) unit," *International Journal of Greenhouse Gas Control,* vol. 4, no. 2, pp. 180-185, Mar 2010, doi: 10.1016/j.ijggc.2009.09.014.

[29] M. Ryden and A. Lyngfelt, "Using steam reforming to produce hydrogen with carbon dioxide capture by chemical-looping combustion," *International Journal of Hydrogen Energy,* vol. 31, no. 10, pp. 1271-1283, Aug 2006, doi: 10.1016/j.ijhydene.2005.12.003.

[30] M. Rydén, A. Lyngfelt, and T. Mattisson, "Synthesis gas generation by chemical-looping reforming in a continuously operating laboratory reactor," *Fuel,* vol. 85, no. 12-13, pp. 1631-1641, 2006.

[31] L. F. de Diego, M. Ortiz, F. García-Labiano, J. Adánez, A. Abad, and P. Gayán, "Hydrogen production by chemical-looping reforming in a circulating fluidized bed reactor using Ni-based oxygen carriers," *Journal of Power Sources,* vol. 192, no. 1, pp. 27-34, 2009/07/01/ 2009, doi: https://doi.org/10.1016/j.jpowsour.2008.11.038.

[32] H. P. Hamers, M. C. Romano, V. Spallina, P. Chiesa, F. Gallucci, and M. v. S. Annaland, "Comparison on process efficiency for CLC of syngas operated in packed bed and fluidized bed reactors," *International Journal of Greenhouse Gas Control,* vol. 28, no. 0, pp. 65-78, 2014, doi: http://dx.doi.org/10.1016/j.ijggc.2014.06.007.

[33] A. Zaabout, S. Cloete, S. T. Johansen, M. van Sint Annaland, F. Gallucci, and S. Amini, "Experimental demonstration of a novel gas switching combustion reactor for power production with integrated CO2 capture," *Industrial & Engineering Chemistry Research,* vol. 52, no. 39, pp. 14241-14250, 2013.

[34] S. Noorman, M. van Sint Annaland, and Kuipers, "Packed Bed Reactor Technology for Chemical-Looping Combustion," *Industrial & Engineering Chemistry Research,* vol. 46, no. 12, pp. 4212-4220, 2007/06/01 2007, doi: 10.1021/ie061178i.

[35] H. P. Hamers, F. Gallucci, P. D. Cobden, E. Kimball, and M. van Sint Annaland, "A novel reactor configuration for packed bed chemical-looping combustion of syngas," *International Journal of Greenhouse Gas Control,* vol. 16, no. 0, pp. 1-12, 2013, doi: http://dx.doi.org/10.1016/j.ijggc.2013.02.021.

[36] A. Zaabout, S. Cloete, and S. Amini, "Hydrodynamic Investigation Into a Novel IC-CLC Reactor Concept For Power Production With Integrated CO2 Capture," in *10th International Conference on Computational Fluid Dynamics In the Oil & Gas, Metallurgical and Process Industries*, Trondheim, Norway, 17-19 June 2014.

[37] M. Usman, W. W. Daud, and H. F. Abbas, "Dry reforming of methane: Influence of process parameters—A review," *Renewable Sustainable Energy Reviews,* vol. 45, pp. 710-744, 2015.

[38] A. Zaabout, S. Cloete, S. T. Johansen, M. v. S. Annaland, F. Gallucci, and S. Amini, "Experimental Demonstration of a Novel Gas Switching Combustion Reactor for Power Production with Integrated CO2 Capture," *Industrial & Engineering Chemistry Research,* vol. 52, no. 39, pp. 14241-14250, Oct 2 2013, doi: 10.1021/ie401810n.

[39] A. Zaabout, S. Cloete, and S. Amini, "Autothermal operation of a pressurized Gas Switching Combustion with ilmenite ore," *International Journal of Greenhouse Gas Control,* vol. 63, pp. 175-183, 2017/08/01/ 2017, doi: https://doi.org/10.1016/j.ijggc.2017.05.018.

[40] A. Zaabout, S. Cloete, J. R. Tolchard, and S. Amini, "A pressurized Gas Switching Combustion reactor: Autothermal operation with a CaMnO3−δ-based oxygen carrier," *Chemical Engineering Research and Design,* vol. 137, pp. 20-32, 2018/09/01/ 2018, doi: https://doi.org/10.1016/j.cherd.2018.06.028.

[41] S. A. Wassie, F. Gallucci, A. Zaabout, S. Cloete, S. Amini, and M. van Sint Annaland, "Hydrogen production with integrated CO2 capture in a novel gas switching reforming reactor: Proof-of-concept," *International Journal of Hydrogen Energy,* vol. 42, no. 21, pp. 14367-14379, 2017/05/25/ 2017, doi: https://doi.org/10.1016/j.ijhydene.2017.04.227.

[42] S. A. Wassie *et al.*, "Hydrogen production with integrated CO2 capture in a membrane assisted gas switching reforming reactor: Proof-of-Concept," *International Journal of Hydrogen Energy,* vol. 43, no. 12, pp. 6177-6190, 2018/03/22/ 2018, doi: https://doi.org/10.1016/j.ijhydene.2018.02.040.

[43] A. Zaabout, P. I. Dahl, A. Ugwu, J. R. Tolchard, S. Cloete, and S. Amini, "Gas Switching Reforming (GSR) for syngas production with integrated CO2 capture using iron-based oxygen carriers," *International Journal of Greenhouse Gas Control,* vol. 81, pp. 170-180, 2019/02/01/ 2019, doi: https://doi.org/10.1016/j.ijggc.2018.12.027.

[44] A. Ugwu, A. Zaabout, J. R. Tolchard, P. I. Dahl, and S. Amini, "Gas Switching Reforming for syngas production with iron-based oxygen carrier-the performance under pressurized conditions," *International Journal of Hydrogen Energy,* 2019.

[45] M. Ortiz, A. Abad, F. Luis, F. García-Labiano, P. Gayán, and J. Adánez, "Optimization of hydrogen production by chemical-looping auto-thermal reforming working with Ni-based oxygen-carriers," *International journal of hydrogen energy,* vol. 36, no. 16, pp. 9663-9672, 2011.

[46] A. Zaabout, S. Cloete, M. van Sint Annaland, F. Gallucci, and S. Amini, "A novel gas switching combustion reactor for power production with integrated CO2 capture: Sensitivity to the fuel and oxygen carrier types," *International Journal of Greenhouse Gas Control,* vol. 39, pp. 185-193, 2015/08/01/ 2015, doi: https://doi.org/10.1016/j.ijggc.2015.05.006.

[47] S. M. Nazir, S. Cloete, O. Bolland, and S. Amini, "Techno-economic assessment of the novel gas switching reforming (GSR) concept for gas-fired power production with integrated CO2 capture," *International Journal of Hydrogen Energy,* vol. 43, no. 18, pp. 8754-8769, 2018.

[48] J. Bolhar-Nordenkampf, T. Proll, P. Kolbitsch, and H. Hofbauer, "Performance of a NiO-based oxygen carrier for chemical looping combustion and reforming in a 120kW unit," in *Greenhouse Gas Control Technologies 9*, vol. 1, J. Gale, H. Herzog, and J. Braitsch Eds., (Energy Procedia, no. 1), 2009, pp. 19-25.

[49] P. Cho, T. Mattisson, and A. Lyngfelt, "Comparison of iron-, nickel-, copper- and manganese-based oxygen carriers for chemical-looping combustion," *Fuel,* vol. 83, no. 9, pp. 1215-1225, Jun 2004, doi: 10.1016/j.fuel.2003.11.013.

[50] A. Zaabout, S. Cloete, M. van Sint Annaland, F. Gallucci, and S. J. I. J. o. G. G. C. Amini, "A novel gas switching combustion reactor for power production with integrated CO2 capture: Sensitivity to the fuel and oxygen carrier types," vol. 39, pp. 185-193, 2015.

[51] S. A. Wassie, F. Gallucci, A. Zaabout, S. Cloete, S. Amini, and M. J. I. J. o. H. E. van Sint Annaland, "Hydrogen production with integrated CO2 capture in a novel gas switching reforming reactor: Proof-of-concept," vol. 42, no. 21, pp. 14367-14379, 2017.

[52] J. Xu and G. F. Froment, "Methane steam reforming, methanation and water-gas shift: I. Intrinsic kinetics," *AIChE journal,* vol. 35, no. 1, pp. 88-96, 1989.

[53] J.-W. Snoeck, G. Froment, and M. Fowles, "Steam/CO2 reforming of methane. Carbon filament formation by the Boudouard reaction and gasification by CO2, by H2, and by steam: kinetic study," *Industrial & engineering chemistry research,* vol. 41, no. 17, pp. 4252-4265, 2002.

[54] J.-W. Snoeck, G. Froment, and M. Fowles, "Kinetic study of the carbon filament formation by methane cracking on a nickel catalyst," *Journal of Catalysis,* vol. 169, no. 1, pp. 250-262, 1997.

[55] M. Najera, R. Solunke, T. Gardner, and G. Veser, "Carbon capture and utilization via chemical looping dry reforming," *Chemical Engineering Research and Design,* vol. 89, no. 9, pp. 1533-1543, 2011.

[56] W.-J. Jang, J.-O. Shim, H.-M. Kim, S.-Y. Yoo, and H.-S. Roh, "A review on dry reforming of methane in aspect of catalytic properties," *Catalysis Today,* 2018.

[57] Z. Hao, Q. Zhu, Z. Jiang, B. Hou, and H. Li, "Characterization of aerogel Ni/Al2O3 catalysts and investigation on their stability for CH4-CO2 reforming in a fluidized bed," *Fuel Processing Technology,* vol. 90, no. 1, pp. 113-121, 2009.

[58] S. Arora and R. J. R. A. Prasad, "An overview on dry reforming of methane: strategies to reduce carbonaceous deactivation of catalysts," vol. 6, no. 110, pp. 108668-108688, 2016.

[59] S. Wang, G. Lu, G. J. J. E. Millar, and fuels, "Carbon dioxide reforming of methane to produce synthesis gas over metal-supported catalysts: state of the art," vol. 10, no. 4, pp. 896-904, 1996.

[60] O. Muraza and A. J. I. J. o. E. R. Galadima, "A review on coke management during dry reforming of methane," vol. 39, no. 9, pp. 1196-1216, 2015.

[61] M. Usman, W. W. Daud, H. F. J. R. Abbas, and S. E. Reviews, "Dry reforming of methane: Influence of process parameters—A review," vol. 45, pp. 710-744, 2015.

[62] M. Osman, A. Zaabout, S. Cloete, and S. Amini, "Internally circulating fluidized-bed reactor for syngas production using chemical looping reforming," *Chemical Engineering Journal,* 2018/10/04/ 2018, doi: https://doi.org/10.1016/j.cej.2018.10.013.

[63] J. Juan-Juan, M. Román-Martínez, and M. Illán-Gómez, "Effect of potassium content in the activity of K-promoted Ni/Al2O3 catalysts for the dry reforming of methane," *Applied Catalysis A: General,* vol. 301, no. 1, pp. 9-15, 2006.

[64] A. E. C. Luna and M. E. Iriarte, "Carbon dioxide reforming of methane over a metal modified Ni-Al2O3 catalyst," *Applied Catalysis A: General,* vol. 343, no. 1-2, pp. 10-15, 2008.

[65] A. Bejan, *Advanced engineering thermodynamics*. John Wiley & Sons, 2016.

[66] D. Kang, H. S. Lim, M. Lee, and J. W. Lee, "Syngas production on a Ni-enhanced Fe2O3/Al2O3 oxygen carrier via chemical looping partial oxidation with dry reforming of methane," *Applied Energy,* vol. 211, pp. 174-186, 2018/02/01/ 2018, doi: https://doi.org/10.1016/j.apenergy.2017.11.018.

[67] Z. Huang *et al.*, "Evaluation of multi-cycle performance of chemical looping dry reforming using CO2 as an oxidant with Fe–Ni bimetallic oxides," *Journal of energy chemistry,* vol. 25, no. 1, pp. 62-70, 2016.

[68] V. V. Galvita, H. Poelman, C. Detavernier, and G. B. Marin, "Catalyst-assisted chemical looping for CO2 conversion to CO," *Applied Catalysis B: Environmental,* vol. 164, pp. 184-191, 2015.

[69] A. Khalesi, H. R. Arandiyan, and M. Parvari, "Effects of lanthanum substitution by strontium and calcium in La-Ni-Al perovskite oxides in dry reforming of methane," *Chinese Journal of Catalysis,* vol. 29, no. 10, pp. 960-968, 2008.

[70] M. K. Nikoo and N. Amin, "Thermodynamic analysis of carbon dioxide reforming of methane in view of solid carbon formation," *Fuel Processing Technology,* vol. 92, no. 3, pp. 678-691, 2011.

[71] D. Pakhare and J. Spivey, "A review of dry (CO 2) reforming of methane over noble metal catalysts," *Chemical Society Reviews,* vol. 43, no. 22, pp. 7813-7837, 2014.

[72] D. Li, Y. Nakagawa, and K. Tomishige, "Methane reforming to synthesis gas over Ni catalysts modified with noble metals," *Applied Catalysis A: General,* vol. 408, no. 1-2, pp. 1-24, 2011.

[73] N. A. K. Aramouni, J. G. Touma, B. A. Tarboush, J. Zeaiter, and M. N. Ahmad, "Catalyst design for dry reforming of methane: analysis review," *Renewable and Sustainable Energy Reviews,* vol. 82, pp. 2570-2585, 2018.

7 Gas-to-Liquid process for CO_2 utilization through gas switching dry reforming.

This chapter has been adapted from **Article IV**

Ugwu, A., A. Zaabout, SM. Nazir and S. Amini, Gas-to-liquid process for CO_2 utilization through gas switching dry reforming. *Chemical Engineering Journal*, 2020. Under review.

Abstract

The Gas Switching Dry Reforming (GSDR) has recently been introduced for efficient CO_2 capture and utilization in syngas production targeting maximizing fuel conversion when integrated into Gas-to-Liquid (GTL) processes. In the GSDR cycle, the oxygen carrier is first reduced using GTL off-gases producing CO_2 (and steam) that is fed to the next reforming stage for syngas production for GTL processes. The oxygen carrier is then oxidized back in a third stage associated with heat generation through the exothermic oxidation reaction with air. The present study further optimizes the GSDR process to solve two major challenges (i: the high carbon deposition and ii: the low syngas quality $H_2/CO < 1$), thus maximizing the environmental and efficiency of the proposed integrated GSDR-GTL processes. Substituting part of the CO_2 feedstock with steam in the reforming stage was found to reduce carbon deposition below 3% and produce syngas with H_2/CO molar ratio ranging between 1 – 2, making the GSDR suitable for integration with GTL. Given that GTL processes operate at high pressure, operating the GSDR process at high pressure is primordial for easy integration to GTL processes. Pressurized operation would avoid a syngas compression step that is associated with additional capital costs and efficiency loss. To this end, the response of the GSDR process to the operating pressure up to 5bar was investigated. Although the reduction stage was not affected significantly by pressure, the performance in the reforming stage was negatively affected by pressure with a decrease in CH_4 and CO_2 conversions. H_2 selectivity was also negatively affected by increased pressure driven by the reverse water-gas shift (RWGS) reaction enhanced by the unconverted CO_2, thus also reducing the H_2/CO ratio. Research on improving the catalytic activity of the oxygen carrier is therefore highly recommended to maximize the benefits of the GSDR process when the integration into GTL technology is targeted. Following a successful experiment demonstration, a preliminary process simulation was completed in ASPEN to illustrate how the proposed GSDR process could be integrated into a methanol production plant.

7.1 Introduction

The increasing concern of climate change and the urgent need to reduce greenhouse gas emissions have made it crucial to explore efficient ways of converting existing fossil fuels to other value-added products. With this, Gas-to-liquids (GTL) technology started gaining interest in the last two decades as it can convert natural gas to a wide variety of liquid products such as gasoline, jet fuel, waxes, methanol, diesel, oxygenates and other industrially relevant chemicals [1-5]. Two common techniques are used for GTL processes: (i) direct methane conversion to methanol and (ii) Fischer–Tropsch processes that convert syngas ($CO+H_2$) to hydrocarbons. This latter is the most commonly used GTL technique [6]. Although Fischer-Tropsch has been around for almost a century, it is just regaining interest because of the low cost of natural gas and the growing value of petroleum products [6].

Currently, six GTL plants are operating globally, with capacities ranging from 2,700 - 140,000 barrels per day [6]. Two of these plants are in Malaysia and managed by Shell, two plants in Qatar which one of the plants is operated by Shell and the other jointly operated by Sasol and Chevron, the 5th plant in South Africa is operated by Sasol, while the 6th plant (Escravos GTL) in Nigeria is operated jointly by Chevron and Sasol. There was a proposal for three new plants in the United States (Lake Charles Louisiana, Karns City, Pennsylvania and Ashtabula, Ohio), out of which only the Lake Charles facility is of large-scale. Shell canceled the plan to build a large-scale GTL facility in Louisiana in December 2013 because of the high estimated CAPEX and market uncertainty of natural gas and petroleum products [6].

Conventionally, the method of producing chemicals/ liquid fuels from natural gas is always indirect and energy-intensive[7-12] largely because the direct conversion of CH_4 is difficult owing to the localized C-H bonds of high bond energy of 413 kJ.mol^{-1}[13, 14]. A state-of-the-art scheme for Fisher-Tropsch proposed by the U.S. Energy Information Administration is considered in this study to illustrate how the GTL process works (*Figure **7-1**a*) [5]. This scheme shows that several complex steps are needed to convert natural gas to the final liquid fuel product making the process energy and cost-intensive. After sulphur removal to prevent catalyst poisoning natural gas is sent to syngas (a mixture of H_2, CO, and CO_2) production step with the desired H_2/CO molar ratio is produced mainly through partial oxidation or autothermal reforming of methane. The produced syngas is sent to the GTL synthesis stage where H_2 and CO combine in different reactions to produce the liquid hydrocarbons of interest (*Reaction **7-1**-Reaction **7-4***). [15, 16] The liquid products are further refined using different technologies such as thermal cracking to obtain the desired product specification.

$$CO + 3H_2 \rightarrow CH_4 + H_2O \qquad (methanation) \qquad \textit{Reaction 7-1}$$

$$nCO + (2n+1)H_2 \rightarrow C_nH_{2n+2} + nH_2O \qquad (paraffins) \qquad \textit{Reaction 7-2}$$

$$nCO + (2n)H_2 \rightarrow C_nH_{2n} + nH_2O \qquad (olefins) \qquad \textit{Reaction 7-3}$$

$$nCO + (2n)H_2 \rightarrow C_nH_{2n+1}OH + (n-1)H_2O \qquad (alcohols) \qquad \textit{Reaction 7-4}$$

Additionally, the process conditions for Fisher-Tropsch are typically around 10-40 bar pressure and temperature (260-500°C) making the GTL plant, even more, energy-intensive and involving high CAPEX [17-19]. As for the commercial-scale GTL technologies, they use autothermal reforming utilizing an air separation unit to produce syngas. This approach has not received many economic benefits due to the high cost of air separation units making the CAPEX high [20]. To this end, several proposals for alternative FT methods have been proposed [21-25], that uses a different reactor design (eg. micro-channel reactor) and proprietary catalysts allowing GTL production at much smaller scales. These approaches remain however insufficient to sustain global demand. A study at the MIT Joint Program on the Science and Policy of Global Change on the long-term viability of GTL, concludes that GTL with the current process configuration is unlikely to emerge as a profitable industry in the coming decades [26]. It is, therefore, important to intensify the efforts to reduce the costs of GTL plants and improve their long-term profitability to boost their industrial deployment.

To this end, a Gas Switching Dry Reforming (GSDR) process was proposed to replace the syngas production train (as illustrated in *Figure **7-1**b)* while capturing and utilizing CO_2 [our recent published GSDR]. This process is based on chemical looping, a promising alternative technology that can provide efficiency, cost, and environmental benefits over existing technologies [7, 27-32]. Integrating chemical looping in the syngas production step will eliminate the need for air separation units and a pre-reformer system that reforms heavier hydrocarbons [20, 33].

A basic schematic of the chemical looping reforming process is depicted in *Figure **7-2**a*, illustrating the three-steps that take place in the process of syngas production with integrated CO_2 capture. In this process, a metal oxide (oxygen carrier) is circulated between interconnected fluidized bed reactors, namely, the air and fuel reactors. In the fuel, the metal oxide is reduced by the reaction between the fuel and the lattice O_2 of the metal oxide in an N_2-free environment (instead of free O_2 from air separation unit (ASU) as in conventional methods

[34, 35]) to produce metallic radical that catalyzes methane reforming reaction (steam/dry) that occurs simultaneously in the same reactor under autothermal conditions. At this stage, the produced syngas is tuned to the desired H_2/CO molar to match the necessary downstream reaction conditions, with minimal undesirable products. The reduced metal oxide is regenerated

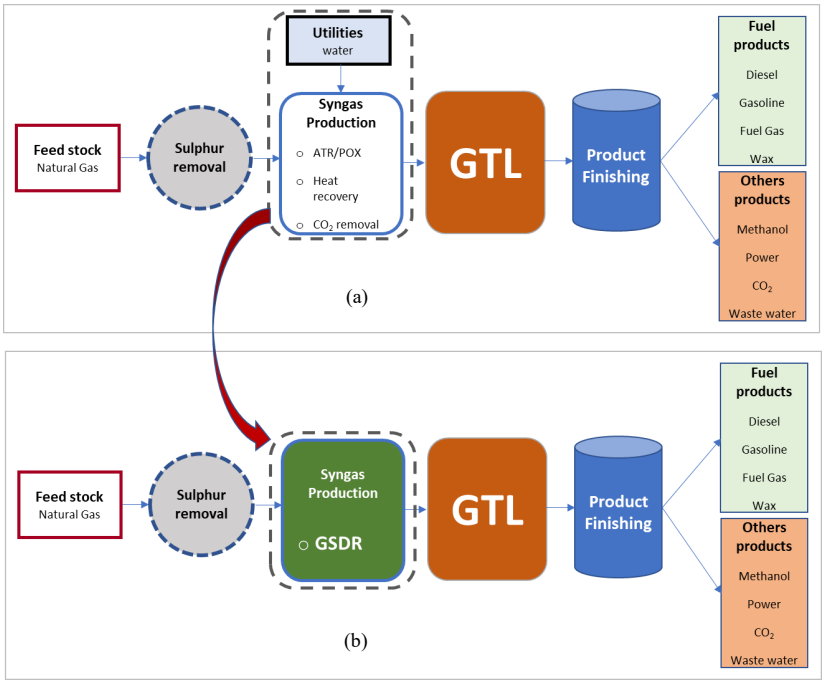

Figure 7-1: (a) state of the art Fisher Tropsch process by U.S. Energy Information Administration, and (b) the proposed GSDR-GTL integration.

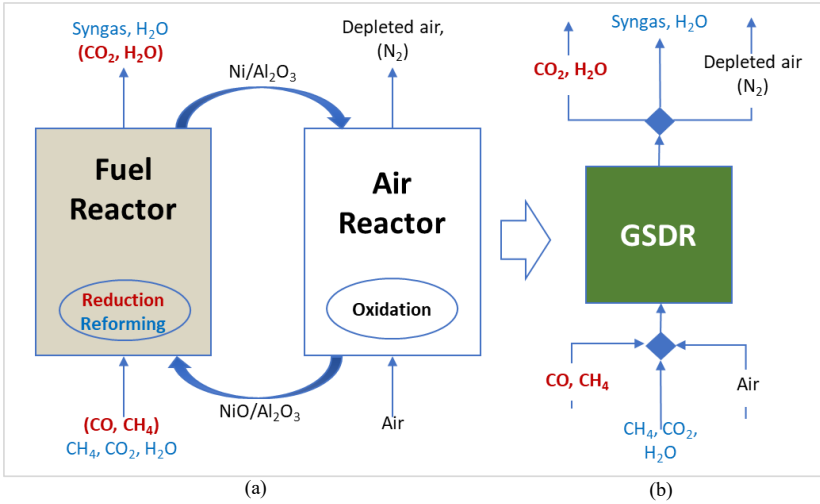

Figure 7-2: Conceptual schemes of the dry reforming process. (a) completed following the chemical looping route. (b) Gas Switching Dry Reforming, GSDR[36].

in the air reactor with inherent air separation and recirculated to the fuel reactor for subsequent redox cycles. Implementing such an arrangement in the conventional chemical looping reforming will require three interconnected reactors (fuel, reformer, and air reactors) which can make the process operation very challenging, especially under high pressure suitable for integration with Fisher-Tropsch (10 - 35 bar for the different applications, while methanol synthesis operates between 40 -100 bar [7, 37, 38]).

To maximize process efficiency, the syngas produced should be conditioned to a pressure near the operating pressure of the downstream GTL process. However, operating conventional chemical looping processes at elevated pressures is difficult [39] considering the need for reliable and precise circulation of large quantities of oxygen carrier material between interconnected reactors at elevated temperatures. Attempts have been made in recent years to address these issues with different reactor configurations that avoid external solid circulation such as Gas Switching Technology (GST)", among others [40-42] with the potential to speed up the scale-up of chemical looping based technologies [41, 43-45]. Unlike the conventional chemical looping, GST utilizes a single fluidized bed reactor where the oxidizing and reducing gases are alternated to complete redox reactions without external circulation of the oxygen carrier (*Figure **7-2***b). This simplified GST configuration makes it easy to pressurize syngas production through the GSDR process, close to the pressure of the downstream GTL process thus enhancing an efficient GSDR-GTL integration.

Furthermore, as syngas remains a building block for GTL processes thus the production of a suitable syngas quality (H_2/CO molar ratio) is important for reducing the processing steps, thus saving costs [46] and having control over adjusting the syngas quality to suit different GTL applications is important; too high H_2/CO ratio $\geq$3 of SMR and too low H_2/CO ratio $\leq$ 1 of dry methane reforming is not optimal for the GTL processes. Syngas quality 1<H_2/CO<3 is most suitable for GTL processes; methanol synthesis requires a 2:1 H_2:CO molar ratio while hydrocarbon synthesis requires 1.5 - 2:1 H_2:CO molar ratio or slightly higher [47-50]. To modify the H_2:CO molar ratio to the optimal value, CO_2 utilization in the reforming process has been proposed in several studies [20, 33, 36, 51-53] including chemical looping making the dry reforming of natural gas more economically and environmentally attractive. With the chemical looping option, the possible reactions at the syngas production step could vary from *Reaction **7-5*** - *Reaction **7-16***.

Reduction Stage

$$CO + NiO \rightarrow Ni + CO_2 \qquad (\Delta H_{298K} = -43.3 kJmol^{-1})$$ *Reaction 7-5*

$$CH_4 + 4NiO \rightarrow 4Ni + CO_2 + 2H_2O \qquad (\Delta H_{298K} = +156.2 kJmol^{-1})$$ *Reaction 7-6*

Reforming stage

$$CH_4 + CO_2 \rightarrow 2CO + 2H_2 \qquad (\Delta H_{298K} = +247.0 kJmol^{-1})$$ *Reaction 7-7*

$$CH_4 + H_2O \rightarrow CO + 3H_2 \qquad (\Delta H_{298K} = +205.9 kJmol^{-1})$$ *Reaction 7-8*

$$CO_2 + H_2 \leftrightarrow CO + H_2O \qquad (\Delta H_{298K} = +41.1 kJmol^{-1})$$ *Reaction 7-9*

$$CH_4 \rightarrow C + 2H_2 \qquad (\Delta H_{298K} = +74.9 kJmol^{-1})$$ *Reaction 7-10*

$$2CO \rightarrow C + CO_2 \qquad (\Delta H_{298K} = -172.4 kJmol^{-1})$$ *Reaction 7-11*

$$C + CO_2 \rightarrow 2CO \qquad (\Delta H_{298K} = +172.4 kJmol^{-1})$$ *Reaction 7-12*

$$C + H_2O \rightarrow CO + H_2 \qquad (\Delta H_{298K} = +131.2 kJmol^{-1})$$ *Reaction 7-13*

Oxidation Stage

$$2Ni + O_2 \rightarrow 2NiO \qquad (\Delta H_{298K} = -479.4 kJmol^{-1})$$ *Reaction 7-14*

$$C + O_2 \rightarrow CO_2 \qquad (\Delta H_{298K} = -393.5 kJmol^{-1})$$ *Reaction 7-15*

$$2C + O_2 \rightarrow 2CO \qquad (\Delta H_{298K} = -221.1 kJmol^{-1})$$ *Reaction 7-16*

From previous studies, it is possible to adjust the syngas quality (H_2/CO ratio of 1) of dry reforming reaction (*Reaction **7-7***) [54-56] to optimal values for GTL processes [57]. This motivated our first study of autothermal Gas Switching Dry Reforming (GSDR) with the proposed process configuration shown in *Figure 7-2*b [36]. The novel approach could circumvent the problem of catalyst deactivation through carbon deposition, by cyclic gasification of the deposited carbon (*Reaction **7-10*** and *Reaction **7-11***) in the oxidation stage. This is however at the expense of reduced CO_2 capture efficiency [36]. Carbon deposition mainly from methane cracking led to a very high H_2/CO ratio (>> 1), imposing the need for process optimization for a successful and cost-effective GTL integration. Feeding larger CO_2/CH_4 was found to minimize carbon deposition but leads to a very low syngas ratio (H_2/CO

molar ratio < 1) [36]. Chunshan et al. suggest steam addition in the reforming stage to achieve a combined dry and steam reforming effect to tune the syngas ratio (H_2/CO molar ratio) and reduce carbon deposition [58] in agreement with a previous study that proposed that high O/C and H/C ratios help to reduce carbon deposition [59]. Recently, Sang Moon Lee et. al. adopted a similar approach using a membrane reactor and could control the H_2/CO ratio by manipulating the $CH_4/CO_2/H_2O$ input ratio [60].

With the aforementioned challenges, this study experimentally explores different options for optimizing the H_2/CO ratio of the GSDR process proposed in our previous study [36] to facilitate its integration to GTL processes and enable better control of GTL products at reduced process steps. Two main approaches were adopted to improve the H_2/CO ratio: i) tuning of the CO_2:CH_4 molar ratio in the gas feed and ii) substitution of part of the CO_2 feedstock with steam. Finally, a sensitivity study at elevated pressure up to 5 bar was completed to highlight the effect of pressure on the H_2/CO ratio. The response of other key performance indicators, such as feed gas conversion, both in the reduction and reforming stages, and carbon deposition, to the different operating parameters, was investigated. If successfully demonstrated, the GSDR process can maximize the environmental (through CO_2 capture in the reduction stage and its utilization in the reforming stage) and the energy efficiency benefits of the GTL technology (through the utilization of GTL off-gas in the reduction stage), thus accelerating the commercial deployment of GTL technology.

7.2 Experiment demonstration

7.2.1 Experimental setup

The experimental set up consists of a fluidized bed reactor with 5 cm inner diameter and 50 cm height, in addition to a freeboard region, expanding from 5cm to 10 cm ID at the top, to minimize particle entrainment (*Figure **6-4***). The total height of the reactor, including the body and the freeboard, is 90cm. The reactor vessel is made of Inconel 600 to withstand high temperatures up to 1000°C. Gas is fed into the reactor using a lance extending towards to bottom of the reactor to create some fountain for effective gas distribution. Heat is supplied to the reactor through an external electrical heating elements wound around the reactor vessel and covered with a 25cm thick insulation. The control of the process parameters, data acquisition

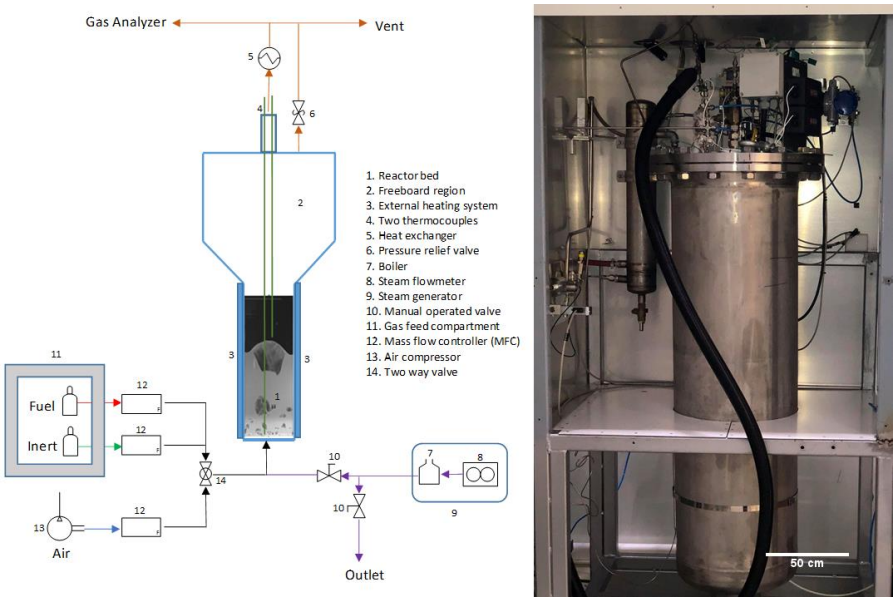

Figure 7-3: GSDR Experimental setup.

and logging is done through a LabVIEW application. Bronkhorst mass flow controllers were used to regulate the gas feed into the reactor. A three-way valve separates the air and fuel feeds during the redox process. The outlet gas stream is passed through a cooler to reduce to temperature to the acceptable level for the gas analyzer and the ventilation system. ETG syngas analyzer is used to measure the gas composition while the temperature is measured using two thermocouples located at 2cm and 20cm inside the bed.

7.2.2 Methodology

This experimental study was completed using a NiO/Al_2O_3 oxygen carrier with 35% active content manufactured by VITO through spray drying. About 623 g of the oxygen carrier was used corresponding to a 0.3m static bed height. The particle size cut-offs D_{10}, D_{50}, and D_{90} are 117.4, 161.7, and 231.3µm respectively. The loosely packed density is 1950 kg/m^3 while the tapped density is 2166 kg/m^3. This oxygen carrier has been used in the first autothermal demonstration of the GSDR process [36] and also used for other previous chemical looping studies including combustion [61-65] with good stability and catalytic performance.

Typical GSDR cycles were completed starting with the reduction stage by feeding a gaseous fuel (CO/CH_4) to react with NiO to produce Ni which catalyzes the reforming reaction. Note that, the GTL off-gases consist mainly of a mixture of CO, H_2, and CH_4 (in addition to CO_2) which converts well with the oxygen carrier in the reduction reactions[66], making GSDR-GTL

integration a feasible option. The reduction stage is followed by the reforming stage where CH_4, CO_2/H_2O are co-fed in the presence of Ni (catalyst) to produce syngas (CO and H_2) through reforming reactions. This stage is energy demanding, justifying the need for the consecutive exothermic oxidation stage where pure air is fed to oxidize Ni back to NiO to produce heat for the process and regenerate the oxygen carrier, in addition to removing any deposited carbon on the catalyst from the precedent stages.

All the experiments were performed at an average temperature of 850°C maintained through a combination of the heat of reactions and external electric heating. For the experiments at atmospheric conditions, 12.8nl/min CO was fed into the reactor for 3min to achieve 50% oxygen carrier utilization at the reduction stage, 3.2nl/min CH_4 (and CO_2 at various CH_4/CO_2 ratios) in the reforming stage and 10nl/min feed of pure air in the oxidation stage. To achieve good mixing and optimal heat transfer, the gas flow was maintained within the bubbling/turbulent fluidization region. Temperature, pressure, and gas composition readings were recorded and the reactor performance was evaluated using the measures as presented in section ***7.2.3***. Process simulation of GSDR integration into the syngas source of a methanol process was completed in ASPEN using the GSDR experiment results at atmospheric conditions.

7.2.3 Reactor performance indicators

Different indicators have been defined in this section to evaluate the GSDR reactor performance bearing in mind that the objective of the GSDR process is to convert CH_4, CO_2/H_2O to syngas (H_2 and CO) with minimal CO_2 emission. It is desired to have maximal fuel conversion in the reduction stage, and maximal CH_4, CO_2, and H_2O conversion in the reforming stage respectively. At the reduction stage, the CO conversion is important since it determines how much Ni that would be available to catalyze the reforming reactions and quantified in *Equation **7-17***. At the reforming stage, the syngas quality H_2/CO molar ratio (*Equation **7-18***) is very important for integration to GTL processes while CH_4, CO_2, and H_2O conversion determine the extent of the reforming reaction, selectivities and overall syngas yield. The CH_4, CO_2, and H_2O conversions at the reforming stage are defined (*Equation **7-19*** - *Equation **7-21***). Carbon deposition may occur at the reforming and fuel stage with the deposited carbon was released in the form of CO and CO_2 at the oxidation stage. It is desired to have minimal carbon deposition to produce syngas with high purity and achieve high CO_2 capture efficiency. The carbon deposition at the reforming stage is quantified in *Equation **7-22***. Carbon affects CO selectivity

(*Equation* ***7-23***), H_2O production through RWGS reaction affects H_2 selectivity (*Equation* ***7-24***) while both carbon and H_2O production affect the overall syngas selectivity (*Equation* ***7-25***). The concentrations and purity of the syngas in the outlet gas stream are affected by the mixing of the carbon, H_2O, and the unconverted reactants in the reforming stage. Thus, syngas yield quantifies this mixing/dilution effect in *Equation* ***7-26***.

$$\gamma_{CO} = 1 - \frac{n_{CO,out\_red}}{n_{CO,in\_red}} \qquad \textit{Equation 7-17}$$

$$\frac{H_2}{CO} = \frac{n_{H_2,out\_ref}}{n_{CO,out\_ref}} \qquad \textit{Equation 7-18}$$

$$\gamma_{CH_4} = 1 - \frac{n_{CH4,out\_ref}}{n_{CH_4,in\_ref}} \qquad \textit{Equation 7-19}$$

$$\gamma_{CO_2} = 1 - \frac{n_{CO_2,out\_ref}}{n_{CO_2,in\_ref}} \qquad \textit{Equation 7-20}$$

$$\gamma_{H_2O} = 1 - \frac{n_{H_2O,out\_ref}}{n_{H_2O,in\_ref}} \qquad \textit{Equation 7-21}$$

$$C_{dep} = \frac{n_{Cin\_ref} - n_{Cout\_ref}}{\gamma_{CH_4} * n_{CH_4,in\_ref} + \gamma_{CO_2} * n_{CO_2,in\_ref}} \qquad \textit{Equation 7-22}$$

$$s_{CO} = \frac{n_{CO,out\_ref}}{\gamma_{CH_4} * n_{CH_4,in\_ref} + \gamma_{CO_2} * n_{CO_2,in\_ref}} \qquad \textit{Equation 7-23}$$

$$s_{H_2} = \begin{Bmatrix} \dfrac{n_{H_2,out_{ref}}}{2\left(\gamma_{CH_4} * n_{CH_4,in_{ref}}\right)} & without\ steam \\ \dfrac{n_{H_2,out_{ref}}}{3\left(\gamma_{CH_4} * n_{CH_4,in_{ref}}\right)} & with\ steam \end{Bmatrix} \qquad \textit{Equation 7-24}$$

$$\emptyset_{syngas} = \frac{n_{CO,out\_ref} + n_{H_2,out\_ref}}{n_{H_2,out\_ref} + n_{CO,out\_ref} + n_{C,out\_ref} + n_{H_2O,out\_ref}} \qquad \textit{Equation 7-25}$$

$$\gamma_{syngas} = \frac{n_{CO,out\_ref} + n_{H_2,out\_ref}}{3 * n_{CH_4,in\_ref} + n_{CO_2,in\_ref} + n_{H_2O,in\_ref}} \qquad \textit{Equation 7-26}$$

7.3 Results and discussion

The first demonstration of the GSDR concept investigated the effect of CO_2:CH_4 ratio between 1-3 which achieved a very low H_2/CO molar ratio that requires optimization before applying to GTL processes [36]. In this study, the GSDR process performance is mapped out for GTL integration by further tuning the CO_2:CH_4 ratio, investigating the effect of steam addition to the reforming stage, and the effect of the pressurized operation. Except for the pressurized case, CO was used as fuel in the reduction stage to show the possibility of utilizing GTL off-gases where CO forms the largest share in the gas mixture. From the previous study, reducing the degree of this Ni-based oxygen carrier reduction impacts positively the process in terms of improved fuel conversion and reduced carbon deposition [36]. Therefore, a 50% degree of oxygen carrier reduction was maintained at the reduction stage in this campaign. At the reforming stage, CH_4, CO_2/H_2O were co-fed in the presence of metallic Ni (catalyst) for different reactions (*Reaction **7-7** - Reaction **7-13***) that produce syngas (CO+H_2). The oxidation stage was kept sufficiently long to ensure complete gasification/combustion of any deposited carbon and to fully oxidize the oxygen carrier before starting a new cycle. As mentioned earlier, this demonstration was not authothermal unlike the previous study [36], instead heat was supplied to maintain the reactor temperature around 800 °C. This choice is to some extent valid given that heat losses in an industrial GSDR scale will be substantially small, besides, that heat integration of between the incoming and outgoing flue gasses would substantially reduce the temperature variation in the cycle.

7.3.1 GSDR behavior

Typical behavior of the GSDR cycle at different CO_2:CH_4 molar ratio from 0.25 – 2, 850°C, and 1bar is shown through the experimental transient gas composition (*Figure **7-4**a*). The gas composition at the reduction stage shows that the transient CO conversion is similar for all the cases indicating that the same degree of reduction of the oxygen carrier was achieved before the start of the reforming stage(*Figure **7-4**a*). The relatively high conversion of CO produces high purity CO_2 at this stage which can be captured directly without further purification. CO conversion decreases towards the end of the reduction stage possibly due to an increase in carbon deposition. The produced CO_2+H_2O (if CH_4 is used as fuel) in the reduction stage could be sent to the reforming stage to improve process efficiency and reduce cost.

At the reforming stage, it was observed in all cases that CH_4 conversion decreased throughout the stage(*Figure **7-4**a*). Interestingly, the CH_4 slippage escalates in the last two-thirds of the

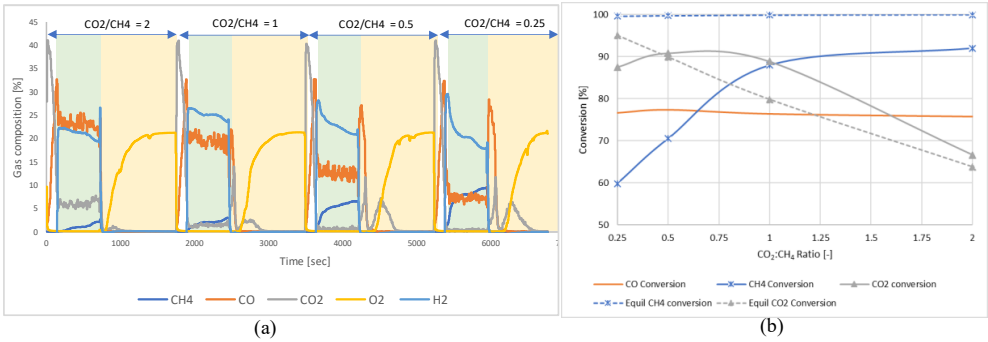

(a) (b)

Figure 7-4: (a) The transient gas composition at the reactor outlet, (b) Gas conversion at different CO_2:CH_4 molar ratios at 850°C and 1bar showing the process behavior at different CO_2:CH_4 molar ratio. The gas flowrate as follows: CO 12.8nl/min at the reduction stage; CH_4 3.2nl/min, CO_2 0.8 - 6.4nl/min at the reforming stage; air_ 10nl/min at the oxidation stage. NOTE: a known amount of N_2 was added both in the reduction and reforming stages respectively to quantify the amount of each species.

reforming stage with an increased magnitude as the CO_2: CH_4 ratio decreases. This behavior is correlated to the extent of carbon deposition that increases rapidly as the CO_2:CH_4 ratio decreases (carbon deposition is detected in the oxidation stage shown in *Figure **7-4**a* in the form of the released CO/CO_2 due to the oxy-gasification of the deposited carbon). Carbon deposition likely becomes more pronounced starting from the last two-thirds of the stage reducing active site availability and thus triggering the escalation in CH_4 slippage. Nevertheless, *Figure **7-4**b* shows that the average CH_4 conversion remains between 60 - 92% for the range of CO_2:CH_4 ratio covered in the study (0.25 to 2) which is acceptable as the unconverted fuel could be recycled in the cycle for reduction of the oxygen carrier. CO_2 conversion remains steady across the reforming stage while H_2 fraction decreases (*Figure **7-4**a*). This could be explained by the fact that the reverse water gas shift - RWGS (*Reaction **7-9***) enhances the conversion of CO_2 and H_2 to produce CO and H_2O despite the decrease in CH_4 conversion; in agreement with the findings in previous studies [67-69]. However, CO_2 conversion decreases with an increase in CO_2:CH_4 ratio driven by the excess CO_2 in the system (*Figure **7-4**b)*. Nonetheless, the achieved gas conversions remain higher than the result reported in a previous study with similar impregnated Ni/Al_2O_3 catalyst in a fluidized bed with 10%wt active content [5] probably due to higher Ni content and lower than the conversion from aerogel Ni/Al_2O_3 catalyst[70] probably due to the difference in surface area as a result of the production method.

CH_4 conversion was lower than the equilibrium prediction while the CO_2 conversion was higher (*Figure 7-4b)* confirming the finding in our previous study and suggesting that kinetics of the different involved mechanisms have a higher influence on the process performance. Substantial

carbon deposition occurred at a lower CO_2:CH_4 ratio but remains below equilibrium predictions (*Figure* ***7-5***a). Carbon deposition was found to decrease significantly with the increase in CO_2:CH_4 ratio (*Figure* ***7-5***a). Previous studies have confirmed that the first intrinsic step of the dry reforming reaction is methane decomposition to produce H_2 and carbon (deposit) followed by the gasification of the deposited carbon to produce CO [5, 71]. This mechanism explains the observed results given that carbon deposition reduces with the increase in the partial pressure of the oxidant (higher O/C ratio) which is in agreement with previous findings [59]. With the decrease in carbon deposition, CO selectivity increases but H_2 selectivity declines (*Figure* ***7-5****b*) as attributed earlier to the RWGS reaction. The high syngas yield achieved is most likely due to the high CO_2 conversion that exceeded equilibrium prediction. The resulting syngas (H_2/CO) molar ratio follows a similar trend with carbon deposition confirming its high dependency to the extent of carbon deposition. The release of CO_2/CO at the air stage (*Figure* ***7-4***a) is due to the combustion/gasification of the deposited carbon thus adversely affecting the CO_2 capture efficiency and CO_2 utilization given that the produced gases are vented to the atmosphere with the depleted air. A post-firing step may be needed to combust the produced CO leading to increased cost. Yet, minimizing carbon deposition in the reduction and reforming stages is crucial for maximizing the environmental and economic impacts of the GSDR process.

In general, varying the CO_2:CH_4 ratio from 0.25 – 2 could produce syngas with optimal quality (1< H_2/CO < 3) and up to 90% syngas purity suitable for GTL processes. However, with this performance carbon deposition and excess of unconverted CO_2 from the reforming remain two major challenges to solve for unlocking the expected environmental and economic benefits of

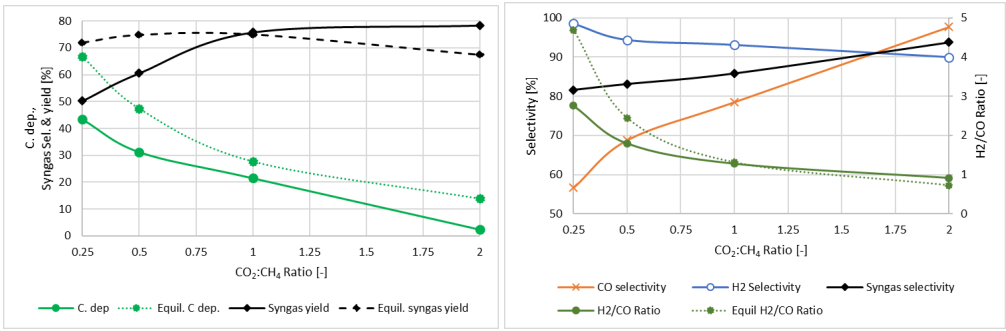

(a) (b)

Figure 7-5: (a)The change in syngas yield and carbon deposition, (b) H_2 and CO selectivity, and syngas quality (H_2/CO molar ratio)against CO_2:CH_4 molar ratio at 850°C and 1bar. The gas flowrate as follows: CO 12.8nl/min at the reduction stage; CH_4 3.2nl/min, CO_2 0.8 - 6.4nl/min at the reforming stage; air 10nl/min at the oxidation stage. NOTE: a known amount of N_2 was fed in the reduction and reforming stages respectively to quantify the amount of each species.

GSDR-GTL integration. Carbon deposition does not only have a negative impact on gas conversion and H_2/CO ratio for GTL applications but also affects CO_2 utilization negatively. For example, the measured carbon deposition at a CO_2:CH_4 molar ratio of 0.25 was ~43% implying that the captured CO_2 for GSDR utilization was barely 57% without accounting for the additional carbon slippage that occurs between the stages. On the other side, the CO_2 capture efficiency increases to ~97% at a CO_2:CH_4 molar ratio of 2 due to the low carbon deposition of 3%, but over 35% of fed CO_2 was unconverted and requires implementing a separation step to avoid substantial dilution of the downstream process that may negatively affect its performance. Nonetheless, the major advantage of varying the CO_2:CH_4 molar ratio in the gas feed is that it creates flexibility in the process performance and syngas quality for different GTL applications. Having an excess of CO_2 in the feed results in high methane conversion, high CO_2 utilization, and reduced carbon deposition but with low syngas purity (high dilution with unconverted CO_2) and H_2/CO ratio <1. On the other hand, low CO_2 feed achieves higher purity syngas and H_2/CO ratio>2 but associated with low methane conversion and high carbon deposition. Further optimization of the GSDR process is therefore needed to minimize the impact of the aforementioned challenges.

7.3.2 Effect of steam addition

Dry methane reforming utilizes CO_2 as feedstock thus offsetting the increasing GHG emission and yields stoichiometric syngas H_2/CO molar ratio of 1 which is too low and requires to be tuned up for GTL processes. Steam methane reforming, on the other hand, is slightly less energy-intensive but produces a stoichiometric H_2/CO ratio of 3, which is too high and requires to be tuned down for the downstream GTL processes. Furthermore, dry reforming has a higher tendency towards carbon deposition than steam methane reforming, in agreement with a previous study [72] which found that steam tends to reduce carbon deposition because of the formation of surface hydroxyl species which inhibits methane decomposition [73]. To leverage the advantages of these two reactions, it is logical to co-feed H_2O, CO_2, and CH_4 in the reforming stage of the GSDR process to combine the effect of steam reforming, dry reforming and partial oxidation of methane to produce syngas with the desired H_2/CO ratio for GTL processes with less energy intensity. This approach aligns with the proposed GSDR-GTL integration where GTL off-gasses contain H_2 and CO (and possibly unconverted CH_4) with different extents depending on the GTL process, that will produce H_2O and CO_2 in the reduction stage and which will be directed to the reforming stage to produce syngas.

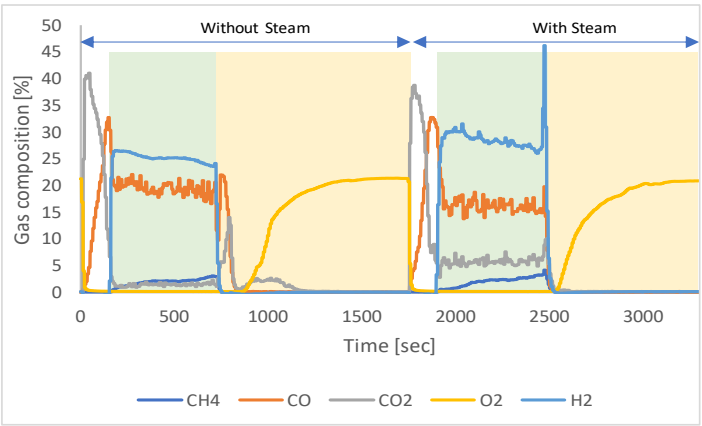

Figure 7-6: Transient gas composition showing GSDR behavior with and without steam at CO_2:CH_4 molar ~1, 850°C, and 1bar. gas flowrate as follows: CO_ 12.8nl/min at the reduction stage; CH_4 3.2nl/min, CO_2 3.2nl/min, (H_2O 3nl/min for the case with steam) at the ref. stage; air 10nl/min at the oxidation stage. NOTE: a known amount of N_2 was fed in the reduction and reforming stages respectively to quantify the amount of each species.

To demonstrate the effect of steam, three cases (with and without steam) were completed by varying CO_2:CH_4 from 0.25 to 1. The range of CO_2:CH_4 was chosen where significant carbon deposition was observed. Experiments were completed at atmospheric conditions, 850°C, and a constant H_2O/CO_2 molar ratio of 1 when H_2O was added. The process behavior could be explained using the transient gas composition at the reactor outlet (*Figure **7-6***). As expected, steam addition improved the syngas (H_2/CO) molar ratio and removed carbon deposition since no CO_2/CO was produced in the oxidation stage.

The effect of steam addition on the different key performance indicators is shown in *Figure **7-7***. Steam addition improved CH_4 conversion, but had a negative effect on CO_2 conversion, with an increased extent for both performance indicators as CO_2:CH_4 ratio is increased. The increase in CH_4 conversion (*Figure 7-7a*) could be attributed to the higher extent of reforming and gasification reactions since steam is a better gasifying agent than CO_2 due to its lower dissociation energy as opposed to CO_2. This behavior conforms with the equilibrium prediction (*Figure 7-7b*). The expected benefit of steam addition on carbon deposition was also demonstrated, reducing it to below 3% when a feed composed of H_2O:CO_2:CH_4 = 1:1:1 was used (*Figure 7-7c*), owing to the resulting increase of the O/C and H/C ratios in the feed. It was also observed that the syngas (H_2/CO) molar ratio follows the same trend as carbon deposition (*Figure 7-7d*). Consequently, CO selectivity was positively affected (*Figure 7-7*e) following the improved gasification reaction with steam (*Reaction **7-13***). However, H_2O addition reduces CO_2 conversion (*Figure 7-7b*) counteracting the RWGS reaction (*Reaction **7-9***), thus positively

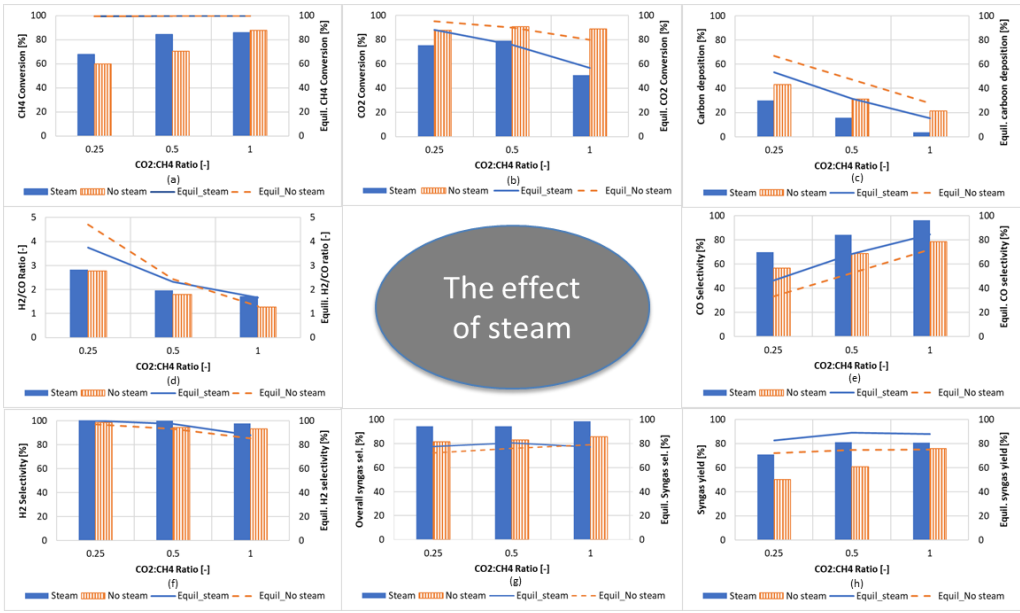

Figure 7-7: The effect of steam at different CO_2:CH_4 molar ratio while maintaining CO_2:H_2O molar ratio of 1, (a) CH_4 Conversion, (b) CO_2 conversion, (c) Carbon deposition, (d) H_2/CO molar ratio, (e) CO selectivity, (f) H_2 selectivity, (g) Overall syngas selectivity, and (h) Syngas yield. Experiments were completed at 850°C and 1bar. The gas flowrate as follows: CO 12.8nl/min at the reduction stage; CH_4 3.2nl/min, CO_2 0.8- 3.2nl/min, H_2O 0.75-3nl/min at the reforming stage; air 10nl/min at the oxidation stage. NOTE: a known amount of N_2 was fed in the reduction and reforming stages respectively to quantify the amount of each species.

affecting H_2 selectivity (*Figure 7-7f)*. The overall syngas selectivity (*Figure 7-7g*) and yield (*Figure 7-7h*) improve with steam addition, while a decline in syngas yield shown when CO_2:CH_4 ratio increased to 1 is due to the considerable decline CO_2 conversion thus causing product dilution.

In summary, steam addition resulted in improvement in syngas quality (H_2/CO molar ratios close to 2 could be achieved at 0.5 <CO_2/CH_4<1 with H_2O feed equal to CO_2) providing an additional variable to further control this important parameter when considering efficient integration with GTL processes. It also minimized carbon deposition thus improving the ability of the GSDR process to efficiently capture carbon for ultimate utilization in GTL. It should be noted that the needed steam could be directly sourced from the reduction stage if methane is used as a reducing agent or if the GTLoff-gases contain unconverted hydrogen. When GSDR is to be operated autothermally, for converting one mole of CH_4 through dry reforming (*Reaction 7-7*), 247 kJ of heat is required to be supplied which is equivalent to the heat generated from the combustion of ~0.3 mol of CH_4 (the standard heat of combustion of CH_4 is

taken as 802 kJ/mol). This will produce 0.3 mole CO_2 and 0.6 mole H_2O to be supplied to the reforming stage to bring the benefits of minimized carbon deposition and adequate syngas quality. This estimation was made assuming adiabatic conditions and no sensible heat is needed to heat the feed gases from room temperature to the reaction operating temperature, otherwise larger CO_2 and H_2O production could be expected.

7.3.3 The effect of pressure

GTL processes operate at elevated pressures; therefore, it is necessary to also operate the syngas production step at high pressures to make the proposed integration to the downstream GTL processes efficient. From a process optimization point of view, high-pressure operations would also increase process capacity, reduce equipment sizes, and cost [74]. Therefore, understanding the effect of operating pressure on the GSDR syngas generation step is essential to the design of the overall system. It should be noted that very limited studies have been published on pressurized chemical looping [75-78] suggesting that the conventional looping configuration may be facing technical challenges hindering its pressurized operation. However, the Gas Switching technology that the current GSDR is based on has been successfully tested for other processes at elevated pressures[43, 79, 80].

The effect of pressure on the GSDR performance was investigated at CO_2/CH_4 ratio of 2 (this value was chosen to reduce carbon deposition as illustrated in section ***7.3.1***). Pure CH_4 was used in the reduction stage, while CO_2 was added only in the reforming stage. The feed rates to each stage were increased proportionally to the pressure to maintain the residence time constant. *Figure* ***7-8*** shows the transient gas composition at the reactor outlet of the GSDR cycle for the different operating pressures investigated in this study. The result shows that CH_4 conversion

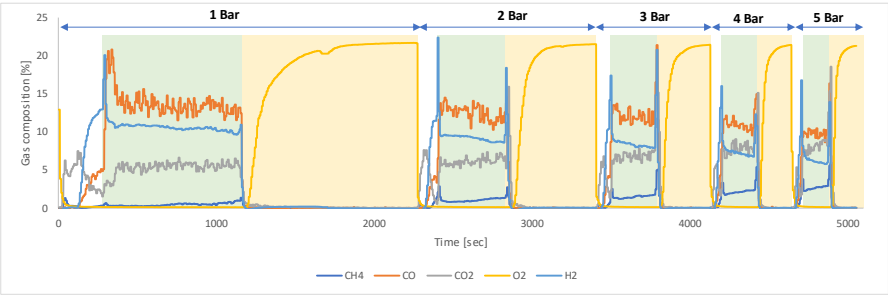

Figure 7-8: The transient gas composition for different pressures (1-5bar) at CO_2:CH_4 molar ratio of 2 and 850°C. The gas flowrate as follows: CH_4 1 - 5nl/min at the reduction stage; CH_4 1 - 2nl/min, CO_2 2-10nl/min at the reforming stage; air 10 - 50nl/min at the oxidation stage. NOTE: a known amount of N_2 was fed in the reduction and reforming stages respectively to quantify the amount of each species.

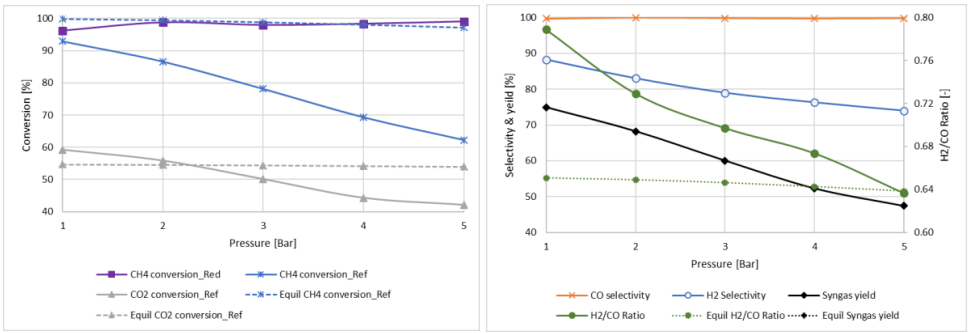

(a) (b)

Figure 7-9: (a) The variation of gas conversion and (b) The variation of selectivity, yield and syngas quality (H_2/CO molar ratio) with pressure at CO_2:CH_4 molar ratio of 2 and 850°C. The gas flowrate as follows: CH_4 1 - 5nl/min at the reduction stage; CH_4 1 - 5nl/min, CO_2 2- 10nl/min at the reforming stage; air 10 - 50nl/min at the oxidation stage. NOTE: a known amount of N_2 was fed in the reduction and reforming stages respectively to quantify the amount of each species.

was high in the reduction stage, although two different sub-stage behaviors were observed: the 1st sub-stage is associated with high selectivity to combustion (CO_2 and H_2O) while in the 2nd sub-stage, CH_4 converts mainly to syngas (H_2+CO). These behaviors were also observed in previous studies [36], where the behavior at the 1st substage is attributed to the easy access to oxygen at the start of the reduction stage leading to full combustion of methane. The partial oxidation of methane to syngas shown at the 2nd substage starts once enough metallic Ni sites become available to catalyze the reforming reactions. Nevertheless, the overall CH_4 conversion in the reduction stage was high and insensitive to the pressure (*Figure **7-9**a)* implying that the oxygen carrier achieves relatively the same reduction level before starting the dry reforming stage. CH_4 and CO_2 conversion in the reforming stage were negatively affected by the pressure showing increased slippage (*Figure **7-8***) and leading to reduced syngas yield as the pressure is increased (*Figure **7-9**b)*. This is in agreement with thermodynamics but with a much larger extent for the experimental results (*Figure **7-9**a)*. This indicates that elevated pressure slows down the kinetics of the dry reforming reaction with this specific oxygen carrier; a challenge that could be compensated for by operating at higher temperatures as suggested in previous studies [16, 81] or by selecting a better oxygen carrier/catalyst to improve the kinetics of the process[16].

CO selectivity was found to improve with an increase in pressure due to the positive effect of pressure in reducing carbon deposition (carbon deposition completely eliminated at 5 bar). Surprisingly H_2 selectivity was negatively affected against equilibrium predictions. This result could be explained by the larger excess of CO_2 left in the system due to the negative effect of

pressure on CO_2 conversion, which counteracted the adverse effect of pressure on RWGS (*Reaction 7-9*) leading to decreased H_2 production. Consequently, this leads to overall syngas quality (H_2/CO molar ratio) deterioration as the pressure is increased (*Figure **7-9**b)*.

Despite the small range of pressure covered in this study, it has given a clear idea of how fast the performance of the reforming stage can deteriorate when the pressure is increased. In principle, a drop of up to 30% in methane conversion could be accommodated given that the unconverted fuel will be utilized in the reduction stage needed for heat supply to the GSDR process. However, the current results revealed that with the current oxygen carrier, CH_4 conversion will drop to 39.36% at 20 bar and to 26.28% at 40 bar while CO_2 conversion drops to 27.62% and 19.91% for the two operating pressures respectively (assuming a fitted logarithmic change of gas conversion with pressure). Obviously, increasing the operating temperature would reduce the impact of pressure on methane conversion, but it is unlikely that thermodynamic conversion could be achieved at economically low temperatures with this oxygen carrier. Extreme operating temperatures would pose new challenges linked to oxygen carrier mechanical stability and involves the need for special expensive alloys to withstand the combined high-pressure high-temperature reactive conditions.

In light of these numbers, finding an oxygen carrier with improved catalytic activity for the dry reforming reaction is necessary for achieving the expected economic and environmental benefits of the GSDR concept for integration with GTL processes. The optimal candidate should achieve at least 70% conversion of methane (70% equilibrium methane conversion is achieved at 850 °C and 50bar) while the unconverted 30% could be recycled to the reduction stage. The improvement in the dry reforming reaction conversion will also drive larger CO_2 conversion that will limit the effect of the RWGS, thus maintaining a high H_2/CO molar ratio for efficient integration with GTL.

7.4 Simulating GSDR-GTL (Methanol synthesis) Integration

As explained in the introduction (*Section **7.1***), the main aim of this study is to replace the syngas production of the state-of-the-art GTL process with GSDR (*Figure **7-1***). Here, the GSDR process will be integrated into the methanol process to supply syngas for reactions *Reaction **7-27***/*Reaction **7-28*** to produce methanol. The three GSDR stages (reduction, reforming, and oxidation) are designed to start with the reduction (white in *Figure **7-10***) by feeding CH_4 and unconverted gas from the methanol process is recycled back to the reduction stage to reduce

the active NiO to Ni. The produced CO_2 and H_2O will be utilized in the reforming stage (green in *Figure* ***7-10***) where CH_4, CO_2, and/Steam react in the presence of Ni/NiO catalyst to produce syngas (CO and H_2). The outlet gases from this stage, containing mainly syngas with the desired H_2/CO molar ratio of ~2, which is sent to the methanol process. The oxidation stage (yellow in *Figure* ***7-10***) starts after the reforming stage where pure air is fed to re-oxidized the reduced oxygen carrier (Ni) to NiO and generate heat. A typical gas composition profile for different stages of one GSDR cycle at 1bar, 850°C and H_2O:CO_2:CH_4 feed composition of 1:1:2 is shown in *Figure* ***7-10***b. It can be shown from the gas composition that CO_2 and CO could also be produced in the oxidation stage due to the combustion and gasification of the deposited carbon in the reduction and reforming stages impacting CO_2 capture efficiency negatively. To minimize this negative effect, the process is designed to achieve a 50% degree of reduction to prevent excessive coking. The proposed GSDR-GTL process integration scheme is shown in *Figure* ***7-11***. One experimental GSDR case where H_2O, CO_2, and CH_4 are co-fed in the reforming stage at atmospheric conditions and H_2O:CO_2:CH_4 molar ratio of 1:1:2 that produced syngas quality H_2/CO molar ratio of ~ 2 (*Figure* ***7-10***b) is considered to demonstrate the proposed GSDR-MeOH integration.

$$CO + 2H_2 \leftrightarrow CH_3OH \quad (\Delta H_{298K} = -90.6 kJmol^{-1}) \qquad \textit{Reaction 7-27}$$

$$CO + 3H_2 \leftrightarrow CH_3OH + H_2O \quad (\Delta H_{298K} = -49.6 kJmol^{-1}) \qquad \textit{Reaction 7-28}$$

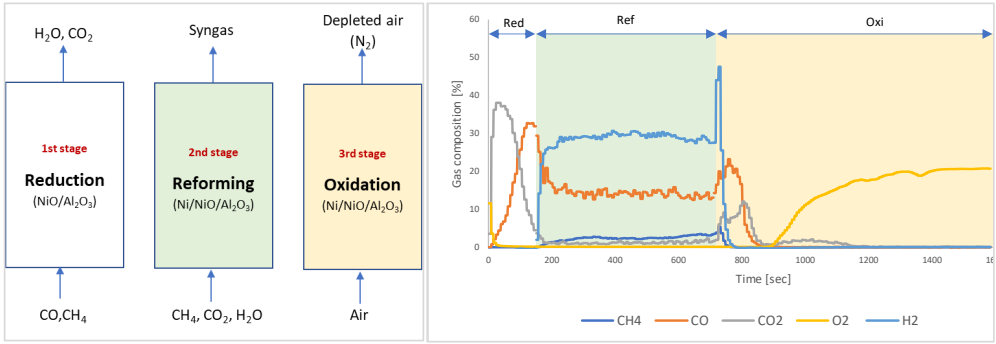

(a) (b)

Figure 7-10: (a) The configuration of the three-stage GSDR process: reduction (white), reforming (green), and oxidation (yellow) stages. (b) Gas composition for case 1 with H_2O:CO_2:CH_4 feed composition of 1.07:1:2 at 850°C and 1bar. The gas flowrate as follows: CO 12.8nl/min at the reduction stage; CH_4 3.2nl/min, CO_2 1.6nl/min, H_2O 1.5nl/min at the reforming stage; air 10nl/min at the oxidation stage. NOTE: a known amount of N_2 was fed in the reduction and reforming stages respectively to quantify the amount of each species.

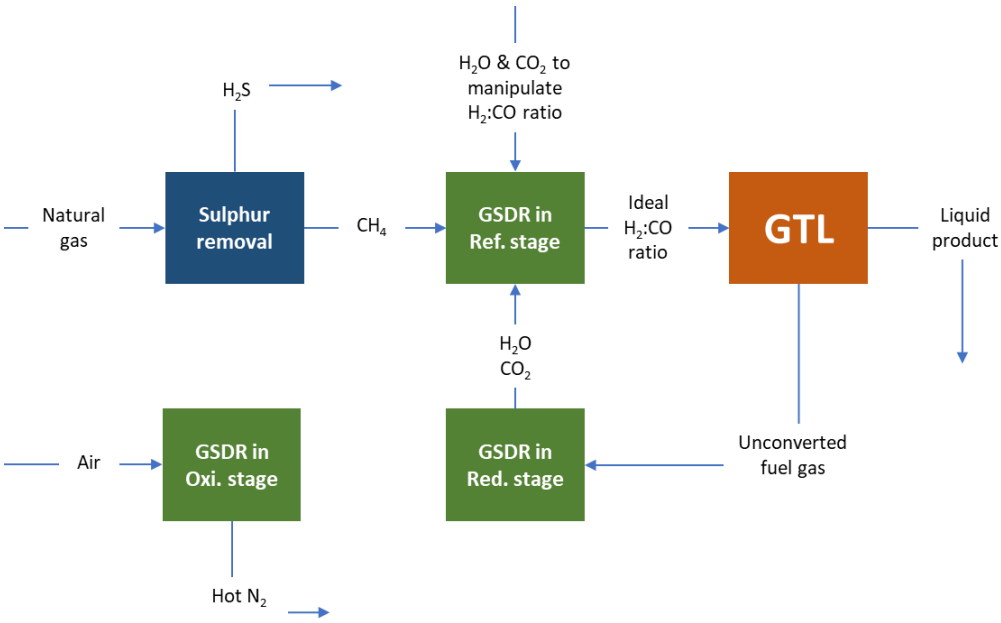

Figure 7-11: Proposed GSDR-GTL integration [36].

7.4.1 Process description

Figure ***7-12*** shows the schematic of the integrated GSDR and the methanol synthesis process. The process design is based on experimental design conditions in the GSDR steps. The methanol synthesis and recovery section are similar to the reference case presented by IEAGHG [82] with some modifications to suit the design conditions in the GSDR process. CH_4 and CO_2 are pre-heated to 850 °C (assuming 830 °C is achieved through pre-heating with the methanol outlet gas stream and the remaining 20 °C with electrical heating), mixed with the reduction step outlet stream and sent to the reforming step to produce syngas quality H_2/CO molar ratio of ~2. The syngas from the reforming step of the GSDR is cooled, firstly to pre-heat the reforming inlet and prepare saturated 2 bar steam with cooling water to 30 °C. The cooled syngas is then compressed in three stages up to 93 bar, which is the design pressure in the methanol synthesis reactor [82]. The methanol synthesis reaction is exothermic, and the reactor is maintained at 260 °C to achieve maximum conversion. The heat from the reactor is recovered to prepare saturated 2 bar steam. The product stream from the methanol synthesis reactor pre-heats the inlet and is further cooled down to 50 °C. The unconverted gas stream is recycled back to the methanol reactor, where the molar ratio of the syngas and recycled gas is 1:11. The liquid stream after cooling the product stream from the methanol synthesis reactor contains the methanol formed during the reaction along with other components. The liquid stream is first

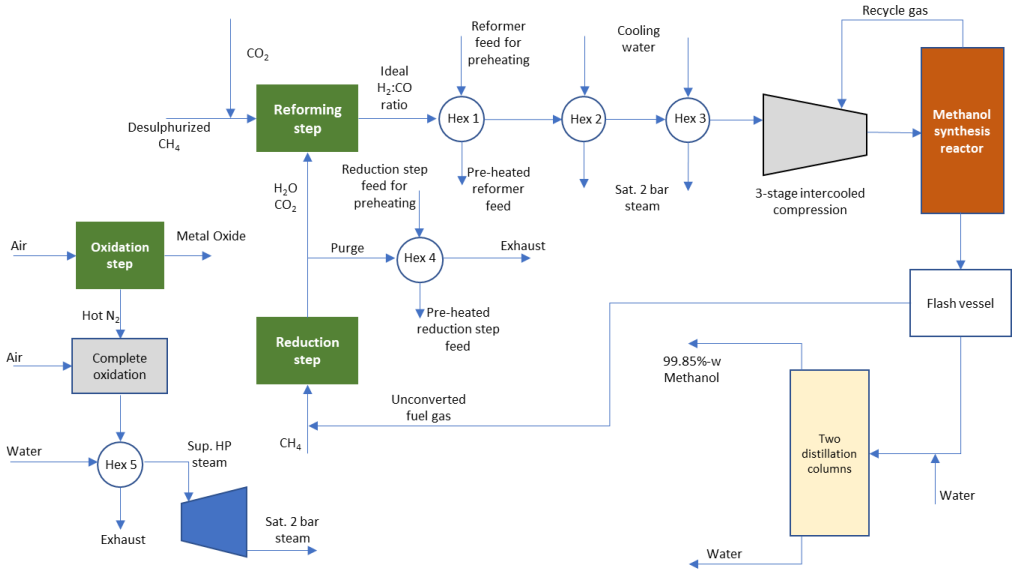

Figure 7-12: Schematic of the integrated GSDR and methanol production process

expanded in a flash vessel to 6 bar, where the gaseous mixture contains unconverted gases that are sent to the reduction stage of the GSDR process. The liquid stream containing mainly methanol is mixed with water to achieve the molar concentration of ~70% methanol. The methanol and water mixture is sent to the distillation column to remove the non-condensable impurities. In the second distillation column, methanol is recovered with 99.85%-wt purity at the top of the distillation column, followed by further cooling to liquefy the produced methanol.

The unconverted fuel gas from the flash vessel of the methanol synthesis process is mixed with additional CH_4 and preheated before the reduction step of GSDR. A fraction (9%) of the reduction outlet stream is purged out to maintain the ideal H_2:CO molar ratio of ~2 at the end of the reforming step. The heat from the purge stream is recovered to pre-heat the inlet gas stream to the reduction step up to 246 °C. It is assumed that the reduction inlet is further heated to 850 °C using electrical heating. The off-gas stream from the oxidation step contains CO, which is mixed with additional air to convert all the CO to CO_2. The heat from the exhaust gases is then recovered to prepare superheated high-pressure steam at 110 bar and 510 °C which is expanded in the steam turbine to 2 bar. The 2 bar streams, from the steam turbine and the steam prepared from heat recovery from methanol reactor, are used to provide a fraction of the heat to the reboiler in the distillation columns for methanol separation. Electrical energy is used to compensate for the remainder of the reboiler duty.

The methanol synthesis process is modeled using Aspen Hysys V10. Peng-Robinson equation of state is used to estimate the property data [83]. The equilibrium reactor module was used to simulate the conditions in the methanol synthesis reactor. 20 stage distillation columns were assumed to recover methanol. The pressure drops, adiabatic efficiency of the pumps, polytropic efficiency of the steam turbine, gas turbine, air compressors, and syngas compressors are assumed similar to the work from Nazir, et al. [84].

7.4.2 The overall process performance

The performance for the GSDR-GTL is compared against the conventional MeOH synthesis using auto-thermal reforming (ATR). Although the results presented here give an understanding of the energy intensity of the processes, we should maintain caution, since ATR is a purely MeOH synthesis technology, whereas GSDR-GTL is a CO_2 utilization technology. The comparison of the key indicators is shown in *Table **7-1***. The heat of the dry reforming reaction is 247 kJ/mol-CH_4 while the overall heat of the reaction in ATR is -0.97 kJ/mol-CH_4 (negative sign indicates, it is an exothermic reaction). Therefore, the specific energy intensity defined as the total LHV input of the fuel per ton of MeOH produced is higher in GSDR-GTL because of the endothermic reactions in the reforming stage of GSDR. However, the higher energy intensity results in utilizing 0.78 t-CO_2 per t-MeOH produced. In the GSDR-GTL process, it is

Table 7-1: The overall simulation results of the proposed GSDR-GTL process and the reference ATR-GTL case.

Indicator	Units	GSDR-GTL	ATR-GTL[82]
Specific energy intensity (LHV of NG per ton of MeOH produced)	GJ/t-MeOH	43.40	30.4
Specific CO_2 utilized (CO_2 utilized per ton of MeOH produced)	t-CO_2/t-MeOH	0.78	0.00
Specific electricity input (electricity per ton MeOH produced)	GJ/t-MeOH	17.76	0.32

assumed that pre-heating of the process streams and the distillation columns are using electrical energy in addition to compressors and pumps. About 83% of the electrical energy is required in distillation columns to separate pure MeOH followed by 14% used in compressors. The resulting specific electrical input to the GSDR-GTL process is significantly higher than the ATR process. The syngas in the ATR process has a higher steam composition, and therefore when the syngas is cooled before compressing it for MeOH synthesis, the heat from condensation is used in distillation columns. However, due to lower steam composition in the syngas from the GSDR process, the condensation heat is not sufficient to be used in distillation columns for MeOH separation. Different design conditions in the process can help in reducing the energy and electrical intensity of the GSDR-GTL process. For instance, as compression work makes up a significant part of the electrical energy requirement (0.85MJ/hr ~14% of the total energy input), a high-pressure operation could improve the electrical efficiency of the process. however, it is also important to remember that syngas production is negatively affected by pressure as explained in section ***7.3.3***. With these observations, a comprehensive process modeling, simulation, and a parametric study are needed to evaluate the best overall process condition for GSDR-GTL integration.

7.5 Conclusion

This study experimentally demonstrates that the novel GSDR process could be optimized for eventual integration into GTL processes to maximize their environmental and efficiency benefits. With GSDR integration to GTL processes, the major greenhouse gases (CO_2 & CH_4) are converted to syngas used to produce a variety of downstream products, making a great impact on carbon capture, utilization, and sequestration (CCUS). The three-stages nature of the GSDR cycle makes it perfectly suited for efficient integration with GTL and maximized fuel conversion through recycling the GTL off-gases for reducing the oxygen carrier in GSDR. This study investigated the effect of CO_2:CH_4 ratio, steam addition, and pressure on syngas quality and other GSDR process performance.

By varying the CO_2:CH_4 ratio from 0.25 – 2, the desired H_2/CO molar ratio between 1-3 was achieved with up to 90% syngas purity suitable for GTL processes. Although carbon deposition was significant for CO_2:CH_4 ratio less than 2, activity and catalyst stability was not negatively affected since the cyclic nature of GSDR ensured that all the produced carbon was gasified/combusted in the oxidation stage on the expenses of reduced CO_2 capture and utilization efficiency. Substituting part of CO_2 in the feed by steam has minimized carbon

deposition while maintaining the desirable syngas quality (H_2/CO molar ratio) between 1 – 3 suitable for GTL processes. Given that steam will be the product of the reduction stage of the GSDR, such a process promises substantial cost by the elimination of the air separation unit used in the conventional tri-reforming/autothermal reforming alternatives.

High-pressure operation negatively affected the reforming stage performance, showing a rapid deterioration of CH_4 and CO_2 conversion with increased pressure. H_2 selectivity was also negatively affected driven by the excess unconverted CO_2 that enhances the RWGS to increase CO selectivity. Interestingly, no carbon deposition has been observed at high pressure. Increased temperature may reduce the negative effect of pressure on the reaction kinetics, but it is unlikely that performance close to equilibrium will be achieved with this specific oxygen carrier at an economically feasible operating temperature, suggesting the need for research on enhancing the catalytic performance of the oxygen carrier.

Finally, the results suggest that there could be enormous benefits to integrate GSDR into gas-to-liquids processes such as improved process efficiency, reduced GHG emission, and improved profitability to enhance commercial deployment. It is therefore important to maximize GSDR performance by creating an optimal combination between CO_2:CH_4 ratio, steam addition, and suitable oxygen carrier with improved kinetics at high pressure. Although a preliminary process modeling was reported to show how GSDR-GTL integration works, comprehensive process modeling, techno-economics, and parametric studies are needed to fully unravel the potentials of the proposed GSDR-GTL process integration.

Acknowledgment

ACT GaSTech project. Project No 271511.

This project has received funding from The Research Council of Norway and is cofounded by the European Commission under the Horizon 2020 programme, ACT Grant Agreement No 691712. The VATL Lab technicians at the Norwegian University of Science and Technology are equally acknowledged for constructing and maintaining the experimental setup.

Nomenclature

Abbreviations

ATR	Auto-thermal Reforming
CCS	Carbon Capture and Storage
CCUS	Carbon Capture Utilization and Storage
CLDR	Chemical Looping Dry Reforming
CLR	Chemical Looping Reforming
GHG	Greenhouse gas
GSDR	Gas Switching Dry Reforming
GSR	Gas Switching Reforming
GTL	Gas-To-Liquid
LHV	Lower Heating Value
NG	Natural Gas
NGCC	Natural Gas Combined Cycle
MeOH	Methanol
RWGS	Reverse Water Gas Shift

Symbols

C_{dep}	Carbon deposition.
D_{10}	Diameter of the catalyst which 10% of a sample mass is smaller than
D_{50}	Diameter of the catalyst which 50% of a sample mass is smaller than
D_{90}	Diameter of the catalyst which 90% of a sample mass is smaller than
n_{C,out_ref}	Mole of C at the gas outlet during reforming stage
n_{CH_4,in_ref}	Mole of CH_4 fed during reforming stage
n_{CH4,out_ref}	Mole of CH_4 at the gas outlet during reforming stage
n_{CO,out_oxi}	Mole of CO at the gas outlet during oxidation stage

n_{CO_2,out_oxi}	Mole of CO_2 at the gas outlet during oxidation stage
n_{CO,out_red}	Mole of CO at the gas outlet during reduction stage
n_{CO,in_red}	Mole of CO fed during reduction stage
n_{CO,out_ref}	Mole of CO at the gas outlet during reforming stage
n_{CO_2,in_ref}	Mole of CO_2 fed during reforming stage
n_{CO_2,out_ref}	Mole of CO_2 at the gas outlet during reforming stage
n_{H_2,out_ref}	Mole of H_2 at the gas outlet during reforming stage
n_{H_2O,out_ref}	Mole of H_2O at the gas outlet during reforming stage
S_{CO}	CO selectivity
S_{H2}	H_2 selectivity
$\emptyset_{syngas}$	Overall syngas selectivity
γ_{CH_4}	CH_4 conversion
γ_{CO}	CO conversion
γ_{CO_2}	CO_2 conversion
γ_{syngas}	Syngas yield

References

[1] U. EIA, "Short-term energy outlook (STEO)," ed: News Release, Feb, 2018.

[2] E. Levelized, "Cost and Levelized Avoided Cost of New Generation Resources in the Annual Energy Outlook 2018," 2018.

[3] M. Asaro, R. M. Smith, and B. H. Davis, "Coal to Liquids Technologies," *Fossil Energy,* pp. 387-426, 2020.

[4] D. C. Dayton, B. Turk, and R. Gupta, "Syngas cleanup, conditioning, and utilization," *Thermochemical Processing of Biomass: Conversion into Fuels, Chemicals and Power,* pp. 125-174, 2019.

[5] M. Usman, W. W. Daud, and H. F. Abbas, "Dry reforming of methane: Influence of process parameters—A review," *Renewable and Sustainable Energy Reviews,* vol. 45, pp. 710-744, 2015.

[6] A. Malik and V. Mantri, "Gas-to-liquids plants face challenges in the US market," *US Energy Information Administration (EIA),* 2014.

[7] P. Sandvik, M. Kathe, W. Wang, F. Kong, and L.-S. Fan, "High-Pressure Chemical Looping Reforming Processes: System Analysis for Syngas Generation from Natural Gas and Reducing Tail Gases," *Energy & fuels,* vol. 32, no. 10, pp. 10408-10420, 2018.

[8] M. Lyubovsky, S. Roychoudhury, and R. LaPierre, "Catalytic partial "oxidation of methane to syngas" at elevated pressures," *Catalysis letters,* vol. 99, no. 3-4, pp. 113-117, 2005.

[9] J. R. Rostrup-Nielsen, "Production of synthesis gas," *Catalysis today,* vol. 18, no. 4, pp. 305-324, 1993.

[10] H. R. Shahhosseini, M. Farsi, and S. Eini, "Multi-objective optimization of industrial membrane SMR to produce syngas for Fischer-Tropsch production using NSGA-II and decision makings," *Journal of Natural Gas Science and Engineering,* vol. 32, pp. 222-238, 2016.

[11] H. J. Venvik and J. Yang, "Catalysis in microstructured reactors: Short review on small-scale syngas production and further conversion into methanol, DME and Fischer-Tropsch products," *Catalysis Today,* vol. 285, pp. 135-146, 2017.

[12] D. Wilhelm, D. Simbeck, A. Karp, and R. Dickenson, "Syngas production for gas-to-liquids applications: technologies, issues and outlook," *Fuel processing technology,* vol. 71, no. 1-3, pp. 139-148, 2001.

[13] R. H. Crabtree, "Current Ideas and Future Prospects in Metal-Catalyzed Methane Conversion," in *Studies in Surface Science and Catalysis*, vol. 81: Elsevier, 1994, pp. 85-92.

[14] P. Tang, Q. Zhu, Z. Wu, and D. Ma, "Methane activation: the past and future," *Energy & Environmental Science,* vol. 7, no. 8, pp. 2580-2591, 2014.

[15] M. Haid, P. Schubert, and C. Bayens, "Synthetic fuel and lubricants production using gas-to-liquids technology," *DGMK Tagungsbericht,* vol. 3, pp. 205-212, 2000.

[16] S. Arora and R. Prasad, "An overview on dry reforming of methane: strategies to reduce carbonaceous deactivation of catalysts," *RSC advances,* vol. 6, no. 110, pp. 108668-108688, 2016.

[17] M. Höök, D. Fantazzini, A. Angelantoni, and S. Snowden, "Hydrocarbon liquefaction: viability as a peak oil mitigation strategy," *Philosophical Transactions of the Royal Society A: Mathematical, Physical and Engineering Sciences,* vol. 372, no. 2006, p. 20120319, 2014.

[18] Y. Huang *et al.*, "Energy use, greenhouse gases emission and cost effectiveness of an integrated high–and low–temperature Fisher–Tropsch synthesis plant from a lifecycle viewpoint," *Applied Energy,* vol. 228, pp. 1009-1019, 2018.

[19] A. Bernardi, J. E. Graciano, and B. Chachuat, "Production of chemicals from syngas: an enviro-economic model-based investigation," in *Computer Aided Chemical Engineering*, vol. 46: Elsevier, 2019, pp. 367-372.

[20] M. Kathe *et al.*, "Utilization of CO 2 as a partial substitute for methane feedstock in chemical looping methane–steam redox processes for syngas production," *Energy & Environmental Science,* vol. 10, no. 6, pp. 1345-1349, 2017.

[21] N. Mohammad, R. Y. Abrokwah, R. G. Stevens-Boyd, S. Aravamudhan, and D. Kuila, "Fischer-Tropsch Studies in a 3D-Printed Stainless Steel Microchannel Microreactor Coated with Cobalt-based Bimetallic-MCM-41 Catalysts," *Catalysis Today,* 2020.

[22] S. Ansari, H. Sarwat, and N. Shahid, "An Investigation of Various Parameters in a Fixed Bed Fisher-Tropsch Reactor," *Nova Journal of Engineering and Applied Sciences,* vol. 3, no. 3, 2016.

[23] H. Kirsch, N. Lochmahr, C. Staudt, P. Pfeifer, and R. Dittmeyer, "Production of CO2-neutral Liquid Fuels by Integrating Fischer-Tropsch Synthesis and Hydrocracking in a Single Micro-

structured Reactor: Performance Evaluation of Different Configurations by Factorial Design Experiments," *Chemical Engineering Journal,* p. 124553, 2020.

[24] M. Ziaei, M. Panahi, M. A. Fanaei, A. Rafiee, and K. R. Khalilpour, "Maximizing the profitability of integrated Fischer-Tropsch GTL process with ammonia and urea synthesis using response surface methodology," *Journal of CO2 Utilization,* vol. 35, pp. 14-27, 2020.

[25] V. B. Borugadda, G. Kamath, and A. K. Dalai, "Techno-economic and life-cycle assessment of integrated Fischer-Tropsch process in ethanol industry for bio-diesel and bio-gasoline production," *Energy,* p. 116985, 2020.

[26] M. Dwortzan. "Is there a future for gas-to-liquids technology?-Study assesses profitability and impact on the transportation sector." https://globalchange.mit.edu/news-media/jp-news-outreach/there-future-gas-liquids-technology (accessed.

[27] S. M. Nazir, S. Cloete, O. Bolland, and S. Amini, "Techno-economic assessment of the novel gas switching reforming (GSR) concept for gas-fired power production with integrated CO2 capture," *International journal of hydrogen energy,* vol. 43, no. 18, pp. 8754-8769, 2018.

[28] S. M. Nazir, J. H. Cloete, S. Cloete, and S. Amini, "Techno-economic Comparison Of Combined Cycle Power Plants With Pre-combustion CO2 Capture Via Two Different Reforming Methods: Chemical Looping Reforming And Gas Switching Reforming," in *14th International Conference on Greenhouse Gas Control Technologies, GHGT-14, 21st-25th October 2018, Melbourne, Australia*, 2018, pp. 21-26.

[29] A. Cabello *et al.*, "Economic analysis of pressurized chemical looping combustion for steam assisted gravity drainage applications," *International Journal of Greenhouse Gas Control,* vol. 90, p. 102786, 2019.

[30] H. Bahzad *et al.*, "Development and techno-economic analyses of a novel hydrogen production process via chemical looping," *International Journal of Hydrogen Energy,* vol. 44, no. 39, pp. 21251-21263, 2019.

[31] M. N. Khan and T. Shamim, "Techno-economic assessment of a plant based on a three reactor chemical looping reforming system," *international journal of hydrogen energy,* vol. 41, no. 48, pp. 22677-22688, 2016.

[32] L. Zhu, Y. He, L. Li, and P. Wu, "Tech-economic assessment of second-generation CCS: Chemical looping combustion," *Energy,* vol. 144, pp. 915-927, 2018.

[33] M. Kathe *et al.*, "Modularization strategy for syngas generation in chemical looping methane reforming systems with CO2 as feedstock," *AIChE Journal,* vol. 63, no. 8, pp. 3343-3360, 2017.

[34] J. Adanez, A. Abad, F. Garcia-Labiano, P. Gayan, and F. Luis, "Progress in chemical-looping combustion and reforming technologies," *Progress in energy and combustion science,* vol. 38, no. 2, pp. 215-282, 2012.

[35] X. Zhu, F. Donat, Q. Imtiaz, C. R. Müller, and F. Li, "Chemical Looping Beyond Combustion–A Perspective," *Energy & Environmental Science,* 2020.

[36] A. Ugwu, A. Zaabout, and S. Amini, "An advancement in CO2 utilization through novel gas switching dry reforming," *International Journal of Greenhouse Gas Control,* vol. 90, p. 102791, 2019/11/01/ 2019, doi: https://doi.org/10.1016/j.ijggc.2019.102791.

[37] W. W. Tso, A. M. Niziolek, O. Onel, C. D. Demirhan, C. A. Floudas, and E. N. Pistikopoulos, "Enhancing natural gas-to-liquids (gtl) processes through chemical looping for syngas production: Process synthesis and global optimization," *Computers & Chemical Engineering,* vol. 113, pp. 222-239, 2018.

[38] H. Gai, K. Zheng, J. Lin, and H. Lou, "Process Simulation, Economic and Environmental Sustainability Assessment of a Gas-To-Liquids Process," *J Chem Eng Process Technol,* vol. 9, p. 373, 2018.

[39] T. Pröll, J. Bolhàr-Nordenkampf, P. Kolbitsch, and H. Hofbauer, "Syngas and a separate nitrogen/argon stream via chemical looping reforming–A 140 kW pilot plant study," *Fuel,* vol. 89, no. 6, pp. 1249-1256, 2010.

[40] M. Osman, A. Zaabout, S. Cloete, and S. Amini, "Internally circulating fluidized-bed reactor for syngas production using chemical looping reforming," *Chemical Engineering Journal,* vol. 377, p. 120076, 2019.

[41] S. Noorman, M. van Sint Annaland, and H. Kuipers, "Packed bed reactor technology for chemical-looping combustion," *Industrial & Engineering Chemistry Research,* vol. 46, no. 12, pp. 4212-4220, 2007.

[42] A. Ugwu *et al.*, "Hydrogen production by water splitting using gas switching technology," *Powder Technology,* 2020.

[43] A. Zaabout, S. Cloete, and S. Amini, "Autothermal operation of a pressurized Gas Switching Combustion with ilmenite ore," *International Journal of Greenhouse Gas Control,* vol. 63, pp. 175-183, 2017/08/01/ 2017, doi: https://doi.org/10.1016/j.ijggc.2017.05.018.

[44] S. M. Nazir, J. H. Cloete, S. Cloete, and S. Amini, "Gas switching reforming (GSR) for power generation with CO2 capture: Process efficiency improvement studies," *Energy,* vol. 167, pp. 757-765, 2019.

[45] H. Hamers, F. Gallucci, P. Cobden, E. Kimball, and M. van Sint Annaland, "A novel reactor configuration for packed bed chemical-looping combustion of syngas," *International Journal of Greenhouse Gas Control,* vol. 16, pp. 1-12, 2013.

[46] O. Glebova, "Gas to Liquids–Historical Development and Future Prospects," 2013.

[47] D. Kang, H. S. Lim, M. Lee, and J. W. Lee, "Syngas production on a Ni-enhanced Fe2O3/Al2O3 oxygen carrier via chemical looping partial oxidation with dry reforming of methane," *Applied Energy,* vol. 211, pp. 174-186, 2018/02/01/ 2018, doi: https://doi.org/10.1016/j.apenergy.2017.11.018.

[48] M. E. Dry, "The fischer–tropsch process: 1950–2000," *Catalysis today,* vol. 71, no. 3-4, pp. 227-241, 2002.

[49] A. Y. Khodakov, W. Chu, and P. Fongarland, "Advances in the development of novel cobalt Fischer− Tropsch catalysts for synthesis of long-chain hydrocarbons and clean fuels," *Chemical reviews,* vol. 107, no. 5, pp. 1692-1744, 2007.

[50] O. Eliseev, "Gas-to-liquid technologies," *Russian Journal of General Chemistry,* vol. 79, no. 11, pp. 2509-2519, 2009.

[51] J. Hu, L. Buelens, S.-A. Theofanidis, V. V. Galvita, H. Poelman, and G. B. Marin, "CO2 conversion to CO by auto-thermal catalyst-assisted chemical looping," *Journal of CO2 Utilization,* vol. 16, pp. 8-16, 2016.

[52] A. More, S. Bhavsar, and G. Veser, "Iron–nickel alloys for carbon dioxide activation by chemical looping dry reforming of methane," *Energy Technology,* vol. 4, no. 10, pp. 1147-1157, 2016.

[53] L. K. Rihko-Struckmann *et al.*, "Hydrogen and carbon monoxide production by chemical looping over iron-aluminium oxides," *Energy Technology,* vol. 4, no. 2, pp. 304-313, 2016.

[54] F. Luis, M. Ortiz, J. Adánez, F. García-Labiano, A. Abad, and P. Gayán, "Synthesis gas generation by chemical-looping reforming in a batch fluidized bed reactor using Ni-based oxygen carriers," *Chemical Engineering Journal,* vol. 144, no. 2, pp. 289-298, 2008.

[55] T. D. Gould, A. Izar, A. W. Weimer, J. L. Falconer, and J. W. J. A. C. Medlin, "Stabilizing Ni catalysts by molecular layer deposition for harsh, dry reforming conditions," vol. 4, no. 8, pp. 2714-2717, 2014.

[56] X. Xie, T. Otremba, P. Littlewood, R. Schomäcker, and A. J. A. C. Thomas, "One-pot synthesis of supported, nanocrystalline nickel manganese oxide for dry reforming of methane," vol. 3, no. 2, pp. 224-229, 2013.

[57] D. Pakhare and J. J. C. S. R. Spivey, "A review of dry (CO 2) reforming of methane over noble metal catalysts," vol. 43, no. 22, pp. 7813-7837, 2014.

[58] C. Song and W. Pan, "Tri-reforming of methane: a novel concept for catalytic production of industrially useful synthesis gas with desired H2/CO ratios," *Catalysis Today,* vol. 98, no. 4, pp. 463-484, 2004.

[59] D. Li, Y. Nakagawa, and K. J. A. C. A. G. Tomishige, "Methane reforming to synthesis gas over Ni catalysts modified with noble metals," vol. 408, no. 1-2, pp. 1-24, 2011.

[60] S. M. Lee, I. H. Hwang, and S. S. Kim, "Enhancement of catalytic performance of porous membrane reactor with Ni catalyst for combined steam and carbon dioxide reforming of methane reaction," *Fuel Processing Technology,* vol. 188, pp. 197-202, 2019.

[61] S. A. Wassie *et al.*, "Hydrogen production with integrated CO2 capture in a membrane assisted gas switching reforming reactor: Proof-of-Concept," *International Journal of Hydrogen Energy,* vol. 43, no. 12, pp. 6177-6190, 2018/03/22/ 2018, doi: https://doi.org/10.1016/j.ijhydene.2018.02.040.

[62] J. Bolhar-Nordenkampf, T. Proll, P. Kolbitsch, and H. Hofbauer, "Performance of a NiO-based oxygen carrier for chemical looping combustion and reforming in a 120kW unit," in *Greenhouse Gas Control Technologies 9*, vol. 1, J. Gale, H. Herzog, and J. Braitsch Eds., (Energy Procedia, no. 1), 2009, pp. 19-25.

[63] P. Cho, T. Mattisson, and A. Lyngfelt, "Comparison of iron-, nickel-, copper- and manganese-based oxygen carriers for chemical-looping combustion," *Fuel,* vol. 83, no. 9, pp. 1215-1225, Jun 2004, doi: 10.1016/j.fuel.2003.11.013.

[64] A. Zaabout, S. Cloete, S. T. Johansen, M. v. S. Annaland, F. Gallucci, and S. Amini, "Experimental Demonstration of a Novel Gas Switching Combustion Reactor for Power Production with Integrated CO2 Capture," *Industrial & Engineering Chemistry Research,* vol. 52, no. 39, pp. 14241-14250, Oct 2 2013, doi: 10.1021/ie401810n.

[65] A. Zaabout, S. Cloete, M. van Sint Annaland, F. Gallucci, and S. J. I. J. o. G. G. C. Amini, "A novel gas switching combustion reactor for power production with integrated CO2 capture: Sensitivity to the fuel and oxygen carrier types," vol. 39, pp. 185-193, 2015.

[66] B. Bao, M. M. El-Halwagi, and N. O. Elbashir, "Simulation, integration, and economic analysis of gas-to-liquid processes," *Fuel Processing Technology,* vol. 91, no. 7, pp. 703-713, 2010.

[67] P. Djinović, I. G. O. Črnivec, B. Erjavec, and A. Pintar, "Influence of active metal loading and oxygen mobility on coke-free dry reforming of Ni–Co bimetallic catalysts," *Applied Catalysis B: Environmental,* vol. 125, pp. 259-270, 2012.

[68] R. Singh, A. Dhir, S. K. Mohapatra, and S. K. Mahla, "Dry reforming of methane using various catalysts in the process," *Biomass Conversion and Biorefinery,* pp. 1-21, 2019.

[69] P. Djinović, J. Batista, and A. Pintar, "Efficient catalytic abatement of greenhouse gases: methane reforming with CO2 using a novel and thermally stable Rh–CeO2 catalyst," *International journal of hydrogen energy,* vol. 37, no. 3, pp. 2699-2707, 2012.

[70] Z. Hao, Q. Zhu, Z. Jiang, B. Hou, and H. Li, "Characterization of aerogel Ni/Al2O3 catalysts and investigation on their stability for CH4-CO2 reforming in a fluidized bed," *Fuel Processing Technology,* vol. 90, no. 1, pp. 113-121, 2009.

[71] D. Li, Y. Nakagawa, and K. Tomishige, "Methane reforming to synthesis gas over Ni catalysts modified with noble metals," *Applied Catalysis A: General,* vol. 408, no. 1-2, pp. 1-24, 2011.

[72] J. Edwards and A. J. F. P. T. Maitra, "The chemistry of methane reforming with carbon dioxide and its current and potential applications," vol. 42, no. 2-3, pp. 269-289, 1995.

[73] T.-J. Huang and T.-C. Yu, "Effect of steam and carbon dioxide pretreatments on methane decomposition and carbon gasification over doped-ceria supported nickel catalyst," *Catalysis Letters,* vol. 102, no. 3-4, pp. 175-181, 2005.

[74] N. Deshpande, A. Majumder, L. Qin, and L.-S. Fan, "High-pressure redox behavior of iron-oxide-based oxygen carriers for syngas generation from methane," *Energy & Fuels,* vol. 29, no. 3, pp. 1469-1478, 2015.

[75] A. Bischi *et al.*, "Design study of a 150 kWth double loop circulating fluidized bed reactor system for chemical looping combustion with focus on industrial applicability and pressurization," *International Journal of Greenhouse Gas Control,* vol. 5, no. 3, pp. 467-474, 2011.

[76] X. Lu *et al.*, "Pressurized chemical looping combustion with CO: Reduction reactivity and oxygen-transport capacity of ilmenite ore," *Applied Energy,* vol. 184, pp. 132-139, 2016.

[77] F. Zerobin, S. Penthor, O. Bertsch, and T. Pröll, "Fluidized bed reactor design study for pressurized chemical looping combustion of natural gas," *Powder Technology,* vol. 316, pp. 569-577, 2017.

[78] M. Rydén and A. Lyngfelt, "Hydrogen and power production with integrated carbon dioxide capture by chemical-looping reforming," in *Greenhouse Gas Control Technologies 7*: Elsevier, 2005, pp. 125-134.

[79] A. Ugwu, A. Zaabout, J. R. Tolchard, P. I. Dahl, and S. Amini, "Gas Switching reforming for syngas production with iron-based oxygen carrier-the performance under pressurized conditions," *International Journal of Hydrogen Energy,* vol. 45, no. 2, pp. 1267-1282, 2020.

[80] A. Zaabout, S. Cloete, J. R. Tolchard, and S. Amini, "A pressurized Gas Switching Combustion reactor: Autothermal operation with a CaMnO3− δ-based oxygen carrier," *Chemical Engineering Research and Design,* vol. 137, pp. 20-32, 2018.

[81] R. Chein, Y. Chen, C. Yu, and J. Chung, "Thermodynamic analysis of dry reforming of CH_4 with CO2 at high pressures," *Journal of Natural Gas Science and Engineering,* vol. 26, pp. 617-629, 2015.

[82] IEAGHG, "Techno-Economic Evaluation of HYCO Plant Integrated to Ammonia / Urea or Methanol Production with CCS , 2017/03," 2017.

[83] C. Ahoba-Sam, L. E. Øi, and K.-J. Jens, "Process Design of a Novel Low Temperature Methanol Synthesis Process Using an Air-blown Autothermal Reformer," presented at the Proceedings of The 59th Conference on Simulation and Modelling (SIMS 59), 26-28 September 2018, Oslo Metropolitan University, Norway, 2018-11-19, 2018, 08.

[84] S. M. Nazir, J. H. Cloete, S. Cloete, and S. Amini, "Efficient hydrogen production with CO2 capture using gas switching reforming," *Energy,* vol. 185, pp. 372-385, 2019.

8 Hydrogen Production by Water Splitting using Gas Switching Technology.

This chapter has been adapted from **Article V**

Ugwu, A., F. Donat, A. Zaabout, C. Müller, K. Albertsen, S. Cloete, G. van Diest and S. Amini, *Hydrogen Production by Water Splitting using Gas Switching Technology*. Powder Technology, 2020. 370: p. 48 - 63

Abstract

This study demonstrates a novel "Gas Switching Water Splitting (GSWS)" technology for the production of pure H_2 with integrated CO_2 capture. The reactor concept is based on the chemical looping technology where an oxygen carrier (metal oxide) is used to transport O_2 from air to the fuel for different redox reactions. Unlike the conventional chemical looping, Gas Switching Technology inherently avoids external circulation of the oxygen carrier by alternating the oxidizing and reducing gases in a single bubbling fluidized bed reactor. This greatly simplifies reactor design leading to an easier scale-up of the technology in comparison with the conventional chemical looping. The first experimental demonstration of the GSWS concept was completed at atmospheric pressure and temperatures ranging between 700°C and 900°C with iron-based oxygen carrier supported on alumina (~35 wt.% Fe_2O_3 on Al_2O_3). Approximately 99% H_2 purity was achieved at ~80% oxygen utilization. Significant fuel slippage was observed especially beyond 33% degree of reduction with some carbon deposition. The deposited carbon was able to combust/gasify completely in the subsequent air stage which makes the concept robust in sustaining oxygen carrier life. However, the gas mixing between the GSWS stages reduced the H_2 purity, CO_2 purity, and CO_2 capture efficiency. To minimize the negative impact of gas mixing, Cu doped $Mg(Fe_{0.9}Al_{0.1})_2O_4$ spinel with 74 wt.% active content was developed specifically for the second experimental demonstration. Despite the high stability and reactivity under redox conditions with TGA, this oxygen carrier did not perform optimally in 5 cm ID fluidized bed reactor because of excessive agglomeration at degree of reduction beyond 34%. In general, a range of the active content between 35 and 70 wt.% of the oxygen carrier was desired for optimal performance of the GSWS concept.

Keywords: *Gas Switching; Hydrogen production; Chemical looping; Carbon capture; zero-emission; production; fluidization; oxygen carrier*

8.1 Introduction.

The Intergovernmental Panel on Climate Change (IPCC) has predicted that the global average temperature would increase between 3.7 and 4.8°C by 2100 above pre-industrial levels if no actions were taken to reduce anthropogenic CO_2 emissions [1]. According to the Paris climate target, these emissions must reduce by approximately 45% from 2010 levels by 2030, reaching net zero in 2050 in order to keep the global temperature rise below 1.5°C [2] (or by ~25% by 2030 and reach net zero in 2070 in the 2°C temperature rise scenario). Despite the urgent warning to reduce greenhouse gas (GHG) emission, CO_2 emission has continued to increase due to the rise in global energy demand and high reliance on fossil fuel [3-5]. This situation is critical with current signs of adverse signs of climate change from the excessive heat waves, wild fire, among others. For the Paris climate agreement target to be achieved to save our planet, it is crucial to switch more towards clean energy carriers such as H_2 in the energy mix [6, 7]. H_2 is considered a clean energy carrier for the future since the combustion is associated with no CO_2 emission and it could be produced from a range of primary energy sources [8] (water, hydrocarbons, and other organic matter). As a secondary energy source, the environmental impact of hydrogen depends greatly on these primary sources and the production process [9]. The major challenge is the ability to extract H_2 economically and efficiently from these primary sources with minimum CO_2 emissions [8-10].

Currently, H_2 is mainly produced at large scale through the steam reforming of natural gas but associated with significant CO_2 emissions as the heat required for the highly endothermic reforming is provided by the combustion of fossil fuel outside the reforming reactor [11]. To address this concern, two main zero-emission technologies have been identified for H_2 production [9]: i) the conversion of fossil fuel with integrated CO_2 capture [12] and ii) the utilization of carbon-free sources such as the electrolysis of water using renewable electricity such as solar, wind, etc. [13]. It is worth mentioning that the energy penalty and cost of these technologies should be competitive compared to other options in order to make them commercially viable [13, 14]. Chemical looping with inherent CO_2 capture has been demonstrated as a technology capable of addressing the high energy penalty and cost relative to other carbon capture and storage (CCS) technologies [12, 15, 16]. This made chemical looping an attractive technology to be extended to energy-intensive processes such as H_2 production [15-20]. Chemical looping process for H_2 production was introduced by Howard Lane and his co-workers as a steam-iron process in 1903 [9, 21, 22]. This process has been demonstrated at lab and pilot scales under atmospheric conditions [23-32].

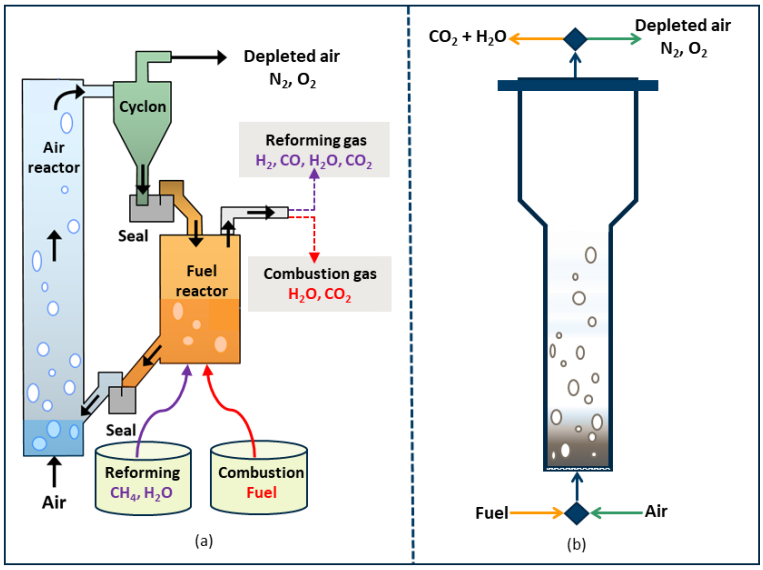

Figure 8-1: Chemical looping and Gas Switching Technology for reforming and combustion applications. a) represents a scheme of conventional chemical looping reforming and combustion [39] while b) represents the simplified Gas Switching configuration of Chemical Looping Combustion [40].

However, high-pressure operation of these chemical looping concepts is necessary for maximizing the energy efficiency and competitiveness with other H_2 production technologies [33]. To date, only a few studies on pressurized chemical looping in an interconnected fluidized bed configuration have been completed [34-37], despite the predicted benefits of such technology in terms of increased energy efficiency [38]. A major challenge is the difficulty to scale up under pressurized conditions, due to the high complexity and the need for precise circulation of large quantities of oxygen carrier material between different interconnected reactors as shown in *Figure **8-1*** (a & b) given that each reactor vessel should be pressurized independently while it is essential to fulfilling the heat and mass balance. In this situation, any instantaneous pressure imbalance between the reactors may induce instabilities in solids circulation, which could, in turn, result in large leakages through the sealing devices. This would reduce the CO_2 purity and capture efficiency and increases explosion risks if unreacted fuel gas mixes with the air. Also, the stress imposed on the material through solid circulation could change the morphology of the oxygen carrier thereby reducing the lifetime through excessive fragmentation.

Attempts have been made in recent years to address these issues through novel reactor concepts with no external solid circulation including gas switching in a packed bed reactor [41, 42], gas switching in a fluidized bed reactor [40, 43-47] and internal circulating reactor [48], but the

focus of this work is on gas-switching fluidized bed reactors. Unlike the conventional chemical looping, this novel technology utilizes a single fluidized bed reactor and avoids the circulation of oxygen carrier by alternating the feeds of the oxidizing and reducing gases to depict different redox stages as shown in *Figure **8-1** b*. With this arrangement, a wide range of inlet flow rates can be accommodated and scale-up challenges can be greatly reduced. Experimental studies have proven that this concept works under atmospheric and high-pressure conditions showing ease of operation and control [49-51]. Gas Switching Technology (GST) has also been proposed for combustion for power generation [52, 53], H_2 production through methane reforming [43, 44, 46, 49, 50], GHG (CO_2 and CH_4) utilization through dry reforming[47] and in some cases provide flexibility in terms of product (H_2 or power) [54].

To capitalize on this success, this study extends the GST to the water splitting using the steam-iron process for efficient H_2 production. *Figure **8-2*** presents a schematic reactor arrangement of a conventional chemical looping technology for H_2 production through water splitting and the gas-switching alternative. The water splitting is a three-step process utilizing the different iron oxide states to produce H_2 with integrated CO_2 capture. In the first stage, Fe_2O_3 is reduced to FeO/Fe using a gaseous fuel (CH_4, CO, syngas, etc). This is followed by the 2nd stage where steam is supplied for the partial oxidation (slightly exothermic) of the FeO/Fe to produce Fe_3O_4 and pure H_2. Air is supplied at the 3rd stage to fully oxidize back the oxygen carrier to Fe_2O_3. This last step (oxidation) is also used to regenerate the oxygen carrier and produce heat for the process.

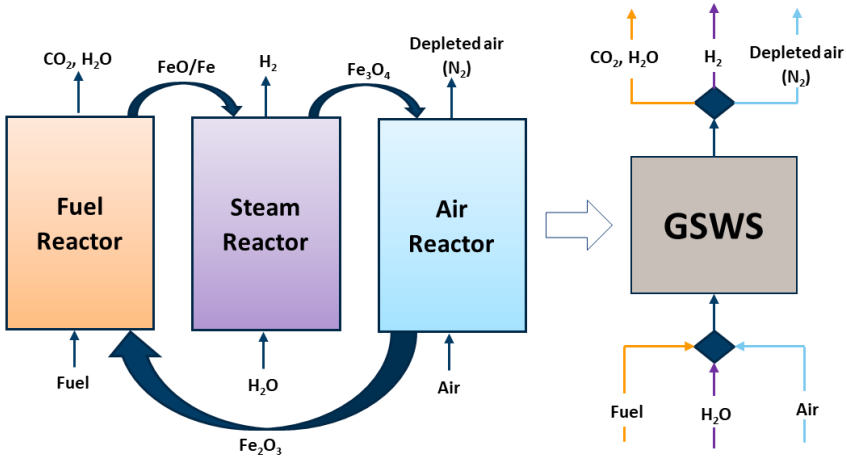

Figure 8-2: a) Water-splitting process completed following the conventional chemical looping route. b) Configuration of a simplified Gas Switching Water Splitting, GSWS.

Following the looping route (*Figure **8-2** a*) for this purpose requires a complex set-up of three interconnected reactors with the circulation of solid oxygen carrier to fulfill both the heat and mass balance requirements [3, 55, 56] whereas the gas switching approach (*Figure **8-2** b*) requires only one fluidized bed reactor with gas feeds alternated in-between stages to achieve the redox reaction without solid circulation. Since the reactions all happen in a single reactor vessel, this new reactor concept enables easy and more effective utilization of heat of reactions to reduce the energy penalty of the process. The reduction of the oxygen carrier (Fe_2O_3 to FeO/Fe) with CH_4 is endothermic and is thermodynamically more favored at high temperatures [3] whereas the oxidation of FeO to Fe_3O_4 with steam is slightly exothermic thus the reaction is more favored at low temperature.

$$CH_4 + 4Fe_2O_3 \rightarrow CO_2 + 2H_2O + 8FeO \qquad \textit{Equation 8-1}$$

$$3CH_4 + 4Fe_2O_3 \rightarrow 3CO_2 + 6H_2O + 8Fe \qquad \textit{Equation 8-2}$$

$$H_2O + 3FeO \rightarrow H_2 + Fe_3O_4 \qquad \textit{Equation 8-3}$$

$$4H_2O + 3Fe \rightarrow 4H_2 + Fe_3O_4 \qquad \textit{Equation 8-4}$$

$$\frac{1}{2}O_2 + 2Fe_3O_4 \rightarrow 3Fe_2O_3 \qquad \textit{Equation 8-5}$$

A conceptual disadvantage that GSWS has over the three-reactor process, is the mixing of gases when switching from one reaction stage to another, affecting CO_2 capture efficiency, CO_2 purity, and H_2 purity. The extent of the gas mixing depends on the flow rates and volume of the reaction vessel. It is therefore important that the fuel and steam stages are long enough to minimize the extent of the mixing of different gases in the system to achieve an acceptable capture efficiency and product gas purity. *Figure **8-3*** shows the separation performance against the redox-active content of the oxygen carrier computed using the mass balance at 20 bar and 800°C assuming a perfectly mixed reactor. The H_2 purity, CO_2 purity, and CO_2 capture efficiency are quantified in section ***8.2.2.1*** (*Equation **8-11** - Equation **8-13***) respectively. 80% oxygen carrier utilization was assumed to achieve a degree of reduction from Fe_2O_3 to FeO using CH_4 as fuel. The assumption to limit the degree of reduction only to FeO was considered because further reduction would i) lead to substantial fuel slip due to equilibrium limitations, ii) cause particle agglomeration and iii) lead to excessive coking. Clearly, CO_2 capture, CO_2 purity and H_2 purity increase substantially with increasing the oxygen carrier active content (Fe_2O_3). Oxygen carrier with higher active content would facilitate longer fuel, steam and air

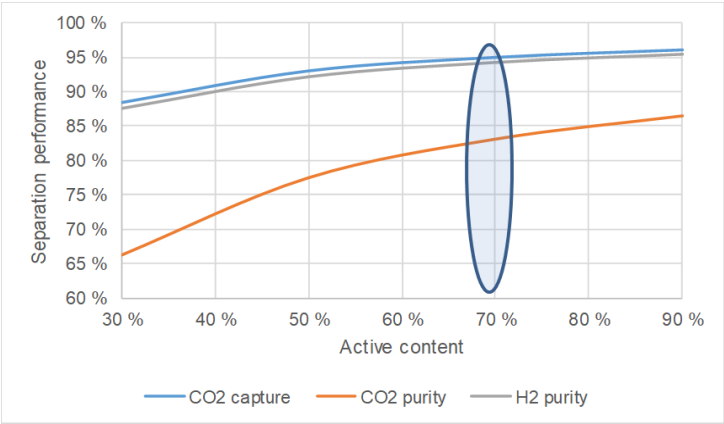

Figure 8-3: The Separation performance at 20 bar and 800 °C assuming 80% degree of reduction from Fe_2O_3 to FeO.

stages, thereby reducing the impact of the undesired mixing when a high-pressure operation is targeted.

In summary, this work demonstrates the experimental operation of the water-splitting process for pure H_2 production which could be coupled with other downstream chemical processes using the Gas Switching configuration. It explicitly highlights the advantages and disadvantages of this configuration in terms of oxygen carrier selection and development, cycle design, and reactor performance (fuel and steam conversion, carbon deposition, CO_2 and H_2 purity, CO_2 capture efficiency, oxygen carrier, agglomeration, etc.).

8.2 Experiments and methods

8.2.1 Experimental setup

The GSWS experiment was completed using a lab-scale fluidized bed reactor (*Figure **8-4***). A fluidized bed is desired to achieve good mixing to minimize concentration and temperature variation in the bed [57-59]. This reactor consists of a cylindrical column (5 cm in inner diameter and 50 cm in height) and a freeboard zone consisting of an expanding conic zone (5 cm in the lower end diameter, 10 cm at the top end diameter and 40 cm height) to minimize particles elutriation. The reactor is made of Inconel 600 with the capability of withstanding high-temperature gas-solids reactive flows (up to 1000 °C). A porous plate distributor made of Inconel 600 with 20 µm mean pore size and 3 mm thickness was used to ensure good gas distribution. The reactor vessel is heated up to a target temperature using an external electrical heating element wound around the reactor. The reactor was also insulated using a 25 cm thick

blanket insulation to prevent excessive heat loss. Automatic gas switching and feed into the reactor were achieved using a three-way electrical automatic switching valve and mass flow controllers from Bronkhorst BV respectively. A cooler was installed at the outlet of the reactor to cool down the stream of hot gases before being sent to the gas analyzer and to the vent. The gas composition was measured using a syngas analyzer (ETG Risorse e Tecnologia) while the bed temperature was measured using two thermocouples inserted at 2 and 20 cm above the gas distributor respectively. A LabVIEW application was used for data acquisition/storage and to control all the measurement instruments and devices.

Thermogravimetric analyzer. The cyclic performance of the oxygen carrier was evaluated in a thermogravimetric analyzer (Mettler Toledo, TGA/DSC 1) at atmospheric pressure. The sample was loaded in a 30 µl alumina crucible that sat on the crucible holder attached to the balance beam and was heated to the desired temperature (usually 850°C) under a reactive gas flow of 125 mL min^{-1} air, measured at normal temperature and pressure, NTP. In addition, a purge gas flow of 25 mL min^{-1} N_2 was present throughout the experiment. The reactant gases were supplied through a fine capillary mounted on the cantilever arm terminating just above,

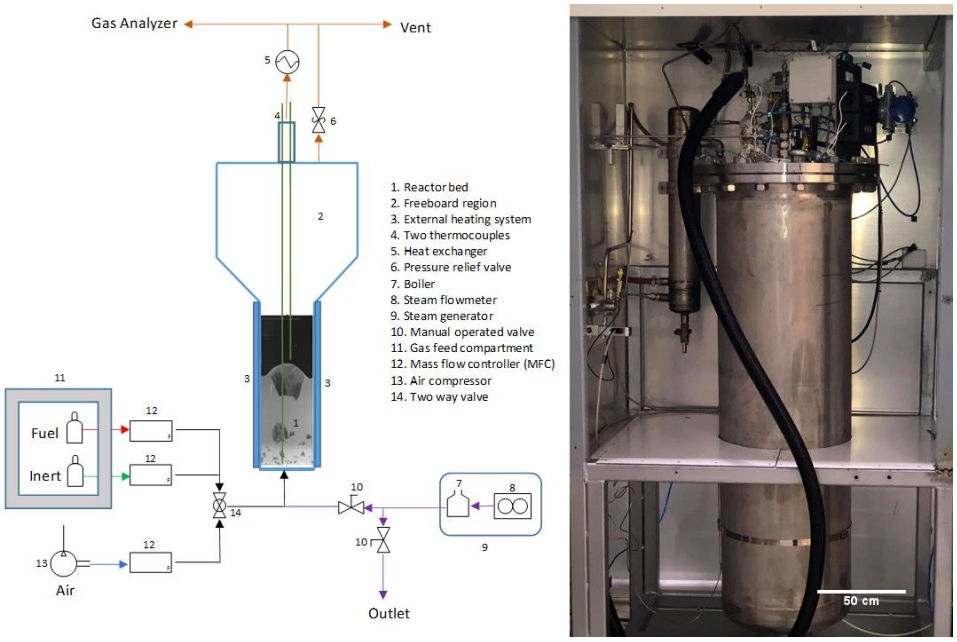

a) b)

Figure 8-4: The experimental setup [43, 44, 47] used for GSWS demonstration tests . a) schematic diagram, b) the actual reactor setup.

and before, the crucible, which means that the measured rate of mass change was largely governed by diffusion in vertical direction from the bulk of the gas to the surface of the sample inside the alumina crucible (note that the gas flowed horizontally over the alumina crucible containing the sample). When the set temperature was reached, the cycling experiment started: The reduction step (25 min) was performed using 6.7 vol.% CH_4 in N_2, followed by a purge step (2 min) and the oxidation step (11 min) using air. Sixty redox cycles were typically carried out. In some experiments, an additional oxidation step was performed using 20 vol.% CO_2 in N_2 (prior to the air oxidation step).

X-ray diffraction. Powder XRD (PANalytical Empyrean) was used to investigate the chemical composition of the crystalline phases of the as-synthesised and cycled oxygen carriers. The diffractometer was operated at 45 kV and 40 mA using CuKα radiation and each sample was scanned over the range of $2\theta = 10 – 90°$ with a step size of 0.0167°. The total time for each measurement was 1 h. For in-situ measurements, the diffractometer was equipped with an Anton Paar XRK 900 high-temperature reactor chamber where the sample was placed onto a glass-ceramic disc made of Macor and exposed to different gas atmospheres at 850°C. For each atmosphere, multiple measurements were made to track the evolution of crystalline phases over the range $2\theta = 20 – 80°$ with a step size of 0.0167 °; each measurement thus lasted 12 min. First, the sample was reduced in 4.4 vol.% CH_4 in N_2 (30 measurements), then re-oxidized in 15 vol.% CO_2 in N_2 (15 measurements) and finally oxidized in 50 vol.% air in N_2 (5 measurements). The cell was purged with pure N_2 for 2 min between the reaction stages. The total flow rate of gas was kept constant at 200 mL min^{-1} (at NTP) and was controlled by a set of mass flow controllers (Bronkhorst, EL-FLOW series) synchronized with the diffractometer and the temperature controller of the high-temperature reaction chamber.

Inductively coupled plasma optical emission spectroscopy (ICP-OES). The molar ratio of Mg:Fe:Al:Cu in the oxygen carrier was determined via ICP-OES using an Agilent 5100 VDV. Matrix effects were lessened by matching the matrix acids for all blanks, standards (multielement standard) and samples.

Scanning electron microscopy. A scanning electron microscope (FEI Quanta 200 FEG) operated at 10 kV was used to characterize the surface morphology of the materials. A double-sided carbon tape was used to attach samples onto an aluminium holder. Prior to SE imaging, the samples were sputter coated (Safematic CCU-010) with an ~ 5 nm-thick layer of PtPd. Transmission electron microscopy (TEM) images of as-synthesized samples were obtained using a FEI Talos F200X microscope operated at 200 kV, equipped with a high-brightness

Schottky field-emission gun (FEG), a high-angle annular dark field (HAADF) detector and a large collection-angle energy-dispersive X-ray spectroscopy (EDX) detector.

Crushing strength. The crushing strength of the oxygen carrier (as-synthesized and after > 40 h of redox operation in the TGA) was obtained by measuring the force required to break individual oxygen carrier particles sieved to 180-212 µm using a force gauge operated at 50 Hz (Shimpo, FGN-20). The crushing strength was defined as the first local maximum in the recorded data when compressing the particle. At least 40 such measurements were performed to give meaningful results.

8.2.2 Methodology

The gas switching water splitting (GSWS) was demonstrated using an iron-based oxygen carrier with the reactor configuration as shown in *Figure **8-2** b* in a fluidized bed reactor (*Figure **8-4***). A three-stage cycle (fuel, steam and air stage) was designed to complete the GSWS process. The cycle starts with the fuel stage where the oxygen carrier is reduced to FeO or Fe using dry fuel (CO or CH_4) with inherent separation of CO_2. The steam stage follows immediately after the fuel stage where steam is fed to partially oxidize FeO/Fe to Fe_3O_4 while producing H_2. The final stage of the GSWS cycle is the air stage for complete oxidation of Fe_3O_4 to Fe_2O_3 associated with heat generation as explain in the introduction (*Section **8.1***). For each reaction condition, real-time temperature, pressure and gas composition were recorded and analyzed. The separation performance was also evaluated through mass balance with the following indicators: CO_2 purity, H_2 purity, and CO_2 capture efficiency as also described in *section **8.2.2.1***. To avoid carbon deposition, the extent of reduction was limited to FeO, although this reduced H_2 yield substantially in line with thermodynamics.

8.2.2.1 Reactor performance measures

The objective of the GSWS process is to convert a hydrocarbon fuel to H_2. Thus, it is desired to maximize the fuel conversion in the fuel stage and maximize H_2 production in the steam stage. From this point of view, the following performance measures have been defined for quantifying the reactor performance. Note that n_i specifies the total moles of species i exiting the reactor during a given stage unless specifically indicated for the moles entering the reactor as $n_{i,in}$. Firstly, the fuel conversion in the fuel stage is quantified as follows:

$$\gamma_{fuel} = \frac{n_{fuel,in} - n_{fuel,out}}{n_{fuel,in}}$$ *Equation 8-6*

However, the conversion of CH_4 to achieve partial oxidation achieves four times less oxygen carrier reduction than the conversion of CH_4 to achieve full oxidation. Thus, the selectivity of CH_4 conversion to CO_2 is also quantified.

$$s_{CO_2} = \frac{n_{CO_2}}{n_{CO} + n_{CO_2}}$$ *Equation 8-7*

One of the goals of the fuel stage is to maximize the degree of oxygen carrier utilization. This parameter is quantified as follows, assuming that oxygen carrier reduction is carried out from Fe_2O_3 to FeO:

$$X_{red} = \frac{oxygen\ transferred\ to\ fuel}{oxygen\ available} = \frac{n_{CO} + 2n_{CO_2} + n_{H_2O}}{3n_{Fe_2O_3}}$$ *Equation 8-8*

When looking at the steam stage, the primary performance measure is the degree of steam conversion:

$$\gamma_{H_2O} = \frac{n_{H_2}}{n_{H_2} + n_{H_2O}}$$ *Equation 8-9*

Significant carbon deposition also took place during the fuel stage and this deposited carbon was released in the steam and air stages. The fraction of carbon deposition is therefore quantified as follows based on the steam and air stages outlet and the total methane entering the fuel stage:

$$C_{dep} = \frac{n_{CO} + n_{CO_2}}{n_{fuel,in}}$$ *Equation 8-10*

The H_2 purity produced during the steam stage is determined by quantifying the amount of other gas present during the steam stage. It is therefore important that the steam stage is long enough to minimize the extent of the mixing of different gases. Hydrogen purity will be reduced as a result of carbon deposition, possibly requiring further purification in a downstream processing step.

$$\sigma_{H_2} = \frac{n_{H_2}}{n_{H_2} + n_{CO} + n_{CO_2}}\Bigg|_{steam} \qquad \textit{Equation 8-11}$$

The CO_2 purity produced during the fuel stage is determined by quantifying the percentage of depleted air (N_2+O_2) and unconverted fuel (CH_4) in the outlet gas stream during the fuel stage as

$$\sigma_{CO_2} = \frac{n_{CO_2}}{n_{CO_2} + n_{CO} + n_{N_2} + n_{O_2} + n_{fuel}}\Bigg|_{fuel} \qquad \textit{Equation 8-12}$$

Finally, the CO_2 capture efficiency is determined to quantify the percentage of CO_2 that escapes to the atmosphere during the air stage (100 % minus the percentage of CO_2 that escapes to the atmosphere).

$$\eta_{CO_2} = 1 - \frac{n_{CO_2,air}}{n_{CO_2,fuel} + n_{CO_2,air} + n_{CO_2,steam}} \qquad \textit{Equation 8-13}$$

8.2.3 Oxygen carrier synthesis

As mentioned earlier, the water-splitting uses the different states oxides of iron to complete the cycle. Two campaigns to demonstrate GSWS concepts were completed with different iron based oxygen carriers. The first demonstration was completed with oxygen carrier of 35 wt.% Fe_2O_3 supported on gamma-alumina. This oxygen carrier has shown very stable performance under redox conditions for methane reforming in a previous study [60]. In the second campaign, an optimized Cu-doped $Mg(Fe_{0.9}Al_{0.1})_2O_4$ spinel with 74 wt.% active content was developed and investigated specifically for this study to meet the requirement of high active content loading for maximizing the separation performance of the GSWS process.

8.2.3.1 Synthesis of 1st campaign oxygen carrier (35 wt.% Fe_2O_3 on Al_2O_3)

An oxygen carrier with 35% active Fe_2O_3 on Al_2O_3 was developed through wet impregnation where spherical gamma-alumina particles from Sasol (Puralox SCCa 150/200) were impregnated in a concentrated aqueous ammonium iron(I) citrate solution (~50 g/100 g water). The aim was to form nanostructured iron oxide inside the mesoporous alumina structure after calcination. Homogenous distribution of the active iron oxide throughout the porous particles was obtained followed by drying steps at 120°C after each step up to a theoretical loading of ~10 wt% metal oxide. After the drying, the material was subjected to heat treatment for about

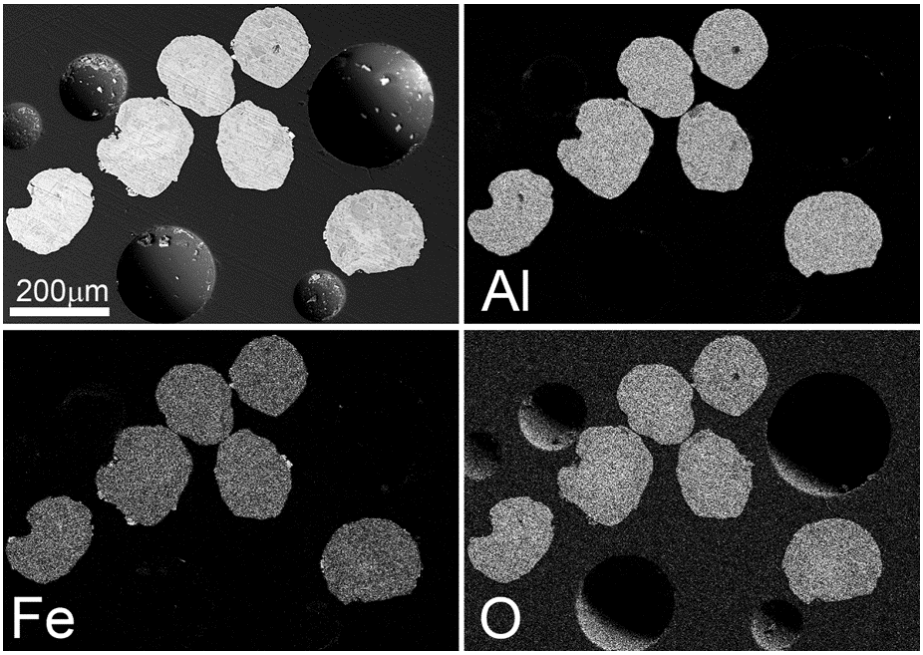

Figure 8-5: SEM/EDS Image of the impregnated alumina particles with a map showing the distribution of Al, Fe and O content[44].

5 hours at 500°C with ramp rate of 1°C/min in ambient air. This procedure was repeated until the theoretical weight loading of the Fe active content to Al_2O_3 was about 1:1. The produced particles were sieved with 100 µm cut-off size to remove fines prior to quality assurance testing. SEM/EDS analysis on particles after sieving indicated the homogenous distribution of the Fe throughout the porous alumina structure (*Figure* ***8-5***). The measured loading of active elements was lower than targeted (Fe:Al ≈ 0.55:1 by weight) due to the loss of active material by sieving, in form of fines which were loosely deposited on the surface of the particles. The BET surface area of the produced Fe-Al_2O_3, impregnated particles was measured to 102.9 m^2/g in comparison with the bare alumina support particles with a BET surface area of 206.0 m^2/g.

8.2.3.2Synthesis of 2nd campaign oxygen carrier (Cu-doped Fe/$MgAl_2O_4$ spinel).

Iron oxide, magnesium carbonate, aluminum oxide, and copper oxide were weighed and dispersed in deionized water with a suitable dispersing agent to create a Cu-doped $Mg(Fe_{0.9}Al_{0.1})_2O_4$ spinel with 74 wt.% active content. Wet ball milling using a horizontal attrition mill (Netzsch, Germany) was employed to homogenize the dispersion and create a stable suspension suitable for spray drying. The resulting slurry was spray-dried using a

pressurized fountain-nozzle atomizing the suspension in the chamber of the spray dryer. The chamber was filled with hot air from the top resulting in a counter-current regime enabling rapid water evaporation forming spherical particles due to surface tension effects. To obtain oxygen carrier particles with sufficient mechanical strength and the desired crystalline phases, the resulting powder was then calcined at 1200°C during 4 hours to yield spheres with an average particle size of 150 μm and tap density of about 1.8 g/cm^3.

8.3 Results and discussion

GSWS experiments were completed with both oxygen carriers (35 wt.% Fe_2O_3on Al_2O_3 tested in a previous study on reforming but not water-splitting [60] and Cu-doped Fe/$MgAl_2O_4$ spinel with 74 wt.% active content developed specifically for this study (*section **8.3.2.2***). Screening and characterization of the oxygen carrier were completed and redox experiments were carried out in the 5 cm ID fluidized bed reactor (*Figure **8-4***) and TGA as explained in section ***8.2.1.*** All experiments were conducted at atmospheric pressure.

8.3.1 1st GSWS demonstration with Fe/Al_2O_3 OC of 35% wt Fe_2O_3

The first GSWS demonstration was done with the 5 cm ID fluidized bed reactor (*Figure **8-4***) using 35% active Fe_2O_3 on Al_2O_3 as described in section ***8.2.3.1***. About 300 g of the oxygen carrier was initially placed in the reactor. Three-stage GSWS cycles (fuel, steam and air stages) were completed with CO and CH_4 as fuel at atmospheric pressure and temperatures between 700 - 900°C. *Figure **8-6*** shows a typical gas composition at the reactor outlet with repeatable behavior over several cycles with temperature profile as shown in *SI Figure **S1***. As presented in a previous study with the same oxygen carrier [60], the fuel stage occurs over two distinct sub-stages. Complete CO conversion was observed at the first sub-stage. This is in line with thermodynamics because CO is fully converted to CO_2 at equilibrium when Fe_2O_3 is present in the first sub-stage. However, CO conversion decreases to ~33% in the second sub-stage as the oxygen carrier is reduced beyond Fe_3O_4. Despite the low conversion achieved in the second sub-stage of the fuel stage, a high degree of oxygen carrier utilization (from Fe_2O_3 to FeO) of about 80% was achieved. The large fuel slippage in the second sub-stage of the fuel stage could be treated properly by recycling or integrating to other downstream processes such as Gas Switching combustion, GSC [40, 61] or reforming, GSR [50, 62], to maximize fuel utilization and process efficiency. Indeed, a previous thermodynamic assessment of the GSC concept

integrated with an IGCC power plant[63] assumed a maximum achievable reactor temperature of 1200 °C, even though state of the art gas turbines can operate well above 1400 °C. Despite this negative aspect, the GSC concept easily outperformed conventional pre-combustion CO_2 capture, achieving 4 %-points higher efficiency [63]. This efficiency advantage can be extended by several additional %-points through an additional combustor after the GSC reactors[64]. H_2 from the GSWS reactors can be used to fuel this combustor and raise the stream temperature to the maximum achievable turbine inlet temperature. This process configuration can, therefore, achieve very high electric efficiencies, while accommodating a large amount of fuel slip in the GSWS fuel stage.

As for the subsequent steam stage, steam conversion of about 30% was achieved, which is higher than equilibrium predictions with FeO [3, 20, 65], indicating some degree of oxygen carrier reduction to metallic Fe. However, steam conversion decreased later in the stage as the active sites available for partial oxidation with steam diminished. It was also be observed from *Figure **8-6***, that no other gas was produced during the steam stage that would contaminate the produced H_2 before switching to another stage, thus making the process promising with the potential of producing high purity H_2 (over 95%).

At the air stage, some traces of CO_2 were produced indicating some carbon deposition in the previous reduction stage. As a result, CO_2 capture efficiency was affected through the release of CO_2 with a stream of depleted air (N_2) at the air stage since CO_2 is captured only during the fuel stage. Fortunately, the deposited carbon could not be gasified during the steam stage thus not affecting H_2 purity. *Figure **8-6*** also shows that O_2 composition approached 21% at the end of the air stage implying that the oxygen carrier was completely oxidized before the start of the next redox cycle. One of the advantages of the GST reactor design like the conventional chemical looping reactor is the capability of preventing deactivation of the oxygen carrier through coking as the deposited carbon are gasified and combusted completely at the air stage before the start of the next cycle.

The sensitivity of steam conversion and oxygen carrier utilization to the reduction time is shown in *Figure **8-7** a*. It could be seen that the oxygen carrier utilization increased only by ~17% when the reduction time was doubled and by ~32% with tripling of the reduction time. The relatively slow increase in oxygen carrier utilization with reduction time originates from the large fuel slippage that occurs when the reduction time is higher than 2 min. Despite this small increase in the oxygen carrier utilization, it has substantially improved the extent of steam conversion to hydrogen. The average steam conversion across the whole steam stage has

increased by ~2.9x when the reduction time was doubled implying a ~5.8x increase the quantity produced in the 3 min reduction time. As for the 9 min reduction time, the average steam conversion remained relatively unchanged in comparison to the 6 min, but the H_2 yield has increased by 50% in comparison to the 6 min (the oxygen carrier utilization has only increased by ~11% opening about 0.145mols additional FeO sites for water-splitting reaction) and is ~8.79 times the 3 min reduction time. This large increase in H_2 yield despite the limited increase in the oxygen carrier utilization could be explained by the creation of Fe sites on the reduced

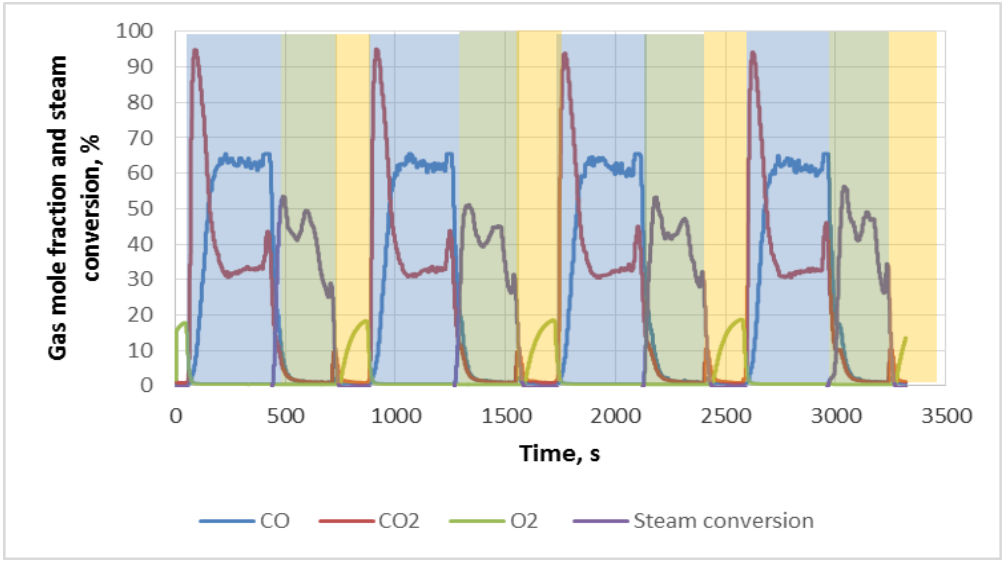

Figure 8-6: The transient gas composition of 4 cycles of GSWS using CO as fuel at 900°C and 1bar. Fuel stage in blue; Steam stage in green; Air stage in yellow. Flowrate: 5 Nl/min CO for 6min (80% degree of OC reduction), 1.9 Nl/min steam for 5min (CO : steam molar ratio feeds=2.5), 10Nl/min Air for 3min.

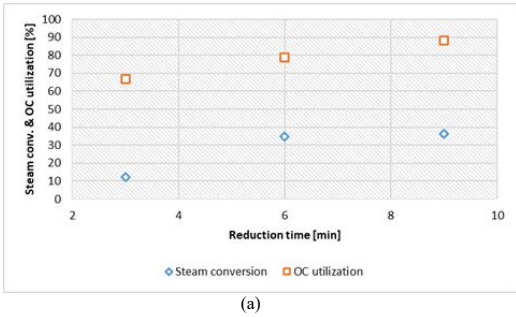

(a)

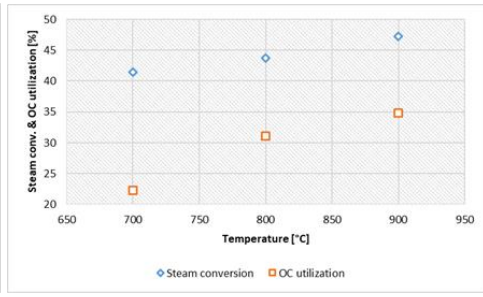

(b)

Figure 8-7: a) The sensitivity of average steam conversion to oxygen carrier utilization of GSWS process using CO as fuel. Fuel stage (5 Nl/min pure CO); steam stage (1.5 g/min); Air stage (10 Nl/min). All the stages were completed at 900°C and 1bar. b) The sensitivity of average steam conversion to operating temperature of GSWS process at 1bar. Fuel stage (5 Nl/min pure CO for 3 min), steam stage (1.9 Nl/min for 5 min); Air stage (10 Nl/min for 3 min).

oxygen carrier that have much higher steam equilibrium conversion to H_2 than FeO [66, 67]. This can clearly be seen in *Figure **8-8*** showing that the transient steam conversion to H_2 peaks in the beginning of the steam stage to values beyond equilibrium predictions of FeO demonstrating existence of Fe sites (with higher extents for the case of 9 min reduction time), but it goes down across the stage as the Fe sites are being consumed. This positive improvement in steam conversion to H_2 would justify accommodating the large fuel slippage occurring in the reduction stage if fuel recycling or GSWS process integration measures are implemented to maximize fuel conversion and energy efficiency.

The increased operating temperature has shown a positive effect on fuel conversion in the reduction stage, leading to increased oxygen carrier utilization (*Figure **8-7** b)* in line with thermodynamics and likely due to improved kinetics [68]. This enhanced the degree of reduction of the oxygen carrier improving steam conversion to H_2. This phenomenon counteracts the negative effect of increased temperature on equilibrium of water splitting reaction *(Equation **8-3*** and *Equation **8-4***) over iron and its oxide.

Further testing of the GSWS concept using CH_4 as fuel shows repeatable cyclic performance (*Figure **8-9***). The major difference observed with CH_4 is that two distinct phenomena occur during the fuel stage. First is the reduction reaction from Fe_2O_3 to FeO associated with CO_2 production. As the lattice oxygen continues to deplete, a point is reached where the reaction switches completely to partial oxidation of methane associated with syngas production of H_2:CO ratio of approximately 2:1. About 60% fuel conversion was achieved in the first phase (reduction phase) of the fuel stage while CH_4 conversion further drops to about 40% in the 2nd

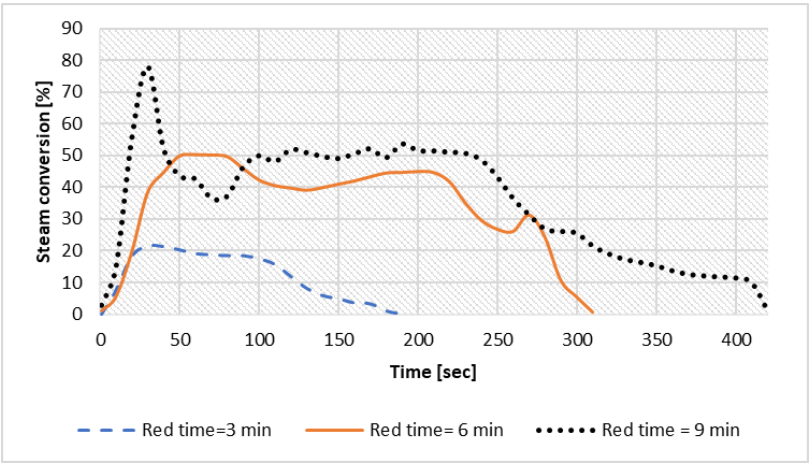

Figure 8-8: The transient steam conversion to H_2 with reduction time. Fuel stage (5 Nl/min pure CO); steam stage (1.9 Nl/min); Air stage (10 Nl/min). All the stages were completed at 900°C and 1bar.

phase (POX) of the fuel stage in line with a thermodynamic analysis of Dohyung Kang et al. [69]. At the start of the steam stage, CO was produced through the gasification of the deposited carbon in the previous fuel stage. This phenomenon increases the partial pressure of CO shifting the equilibrium of Boudouard reaction to the right to convert the produced CO to CO_2 and redepositing carbon. The CO and CO_2 concentrations in the steam thus affect H_2 purity negatively. This could be due to the steam gasification of the deposited carbon at the steam steam.

8.3.2 2nd GSWS demonstration with Cu-doped Fe/$MgAl_2O_4$ spinel OC

8.3.2.1 Oxygen carrier chemistry and screening

From *Figure* ***8-3*** it is clear that an oxygen carrier with 35 wt.% of redox-active Fe_2O_3 is not sufficient to obtain hydrogen of high purity at elevated operating pressures. Initially, it was planned to produce oxygen carriers via spray-drying using promising material formulations (based on Fe_2O_3) that have been reported in the literature in the context of chemical looping water-splitting [9, 32, 70]. The majority of these materials showed good cyclic stability only with low Fe_2O_3 contents (< 30 wt.%) and/or under mild reaction conditions (< 900°C) with the incomplete conversion of the oxygen carrier. Further, only a few studies dealt with using CH_4 during reduction, which has a much lower reactivity with Fe_2O_3 than CO or H_2, and hardly any work investigated the suitability of the oxygen carriers for fluidized bed reactors, where also mechanical properties are important. Most importantly, sintering and agglomeration of oxygen carrier particles has widely been neglected but is arguably the most important aspect when using oxygen carrier particles in a fluidized bed system at a large scale. Agglomeration of particles in the reactor would terminate operation immediately. Almost none of the previous works on oxygen carrier development addressed challenges associated with scale-up and actual large-scale operation. Specifically, the oxygen carrier particles had to possess high oxygen storage capacity (> 0.2 g O_2 per g OC, corresponding to ~ 70 wt.% Fe_2O_3 in the oxygen carrier), high reactivity with CH_4, high resistance towards sintering at high temperature (up to 1000°C), high resistance towards coke deposition that would contaminate the H_2 generated in the subsequent steam oxidation step, and reasonable mechanical strength (~ 50 MPa). The material formulation had to be suitable for a production process via spray-drying, followed by calcination at high temperature (1200 – 1300°C) to ensure sufficient mechanical strength. The resulting oxygen c

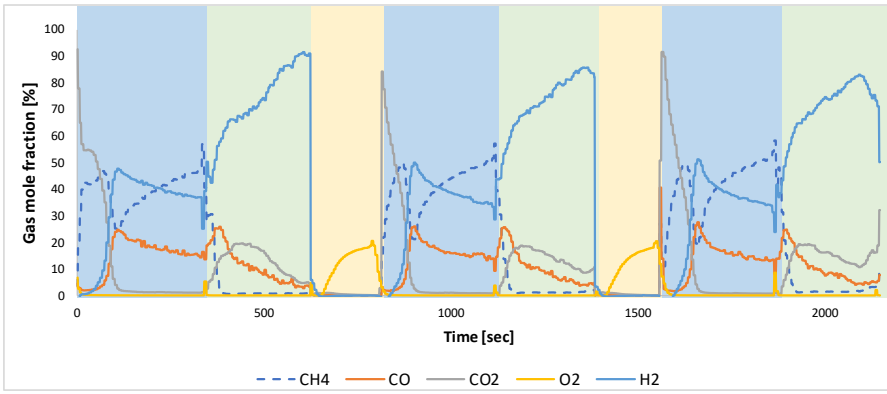

Figure 8-9: The Transient gas composition of 4 GSWS cycles with CH_4 as fuel. Fuel stage in blue, steam stage in green, air stage in yellow. Flowrate: 1.7 Nl/min CH_4 for 6min; 1.9 Nl/min steam for 5min (H_2O:CH_4 molar ratio =3:1), 10Nl/min air for 3min.

arrier particles produced through spray-drying are naturally of very low surface area (< 1 m^2/g), which requires good solid-state properties to achieve high reactivity [71]. The cyclic performance of newly developed oxygen carriers (their synthesis is described in the experimental *section* ***8.2.3.2***) was assessed using thermogravimetric analysis (TGA) at 850°C and they were characterized by electron microscopy and X-ray diffraction (XRD) before and after the cycling experiments.

8.3.2.1.1 Material development and assessment of the cyclic redox performance in the TGA

The material development work focused initially on Fe_2O_3 supported on La-doped CeO_2 and variations thereof [56, 72-74]. When cycled in the TGA at 850°C, none of them was found to be cyclically stable and the oxygen carriers deactivated quickly due to sintering (data not shown in this work). Promising results were reported by Imtiaz et al. [75], and so similar oxygen carriers were produced from nitrates, which contained 70 wt.% Fe_2O_3, 22 wt.% $MgAl_2O_4$ and 8 wt.% CuO. Cu-species have high mobility and they were found to migrate to the surface and cover Fe-sites during reduction, thus reducing their catalytic effect for CH_4 decomposition ($CH_4 \rightarrow C + 2H_2$) substantially [75]. The oxygen carriers produced in this work were calcined at much higher temperature than in the original work by Imtiaz et al. due the requirement for obtaining stable spheres after spray-drying in a scaled production process; the corresponding X-ray diffractograms are compared in *Figure* ***8-10*** a – *c.*

It is clear that at the lower calcination temperatures, both Fe_2O_3 (PDF 01-080-5406) and a cubic (Mg,Al,Fe) spinel phase existed within the oxygen carrier (*Figure* ***8-10*** a *& b).* A crystalline

CuO phase was not observed, suggesting the dissolution of CuO in the spinel phase. With increasing calcination temperature, there was a gradual decrease in the amount of Fe_2O_3 and after calcination at 1300°C (*Figure **8-10** c*), almost all Fe_2O_3 existed in a mixed (Mg,Al,Fe) spinel phase (identified as $Mg(Fe_{0.5}Al_{0.5})_2O_4$, PDF 01-080-3010), which most likely included also the Cu, since no reflections from isolated CuO were detected. If CuO is incorporated in the spinel structure, its mobility is lowered and all elements within the spinel structure are effectively anchored[76]. It was recently shown that Cu can be exsolved from the spinel under reducing conditions, thereby improving the material's reactivity [77]; this is discussed below together with results from the in-situ XRD measurements.

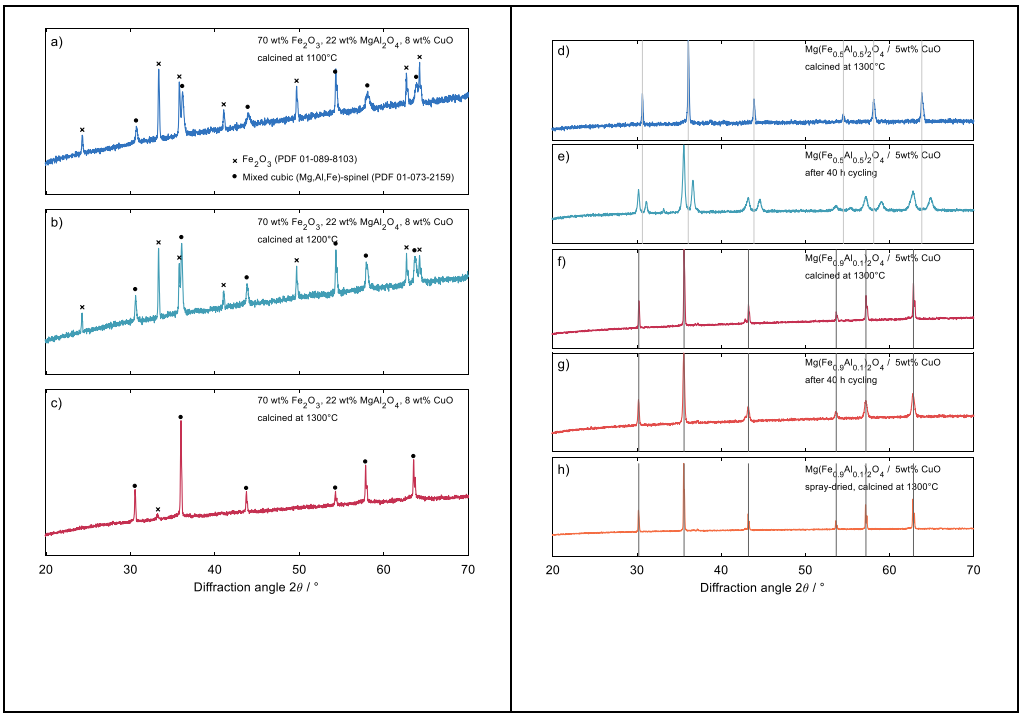

Figure 8-10: The results from X-ray diffraction. a) – c) Effect of calcination temperature on the crystalline phases formed for an oxygen carrier with 70 wt.% Fe_2O_3, 22 wt.% $MgAl_2O_4$ and 8 wt.% CuO. d) As-prepared oxygen carrier $Mg(Fe_{0.5}Al_{0.5})_2O_4$ with 5 wt.% CuO calcined at 1300°C. e) Oxygen carrier $Mg(Fe_{0.5}Al_{0.5})_2O_4$ with 5 wt.% CuO calcined at 1300°C after 40 h of redox cycling in the TGA at 850°C. f) As-prepared oxygen carrier $Mg(Fe_{0.9}Al_{0.1})_2O_4$ with 5 wt.% CuO calcined at 1300°C. g) Oxygen carrier $Mg(Fe_{0.9}Al_{0.1})_2O_4$ with 5 wt.% CuO calcined at 1300°C after 40 h of redox cycling in the TGA at 850°C. h) Spray-dried, as-prepared oxygen carrier $Mg(Fe_{0.9}Al_{0.1})_2O_4$ with 5 wt.% CuO calcined at 1300°C. The vertical light grey lines in d) and e) indicate the peak positions of the reference pattern for $Mg(Fe_{0.5}Al_{0.5})_2O_4$, PDF 01-080-3010. The vertical dark grey lines in f) – h) indicate the peak positions of the reference pattern for $Mg(Fe_{0.9}Al_{0.1})_2O_4$, PDF 01-071-1233.

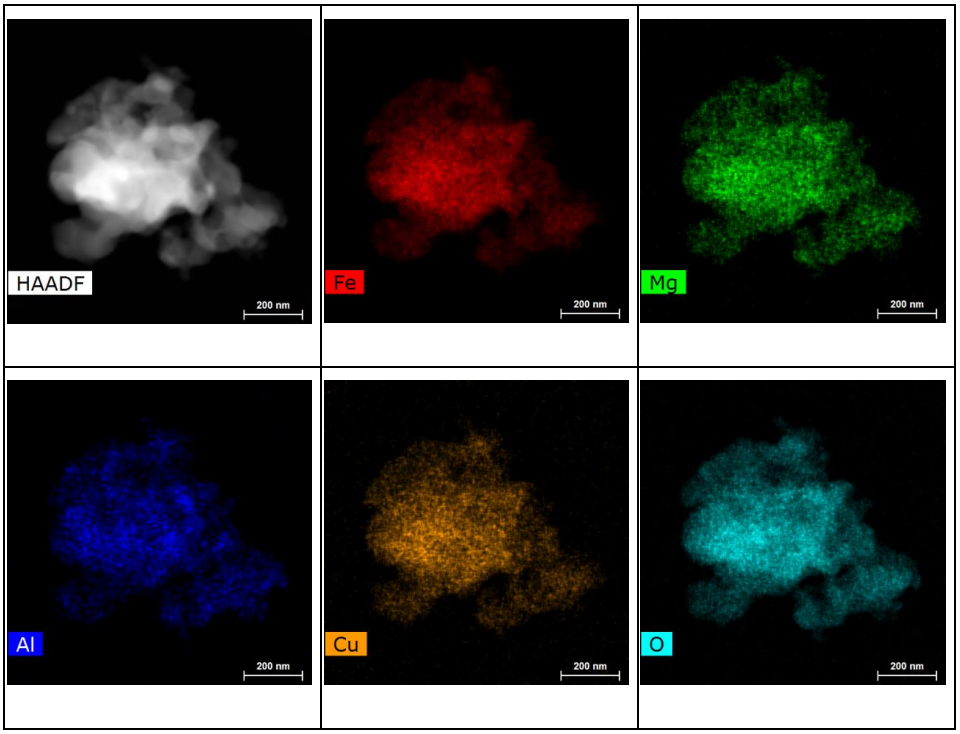

Figure 8-11: TEM images of the as-prepared oxygen carrier $Mg(Fe_{0.5}Al_{0.5})_2O_4$ with 5 wt.% CuO calcined at 1300°C, and the corresponding elemental maps.

Owing to the formation of the mixed spinel phase upon calcination at high temperature, a stoichiometric compound was synthesized and used as an oxygen carrier, $Mg(Fe_{0.5}Al_{0.5})_2O_4$ doped with 5 wt.% CuO (calcined at 1300°C). From the XRD pattern presented in *Figure **8-10** d* the oxygen carrier was nearly phase-pure and the corresponding EDX maps shown in *Figure **8-11*** confirm a uniform distribution of elements within the material. Measurements via ICP-OES gave a ratio of Mg:Fe:Al:Cu of 0.310:0.585:0.061:0.044, which was in good agreement with the theoretical ratio (Mg:Fe:Al:Cu = 0.320:0.575:0.064:0.041).

The oxygen carrier was cycled (reduction in ~ 7 vol.% CH_4 and oxidation in ~ 83 vol.% air) in the TGA at 850°C, with the results of the first eight cycles shown in *Figure **8-12** a* & b. Initially, there was hardly any reduction (*Figure **8-12** a*), but the oxygen carrier gradually activated, as can be seen from the increasing weight loss during reduction. The subsequent weight increase measured during reduction was due to the decomposition of CH_4, resulting in coke deposits on the surface of the oxygen carrier. The weight loss curve thus reflects two different mechanisms: The loss of lattice oxygen due to the conversion of CH_4, and a weight

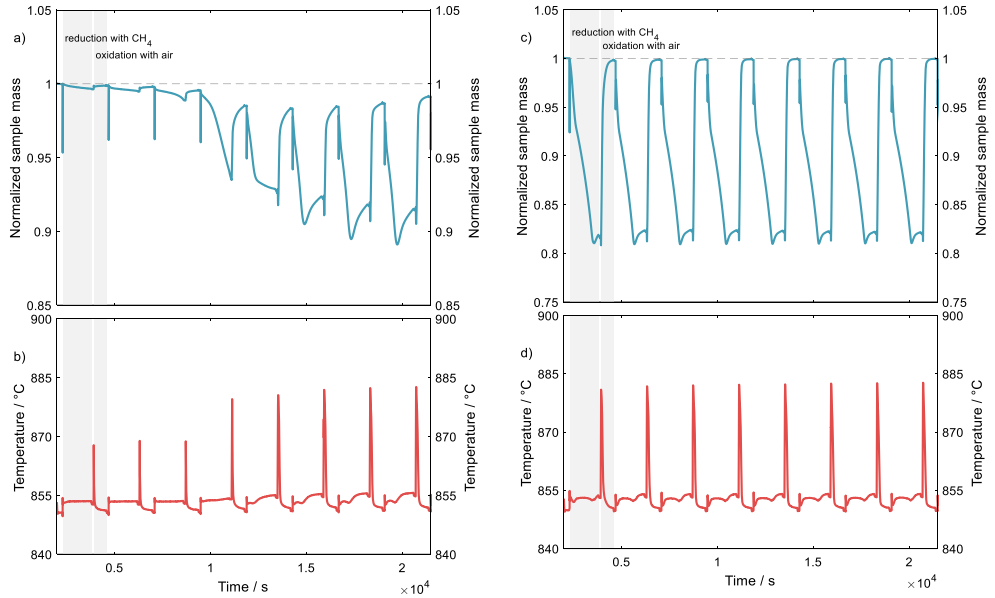

Figure 8-12: The results from the redox cycling experiments using the TGA at 850°C. Reduction was performed with CH_4 and oxidation was performed with air. a) and b) show the normalized sample mass and sample temperature, respectively, measured during the initial eight (of 60) cycles for the oxygen carrier $Mg(Fe_{0.5}Al_{0.5})_2O_4$ with 5 wt.% CuO. c) and d) show the normalized sample mass and sample temperature, respectively, measured during the initial eight (of 60) cycles for the oxygen carrier $Mg(Fe_{0.9}Al_{0.1})_2O_4$ with 5 wt.% CuO.

increase due to coke depositing on the sample surface. After 30 cycles, the measured oxygen storage capacity prior coking was ~ 10.9 wt.%, which corresponds to 76 % of the theoretical oxygen storage capacity assuming the equivalent amounts of Fe_2O_3 and CuO were the only redox-active species. It was thus expected that coking would not become a major problem in fluidized bed experiments by limiting the time of the reduction since the oxygen carrier is reduced uniformly inside the reactor.

*Figure **8-10*** d & e compare the diffractograms acquired before and after the cycling experiment respectively. The peaks corresponding to the (Cu-doped) $Mg(Fe_{0.5}Al_{0.5})_2O_4$ spinel split into pairs of peaks, indicating the separation of the $Mg(Fe_{0.5}Al_{0.5})_2O_4$ spinel into an Fe-rich and an Fe-depleted spinel phase. The Fe-rich spinel phase was identified as $Mg(Fe_{0.9}Al_{0.1})_2O_4$ spinel (PDF 01-071-1233), containing theoretically 74 wt.% of redox-active Fe_2O_3. Since this phase appeared to be the thermodynamically stable phase under the reaction conditions employed, a phase pure $Mg(Fe_{0.9}Al_{0.1})_2O_4$ oxygen carrier doped with 5 wt.% CuO was synthesized and investigated in the TGA under identical reaction conditions. The results are plotted in *Figure **8-12*** c *&* *d* and show that the material was active from the first cycle and no activation period

was required. The diffractogram of the oxygen carrier after the cycling experiment (after 60 cycles after the air oxidation step, corresponding to ~ 40 h of cycling operation) was identical with that of the as-synthesized oxygen carrier, demonstrating that no irreversible phase changes occurred during redox cycling (*Figure **8-10** f & g*). The extent of coking was much lower than that seen for the Cu-doped $Mg(Fe_{0.5}Al_{0.5})_2O_4$ and the oxygen storage capacity was 18.8 wt.%, utilizing ~ 85% of the total redox-active lattice oxygen prior coking. The material collected from the TGA after the 60 cycle experiment appeared fused together (note that fine powder was used as the starting material) and could not easily be separated by slight agitation, confirming that surface area played only a minor role for the material's reactivity. In the TGA experiments, fine powder of oxygen carrier remained stagnant in the crucible during redox cycling, which clearly facilitated sinter processes. In fluidized bed operation, discussed below in *section **8.3.2.2** the* oxygen carrier particles were much larger (100-180 μm) and under vigorous movement with fast heat transfer; it was thus expected that sinter processes causing particle agglomeration would not be significant or could at least be controlled by varying the flow rate of gas and the extent of reduction.

8.3.2.1.2 Material characterization

Most oxygen carriers deactivate owing to either irreversible phase changes occurring during redox cycling or sintering decreasing the surface area and accessible pore-volume, or both. From the TGA experiments it appeared that the reactivity of the Cu-doped $Mg(Fe_{0.9}Al_{0.1})_2O_4$ oxygen carrier particles did not depend on surface area (N_2 sorption measurements of fresh and cycled material gave BET surface areas < 1 m^2/g). Since no irreversible phase changes occurred during redox cycling (*Figure **8-10** f & g*), the oxygen carrier was inherently stable.

The experiments described above have, so far, neglected the re-oxidation with steam to produce H_2. Using high steam concentrations in TGAs is usually difficult, and so CO_2 was used as an oxidant instead. At 850°C, CO_2 and H_2O possess roughly the same oxidation potential [77]. *Figure **8-13** a & b* show the results from a TGA experiment (first five redox cycles), where the Cu-doped $Mg(Fe_{0.9}Al_{0.1})_2O_4$ oxygen carrier was reduced in CH_4 and re-oxidized using first CO_2 and then air. Oxidation with CO_2 restored 89 % of the total redox-active lattice oxygen of the material within the given time. Nonetheless, a significant amount of heat was produced when replenishing the remaining lattice oxygen with air, with the oxidation in CO_2 being nearly heat neutral (*Figure **8-13** b*). No adverse effects on the cyclic redox stability have been observed when the oxygen carrier was not re-oxidized in air, although it has been reported for mixed Fe-based oxygen carriers that an air oxidation step may be required [77] to prevent the material's

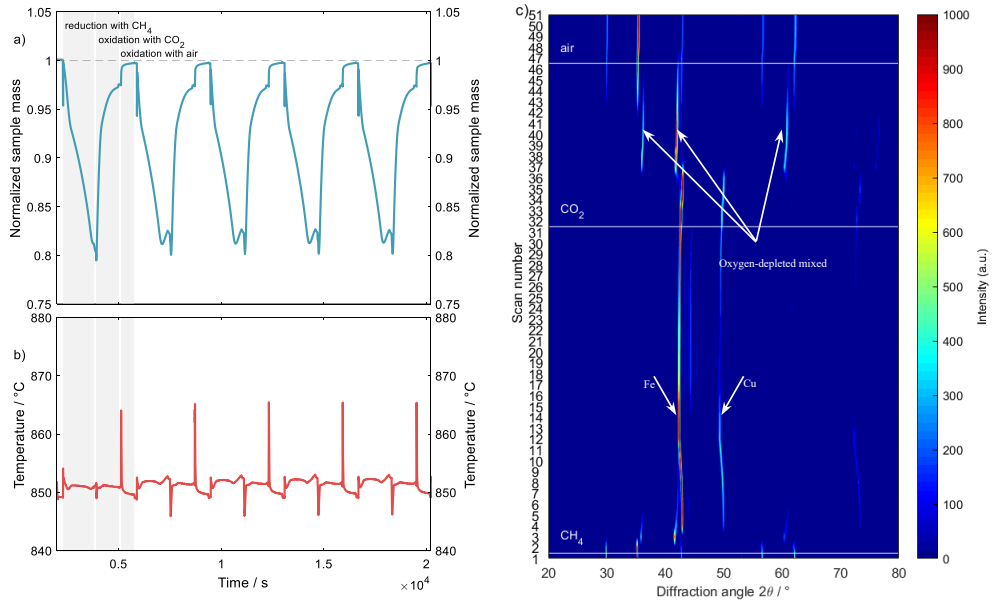

Figure 8-13: The results from the redox cycling experiments using the TGA and In-situ XRD at 850°. a) and b) show the normalized sample mass and sample temperature, respectively, measured during the initial five cycles for the oxygen carrier $Mg(Fe_{0.9}Al_{0.1})_2O_4$ with 5 wt.% CuO. c) shows a 2D intensity map measured during an in-situ XRD experiment at 850°C in which the oxygen carrier $Mg(Fe_{0.9}Al_{0.1})_2O_4$ with 5 wt.% CuO was reduced in CH_4 (scans 2-31) and oxidized in CO_2 (scans 32-46) and oxidized in air (scans 47-51).

deactivation due to gradual phase segregation. Material collected from the TGA appeared less sintered compared to that which had been re-oxidized using air only, implying that the re-oxidation with CO_2 (or steam in the actual hydrogen generation step) aided in restoring transient phases of lower sinter temperatures.

Temperature-programmed reduction (TPR) in the presence of 7 vol.% CH_4/N_2 using the TGA showed that the Cu-doped $Mg(Fe_{0.9}Al_{0.1})_2O_4$ oxygen carrier reduced in two principal steps (SI *Figure* ***S2*** c)**.** The results were confirmed by in-situ XRD (*Figure* ***8-13*** *c*), which was performed under similar reaction conditions as the cycling experiment (i.e. reduction with CH_4, oxidation with CO_2 followed by air at 850°C). *Figure* ***8-13*** c shows that upon exposure to CH_4, the oxygen carrier reduced to metallic iron via a different mixed (Mg,Al,Fe) phase. Interestingly, separate reflections from Cu-species were not seen until also metallic iron formed. Separate crystalline Al-containing phases such as Al_2O_3 were not detected during reduction. Upon re-oxidation with CO_2 (scans 32 – 46 in *Figure* ***8-13*** c metallic Cu (peak near 50°) was re-incorporated in the mixed spinel environment, which is different from what has been observed for Fe-based

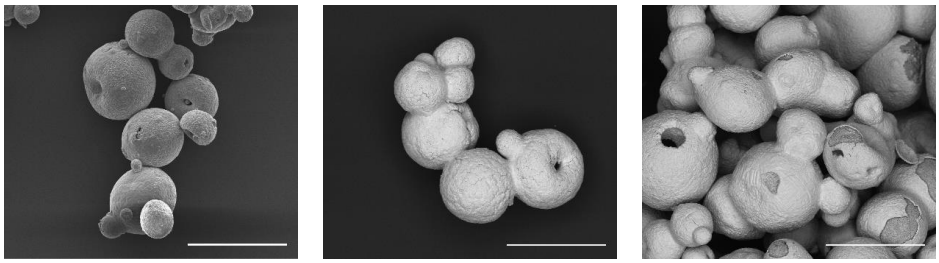

a) b) c)

Figure 8-14: SEM images of the spray-dried oxygen carrier $Mg(Fe_{0.9}Al_{0.1})_2O_4$ with 5 wt.% CuO. a) As-prepared oxygen carrier particles, b) oxygen carrier particles after redox cycling in the fluidized bed, and c) oxygen carrier particles after redox cycling in the fluidized bed when the bed partially defluidized and the oxygen carrier particles fused together. The length of the white bar is 200 µm.

brownmillerite structures, where Cu could only be re-incorporated upon exposure to air (i.e. at higher partial pressures of oxygen)[77]. Before the atmosphere in the reaction chamber was changed from CO_2 to air, there was, somewhat unexpected, a gradual transition towards the initial spinel phase, which suggests that a near-complete recovery of lattice oxygen with CO_2 was possible. To confirm this, an isothermal cycling experiment was performed at 850°C, in which after the fourth reduction the material was re-oxidized for 4 h in 20 vol.% CO_2 only (*SI Figure **S2** c*). Indeed, there was an increase in sample mass throughout the oxidation period, although at a very low rate that would prevent the complete re-oxidation withing a reasonable time. However, this result also implies that the complete combustion of CH_4 to generate CO_2 and H_2O only during the reduction of the fully-oxidized oxygen carrier (as is the case for the transition $Fe_2O_3 \rightarrow Fe_3O_4$) is probably not possible thermodynamically. At the beginning and the end of the in-situ XRD experiment (scan 1 and 51), the same crystalline spinel phase (PDF 01-071-1233) was observed, confirming the fully reversible phase changes within the oxygen carrier.

In the actual gas switching reactor, a fluidized bed, spray-dried particles were used (their synthesis is described in the experimental *section **8.3.2.2.*** Most of the freshly calcined particles were of spherical shape, but some particles had the shape of a torus with a large void in the center, as can be seen in *Figure **8-14** a*. In addition, smaller satellite particles stuck to larger ones, thus forming agglomerates of particles. The compression strength of the as-synthesized spray-dried Cu-doped $Mg(Fe_{0.9}Al_{0.1})_2O_4$ oxygen carrier particles was 4.25 +/- 1.29 N, which is equivalent to ~ 142 MPa when normalizing force by the average geometrical diameter of the particles. The relatively large standard deviation of the measured crushing strength was probably due to the inhomogeneity of some of the particles, as seen in *Figure **8-14** a*.After 60

redox cycles in the TGA, the crushing strength reduced to 3.44 +/- 1.46 N (equivalent to ~ 115 MPa), which is comparable to what has been reported as state-of-the-art in the context of oxygen carriers for chemical looping[78].

8.3.2.2 Fluidized bed experiment with optimized Cu-doped $Mg(Fe_{0.9}Al_{0.1})_2O_4$ spinel OC.

The oxygen carrier material was investigated in the 5 cm ID reactor (*Figure **8-4***) under atmospheric condition. The mass of the oxygen carrier originally placed in the reactor was 460 g making about 3 moles of lattice oxygen. It is important to note the reduction behavior and the thermodynamic properties of the Cu-doped $Mg(Fe_{0.9}Al_{0.1})_2O_4$ are fundamentally different from the Fe_2O_3-system, for which three-phase transitions occur upon reduction (Fe_2O_3-Fe_3O_4, Fe_3O_4-Fe, FeO-Fe). Cu-doped $Mg(Fe_{0.9}Al_{0.1})_2O_4$ reduces in two steps, where the first step (transition between two different spinel environments, *Figure **8-10** c*) would require the consumption ~ 1/3 of the total redox-active lattice oxygen (*Figure **8-12** a*), equivalent to Fe_2O_3→ FeO transition. In the second transition the redox-active Fe-species transform from the spinel environment to metallic Fe at a relatively low equilibrium constant (equivalent to FeO → Fe transition), which implies that upon reduction no pure CO_2 can be generated, but upon oxidation with steam even higher yields of H_2 can be obtained than for the transition Fe → FeO. In fact, in preliminary studies the measured equilibrium constant $K_{eq} = pCO_2/pCO$ (CO_2 was used as a surrogate for H_2O) at 800°C was 0.33 compared to $K_{eq} = 0.54$ for the transition Fe → FeO.

8.3.2.2.1 Reactor performance

From *Figure **8-15***, the cyclic behavior of the oxygen carrier was repeatable over the three cycles. The degree of fuel conversion in the fuel stage was, unfortunately, low, with a large quantity of unconverted CH_4, CO and H_2 exiting the reactor. It is possible that conversion will be improved in a larger reactor with a greater gas residence time, but the general degree of fuel utilization in these experiments was below expectations when comparing it with the results from the TGA experiments (*Figure **8-12** c)*. It is clear that such a large amount of fuel slip will require integration with another process capable of combusting this large quantity of slipped fuel as discussed earlier. From *Figure **8-15***, about 13% steam conversion was achieved at 800°C, which was much lower than expected from K_{eq} (note that $K_{eq} = 0.33$ implies a steam conversion of 75

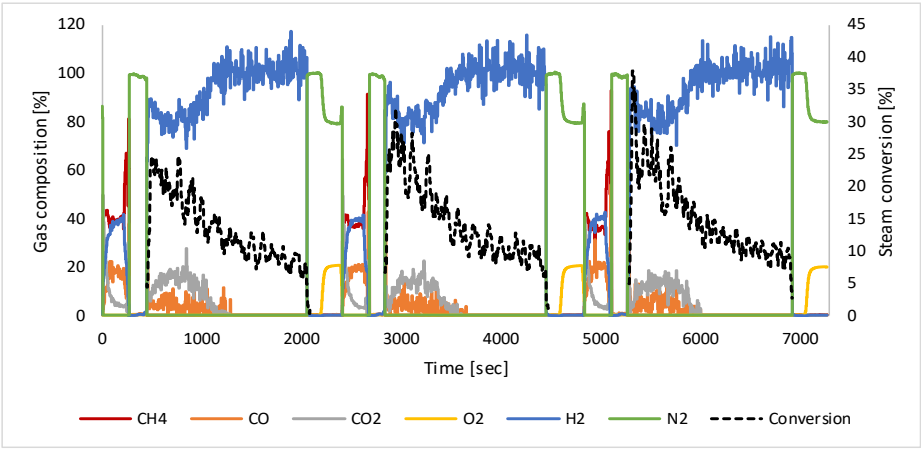

Figure 8-15: Three cycles of reactor operation with a fuel time of 4 minutes at 800°C and 1bar.

% is feasible). It thus appeared that the oxygen carrier was not reduced sufficiently to exploit the low value of K_{eq} for this material. Carbon deposition from the fuel stage was also eminent and unlike the behavior with the oxygen carrier containing 35 wt.% Fe_2O_3, the deposited carbon was gasified in the steam stage to produce syngas (CO + H_2), thus reducing the H_2 purity.

Even though such large degrees of fuel slip can be accommodated by more complex process integration, it remains desirable to greatly improve the fuel utilization in the GSWS fuel stage. High fuel conversion, therefore, remains an important priority for future oxygen carrier development studies. Apart from the low fuel utilization, the new oxygen carrier presented additional challenges in the reactor tests: agglomeration (*Figure **8-14** b & c)* at higher degrees of reduction and carbon deposition in all cases. When the fuel time was increased beyond 4 minutes, the oxygen carrier started to agglomerate at the air stage after 10 cycles (*SI Figure **S3***). This was probably because of non-uniform reduction arising from dead zones in the reactor above the distributor plate, making some part of the oxygen carrier much more reduced than others. This phenomenon made the reactor inoperable. The produced agglomerate was brittle and could relatively easily be reduced to a fluidizable and reactive powder again. It is also desired to reduce the oxygen carrier uniformly in the bed to prevent coking as seen in the TGA experiments *section **8.3.2.1** (Figure **8-12** c).*

However, it is very important for the GSWS process to be able to achieve a large degree of oxygen carrier utilization to maximize CO_2 separation efficiency. As outlined in the introduction, lower degrees of oxygen carrier utilization will magnify the effect of the mixing of different gases when switching between stages, resulting in lower CO_2 capture efficiency

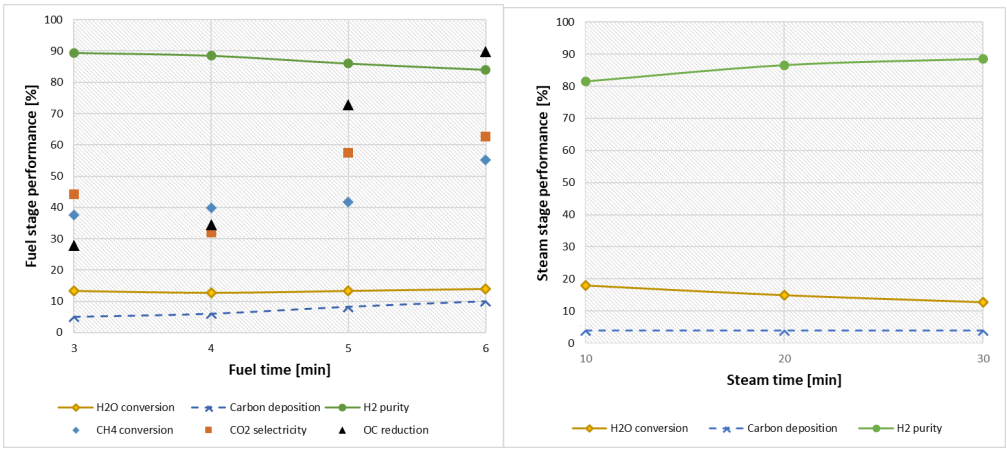

a) b)

Figure 8-16: The reactor performance at the fuel and steam stages at 800°C and 1bar. a) The performance at the fuel stage against fuel time at a constant steam time (5mins). b) The performance at the steam stage against steam time at constant fuel time (4mins).

and purities of H_2 and CO_2. As illustrated later in the achieved oxygen carrier utilization in the case with 4 minutes fuel time was only 34% (*Figure* ***8-16***), implying that the onset of agglomeration at the oxidation stage is greatly restricting the degree of oxygen carrier utilization and thus also the CO_2 separation performance of the reactor. This is in agreement with the TPR results (*SI Figure* ***S2***) and in-situ XRD experiments (*Figure* ***8-13*** c). The onset of both coking and agglomeration appears to be related to the formation of the metallic iron phase.

As outlined in *section* ***8.3.2.1*** agglomeration was observed in TGA experiments only when a fine powder was used. It is therefore difficult to ascertain why agglomeration of the spray-dried particles was experienced in the larger reactor, but one possibility could be the large reactor aspect ratio, which limited the axial mixing in the reactor. Lower quality of mixing will increase the likelihood of particle agglomerates forming. Agglomeration will be a self-strengthening phenomenon in this case, with initial agglomerates further reducing the quality of mixing in the bed, thus allowing additional agglomerates to form.

Regarding carbon deposition, *Figure* ***8-15*** clearly shows the formation of CO and CO_2 in the steam stage due to the gasification of deposited carbon by steam. It is shown that the concentration of CO_2 was significantly higher than that of CO, suggesting that the oxygen carrier catalyzes the water-gas shift reaction, which converts CO and excess steam to CO_2 and H_2. These released carbon-containing gases will reduce the CO_2 capture efficiency if the resulting H_2-rich stream is combusted for heat or power production.

Figure ***8-16*** summarizes the reduction performance of the oxygen carrier as a function of the fuel and steam times. In these cases, data was extracted from a stage before significant agglomeration started, but it is possible that some initial agglomeration behavior already caused the reactor to exhibit some plug-flow behavior in these cases, thus increasing fuel conversion due to increased gas contact and residence time. Looking at the effect of fuel time (*Figure* ***8-16*** *a*), higher H_2 yield was achieved with fuel times of 5 and 6 minutes (evident from H_2O conversion), but associated with higher carbon deposition and less H_2 purity as opposed to the fuel times of 3 and 4 minutes. At lower fuel time, the degree of fuel utilization with methane conversion (40%) mostly occurring through partial oxidation to syngas instead of full oxidation (CO_2 selectivity was in the range of 30-45%). Steam conversion of about 13% was obtained for all cases; more than 50% lower than the Fe_3O_4-FeO equilibrium at 800 °C. Carbon deposition at the fuel stage resulted in about 6% of the incoming carbon to end up in the H_2-rich stream from the steam stage. On a dry basis, these carbon-containing gases will reduce the H_2 purity to about 90%. At shorter steam stage (*Figure* ***8-16*** *b*), higher steam conversion to H_2 was achieved but also with lower H_2 purity due to more of CO_2 and CO mixed into the released H_2. As shown in *Figure* ***8-15***, H_2O conversion, through the gasification of the deposited carbon and water-gas-shift reaction are higher at the start of the steam stage, explaining these trends.

8.4 Conclusion

Two GSWS experimental campaigns were completed using 35 wt.% Fe_2O_3 on Al_2O_3 and Cu-doped Fe/$MgAl_2O_4$ spinel of high iron content developed specifically in this study. The 1st GSWS demonstration was completed with 35 wt.% Fe_2O_3 on Al_2O_3 OC in 5 cm ID fluidized bed reactor. Good reactor performance was achieved with no agglomeration but H_2 purity was compromised due to gas mixing while switching between reactor stages. To improve H_2 purity, a mass balance calculation showed that up to 70 wt.% iron content oxygen carrier is desired to keep the GSWS stages sufficiently long to minimize gas mixing effect on GSWS gas separation performance. On this ground, an optimized Cu-doped $Mg(Fe_{0.9}Al_{0.1})_2O_4$ spinel OC with 74 wt.% active content was developed, screened and characterized using TGA, XRD, ICP-OES, SEM, ICP and crushing test for the 2nd GSWS demonstration in the 5 cm ID fluidized bed reactor. High oxygen-carrying capacity up to 20% was achieved and TGA result at 850°C shows that the oxygen carrier is very reactive and exhibited good redox behavior.

However, the 2nd GSWS demonstration with the optimized Cu-doped $Mg(Fe_{0.9}Al_{0.1})_2O_4$ spinel OC with 74 wt.% active content revealed three key challenges with the proposed high active

content. All three of these challenges need to be addressed in future work to increase the attractiveness of the GSWS concept. Firstly, the degree of fuel utilization in the fuel stage was low, resulting in high fuel slippage. Such slipped fuel can be productively integrated with a downstream process, but it will certainly increase the attractiveness of the GSWS concept if fuel slip can be minimized. Secondly, the oxygen carrier started to agglomerate after about 34% of reduction. This issue does not allow the process to utilize even half of the oxygen-carrying capacity and will seriously hamper the CO_2 separation performance of the process. It is possible that this challenge can be overcome in a larger reactor where more vigorous fluidization is possible, but this needs to be confirmed in future experiments. Thirdly, the oxygen carrier showed significant carbon deposition, resulting in CO_2 and CO being released in the steam stage. When the H_2-rich stream is combusted, this will result in CO_2 emissions of about 20 kg/GJ_{LHV} of H_2. Alternatively, a downstream pressure swing adsorption unit can be used to purify the H_2 before utilization. The results from TGA appeared as if coking was delayed until 85% lattice oxygen conversion was achieved. This was possible because the rate of reduction was much faster in TGA than the rate of coking so that the net effect was mass loss even though coking occurred. This shows that TGA alone is not suitable to relate conversion with onset of coking.

To summarize, the following points could be noted:

- Gas Switching water-splitting could be an efficient technique for H_2 production with zero-emission.
- Oxygen carrier with 35 wt.% active content performed well but with less H_2 purity without agglomeration, while the oxygen carrier with 74 wt.% active content tends to agglomerate faster.
- A compromise in the active content is therefore required to achieve an optimum GSWS performance.
- Relying on a TGA alone is not so sufficient as many other factors, such as coking, agglomeration, could differ with large-scale setup.

Acknowledgment

ACT GaSTech project. Project No 271511.

This project has received funding from The Research Council of Norway and is cofounded by the European Commission under the Horizon 2020 program, ACT Grant Agreement No 691712. This project also received the 2019 Equinor Publication Grant. VATL Lab technicians at the Norwegian University of Science and Technology are equally acknowledged for constructing and maintaining the experimental setup.

Nomenclature

Abbreviations

BET	Brunauer–Emmett–Teller
CCS	Carbon capture and storage
CFB	Circulation Fluidized Bed
CLC	Chemical Looping Combustion
CLR	Chemical Looping Reforming
EDS	Energy Dispersive Spectroscopy
EDX	Energy Dispersive X-Ray Spectroscopy
GHG	Gashouse Gas
GSC	Gas Switching Combustion
GST	Gas Switching Technology
GSWS	Gas Switching Water Splitting
ICP-OES	Inductively coupled plasma optical emission spectroscopy
OC	Oxygen carrier
POX	Partial Oxidation of Methane
SEM	Scanning Electron Microscopy
TEM	Transmission Electron Microscopy
XRD	X-ray Diffraction
TGA	Thermogravimetric Analysis

Symbols

C_{dep}	Carbon deposition
D_{50}	Diameter of the catalyst which 50% of a sample mass is smaller than
n_{CO}	Mole of CO at the gas outlet
n_{CO_2}	Mole of CO_2 at the gas outlet
$n_{CO_2,air}$	Mole of CO_2 in the outlet gas at the air stage
$n_{CO_2,fuel}$	Mole of CO_2 in the outlet gas at the fuel stage
$n_{CO_2,steam}$	Mole of CO_2 in the outlet gas at the steam stage
$n_{fuel,in}$	Mole of fuel input
$n_{fuel,out}$	Mole of fuel at the gas outlet
$n_{Fe_2O_3}$	Mole of Fe_2O_3
n_{H_2}	Mole of H_2 at the gas outlet
n_{H_2O}	Mole of H_2O at the gas outlet
n_{N_2}	Mole of N_2 at the gas outlet
n_{O_2}	Mole of O_2 at the gas outlet
s_{CO_2}	CO_2 selectivity
η_{CO_2}	CO_2 capture efficiency
σ_{H_2}	H_2 purity
σ_{CO_2}	CO2 purity
γ_{fuel}	Fuel conversion
γ_{H_2O}	Steam conversion

References

[1] C. IEAGHG, "Migration in the Overburden," IEAGHG Technical Reports, 2017.

[2] IPCC, "Global Warming of 1.5C- An IPCC Special Report on the impacts of global warming of 1.5C above pre-industrial levels and related global greenhouse gas emission pathways, in the context of strengthening the global response to the threat of climate change, sustainable development, and efforts to eradicate poverty. Summary for Policymakers," IPCC, Switzerland, 2018. [Online]. Available: https://report.ipcc.ch/sr15/pdf/sr15_spm_final.pdf

[3] F. He and F. Li, "Perovskite promoted iron oxide for hybrid water-splitting and syngas generation with exceptional conversion," *Energy & Environmental Science,* vol. 8, no. 2, pp. 535-539, 2015.

[4] P. Nejat, F. Jomehzadeh, M. M. Taheri, M. Gohari, and M. Z. A. Majid, "A global review of energy consumption, CO2 emissions and policy in the residential sector (with an overview of

the top ten CO2 emitting countries)," *Renewable and sustainable energy reviews,* vol. 43, pp. 843-862, 2015.

[5] J. Cook *et al.*, "Quantifying the consensus on anthropogenic global warming in the scientific literature," *Environmental research letters,* vol. 8, no. 2, p. 024024, 2013.

[6] R. K. Pachauri *et al.*, *Climate change 2014: synthesis report. Contribution of Working Groups I, II and III to the fifth assessment report of the Intergovernmental Panel on Climate Change*. IPCC, 2014.

[7] U. N. "Adoption of the Paris Agreement Proposal by the President." https://unfccc.int/resource/docs/2015/cop21/eng/l09r01.pdf (accessed May, 2018).

[8] C. C. Elam, C. E. G. Padró, G. Sandrock, A. Luzzi, P. Lindblad, and E. F. Hagen, "Realizing the hydrogen future: the International Energy Agency's efforts to advance hydrogen energy technologies," *International Journal of Hydrogen Energy,* vol. 28, no. 6, pp. 601-607, 2003.

[9] G. Voitic and V. Hacker, "Recent advancements in chemical looping water splitting for the production of hydrogen," *RSC Advances,* vol. 6, no. 100, pp. 98267-98296, 2016.

[10] P. P. Edwards, V. L. Kuznetsov, W. I. David, and N. P. Brandon, "Hydrogen and fuel cells: towards a sustainable energy future," *Energy policy,* vol. 36, no. 12, pp. 4356-4362, 2008.

[11] J. D. Holladay, J. Hu, D. L. King, and Y. Wang, "An overview of hydrogen production technologies," *Catalysis today,* vol. 139, no. 4, pp. 244-260, 2009.

[12] J. Adanez, A. Abad, F. Garcia-Labiano, P. Gayan, and F. Luis, "Progress in chemical-looping combustion and reforming technologies," *Progress in energy and combustion science,* vol. 38, no. 2, pp. 215-282, 2012.

[13] S. K. Ngoh and D. Njomo, "An overview of hydrogen gas production from solar energy," *Renewable and Sustainable Energy Reviews,* vol. 16, no. 9, pp. 6782-6792, 2012.

[14] R. Chaubey, S. Sahu, O. O. James, and S. Maity, "A review on development of industrial processes and emerging techniques for production of hydrogen from renewable and sustainable sources," *Renewable and Sustainable Energy Reviews,* vol. 23, pp. 443-462, 2013.

[15] E. J. Anthony, "Solid looping cycles: a new technology for coal conversion," *Industrial & Engineering Chemistry Research,* vol. 47, no. 6, pp. 1747-1754, 2008.

[16] M. Rydén and M. Arjmand, "Continuous hydrogen production via the steam–iron reaction by chemical looping in a circulating fluidized-bed reactor," *International Journal of Hydrogen Energy,* vol. 37, no. 6, pp. 4843-4854, 3// 2012, doi: http://dx.doi.org/10.1016/j.ijhydene.2011.12.037.

[17] T.-L. Hsieh *et al.*, "250 kWth high pressure pilot demonstration of the syngas chemical looping system for high purity H2 production with CO2 capture," *Applied energy,* vol. 230, pp. 1660-1672, 2018.

[18] M. N. Khan and T. Shamim, "Investigation of hydrogen generation in a three reactor chemical looping reforming process," *Applied Energy,* vol. 162, pp. 1186-1194, 2016.

[19] M. N. Khan and T. Shamim, "Exergoeconomic analysis of a chemical looping reforming plant for hydrogen production," *International Journal of Hydrogen Energy,* vol. 42, no. 8, pp. 4951-4965, 2017.

[20] M. V. Kathe, A. Empfield, J. Na, E. Blair, and L.-S. Fan, "Hydrogen production from natural gas using an iron-based chemical looping technology: Thermodynamic simulations and process system analysis," *Applied energy,* vol. 165, pp. 183-201, 2016.

[21] H. Lane, "Apparatus for producing hydrogen gas," ed: Google Patents, 1912.

[22] L.-S. Fan and F. Li, "Chemical looping technology and its fossil energy conversion applications," *Industrial & Engineering Chemistry Research,* vol. 49, no. 21, pp. 10200-10211, 2010.

[23] T. Proell, J. Bolhar-Nordenkampf, P. Kolbitsch, and H. Hofbauer, "Syngas and a separate nitrogen/argon stream via chemical looping reforming - A 140 kW pilot plant study," *Fuel,* vol. 89, no. 6, pp. 1249-1256, Jun 2010, doi: 10.1016/j.fuel.2009.09.033.

[24] B. Kronberger, E. Johansson, G. Loffler, T. Mattisson, A. Lyngfelt, and H. Hofbauer, "A two-compartment fluidized bed reactor for CO2 capture by chemical-looping combustion," *Chemical Engineering & Technology,* vol. 27, no. 12, pp. 1318-1326, Dec 2004, doi: 10.1002/ceat.200402137.

[25] C. Linderholm, A. Abad, T. Mattisson, and A. Lynyfelt, "160 h of chemical-looping combustion in a 10 kW reactor system with a NiO-based oxygen carrier," *International Journal of Greenhouse Gas Control,* vol. 2, no. 4, pp. 520-530, Oct 2008, doi: 10.1016/j.ijggc.2008.02.006.

[26] E. Johansson, T. Mattisson, A. Lyngfelt, and H. Thunman, "A 300 W laboratory reactor system for chemical-looping combustion with particle circulation," *Fuel,* vol. 85, no. 10-11, pp. 1428-1438, Jul-Aug 2006, doi: 10.1016/j.fuel.2006.01.010.

[27] N. Ding, W. R. Wang, Y. Zheng, C. Luo, P. F. Fu, and C. G. Zheng, "Development and Testing of an Interconnected Fluidized-Bed System for Chemical Looping Combustion," *Chemical Engineering & Technology,* vol. 35, no. 3, pp. 532-538, Mar 2012, doi: 10.1002/ceat.201100560.

[28] P. Kolbitsch, J. Bolhar-Nordenkampf, T. Proll, and H. Hofbauer, "Operating experience with chemical looping combustion in a 120 kW dual circulating fluidized bed (DCFB) unit," *International Journal of Greenhouse Gas Control,* vol. 4, no. 2, pp. 180-185, Mar 2010, doi: 10.1016/j.ijggc.2009.09.014.

[29] M. Ryden and A. Lyngfelt, "Using steam reforming to produce hydrogen with carbon dioxide capture by chemical-looping combustion," *International Journal of Hydrogen Energy,* vol. 31, no. 10, pp. 1271-1283, Aug 2006, doi: 10.1016/j.ijhydene.2005.12.003.

[30] M. Rydén, A. Lyngfelt, and T. Mattisson, "Synthesis gas generation by chemical-looping reforming in a continuously operating laboratory reactor," *Fuel,* vol. 85, no. 12-13, pp. 1631-1641, 2006.

[31] L. F. de Diego, M. Ortiz, F. García-Labiano, J. Adánez, A. Abad, and P. Gayán, "Hydrogen production by chemical-looping reforming in a circulating fluidized bed reactor using Ni-based oxygen carriers," *Journal of Power Sources,* vol. 192, no. 1, pp. 27-34, 2009/07/01/ 2009, doi: https://doi.org/10.1016/j.jpowsour.2008.11.038.

[32] M. Luo *et al.*, "Review of hydrogen production using chemical-looping technology," *Renewable and Sustainable Energy Reviews,* vol. 81, pp. 3186-3214, 2018.

[33] H. P. Hamers, M. C. Romano, V. Spallina, P. Chiesa, F. Gallucci, and M. v. S. Annaland, "Comparison on process efficiency for CLC of syngas operated in packed bed and fluidized bed reactors," *International Journal of Greenhouse Gas Control,* vol. 28, no. 0, pp. 65-78, 2014, doi: http://dx.doi.org/10.1016/j.ijggc.2014.06.007.

[34] R. Xiao, L. Chen, C. Saha, S. Zhang, and S. Bhattacharya, "Pressurized chemical-looping combustion of coal using an iron ore as oxygen carrier in a pilot-scale unit," *International Journal of Greenhouse Gas Control,* vol. 10, pp. 363-373, 2012.

[35] L. Chen, Z. Fan, R. Xiao, and K. Liu, "Pressurized Chemical Looping Combustion for Solid Fuel," *Handbook of Chemical Looping Technology,* pp. 123-158, 2018.

[36] S. Zhang, R. Xiao, and W. Zheng, "Comparative study between fluidized-bed and fixed-bed operation modes in pressurized chemical looping combustion of coal," *Applied energy,* vol. 130, pp. 181-189, 2014.

[37] A. Bischi *et al.*, "Design study of a 150 kWth double loop circulating fluidized bed reactor system for chemical looping combustion with focus on industrial applicability and pressurization," *International Journal of Greenhouse Gas Control,* vol. 5, no. 3, pp. 467-474, 2011.

[38] J. Adanez, A. Abad, F. Garcia-Labiano, P. Gayan, and L. F. de Diego, "Progress in Chemical-Looping Combustion and Reforming technologies," *Progress in Energy and Combustion Science,* vol. 38, no. 2, pp. 215-282, Apr 2012, doi: 10.1016/j.pecs.2011.09.001.

[39] N. M. F. Science. "Chemical Looping Combustion." https://mfix.netl.doe.gov/research/chemical-looping-combustion/ (accessed June, 2019).

[40] A. Zaabout, S. Cloete, S. T. Johansen, M. van Sint Annaland, F. Gallucci, and S. Amini, "Experimental Demonstration of a Novel Gas Switching Combustion Reactor for Power Production with Integrated CO2 Capture," *Industrial & Engineering Chemistry Research,* vol. 52, no. 39, pp. 14241-14250, 2013/10/02 2013, doi: 10.1021/ie401810n.

[41] S. Noorman, M. van Sint Annaland, and H. Kuipers, "Packed bed reactor technology for chemical-looping combustion," *Industrial & Engineering Chemistry Research,* vol. 46, no. 12, pp. 4212-4220, 2007.

[42] H. Hamers, F. Gallucci, P. Cobden, E. Kimball, and M. van Sint Annaland, "A novel reactor configuration for packed bed chemical-looping combustion of syngas," *International Journal of Greenhouse Gas Control,* vol. 16, pp. 1-12, 2013.

[43] A. Ugwu, A. Zaabout, J. R. Tolchard, P. I. Dahl, and S. Amini, "Gas Switching Reforming for syngas production with iron-based oxygen carrier-the performance under pressurized conditions," *International Journal of Hydrogen Energy,* 2019.

[44] A. Zaabout, P. I. Dahl, A. Ugwu, J. R. Tolchard, S. Cloete, and S. Amini, "Gas Switching Reforming (GSR) for syngas production with integrated CO2 capture using iron-based oxygen carriers," *International Journal of Greenhouse Gas Control,* vol. 81, pp. 170-180, 2019.

[45] S. M. Nazir, J. H. Cloete, S. Cloete, and S. Amini, "Gas switching reforming (GSR) for power generation with CO2 capture: Process efficiency improvement studies," *Energy,* vol. 167, pp. 757-765, 2019.

[46] S. M. Nazir, J. H. Cloete, S. Cloete, and S. Amini, "Efficient hydrogen production with CO2 capture using gas switching reforming," *Energy,* 2019.

[47] A. Ugwu, A. Zaabout, and S. Amini, "An advancement in CO2 utilization through novel gas switching dry reforming," *International Journal of Greenhouse Gas Control,* vol. 90, p. 102791, 2019.

[48] M. Osman, A. Zaabout, S. Cloete, and S. Amini, "Internally circulating fluidized-bed reactor for syngas production using chemical looping reforming," *Chem. Eng. J.,* 2018/10/04/ 2018, doi: https://doi.org/10.1016/j.cej.2018.10.013.

[49] S. A. Wassie, F. Gallucci, A. Zaabout, S. Cloete, S. Amini, and M. van Sint Annaland, "Hydrogen production with integrated CO2 capture in a novel gas switching reforming reactor: Proof-of-concept," *International Journal of Hydrogen Energy,* vol. 42, no. 21, pp. 14367-14379, 5/25/ 2017, doi: https://doi.org/10.1016/j.ijhydene.2017.04.227.

[50] S. A. Wassie *et al.*, "Hydrogen production with integrated CO2 capture in a membrane assisted gas switching reforming reactor: Proof-of-Concept," *International Journal of Hydrogen Energy,* vol. 43, no. 12, pp. 6177-6190, 2018/03/22/ 2018, doi: https://doi.org/10.1016/j.ijhydene.2018.02.040.

[51] A. Zaabout, S. Cloete, and S. Amini, "Autothermal operation of a pressurized Gas Switching Combustion with ilmenite ore," *International Journal of Greenhouse Gas Control,* vol. 63, pp. 175-183, 2017/08/01/ 2017, doi: https://doi.org/10.1016/j.ijggc.2017.05.018.

[52] A. Zaabout, S. Cloete, S. T. Johansen, M. v. S. Annaland, F. Gallucci, and S. Amini, "Experimental Demonstration of a Novel Gas Switching Combustion Reactor for Power Production with Integrated CO2 Capture," *Industrial & Engineering Chemistry Research,* vol. 52, no. 39, pp. 14241-14250, Oct 2 2013, doi: 10.1021/ie401810n.

[53] S. M. Nazir, S. Cloete, O. Bolland, and S. Amini, "Techno-economic assessment of the novel gas switching reforming (GSR) concept for gas-fired power production with integrated CO2 capture," *International Journal of Hydrogen Energy,* vol. 43, no. 18, pp. 8754-8769, 2018/05/03/ 2018, doi: https://doi.org/10.1016/j.ijhydene.2018.02.076.

[54] S. Szima *et al.*, "Gas switching reforming for flexible power and hydrogen production to balance variable renewables," *Renewable and Sustainable Energy Reviews,* vol. 110, pp. 207-219, 2019/08/01/ 2019, doi: https://doi.org/10.1016/j.rser.2019.03.061.

[55] P. Chiesa, G. Lozza, A. Malandrino, M. Romano, and V. J. I. j. o. h. e. Piccolo, "Three-reactors chemical looping process for hydrogen production," vol. 33, no. 9, pp. 2233-2245, 2008.

[56] P. Chiesa, G. Lozza, A. Malandrino, M. Romano, and V. Piccolo, "Three-reactors chemical looping process for hydrogen production," *International Journal of Hydrogen Energy,* vol. 33, no. 9, pp. 2233-2245, 2008/05/01/ 2008, doi: https://doi.org/10.1016/j.ijhydene.2008.02.032.

[57] C. E. Agu *et al.*, "Investigation of Bubbling Behaviour in Deep Fluidized Beds at Different Gas Velocities using Electrical Capacitance Tomography," 2019.

[58] C. E. Agu, L.-A. Tokheim, M. Eikeland, and B. M. J. C. E. J. Moldestad, "Determination of onset of bubbling and slugging in a fluidized bed using a dual-plane electrical capacitance tomography system," vol. 328, pp. 997-1008, 2017.

[59] J. C. Abanades, E. J. Anthony, J. Wang, J. E. J. E. S. Oakey, and Technology, "Fluidized bed combustion systems integrating CO2 capture with CaO," vol. 39, no. 8, pp. 2861-2866, 2005.

[60] A. Ugwu *et al.*, "The demonstration of pressurized Gas Switching Partial Oxidation (GSPOX) of methane using Lanthanum based oxygen carrier " *Industrial & Engineering Chemistry,* vol. In view, 2019.

[61] A. Zaabout, S. Cloete, M. van Sint Annaland, F. Gallucci, and S. Amini, "A novel gas switching combustion reactor for power production with integrated CO2 capture: Sensitivity to the fuel and oxygen carrier types," *International Journal of Greenhouse Gas Control,* vol. 39, pp. 185-193, 8// 2015, doi: http://dx.doi.org/10.1016/j.ijggc.2015.05.006.

[62] S. A. Wassie, F. Gallucci, A. Zaabout, S. Cloete, S. Amini, and M. J. I. J. o. H. E. van Sint Annaland, "Hydrogen production with integrated CO2 capture in a novel gas switching reforming reactor: Proof-of-concept," vol. 42, no. 21, pp. 14367-14379, 2017.

[63] S. Cloete, M. C. Romano, P. Chiesa, G. Lozza, and S. Amini, "Integration of a Gas Switching Combustion (GSC) system in integrated gasification combined cycles," *International Journal of Greenhouse Gas Control,* vol. 42, pp. 340-356, 2015.

[64] C. A. del Pozo, S. Cloete, J. H. Cloete, Á. J. Álvaro, and S. Amini, "The potential of chemical looping combustion using the gas switching concept to eliminate the energy penalty of CO2 capture," *International Journal of Greenhouse Gas Control,* vol. 83, pp. 265-281, 2019.

[65] K. Svoboda, G. Slowinski, J. Rogut, and D. Baxter, "Thermodynamic possibilities and constraints for pure hydrogen production by iron based chemical looping process at lower temperatures," *Energy conversion and management,* vol. 48, no. 12, pp. 3063-3073, 2007.

[66] N. Saithong, S. Authayanun, Y. Patcharavorachot, and A. Arpornwichanop, "Thermodynamic analysis of the novel chemical looping process for two-grade hydrogen production with CO2 capture," *Energy Conversion and Management,* vol. 180, pp. 325-337, 2019.

[67] Y. De Vos, M. Jacobs, I. Van Driessche, P. Van Der Voort, F. Snijkers, and A. Verberckmoes, "Processing and characterization of Fe-based oxygen carriers for chemical looping for hydrogen production," *International Journal of Greenhouse Gas Control,* vol. 70, pp. 12-21, 2018.

[68] H. Chen, Z. Zheng, Z. Chen, and X. T. Bi, "Reduction of hematite (Fe2O3) to metallic iron (Fe) by CO in a micro fluidized bed reaction analyzer: A multistep kinetics study," *Powder technology,* vol. 316, pp. 410-420, 2017.

[69] D. Kang, H. S. Lim, M. Lee, and J. W. Lee, "Syngas production on a Ni-enhanced Fe2O3/Al2O3 oxygen carrier via chemical looping partial oxidation with dry reforming of methane," *Applied Energy,* vol. 211, pp. 174-186, 2018/02/01/ 2018, doi: https://doi.org/10.1016/j.apenergy.2017.11.018.

[70] L. Protasova and F. Snijkers, "Recent developments in oxygen carrier materials for hydrogen production via chemical looping processes," *Fuel,* vol. 181, pp. 75-93, 2016.

[71] F. Li, Z. Sun, S. Luo, and L.-S. Fan, "Ionic diffusion in the oxidation of iron—effect of support and its implications to chemical looping applications," *Energy & Environmental Science,* vol. 4, no. 3, pp. 876-880, 2011.

[72] D. Sanfilippo, "One-step hydrogen through water splitting with intrinsic CO2 capture in chemical looping," *Catalysis Today,* vol. 272, pp. 58-68, 9/1/ 2016, doi: http://dx.doi.org/10.1016/j.cattod.2016.02.021.

[73] W. Liu *et al.*, "Inhibiting the interaction between FeO and Al 2 O 3 during chemical looping production of hydrogen," *RSC Advances,* vol. 5, no. 3, pp. 1759-1771, 2015.

[74] R. D. Solunke and G. t. Veser, "Hydrogen production via chemical looping steam reforming in a periodically operated fixed-bed reactor," *Industrial & Engineering Chemistry Research,* vol. 49, no. 21, pp. 11037-11044, 2010.

[75] Q. Imtiaz *et al.*, "Development of MgAl 2 O 4-stabilized, Cu-doped, Fe 2 O 3-based oxygen carriers for thermochemical water-splitting," *Journal of Materials Chemistry A,* vol. 4, no. 1, pp. 113-123, 2016.

[76] J. Y. Do *et al.*, "Reliable oxygen transfer in MgAl2O4 spinel through the reversible formation of oxygen vacancies by Cu2+/Fe3+ anchoring," *Applied energy,* vol. 219, pp. 138-150, 2018.

[77] D. Hosseini, F. Donat, P. M. Abdala, S. M. Kim, A. M. Kierzkowska, and C. R. Müller, "Reversible exsolution of dopant improves the performance of Ca2Fe2O5 for chemical looping hydrogen production," *ACS applied materials & interfaces,* 2019.

[78] C. Chung, L. Qin, V. Shah, and L.-S. Fan, "Chemically and physically robust, commercially-viable iron-based composite oxygen carriers sustainable over 3000 redox cycles at high temperatures for chemical looping applications," *Energy & Environmental Science,* vol. 10, no. 11, pp. 2318-2323, 2017.

9 Combined Syngas and Hydrogen Production using Gas Switching Technology

This chapter has been adapted from **Article VI**

Ugwu, A., A. Zaabout, F. Donat, C. Müller, K. Albertsen, G. van Diest, S. Amini, Combined Syngas and Hydrogen Production using Gas Switching Technology. *Industrial & Engineering Chemistry*, 2020. Under review.

Abstract

In this study, a three-stage GST (Gas Switching Technology) process (fuel, steam/CO_2, and air stage) for syngas production in the fuel stage and H_2/CO production in the steam/CO_2 stage was investigated using a lanthanum-based oxygen carrier ($La_{0.85}Sr_{0.15}Fe_{0.95}Al_{0.05}O_3$). The experiments were performed at temperatures between 750 - 950 °C and pressures up to 5 bar. The results show that the oxygen carrier exhibits high selectivity to syngas production at the fuel stage with the process performance observed to improve with increasing temperature although carbon deposition could not be avoided. Co-feeding CO_2 with CH_4 at the fuel stage could reduce carbon deposition significantly and improve the purity of the H_2 produced at the steam stage but reduced the syngas H_2/CO molar ratio from 3.75 to 1 (at CO_2/CH_4 ratio of 1, 950 °C and 1 bar). The demonstration of CO_2 utilization at the fuel stage showed a stable syngas production over twelve hours and maintained the H_2/CO ratio at almost unity, suggesting that the oxygen carrier was exposed to simultaneous partial oxidation of CH_4 with the lattice oxygen which is restored instantly by the incoming CO_2. This observation is supported by a similar trend of the re-oxidation step and H_2 composition in the steam stage compared to the case with less fuel duration indicating that the oxidation and reduction of the oxygen carrier happened almost at the same time and rate in the fuel. The addition of steam could tune up the H_2/CO ratio up to a value of 4 without carbon deposition at H_2O/CH_4 ratio of 1, 950 °C and 1 bar; making the syngas from Gas Switching Partial Oxidation (GSPOX) suitable for any downstream process, e.g. gas-to-liquid (GTL) processes. The process was also demonstrated at higher pressures with over 70 % fuel conversion achieved at 5 bar and 950 °C.

Keywords: Chemical looping; Gas Switching; Syngas; Hydrogen; Partial oxidation; Climate change; Low carbon technology; Natural gas; CCUS

9.1 Introduction

Natural gas is considered to be an important energy source in the decarbonization roadmap of fossil fuels considering its availability and low carbon footprint compared to other fossil fuels such as crude oil or coal [1]. However, the direct utilization of natural gas is associated with CO_2 emissions, thus shifting the focus towards its conversion to syngas (a mixture of hydrogen and carbon monoxide), hydrogen, and other valuable chemicals [2]. Syngas can be produced from natural gas through six different ways [3]: (i) Steam methane reforming (SMR), (ii) partial oxidation of methane (POX), (iii) dry methane reforming (DMR), (iv) combined methane reforming (CMR, a combination of SMR and DMR), (v) Autothermal reforming (ATR, a combination of SMR and POX), and (vi) tri reforming (TMR, a combination of SMR, DMR, and POX). However, only three (POX, SMR, and ATR) of the six technologies have been commercialized [4, 5]. Although SMR is commercialized, this technology is very energy-intensive and usually associated with high CO_2 emissions. Partial oxidation of methane (POX) is more energy-efficient than SMR [6], but the conventional route (*Reaction **9-1***) requires an air separation unit (ASU) for oxygen production, which increases the investment/capital costs and is also associated with CO_2 emissions if non-renewable electricity is used for powering the ASU. Nevertheless, POX remains an attractive technology when targeting its integration with gas-to-liquid (GTL) technologies for producing fuels, such as methanol or other higher hydrocarbons, because the produced syngas has a H_2:CO ratio ranging between 1-2 [7-10].

$$CH_4 + 0.5O_2 \rightarrow CO + 2H_2 \qquad (\Delta H_{298K} = -35.6\ kJmol^{-1}) \qquad \textit{Reaction 9-1}$$

Chemical looping partial oxidation (CLPOX) of methane has been introduced to remove the need for the capital-intensive ASU by utilizing metal oxide-based oxygen carriers that can provide the oxygen for the partial oxidation reaction. The CLPOX of methane occurs through a heterogeneous reaction with the lattice oxygen of the oxygen carrier (*Reaction **9-2***) in the fuel reactor. The oxygen carrier is circulated to a second reactor, the air reactor, for the regeneration of its lattice oxygen with air in an exothermic reaction (*Reaction **9-11***). CLPOX shares a similar advantage of the conventional chemical looping reforming (CLR), which has received increasing attention over the last two decades due to its prospects of increasing the process efficiency through heat integration [6, 11-14]. The heat generated in the oxidation reaction of the oxygen carrier can be utilized to supply heat for the partial oxidation reaction that becomes endothermic when gaseous oxygen is substituted with lattice oxygen. For material development, CLPOX exhibits an advantage over CLR in terms of cost and availability since

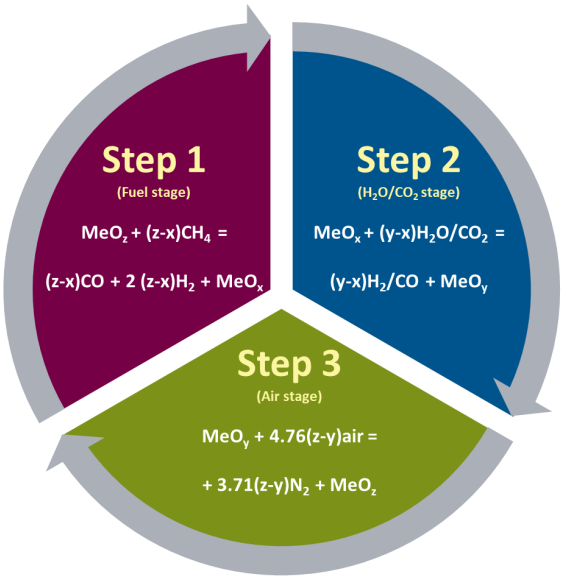

Figure 9-1: The redox cycle for the three-step chemical looping (CLPOX) process for the combined syngas and H_2/CO production.

metal oxides (oxygen carrier) are not required to be catalytically active for the hydrocarbon. CLPOX offers the flexibility to control the H_2/CO ratio of the produced syngas by simply adjusting the process conditions, co-feeding CH_4, H_2O, and/or CO_2 in the syngas production step [15, 16].

In this study, this technology has been extended to combine syngas and pure hydrogen production in a three-step process (CLPOX-H_2) with integrated CO_2 capture (*Figure* ***9-1***). The three steps of the CLPOX-H_2 are as follows: In step 1, the oxygen carrier is exposed to CH_4 for the partial oxidation of methane by lattice oxygen to produce syngas (*Reaction* ***9-2***). In this step, CO_2 and H_2O could be utilized to control the syngas quality (i.e. H_2/CO molar ratio). In step 2, H_2O/CO_2 is fed to partially oxidize the oxygen carrier and produce H_2/CO (*Reaction* ***9-3***). In step 3, the oxygen carrier is further oxidized by oxygen from the air for regeneration and production of heat (*Reaction* ***9-4***). Step 3 could be avoided but that would reduce the overall heat generated from the process, implying that the endothermic step 1 starts at a lower temperature for autothermal operations.

To maximize the economic and environmental benefits of CLPOX (or CLPOX-H_2), a pressurized operation is required to improve the overall process efficiency and simplify its integration with downstream GTL processes. Chemical looping-based processes have been investigated at larger scales using interconnected circulating fluidized beds (CFB) [17, 18].

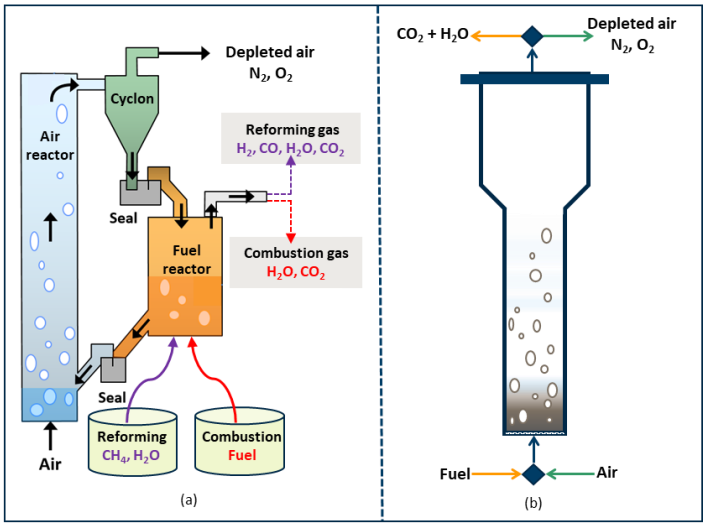

Figure 9-2: (a) Conventional Chemical looping Technology using CFB configuration [19]. (b) Gas Switching Technology proposed in this study [20].

Although the CFB configuration has been demonstrated at the lab [21-23] and pilot [24-33] scales for several chemical looping processes, pressurizing this configuration (*Figure **2-4***a) is difficult considering that each reactor needs to be pressurized individually with the need for precise control of the circulation of the oxygen carriers to fulfill the heat and mass balances of the process. The challenges magnify in three-steps processes such as CLPOX-H_2, which would require three interconnected reactors with an oxygen carrier circulating between them. As a consequence, the studies on pressurized chemical looping operations are still very limited [34-37].

Alternative reactor configurations have been proposed to address the need for pressurized operation. Among these alternatives, the gas switching technology (GST) reactor concept has been proven to be promising [38-41]. The GST reactor concept utilizes a single fluidized bed vessel, where gas feeds are alternated between the different reaction stages to oxidize and reduce the oxygen carrier (metal oxide) without requiring external solids circulation (*Figure **2-4b***). With this arrangement, load fluctuations can be greatly reduced since the oxygen carrier is confined in one pressurized vessel. Heat integration is also easier because the reactions occur in one confinement as opposed to the traditional chemical looping concept that requires the circulation of oxygen carriers between separated reactors. Operation of the three-steps process CLPOX-H_2 would be simpler in GST as only gas feeds into the same reactor need to be alternated. The CLPOX process adopted is referred to as gas switching partial oxidation (GSPOX) and is illustrated in *Figure **9-3***.

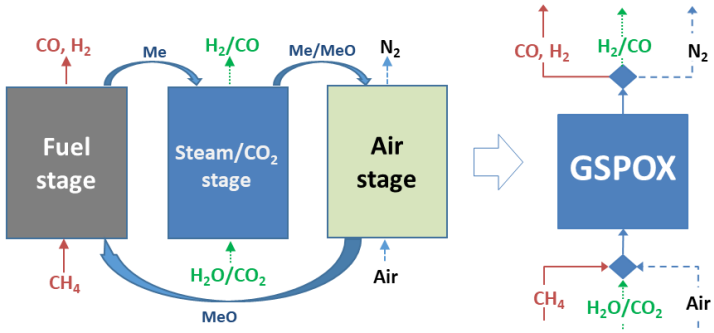

Figure 9-3: Three-stage chemical looping process for combined syngas production with integrated CO_2/steam utilization to produce H_2/CO. (a): Conventional chemical looping arrangement. (b): The simplified Gas Switching Technology under investigation.

Fuel Stage

$$MeO_z + (z-x)CH_4 \rightarrow (z-x)CO + 2(z-x)H_2 + MeO_x \qquad \textit{Reaction 9-2}$$

$$CH_4 + CO_2 \rightarrow 2CO + 2H_2 \qquad (\Delta H_{298K} = +247.0\ kJ\ mol^{-1}) \qquad \textit{Reaction 9-3}$$

$$CH_4 + H_2O \rightarrow CO + 3H_2 \qquad (\Delta H_{298K} = +205.9\ kJ\ mol^{-1}) \qquad \textit{Reaction 9-4}$$

$$CO_2 + H_2 \rightarrow CO + H_2O \qquad (\Delta H_{298K} = +41.1\ kJ\ mol^{-1}) \qquad \textit{Reaction 9-5}$$

$$CH_4 \rightarrow C + 2H_2 \qquad (\Delta H_{298K} = +74.9\ kJ\ mol^{-1}) \qquad \textit{Reaction 9-6}$$

$$C + CO_2 \rightarrow 2CO \qquad (\Delta H_{298K} = +172.4\ kJ\ mol^{-1}) \qquad \textit{Reaction 9-7}$$

Steam/CO_2 stage

$$MeO_x + (y-x)H_2O/CO_2 \rightarrow (y-x)H_2/\mathrm{CO} + MeO_y \qquad \textit{Reaction 9-8}$$

$$C + H_2O \rightarrow CO + H_2 \qquad (\Delta H_{298K} = +131.2\ kJ\ mol^{-1}) \qquad \textit{Reaction 9-9}$$

$$CO + H_2O \rightarrow CO_2 + H_2 \qquad (\Delta H_{298K} = -41.1\ kJ\ mol^{-1}) \qquad \textit{Reaction 9-10}$$

Air Stage

$$MeO_y + 4.76(z-y)air \rightarrow 3.71(z-y)N_2 + MeO_z \qquad \textit{Reaction 9-11}$$

***NOTE**: z, y and z represents the oxidation states of the oxygen carrier ($z > y > x$)*

Like any other chemical looping-based process, the feasibility of GSPOX depends to a great extent on the oxygen carriers, which should be of low cost, and enable a high selectivity towards syngas production in the fuel stage and hydrogen production in the oxidation stage with steam [42]. Perovskite-based metal oxides have demonstrated good performance for the production of syngas from CH_4 [43-46]. Perovskites have the general formula of ABO_3, where A represents a rare earth metal and/or an alkaline earth metal, and B is a transition metal [47, 48]. Perovskites generally possess good redox properties under the appropriate temperature and pressure conditions [47, 48], offer more resistance to carbon deposition and are thermodynamically suitable to convert CH_4 to syngas [10, 49-51]. Perovskites have also been applied in the combined partial oxidation and H_2O/CO_2 splitting to produce syngas in the reduction step and H_2/CO in the oxidation step [52-55]. In this study, a La-Fe-based perovskite was used as the oxygen carrier and its production scaled up to the kg-scale via spray-drying for utilization in the GST fluidized bed reactor. The A-site (i.e. La) was partially substituted with Sr while the B-site was doped with Al to yield an oxygen carrier with the composition $La_{0.85}Sr_{0.15}Fe_{0.95}Al_{0.05}O_3$. This oxygen carrier has demonstrated excellent performance with about 99 % selectivity to syngas in a gram-scale setup [56, 57].

In summary, this study experimentally investigates the GSPOX performance of a spray-dried oxygen carrier in a novel gas switching reactor as an alternative to pressurized CLPOX. A sensitivity study of CH_4 molar ratio, flowrate, operating temperature, and pressure was conducted to gain insight and understanding of the process behavior, and also to ascertain the best process conditions for the eventual scale-up of the process.

9.2 Experimental demonstration

9.2.1 Oxygen carrier

The oxygen carrier used had the composition $La_{0.85}Sr_{0.15}Fe_{0.95}Al_{0.05}O_3$ and was prepared from La_2O_3, $SrCO_3$, Fe_2O_3, and Al_2O_3 (technical grades) by solid-state processing. The starting materials were mixed in the given ratio and then milled to the specific particle size (D10: 0.263 µm, D50: 0.620 µm, D90: 1.355 µm, D99: 2.1587 µm), followed by drying and calcination at 1250 °C for 4 h (5 °C/min increment, 25 °C/min decrement). Small samples of the prepared materials were characterized first by X-ray diffraction (XRD) to ensure a phase-pure perovskite had formed. The performance towards the partial oxidation of methane was evaluated in previous work, including a detailed characterization of the oxygen carrier material [57]. Due to

the relatively small scale of the material production (few kgs), the size of the spray dryer was limited. The smaller spray dryer was unable to produce homogeneous large spheres, therefore the material needed to be screened and sieved before the application in the fluidized bed reactor. *Figure **9-4*** shows the SEM image of the synthesized $La_{0.85}Sr_{0.15}Fe_{0.95}Al_{0.05}O_3$ spheres produced by spray-drying. Initially, the PSD of the calcined spheres was quite wide (*Figure **9-5a***), but the samples used in the GST reactor were sieved between 137 – 225 µm for the experimental demonstration (*Figure **9-5b***). The particles were porous and had a relatively low density (bulk density 1901 kg/m^3) given the heavy elements included. The oxygen carrier was phase-pure, as is evident from the diffractogram shown in *Figure **9-6***. The effective oxygen storage capacity was 9 wt.% at 900 °C [57].

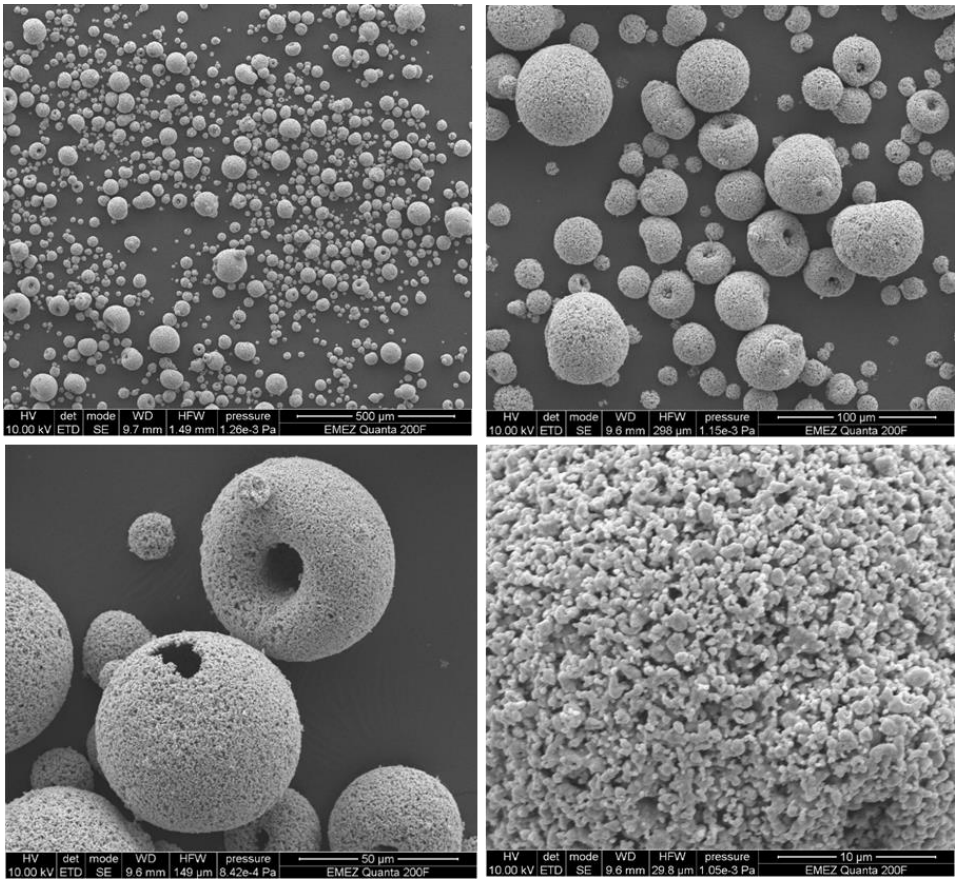

Figure 9-4: The SEM image showing the particle distribution of the freshly synthesized $La_{0.85}Sr_{0.15}Fe_{0.95}Al_{0.05}O_3$ oxygen carrier under investigation in this study.

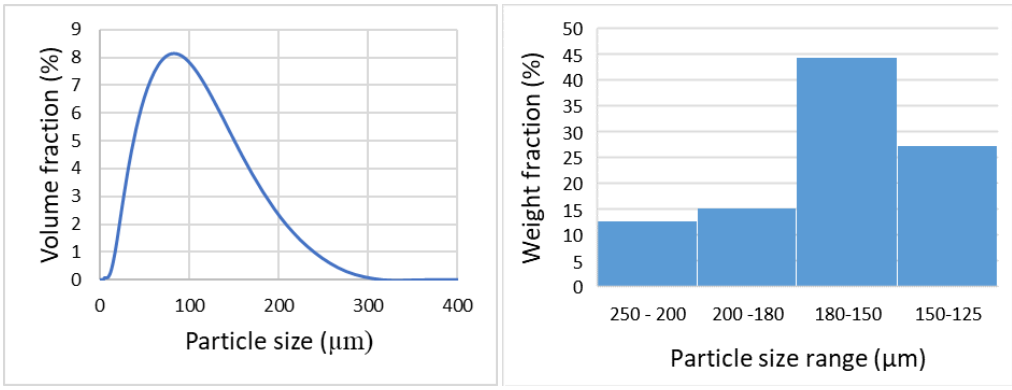

(a) (b)

Figure 9-5: (a) Particle size distribution of calcined oxygen carrier spheres before sieving, and (b) Particle size distribution of material screened used in the reactor after sieving

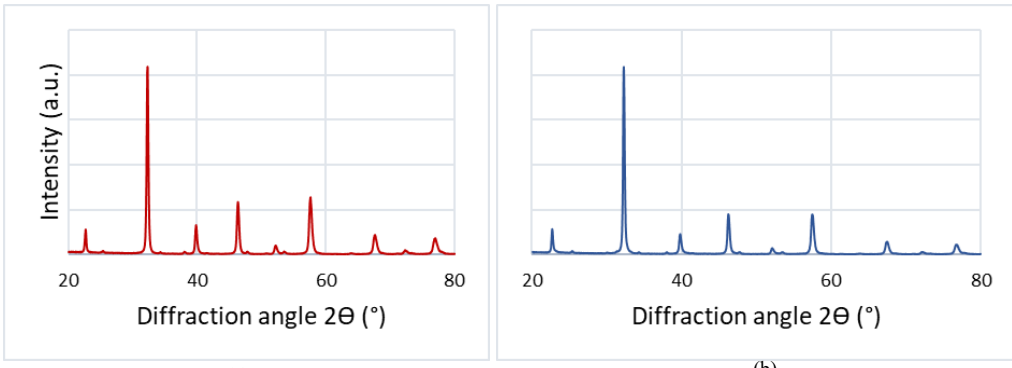

(a) (b)

Figure 9-6: The XRD patterns of the synthesized oxygen carrier ($La_{0.85}Sr_{0.15}Fe_{0.95}Al_{0.05}O_{3-\delta}$). a) fully oxidized state, and b) state at the end the fuel stage (before the air oxidation step). All diffraction peaks correspond to the perovskite phase [57]. *The diffraction peaks in b) are shifted towards lower diffraction angles owing to the slightly lower amount of lattice oxygen.*

9.2.2 Experimental setup

The experimental set up consisted of a fluidized bed reactor, the gas switching reactor, with 5 cm inner diameter and 50 cm height with a freeboard region at the top (expanding from a 5 cm to a 10 cm diameter) to minimize particle entrainment (*Figure **6-4***). The total height of the reactor, including the body and the freeboard, was 90 cm. The reactor vessel was made of Inconel 600 to withstand high temperatures up to 1000 °C. Gas was fed into the reactor using a lance extending towards to bottom of the reactor. Heat was supplied to the reactor through an external electrical heating element wound around the reactor vessel and covered with a 25 cm thick insulation. The process parameters, data acquisition, and logging were controlled through a LabVIEW application. Bronkhorst mass flow controllers were used to measure and control

the gas feed into the reactor. A three-way valve separated the air and fuel feeds during the redox process. The outlet gas stream was cooled down through the heat exchanger before it was sent to ventilation. Gas was sampled after the cooler and sent to a gas analyzer for measuring the gas composition. A syngas analyzer (Model: ETG MCA 100 SYN P) was used to measure the gas composition. The temperature was measured using two thermocouples located 2 cm and 20 cm from the bottom inside the reactor. The pressure was measured at different locations and used for monitoring reactor operation. A back-pressure valve was placed after the cooler and used for maintaining the target set pressure up to 5 bar.

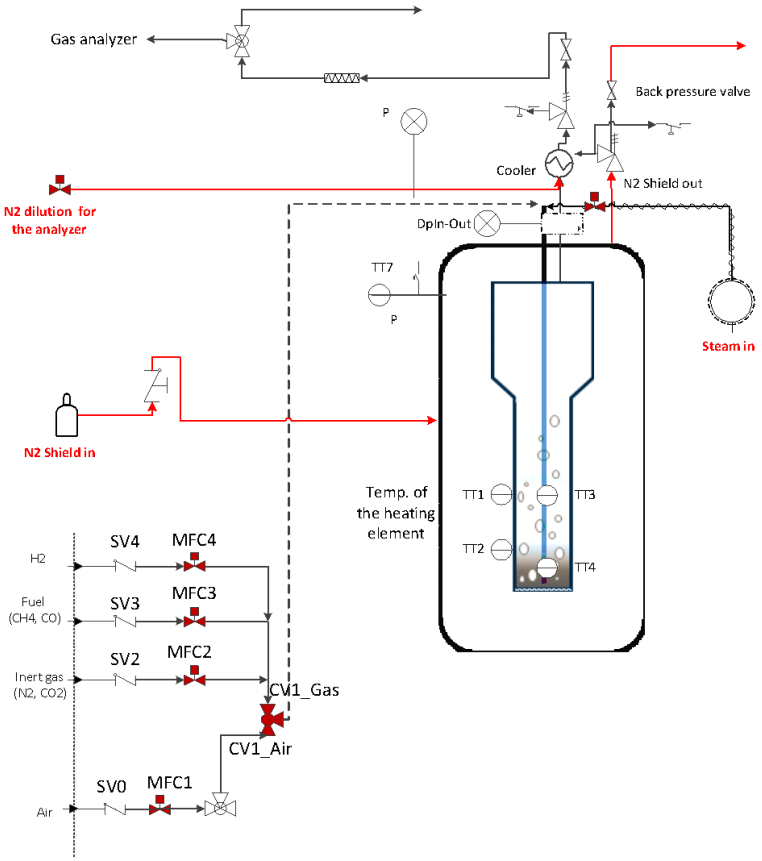

Figure 9-7: Experimental setup. SV04 represents stop valves and MFC1-4 represents mass flow controllers for air, the inert gas (N_2 and CO_2), the fuel (CH_4, CO), and H_2 respectively. TT1 and TT2 represent the temperature transmitter (thermocouple) that measures the temperature of the heating element on the reactor external circumference, while TT3 and TT4 represent temperature transmitters (thermocouple) that measure the bed temperature inside the reactor. P is pressure sensors while TT7 is the temperature transmitter (thermocouple) that measures the temperature inside the reactor shell.

9.2.3 Methodology

9.2.3.1GSPOX operation

Lab-scale experiments were conducted using the La-based oxygen carrier described in section 9.2.1 and the experimental setup shown in (*Figure **6-4***). About 460 g of the oxygen carrier was placed inside the reactor, corresponding to a 0.3 m static bed height. The GSPOX cycle consists of three stages: fuel, steam, and air stage (*Figure **9-3***). The reactor was first heated up to the target temperature at a ramp rate of 5 °C/min, followed by approximately 30 short redox cycles (oxidation and reduction) for 1 h to enhance the activity of the oxygen carrier ("activation"). After activation, the actual GSPOX cycling experiments started with the fuel stage, where CH_4 was fed. The net reaction at this stage is endothermic thus requires heat addition to ensure that gas conversion does not decrease extensively across the stage. It is possible to co-fed CH_4 with CO_2 and/or H_2O to control the syngas quality (i.e. H_2/CO molar ratio) and carbon deposition. The steam stage proceeded the fuel stage to partially re-oxidize the oxygen carrier while producing hydrogen and gasifying any deposited carbon from the fuel stage. Air was fed after the steam stage to ensure complete oxidation of the oxygen carrier and the generation of heat to drive the process. A known amount of inert N_2 gas was fed across the fuel stage to quantify the amount of all the species formed or converted through carbon and hydrogen balances. There was also a purging step included between the redox stages to avoid the direct contact of the fuel and the oxidant. The total gas flowrate ranged between 1 – 50 nl/min in all stages. The gas flowrate was chosen to ensure that the bed was fluidized and maintain the flow ($U/U_{mf} \sim 10$) within the bubbling/turbulent regime to achieve good solid mixing/heat transfer across the bed. The experiments were performed by varying the CH_4 molar ratio from 10 - 60%, temperatures from 750 – 950 °C, and reactor pressures from 1 - 5 bar. The reactor behavior, effect of temperature, pressure, CH_4 molar fraction, flowrate and CO_2/H_2O utilization were evaluated using reactor performance indicators in *section **7.2.3.***

9.2.3.2Reactor performance indicators

Different performance indicators were defined to evaluate the GSPOX process and identify appropriate conditions to achieve the maximum conversion of CH_4 to syngas (H_2 and CO). Note that the amount of other gaseous species was quantified based on a known amount of inert gas (N_2) fed into the reactor and the mole fractions recorded in the gas analyzer (*Equation **9-12***). It is desired to have maximal gas conversion in the fuel stage, and H_2O/CO_2 conversion in the steam/CO_2 stage. The CH_4 conversion and the fuel stage and H_2O conversion are defined in

*Equation **7-19*** and *Equation **7-21*** respectively. It is important to tune the syngas H_2/CO ratio (*Equation **7-18***) to be suitable for the downstream process where the produced syngas could be utilized. Carbon deposition (*Equation **7-22***) may occur in the fuel stage, while the deposited carbon is then released in the form of CO and CO_2 in the steam and air stages, thus negatively affecting the purity of produced H_2 in the steam stage. The amount of deposited carbon was quantified through a carbon balance. During the partial oxidation of methane, many competing reactions can occur; it is, therefore, important to quantify the selectivity to the different species formed. Carbon deposition affects the CO selectivity (*Equation **7-23***), while the H_2O production from the total oxidation of the fuel or the reverse water gas shift (RWGS) reaction affects the H_2 selectivity (*Equation **7-24***). Both carbon deposition and H_2O production affect the overall syngas selectivity (*Equation **7-25***).

$$n_{i,out} = \frac{x_{i,out}}{x_{N_2,out}} * n_{N_2,in} \qquad \textit{Equation 9-12}$$

$$\gamma_{CH_4} = 1 - \frac{n_{CH4,out\_fuel}}{n_{CH_4,in\_fuel}} \qquad \textit{Equation 9-13}$$

$$\gamma_{H_2O} = 1 - \frac{n_{H_2O,out\_steam}}{n_{H_2O,in\_steam}} \qquad \textit{Equation 9-14}$$

$$\frac{H_2}{CO} = \frac{n_{H_2,out\_fuel}}{n_{CO,out\_fuel}} \qquad \textit{Equation 9-15}$$

$$C_{dep} = \frac{n_{C,out\_fuel}}{\gamma_{CH_4} * n_{CH_4,in\_fuel} + \gamma_{CO_2} * n_{CO_2,in\_fuel}} * 100 \qquad \textit{Equation 9-16}$$

$$s_{CO} = \frac{n_{CO,out\_fuel}}{\gamma_{CH_4} * n_{CH_4,in\_fuel} + \gamma_{CO_2} * n_{CO_2,in\_fuel}} \qquad \textit{Equation 9-17}$$

$$s_{CO2} = 100 - s_{CO} - C_{dep} \qquad \textit{Equation 9-18}$$

$$s_{H2} = \begin{cases} \dfrac{n_{H2,out_{fuel}}}{2\left(\gamma_{CH_4} * n_{CH_4,in_{fuel}}\right)} & without\ steam \\ \dfrac{n_{H2,out_{fuel}}}{3\left(\gamma_{CH_4} * n_{CH_4,in_{fuel}}\right)} & with\ steam \end{cases} \qquad \textit{Equation 9-19}$$

$$S_{syngas} = \frac{n_{CO,out\_fuel} + n_{H_2,out\_fuel}}{\left(\begin{matrix} n_{H_2,out_{fuel}} + n_{CO,in_{fuel}} + n_{C,out_{fuel}} + n_{H_2O,out_{fuel}} \\ +s_{CO2} * n_{CH_4,in\_fuel} \end{matrix}\right)} \qquad \textit{Equation 9-20}$$

9.3 Result and Discussion

9.3.1 The GSPOX process behavior

A complete GSPOX cycle performed at atmospheric pressure and temperatures from 750 °C to 950 °C is shown in *Figure **9-8a***. The oxygen carrier reactivity was stable over the entire experimental campaign, with no signs of sintering/agglomeration observed despite being exposed to thermal stress and redox cycles throughout hundreds of GSPOX cycles. The cycle starts with the fuel (reduction) stage where the oxygen carrier was exposed to CH_4 (diluted with 50 % N_2). The overall reaction in the fuel stage is endothermic, unlike the conventional partial oxidation process using gaseous O_2 feed. At the start of the fuel stage for the three temperatures, the CH_4 was oxidized completely to CO_2 and H_2O, followed by a sharp transition towards partial oxidation with mostly syngas being produced. For this particular oxygen carrier composition, ~ 4 % of the redox-active lattice oxygen is selective for the total oxidation of CH_4, whereas ~ 96 % of the redox-active lattice oxygen is selective for the partial oxidation of CH_4 [57]. During the reduction of the oxygen carrier, the perovskite phase transitions to La_2O_3, $La_xSr_{2-x}Fe_yAl_{1-y}O_4$, and metallic Fe in a single step. The high oxygen storage capacity of ~ 9 wt.% is associated with a change in the oxidation state of the iron component from Fe^{3+}/Fe^{4+} to Fe^0. Metallic Fe, i.e. Fe^0, catalyzes the decomposition of CH_4 (*Reaction **9-6***), which was apparent when the ratio H_2/CO measured in the off-gas increased above the theoretical value of 2. This is different from the results reported in previous studies using $La_{0.6}Sr_{0.4}Fe_{0.8}Al_{0.2}O_{3-\delta}$ oxygen carrier with an oxide shell, that acts like a micro-membrane via a thermochemical process [58] and $La_{1-x}Sr_xFeO_{3-\delta}$ via chemical looping [59] with a H_2O ratio ~2 respectively due to the different synthesis method. However, the transient H_2/CO ratio is similar to the first study completed with the same oxygen carrier in a gram-scale setup [56].

At the steam stage, it can be seen that H_2 was produced through the water-splitting reaction (*Reaction* ***9-8***) - partial oxidation of the oxygen carrier with steam. There was also gasification of the deposited carbon with steam (*Reaction* ***9-9***) resulting in a large amount of CO produced in the first third of the steam stage. When all the deposited carbon was fully gasified, pure H_2 production dominated the rest of the stage. In the oxidation stage with air, the rapid oxygen

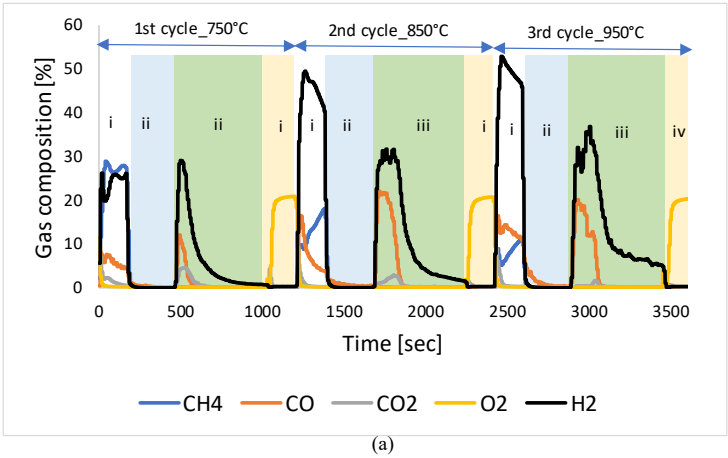

(a)

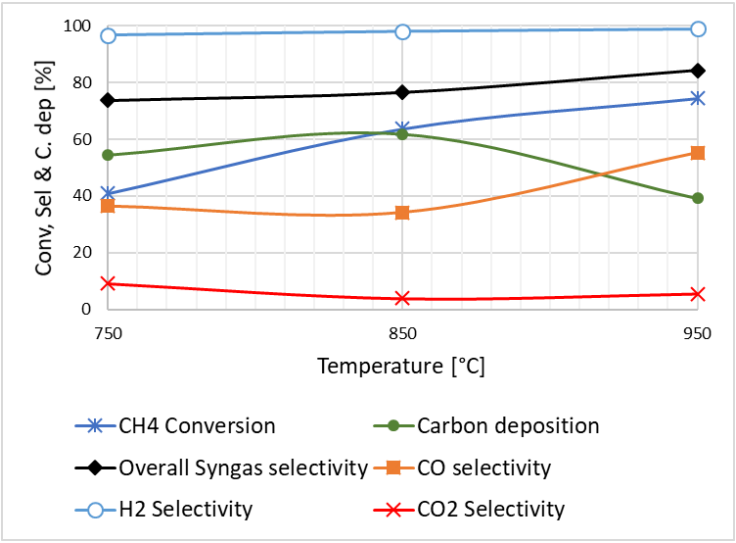

(b)

Figure 9-8: a) Three cycles showing the transient gas composition under Gas Switching Partial Oxidation (GSPOX); b) sensitivity of time-averaged values of key performance indicators in the fuel stage. CH_4 molar fraction of 50 % diluted in N_2, 1 bar, and temperature from 750 to 950 °C. i: fuel stage (Gas input: CH_4 4.1 nl/min, N_2 4.1 nl/min for 2.93 min); ii. N_2 purge (Gas input: N_2 10 nl/min for 5 min); iii: steam stage (Gas input: H_2O 2 nl/min for 10 min); iv: Air stage (Gas input: air 10 nl/min for 3 min).

breakthrough suggests that most of the oxidation has been completed in the steam stage. As mentioned above, ~ 96 % of the redox-active lattice oxygen can be regenerated using mild oxidants such as H_2O or CO_2. It is worth to know that the observed rate of H_2 production was about the double of the gaseous carbon products (CO and CO_2) in the fuel stage, suggesting that both partial oxidation and carbon gasification occurred simultaneously. A small amount of CO_2 was also observed during the steam stage indicating the occurrence of the WGS (*Reaction **9-10***), which decreased with temperature due to its exothermic nature. Finally, at the air stage, the partially reduced oxygen carrier was regenerated completely. The reaction in this stage was highly exothermic generating part of the heat required to drive the endothermic reactions in the fuel stage to achieve autothermal operation.

Comparing the GSPOX behavior for the three operating temperatures tested (*Figure **9-8a)***, it can be seen that the CH_4 conversion almost doubled when the temperature was increased from 750 to 950 °C (*Figure **9-8b)***, indicating an improvement in the reaction kinetics as the temperature increases. The extent of carbon deposition also reduced with the increase in temperature (especially at 950 °C) in favor of an increased CO production, to a large extent contributing to an improved syngas selectivity. The hydrogen selectivity increased when the temperature was increased from 750 °C to 850 °C and remained insensitive when increasing the temperature further to 950 °C. The interpretation of these results come from *Figure **9-8a,*** where it can be seen that CO_2 was present in the entire fuel stage of 750 °C together with syngas, indicating that the WGS occurred in parallel with the partial oxidation throughout the stage.

Despite the improvement in the degree of carbon deposition especially at 950 °C, the syngas H_2/CO ratio remained above the expected value of 2 in the fuel stage (*Figure **9-8a***), and less than 80% H_2 purity was achieved at the steam stage. It is worth mentioning that if syngas production is targeted, carbon deposition will not be an issue for this process as it is completely gasified within the subsequent steam stage, thus sustaining the oxygen carrier reactivity. Surprisingly, the carbon deposition reported in this study when less than 70 % of the active lattice oxygen was consumed during the fuel stage was not observed in the gram-scale study with the same material [57], bringing into question a possible scale effect of the proposed gas switching technology as also reported in another study for H_2 production through water splitting[60]. It should, however, be noted that the gram-scale was performed with only 8 mol% CH_4 molar fraction as against 50 % in the current study. The following section reports the results of a sensitivity study varying several operating parameters to evaluate their influence on key GSPOX process parameters.

9.3.2 Sensitivity study

9.3.2.1 The effect of CH_4 molar fraction

The effect of the CH_4 molar fraction at the fuel stage was investigated under atmospheric conditions and 950 °C (*Figure **9-9***) while keeping the total gas flow rate constant. The time of the fuel stage was increased proportionally with the CH_4 molar fraction such that the total amount of CH_4 fed during the fuel stage was kept constant. From the results shown in *Figure **9-9***, it can be seen that carbon deposition increased with the CH_4 molar fraction. This finding further supports the GSPOX behavior explained in *section **9.3.1***, where it was shown that different active sites determine the dominant reactions/output of the GSPOX process. Although the fuel stage always started with a fully oxidized oxygen carrier, it is likely that the increased CH_4 concentration in the reducing gas increased the rate of carbon deposition by locally reducing the oxygen carrier faster than expected. This increased carbon deposition reduced the CO selectivity, which in turn led to an increase of the H_2:CO ratio to ~ 3.7 when the CH_4 molar

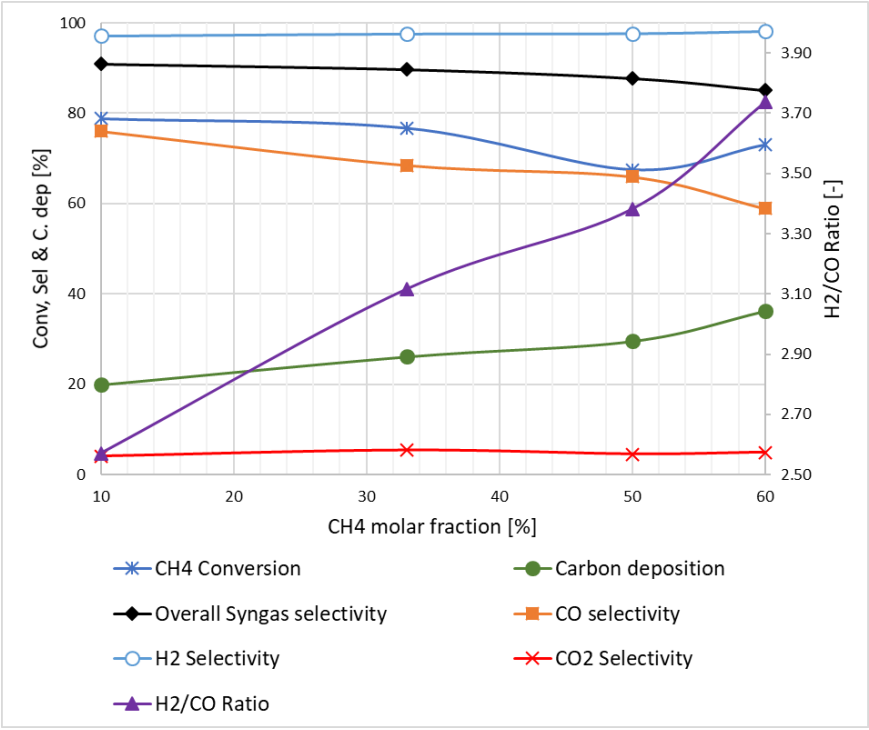

Figure 9-9: Sensitivity of key performance indicators to CH_4 molar fraction at 1 bar operating pressure and 950 °C. i: fuel stage (Gas input range: CH_4 0.6 – 3.72 nl/min, N_2 5.6 – 2.48 nl/min for 20 – 3.2min) ii. N_2 purge (Gas input: N_2 10 nl/min for 5 min); iii: steam stage (Gas input: H_2O 2 nl/min for 10 min; iv: Air stage air 10 nl/min for 3 min).

fraction was 60 %. Consequently, CH_4 conversion was marginally affected by the carbon deposition. By inspecting *Figure **9-8a*** it can be seen that in the fuel stage, the CH_4 conversion decreased with time accompanied by a decrease in CO generation; a sign of increased carbon deposition which blocks the pores and limits the diffusion of gas into the active surface of the metal oxide.

Interestingly, the total amount of CO_2 produced during the fuel stage was insensitive to the CH_4 molar fraction, implying that the oxygen carrier was reduced to the same extent. This also confirms that the reduction of the oxygen carrier in the fuel stage occurred in two principal steps, where the first short step involved complete methane combustion to produce CO_2 and H_2O, while the second step involved the partial oxidation of methane after a certain amount of lattice oxygen had been removed from the oxygen carrier (850 °C and 950 °C in *Figure **9-8a*** illustrate this behavior). From our previous work, the transition from the total to the partial oxidation of CH_4 occurred when ~ 3 – 4 % of the redox-active lattice oxygen was removed from the oxygen carrier [57]. The H_2/CO ratio of the syngas increased with carbon deposition indicating that the mechanism of carbon deposition is mainly methane cracking (*Reaction **9-6***). The absence of CO_2 and H_2O in the second step (partial oxidation) reduced the extent of side reactions, thus making H_2 selectivity insensitive towards CH_4 molar fraction. Despite that, the H_2 selectivity remains unaffected, and the syngas selectivity decreased following the decrease in CO selectivity due to carbon deposition.

9.3.2.2The effect of flowrate

The effect of flowrate was investigated at 50 % CH_4 molar fraction (50 % dilution with N_2), 950 °C, and 1 bar by varying the flowrate from 6.2 nl/min to 10.2 nl/min (*Figure **9-10***). This flow rate range was selected to ensure that the reacting bed was always kept within the bubbling/turbulent fluidization regime. Similar to *section **9.3.2.1***, the total amount of CH_4 fed during the fuel stage was kept the same by proportionally decreasing the stage time with the gas flow rate. The transient gas composition (*Figure **9-10a***) shows that the cycle for the three tested flow rates was almost identical, implying that the reactions involved in the three stages were fast enough to be independent of the gas residence time in the bed. This also suggests that the gas-solid contact was good in the studied range of the gas flow rates and that slippage of the reactant gases through the bed was avoided. Carbon deposition was apparent for the three cases, as can be seen by the released CO and CO_2 in the steam stage (after the fuel stage)

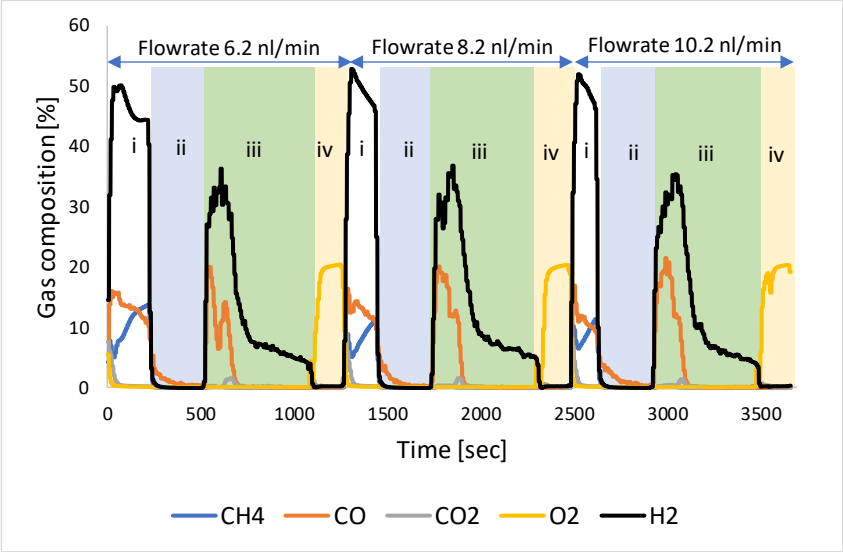

(a)

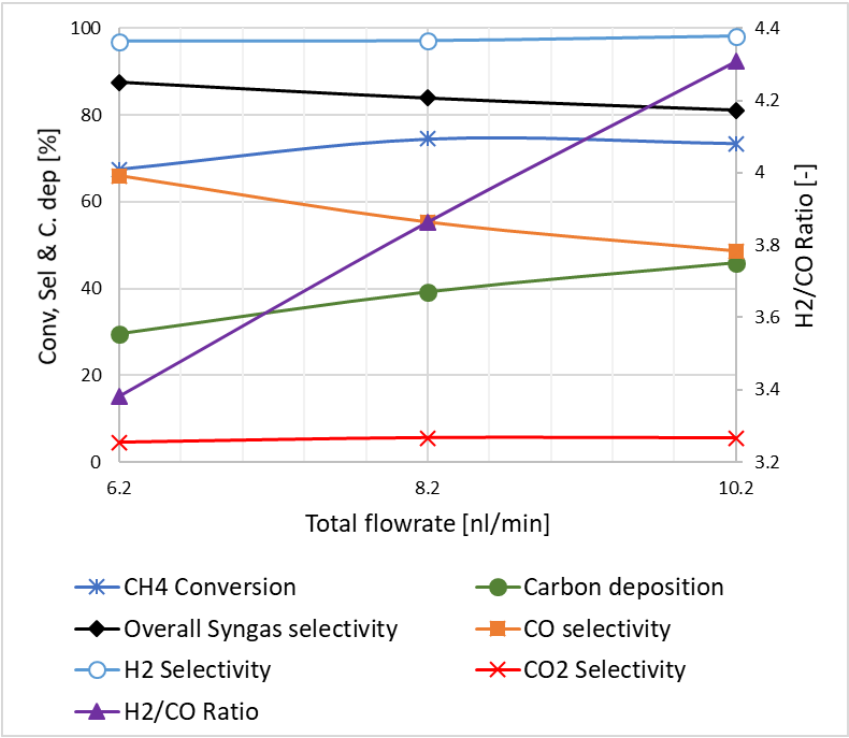

(b)

Figure 9-10: (a) The transient gas composition for different flowrates, and (b) sensitivity of key performance indicators to at 50 % CH_4 molar fraction, 1 bar, and 950 °C. i: fuel stage (Gas input: CH_4 3.1 – 5.1 nl/min, N_2 3.1 – 5.1 nl/min for 3.87 – 2.35 min); ii. N_2 purge (Gas input: N_2 10 nl/min for 5min; iii: steam stage H_2O 2 nl/min for 10 min); iv: Air stage (Gas input: air 10 nl/min for 3 min).

marking the gasification of deposited carbon. H_2 production through the partial oxidation of the oxygen carrier by steam was visible for the three tested cases. It can be clearly seen that the H_2 concentration was around twice that of CO when carbon gasification occurred, while pure hydrogen was produced for the rest of the steam stage after all the carbon had been gasified.

From the time-averaged values shown in *Figure **9-10b***, the CH_4 conversion increased slightly when the flowrate was increased from 6.2 to 8.2 nl/min, but it then remained relatively constant with a further increase. The improvement in CH_4 conversion is a sign of improved mixing/gas-solids contact that counteracted the possible negative effect of reduced residence time. As expected, such improvement in the mixing of the gas and the particles would reduce bed segregation, prevent some of the solids to form a packed bed, ensures that the oxygen carrier is reduced uniformly in the entire bed, and reduces carbon deposition. However, Figure 9-10 contrarily shows that with increasing flowrate the carbon deposition increased. This may be as a result of the increased rate of reduction at higher flowrates which enhances carbon deposition (type 3 active site of Mihai et al. [61]) as described in *section **9.3.1***. Consequently, the CO selectivity increased with decreasing carbon deposition and the absence of RWGS (*Reaction **9-5***). Interestingly, the selectivity to CO_2 remained constant confirming that the oxygen carrier achieved the same level of reduction as described in *section **9.3.2.1***. As also explained in *section **9.3.2.1**,* the H_2 selectivity is also insensitive to the flow rate due to well distinctive behavior of the two sub-steps of the fuel stage.

9.3.2.3The effect of CO_2 and H_2O utilization.

In an attempt to reduce carbon deposition and control the syngas quality, CO_2 and H_2O were co-fed during the fuel stage. Four cases were investigated at atmospheric condition, 50% CH_4 molar fraction and a temperature of 950°C as follows: i) Base case - without CO_2 and H_2O addition (50% N_2 and 50% CH_4 molar fraction at fuel stage), ii) CO_2 case (50% CO_2 and 50% CH_4 molar fractions at fuel stage), iii) H_2O case (50% H_2O and 50% CH_4 at fuel stage), and iv) CO_2 + H_2O case – (25% CO_2 , 25% H_2O and 50% CH_4 at fuel stage). The transient gas composition of the four cases (*Figure **9-11***) shows that the use of CO_2 and H_2O had a positive influence on the extent of carbon deposition, gas feed conversion, and syngas quality.

The CO_2 case shows that carbon deposition was reduced significantly (from 40% to 0) with a resultant improvement in the purity of the H_2 produced in the subsequent steam stage (*Figure **9-11***). A similar approach was applied in chemical looping reforming using a perovskite-based oxygen carrier where a combined effect of POX (*Reaction **9-2***) and DMR (*Reaction **9-3***) was

achieved [1, 62]. The attractiveness of this strategy is the ability to utilize CO_2 to produce valuable products and offset GHG emissions. The H_2O case was considered to achieve a combined effect of POX (*Reaction* ***9-2***) and SMR (*Reaction* ***9-4***). With this arrangement, carbon deposition was significantly reduced achieving a high H_2/CO ratio, which was found to be close to 4 (*Figure* ***9-12****b*) due to the WGS reaction (*Reaction* ***9-10***). The converted steam reacted with the produced CO to form CO_2 (and H_2) through the aforementioned WGS reaction (evidenced by the presence of CO_2 as a product in the fuel stage as shown in *Figure* ***9-11***). It is also possible to synergize CO_2 and H_2O utilization in the fuel stage to achieve a combined effect of POX, DMR, and SMR (*Reaction* ***9-21***) known as tri-methane reforming (TMR). TMR is expected to eliminate the disadvantages of the conventional individual reactions, improve overall process performance, efficiency, prolong catalyst life, and mitigate coking [3, 63]. TMR also provides the flexibility to tune the produced syngas to a desired quality. This approach has been previously demonstrated to produce syngas with H_2/CO ratio between 1-2 suitable for Gas-to-Liquid processes [63].

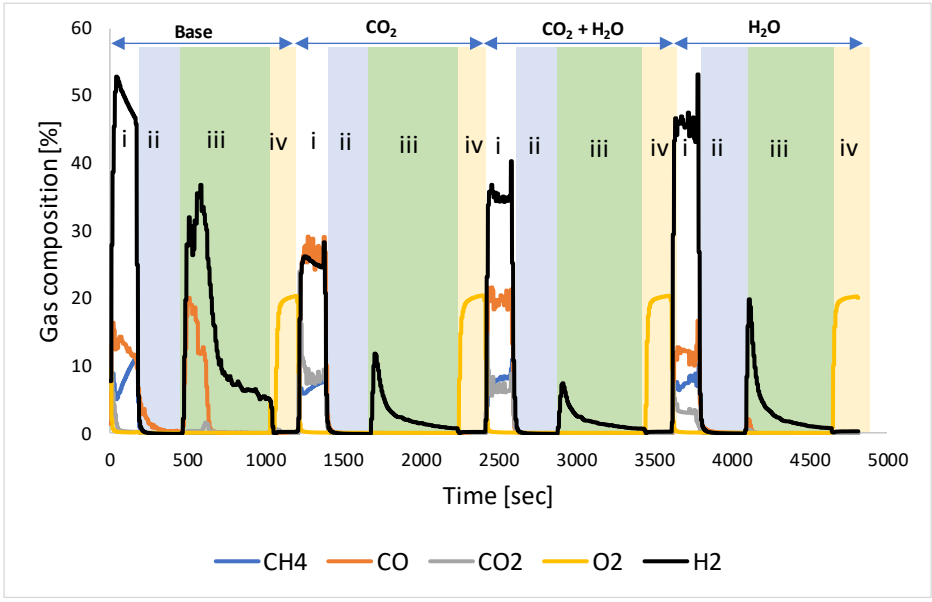

Figure 9-11:The transient gas composition for the base case without H_2O/CO_2 addition and other cases with H_2O/CO_2 addition as indicated in the plot at 50 % CH_4 molar fraction, 950 °C, and 1 bar. i: fuel stage Base case (Gas input: CH_4 4.1nl/min, N_2 4.1 nl/min for 2.93 min), CO_2 case (Gas input: CH_4 4.1 nl/min, CO_2 4.1 nl/min for 2.93 min), CO_2+H_2O case (Gas input: CH_4 4.1nl/min, CO_2 2.05 nl/min, H_2O 2.05 nl/min for 2.93 min), H_2O case (Gas input: CH_4 4.1 nl/min, H_2O 4.1 nl/min for 2.93 min); ii. N_2 purge (Gas input: N_2 10 nl/min for 5 min); iii: steam stage (Gas input: H_2O 2 nl/min for 10 min); iv: Air stage (Gas input: air 10 nl/min for 3 min).

$$20CH_4 + H_2O + MeO + CO_2 \rightarrow 21CO + 41H_2 + Me \qquad \textit{Reaction 9-21}$$

It was observed that the three cases with the addition of an oxidant (H_2O, and/CO_2), syngas production was favored from the start of the fuel step, thus eliminating the initial reduction of the oxygen carrier that produced CO_2 and steam. This has resulted in a slight decrease in the

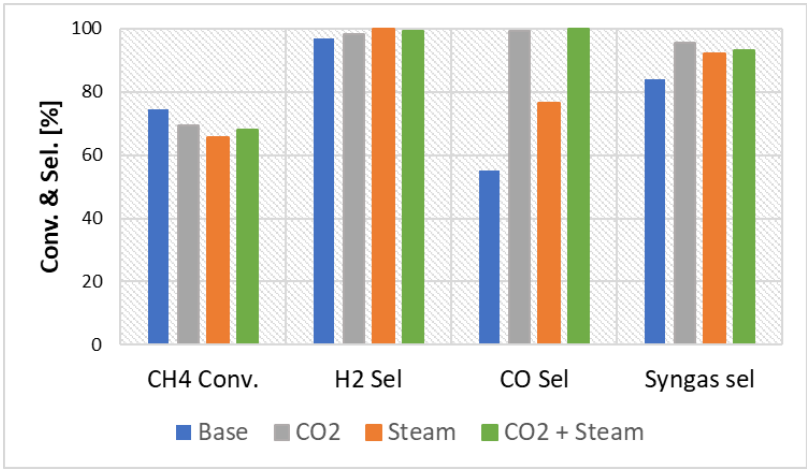

(a)

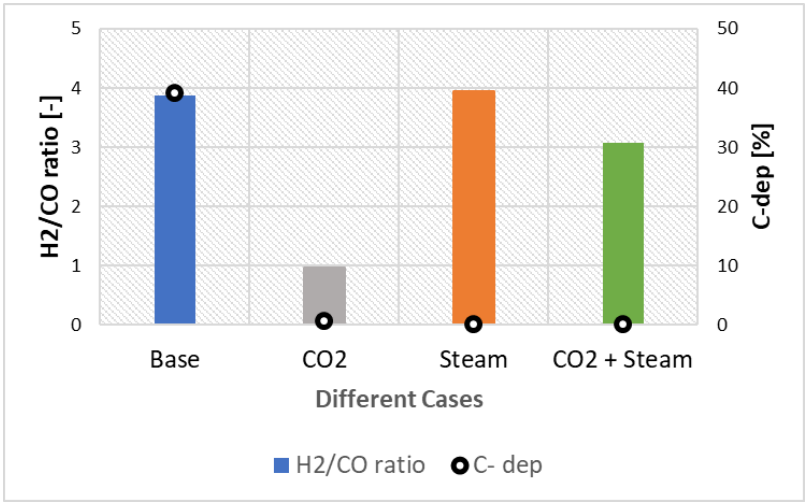

(b)

Figure 9-12:(a)The effect of steam and CO_2 utilization at the fuel stage on fuel conversion and selectivity, and (b) the effect of steam and CO utilization at the fuel stage on syngas quality (H_2/CO ratio) and carbon deposition at 50% CH_4 molar fraction, 950°C and 1 bar. i: fuel stage Base case (Gas input: CH_4 4.1 nl/min, N_2 4.1 nl/min for 2.93 min), CO_2 case (Gas input: CH_4 4.1 nl/min, CO_2 4.1 nl/min for 2.93min), CO_2+H_2O case (Gas input: CH_4 4.1nl/min, CO_2 2.05 nl/min, H_2O 2.05 nl/min for 2.93 min), H_2O case (Gas input: CH_4 4.1 nl/min, H_2O 4.1 nl/min for 2.93min); ii. N_2 purge (Gas input: N_2 10nl/min for 5 min); iii: steam stage (Gas input: H_2O 2 nl/min for 10 min); iv: Air stage (Gas input: air 10 nl/min for 3 min).

overall methane conversion for those three cases as can be seen in *Figure* ***9-12***a. On the other hand, the overall H_2, CO, and syngas selectivities improved compared with the base case (*Figure* ***9-12****a*). The slight improvement in H_2 selectivity resulted from the disappearance of the reduction step (usually happens at the beginning of the fuel stage) which eliminates steam production that affects H_2 selectivity. Instead, methane was reformed to syngas (H_2 + CO) in the presence of the oxidant. Carbon deposition decreased substantially in the presence of the oxidant, thus considerably improving the CO selectivity (*Figure* ***9-12****b*). The improvement in CO selectivity was however lower for the case of pure steam addition, which could be attributed to the occurrence of the WGS reaction in the presence of steam thus maximizing hydrogen production. With these results, the CO_2 and the CO_2 + steam cases could safely be recommended for GTL applications due to the moderate H_2/CO ratio, the elimination of carbon deposition with high syngas selectivity, but interestingly, they can also produce high purity H_2 in the steam stage.

The improvement of *Figure* ***9-12*** in the fuel stage when co-feeding an oxidant with methane could be attributed to two mechanisms: i) simultaneous redox reactions occur in the presence of the oxidant leading to the immediate restoration of the lattice oxygen in the reduced perovskite, [45, 64], ii) oxidant addition could also ensure simultaneous gasification of the deposited carbon to CO thus eliminating its negative effect on syngas quality (H_2/CO ratio). An additional experiment was performed by co-feeding CO_2 and CH_4 (50% molar fractions each) for more than 12 h (*Figure* ***9-13***), which demonstrated that syngas production could be sustained continuously with only a very small drop (< 5 %) in the conversion of CH_4. This indicates that the oxygen carrier performed similarly to a catalyst in the dry reforming reaction. At the start of the fuel stage, CH_4 conversion was slightly higher than CO_2 conversion but gradually decreased and stabilized at the same value as CO_2 conversion for the rest of the stage (CO_2 conversion remained constant in the entire duration of the fuel stage).

From an XRD measurement (*Figure* ***9-6b***) of the oxygen carrier sample collected immediately after the fuel stage (before the re-oxidation step), it is evident that the oxygen carrier was not reduced significantly when CH_4 and CO_2 were co-fed. The small shift in peak position towards lower diffraction angles indicates that only a small amount of lattice oxygen was removed (~ 0.4 wt%), most likely at the beginning of the experiment shown in ***Figure 9-13***. It was observed

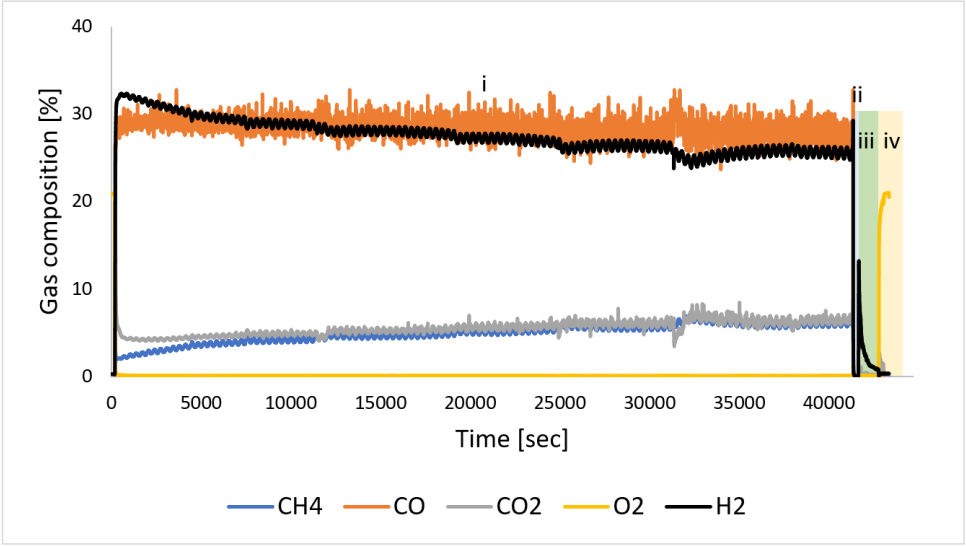

Figure 9-13: Transient gas composition of GSPOX after 12 h at CH_4 CH_4 molar fraction of 50% in the fuel stage (CO_2:CH_4 ratio= 1:1) at 1 bar, and 950 °C. i: fuel stage (Gas input: CH_4 4.1 nl/min, CO_2 4.1 nl/min for 12 h); ii. N_2 purge (Gas input: N_2 10 nl/min for 5 min); iii: steam stage- (Gas input: H_2O 2 nl/min for 10 min); iv: Air stage (Gas input: air 10 nl/min for 3 min).

that a ratio of $CH_4/CO_2 > 3$ was required to reduce the oxygen carrier further and utilize its complete oxygen storage capacity of ~ 9 wt%. Below that ratio, the oxygen carrier maintained its high oxidation state without undergoing a bulk phase transition; however, full recovery of its lattice oxygen required a stronger oxidant, i.e. air (*Reaction* ***9-11***). Therefore, the observations made do not suggest the catalytic activation of CH_4, since the perovskite itself is not catalytically active. The trend seen in *Figure* ***9-13*** was rather the result of the simultaneous reduction/oxidation of the oxygen carrier utilizing only a small amount of its lattice oxygen.

At the beginning of the fuel stage, the H_2 generation was higher but gradually decreased and remained constant following the same trend as CH_4 conversion. Altogether *Figure* ***9-13*** suggests that syngas production was likely following the aforementioned mechanism (i) exposing the oxygen carrier to simultaneous reduction through partial oxidation by CH_4 and oxidation by CO_2. Though the reduction rate exceeded the rate of oxidation at the beginning of the stage, with a gradual decreasing difference, resulting in an overall reduction of the oxygen carrier (9%wt oxygen-carrying capacity) that led to hydrogen production when steam was fed in the subsequent stage oxidizing back the oxygen carrier. This suggests that when co-feeding an oxidant with CH_4 into this oxygen carrier, simultaneous redox reactions (oxidation and reduction) can take place at equal rates, when the oxygen carrier is reduced to 35 %, resulting

as observed in *Figure* ***9-13***. Further research is needed for drawing firm conclusions about the mechanisms by which syngas is produced when co-feeding an oxidant with CH_4 to the oxygen carrier.

9.3.3 The effect of pressure

Pressurized operation is necessary to reduce downstream compression work, improve process efficiency, and explore the feasibility of integration with other downstream processes. For these reasons, a further investigation of GSPOX at pressures from 1 – 5 bar was performed at 50% CH_4 molar fraction, the addition of CO_2 (CO_2/CH_4 ratio of 1), and an operating temperature of 950°C. The gas feed was increased proportionally to the pressure to maintain a constant superficial gas velocity of about 0.1 m/s in the reactor. The achieved performance is summarized in *Figure* ***9-14***. It can be seen that increasing the pressure led to a decrease in CH_4 and CO_2 conversions, similar to a previous study [65]. Since the reactions are heterogeneous (gas/solid reaction) and mainly endothermic, it is possible that the pressure would have negative

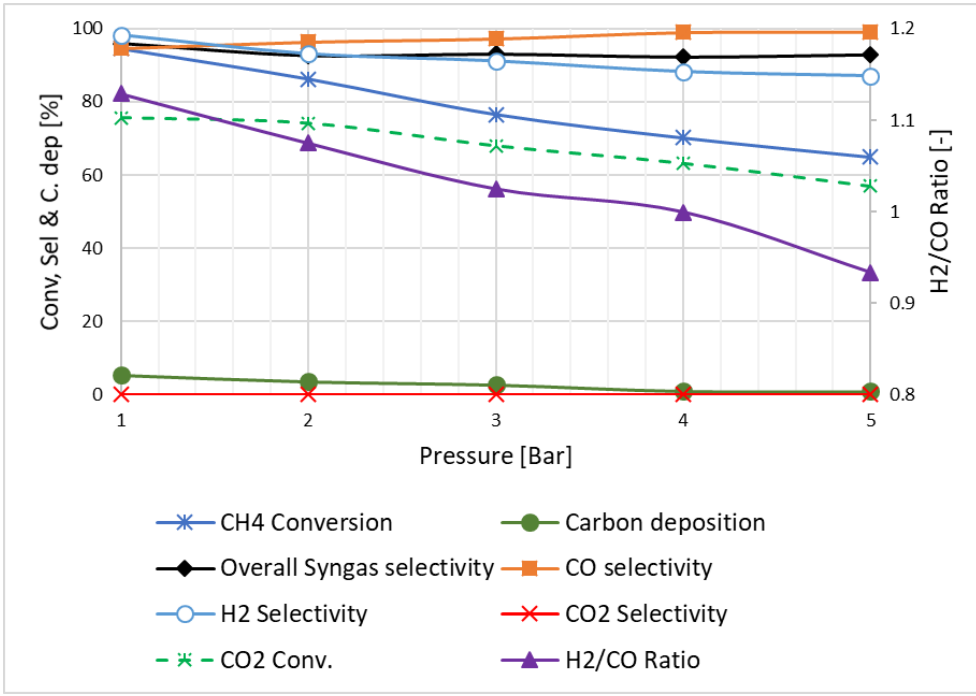

Figure 9-14: The variation of gas composition with pressure at 50% CH_4 molar fraction and 950°C. i: fuel stage (Gas input: CH_4 2.1 – 10.5 nl/min, CO_2 2.1 – 10.5 nl/min for 11.74 – 2.35 min); ii. N_2 purge (Gas input: N_2 10 – 50 nl/min for 10 – 2 min); iii: steam stage (Gas input: H_2O 2 – 10 nl/min for 20 – 4 min); iv: Air stage (Gas input: air 10 – 50nl/min for 10 – 2 min).

effects both on the equilibrium and the reaction kinetics. The overall CO_2 conversion was lower than the CH_4 conversion, confirming that the partial oxidation of CH_4 occurs at a faster rate than the oxidation of the metal oxide by CO_2 at the beginning of the fuel stage as shown earlier in *Figure **9-13***. However, the difference between the two reactions was found to decrease with the pressure, indicating that CH_4 conversion is affected more negatively by pressure than CO_2 conversion. This could be attributed to the fact that CH_4 is involved in more reaction pathways (*Reaction **9-2***, *Reaction **9-3***, *Reaction **9-4*** & *Reaction **9-6***) while CO_2 is involved in fewer reactions (*Reaction **9-3*** & *Reaction **9-5***). The decrease in H_2 selectivity indicates that pressure improves the kinetics of RWGS (*Reaction **9-5***) where CO_2 reacts with the H_2 to form H_2O and CO indicating that kinetics was playing more role than thermodynamics. This makes the syngas H_2/CO ratio to decrease with pressure (even below 1 at pressures higher than 4 bar). Overall, further work is needed to optimize this oxygen carrier to minimize the negative effect of pressure on its performance before the scale-up of the GSPOX process.

9.4 Conclusion

The coupling of CH_4 partial oxidation and water splitting for syngas and hydrogen production as an efficient pathway for natural gas decarbonization was investigated in this work using a lanthanum strontium ferrite oxygen carrier. Unlike previous studies on related topics, the experiments were completed in a novel chemical looping reactor concept known as gas switching technology (GST) that uses a single fluidized bed reactor cycling multiple stages of the process (fuel, steam, and air stages). The results showed that the oxygen carrier exhibits high selectivity to syngas production at the fuel stage but with substantial carbon deposition when pure methane was fed, resulting in syngas production with very high H_2/CO in the fuel stage and very low purity H_2 production in the consecutive steam stage. If only syngas is targeted, carbon deposition will not be problematic as the deposited carbon could totally be gasified in the steam stage producing valuable syngas and also ensuring complete regeneration of the oxygen carrier thus prolonging its lifetime with sustained chemical reactivity.

Co-feeding an oxidant, such as CO_2, H_2O, or both, together with CH_4 at the fuel stage resulted in a significant decrease in carbon deposition and an H_2/CO ratio of $\sim$ 1 - 4 (the CO_2 case was the lowest H_2/CO while the H_2O case resulted in the highest value driven by the WGS reaction due to the presence of the unreacted H_2O). For all cases of H_2O and CO_2 (or combination) utilization at the fuel stage, an improved H_2 purity at the steam stage was achieved following

the reduction in carbon deposition with less CO contamination through the gasification of the deposited carbon with H_2O.

An important observation of continuous syngas production with ($H_2/CO \approx 1$) by co-feeding CO_2 and CH_4 at the fuel stage for over 12 h indicated that the oxygen carrier was exposed to simultaneous redox reactions through CH_4 partial oxidation with the lattice oxygen which is restored instantly by the fed CO_2. This process occurs at a higher rate for the CH_4 partial oxidation but reduces gradually to equalize the reversed oxidation reaction by CO_2 resulting in a behavior similar to methane reforming that occurs continuously as long as heat is supplied.

Operating at high pressures was found to have negative effects on both CH_4 and CO_2 conversions. This could be due to a combined equilibrium and kinetic limitations of the involved endothermic heterogeneous reactions. CO_2 conversion was less sensitive to the pressure than CH_4 conversion since CH_4 is involved in more dominating reaction pathways than CO_2. Pressure improves the kinetics of the RWGS reaction contrarily to equilibrium prediction, thus affecting the H_2 selectivity and the syngas H_2/CO ratio negatively. This calls for further research to explore approaches to minimize the negative impact of the pressure on the GSPOX performance before scale-up.

Acknowledgment

ACT GaSTech project. Project No 271511.

This project has received funding from The Research Council of Norway, Swiss Office of Energy, and is cofounded by the European Commission under the Horizon 2020 programme, ACT Grant Agreement No 691712. VATL Lab technicians at the Norwegian University of Science and Technology are equally acknowledged for constructing and maintaining the experimental setup.

Nomenclature

Abbreviations

ASU	Air Separation Unit
ATR	Autothermal reforming
CAPEX	Capital Expenditure
CCUS	Carbon Capture Utilization and Storage
CFB	Circulating Fluidized Bed
CLPOX	Chemical Looping Partial oxidation
CLR	Chemical Looping Reforming
CMR	Combined Methane Reforming
DMR	Dry Methane Reforming
GSPOX	Gas Switching Partial Oxidation
GSR	Gas Switching Reforming
GST	Gas Switching Technology
GTL	Gas-To-Liquid
Me (MeO)	Metal (Metal oxide)
OC	Oxygen Carrier
POX	Partial Oxidation
RWGS	Reverse Water Gas Shift
SMR	Steam methane reforming
TMR	Tri-reforming
U	Fluidization velocity
U_{mf}	Minimum fluidization velocity
WGS	Water Gas Shift
XRD	X-ray diffraction

Symbols

C_{dep}	Carbon deposition
D_{10}	Diameter of the catalyst which 10% of a sample mass is smaller than
D_{50}	Diameter of the catalyst which 50% of a sample mass is smaller than
D_{90}	Diameter of the catalyst which 90% of a sample mass is smaller than
n_{C,out_ref}	Mole of C at the gas outlet during reforming stage
n_{CH_4,in_fuel}	Mole of CH_4 fed in the fuel stage
n_{CH4,out_fuel}	Mole of CH_4 at the gas outlet in the fuel stage
n_{CO,out_oxi}	Mole of CO at the gas outlet in the oxidation stage
n_{CO_2,out_oxi}	Mole of CO_2 at the gas outlet in the oxidation stage
n_{CO,out_fuel}	Mole of CO at the gas outlet in the fuel stage
n_{CO_2,in_fuel}	Mole of CO_2 fed in the fuel stage
n_{CO_2,out_fuel}	Mole of CO_2 at the gas outlet in the fuel stage
n_{H_2,out_fuel}	Mole of H_2 at the gas outlet in the fuel stage
n_{H_2O,out_fuel}	Mole of H_2O at the gas outlet in the fuel stage
$n_{i,out}$	Mole of any gas species at the gas outlet
$n_{N_2,in}$	A known mole of N_2 gas fed in the fuel stage
s_{CO}	CO selectivity
s_{CO_2}	CO_2 selectivity
s_{H2}	H_2 selectivity
S_{syngas}	Overall syngas selectivity
$x_{i,out}$	Mole fraction of any gas species as recorded in the gas analyzer
$x_{N_2,out}$	Mole fraction of N_2 gas as recorded in the gas analyzer
γ_{CH_4}	CH_4 conversion
γ_{CO_2}	CO_2 conversion
γ_{syngas}	Syngas yield

References

[1] K. Zhao, J. Chen, H. Li, A. Zheng, and F. He, "Effects of Co-substitution on the reactivity of double perovskite oxides LaSrFe2-xCoxO6 for the chemical-looping steam methane reforming," *Journal of the Energy Institute,* vol. 92, no. 3, pp. 594-603, 2019.

[2] Y. Bai *et al.*, "Catalytic performance of perovskite-like oxide doped cerium (La2− xCexCoO4±y) as catalysts for dry reforming of methane," *Chinese Journal of Chemical Engineering,* vol. 27, no. 2, pp. 379-385, 2019.

[3] S. Arora and R. Prasad, "An overview on dry reforming of methane: strategies to reduce carbonaceous deactivation of catalysts," *RSC advances,* vol. 6, no. 110, pp. 108668-108688, 2016.

[4] V. Papavassiliou *et al.*, "Catalytic Partial Oxidation Pilot Plant Study," *Industrial & engineering chemistry research,* vol. 49, no. 1, pp. 94-103, 2010.

[5] A. M. Silva *et al.*, "Partial oxidation and water–gas shift reaction in an integrated system for hydrogen production from ethanol," *Applied Catalysis A: General,* vol. 334, no. 1-2, pp. 179-186, 2008.

[6] G. P. Berrocal, A. L. Da Silva, J. M. Assaf, A. Albornoz, and M. do Carmo Rangel, "Novel supports for nickel-based catalysts for the partial oxidation of methane," *Catalysis Today,* vol. 149, no. 3-4, pp. 240-247, 2010.

[7] M. Rydén, A. Lyngfelt, and T. Mattisson, "Synthesis gas generation by chemical-looping reforming in a continuously operating laboratory reactor," *Fuel,* vol. 85, no. 12-13, pp. 1631-1641, 2006.

[8] F. He, Y. Wei, H. Li, and H. Wang, "Synthesis gas generation by chemical-looping reforming using Ce-based oxygen carriers modified with Fe, Cu, and Mn oxides," *Energy & Fuels,* vol. 23, no. 4, pp. 2095-2102, 2009.

[9] F. Luis, M. Ortiz, J. Adánez, F. García-Labiano, A. Abad, and P. Gayán, "Synthesis gas generation by chemical-looping reforming in a batch fluidized bed reactor using Ni-based oxygen carriers," *Chemical Engineering Journal,* vol. 144, no. 2, pp. 289-298, 2008.

[10] M. Tang, L. Xu, and M. Fan, "Progress in oxygen carrier development of methane-based chemical-looping reforming: A review," *Applied Energy,* vol. 151, pp. 143-156, 2015.

[11] D. Ma, D. Mei, X. Li, M. Gong, and Y. Chen, "Partial Oxidation of Methane to Syngas over Monolithic Ni/γ-Al2O3 Catalyst——Effects of Rare Earths and Other Basic Promoters," *Journal of Rare Earths,* vol. 24, no. 4, pp. 451-455, 2006.

[12] A. Beretta, G. Groppi, and E. Tronconi, "Monolithic catalysts for gas-phase synthesis of chemicals," 2006.

[13] M. Fathi, E. Bjorgum, T. Viig, and O. Rokstad, "Partial oxidation of methane to synthesis gas:: Elimination of gas phase oxygen," *Catalysis Today,* vol. 63, no. 2-4, pp. 489-497, 2000.

[14] R.-J. Li, C.-C. Yu, W.-J. Ji, and S.-K. Shen, "Methane oxidation to synthesis gas using lattice oxygen in La1− xSrxFeO3 perovskite oxides instead of molecular oxygen," in *Studies in surface science and catalysis*, vol. 147: Elsevier, 2004, pp. 199-204.

[15] T. H. Nguyen, A. Łamacz, A. Krztoń, B. Liszka, and G. Djéga-Mariadassou, "Partial oxidation of methane over Ni0/La2O3 bifunctional catalyst III. Steady state activity of methane total oxidation, dry reforming, steam reforming and partial oxidation. Sequences of elementary steps," *Applied Catalysis B: Environmental,* vol. 182, pp. 385-391, 2016.

[16] D. Kang, M. Lee, H. S. Lim, and J. W. Lee, "Chemical looping partial oxidation of methane with CO2 utilization on the ceria-enhanced mesoporous Fe2O3 oxygen carrier," *Fuel,* vol. 215, pp. 787-798, 2018.

[17] A. Lyngfelt, A. Brink, Ø. Langørgen, T. Mattisson, M. Rydén, and C. Linderholm, "11,000 h of chemical-looping combustion operation—Where are we and where do we want to go?," *International Journal of Greenhouse Gas Control,* vol. 88, pp. 38-56, 2019.

[18] R. W. Breault, *Handbook of chemical looping technology*. John Wiley & Sons, 2018.

[19] N. M. F. Science. "Chemical Looping Combustion." https://mfix.netl.doe.gov/research/chemical-looping-combustion/ (accessed June, 2019).

[20] A. Zaabout, S. Cloete, S. T. Johansen, M. van Sint Annaland, F. Gallucci, and S. Amini, "Experimental Demonstration of a Novel Gas Switching Combustion Reactor for Power Production with Integrated CO2 Capture," *Industrial & Engineering Chemistry Research,* vol. 52, no. 39, pp. 14241-14250, 2013/10/02 2013, doi: 10.1021/ie401810n.

[21] X. Zhu, F. Donat, Q. Imtiaz, C. R. Müller, and F. Li, "Chemical Looping Beyond Combustion–A Perspective," *Energy & Environmental Science,* 2020.

[22] P. Moldenhauer, M. Rydén, T. Mattisson, and A. Lyngfelt, "Chemical-looping combustion and chemical-looping reforming of kerosene in a circulating fluidized-bed 300 W laboratory reactor," *International Journal of Greenhouse Gas Control,* vol. 9, pp. 1-9, 2012.

[23] R. Larsén, "Construction and initial testing of a lab-scale Chemical Looping system," 2014.

[24] T. Pröll, P. Kolbitsch, J. Bolhàr-Nordenkampf, and H. Hofbauer, "A novel dual circulating fluidized bed system for chemical looping processes," *AIChE journal,* vol. 55, no. 12, pp. 3255-3266, 2009.

[25] S. Penthor *et al.*, "The EU-FP7 project SUCCESS–Scale-up of oxygen carrier for chemical looping combustion using environmentally sustainable materials," *Energy Procedia,* vol. 114, pp. 395-406, 2017.

[26] Ø. Langørgen, I. Saanum, and N. E. L. Haugen, "Chemical looping combustion of methane using a copper-based oxygen carrier in a 150 kW reactor system," *Energy Procedia,* vol. 114, pp. 352-360, 2017.

[27] P. Kolbitsch, J. Bolhar-Nordenkampf, T. Pröll, and H. Hofbauer, "Comparison of two Ni-based oxygen carriers for chemical looping combustion of natural gas in 140 kW continuous looping operation," *Industrial & engineering chemistry research,* vol. 48, no. 11, pp. 5542-5547, 2009.

[28] K. Whitty, J. Lighty, and A. Fry, "Development and Scale-Up of Copper-Based Chemical Looping with Oxygen Uncoupling," in *4th International Conference on Chemical Looping*, 2016.

[29] J. Weber, "Single and Double Loop Reacting Systems," *Handbook of Chemical Looping Technology,* pp. 41-60, 2018.

[30] J. Ströhle, M. Orth, and B. Epple, "Design and operation of a 1 MWth chemical looping plant," *Applied Energy,* vol. 113, pp. 1490-1495, 2014.

[31] T. B. Vilches, F. Lind, M. Rydén, and H. Thunman, "Experience of more than 1000 h of operation with oxygen carriers and solid biomass at large scale," *Applied Energy,* vol. 190, pp. 1174-1183, 2017.

[32] P. Ohlemüller, J. Ströhle, and B. Epple, "Chemical looping combustion of hard coal and torrefied biomass in a 1 MWth pilot plant," *International Journal of Greenhouse Gas Control,* vol. 65, pp. 149-159, 2017.

[33] P. Kolbitsch, J. Bolhàr-Nordenkampf, T. Pröll, and H. Hofbauer, "Operating experience with chemical looping combustion in a 120 kW dual circulating fluidized bed (DCFB) unit," *International Journal of Greenhouse Gas Control,* vol. 4, no. 2, pp. 180-185, 2010.

[34] L. Chen *et al.*, "Experimental evaluations of solid-fueled pressurized chemical looping combustion–The effects of pressure, solid fuel and iron-based oxygen carriers," *Applied energy,* vol. 195, pp. 1012-1022, 2017.

[35] R. Xiao, Q. Song, S. Zhang, W. Zheng, and Y. Yang, "Pressurized chemical-looping combustion of Chinese bituminous coal: cyclic performance and characterization of iron ore-based oxygen carrier," *Energy & fuels,* vol. 24, no. 2, pp. 1449-1463, 2010.

[36] R. Xiao, L. Chen, C. Saha, S. Zhang, and S. Bhattacharya, "Pressurized chemical-looping combustion of coal using an iron ore as oxygen carrier in a pilot-scale unit," *International Journal of Greenhouse Gas Control,* vol. 10, pp. 363-373, 2012.

[37] Z. Fan, L. Chen, F. Liu, J. Bao, H. Nikolic, and K. Liu, "Coal based pressurized chemical looping combustion combined cycle process development and analysis," in *Proceedings of the 4th International Conference on Chemical Looping*, 2016.

[38] A. Zaabout, P. I. Dahl, A. Ugwu, J. R. Tolchard, S. Cloete, and S. J. I. J. o. G. G. C. Amini, "Gas Switching Reforming (GSR) for syngas production with integrated CO2 capture using iron-based oxygen carriers," vol. 81, pp. 170-180, 2019.

[39] A. Zaabout *et al.*, "Experimental demonstration of a novel gas switching combustion reactor for power production with integrated CO2 capture," vol. 52, no. 39, pp. 14241-14250, 2013.

[40] S. A. Wassie, F. Gallucci, A. Zaabout, S. Cloete, S. Amini, and M. J. I. J. o. H. E. van Sint Annaland, "Hydrogen production with integrated CO2 capture in a novel gas switching reforming reactor: Proof-of-concept," vol. 42, no. 21, pp. 14367-14379, 2017.

[41] A. Ugwu, A. Zaabout, J. R. Tolchard, P. I. Dahl, and S. Amini, "Gas Switching reforming for syngas production with iron-based oxygen carrier-the performance under pressurized conditions," *International Journal of Hydrogen Energy,* vol. 45, no. 2, pp. 1267-1282, 2020.

[42] D. Chen *et al.*, "Investigation of the role of surface lattice oxygen and bulk lattice oxygen migration of cerium-based oxygen carriers: XPS and designed H2-TPR characterization," *Applied Catalysis B: Environmental,* vol. 218, pp. 249-259, 2017.

[43] D. D. Taylor, N. J. Schreiber, B. D. Levitas, W. Xu, P. S. Whitfield, and E. E. Rodriguez, "Oxygen Storage Properties of La1–x Sr x FeO3− δ for Chemical-Looping Reactions · An In Situ Neutron and Synchrotron X-ray Study," *Chemistry of Materials,* vol. 28, no. 11, pp. 3951-3960, 2016.

[44] I. S. Metcalfe *et al.*, "Overcoming chemical equilibrium limitations using a thermodynamically reversible chemical reactor," *Nature chemistry,* vol. 11, no. 7, pp. 638-643, 2019.

[45] E. Marek, W. Hu, M. Gaultois, C. P. Grey, and S. A. Scott, "The use of strontium ferrite in chemical looping systems," *Applied Energy,* vol. 223, pp. 369-382, 2018.

[46] X. Shen *et al.*, "The coupling of CH4 partial oxidation and CO2 splitting for syngas production via double perovskite-type oxides LaFexCo1− xO3," *Fuel,* vol. 268, p. 117381, 2020.

[47] K. Zhao *et al.*, "Exploration of the mechanism of chemical looping steam methane reforming using double perovskite-type oxides La1. 6Sr0. 4FeCoO6," *Applied Catalysis B: Environmental,* vol. 219, pp. 672-682, 2017.

[48] H. Ding *et al.*, "A novel composite perovskite-based material for chemical-looping steam methane reforming to hydrogen and syngas," *Energy Conversion and Management,* vol. 171, pp. 12-19, 2018.

[49] X. Zhu, K. Li, L. Neal, and F. Li, "Perovskites as geo-inspired oxygen storage materials for chemical looping and three-way catalysis: a perspective," *ACS Catalysis,* vol. 8, no. 9, pp. 8213-8236, 2018.

[50] L. Zeng, Z. Cheng, J. A. Fan, L.-S. Fan, and J. Gong, "Metal oxide redox chemistry for chemical looping processes," *Nature Reviews Chemistry,* vol. 2, no. 11, pp. 349-364, 2018.

[51] H. Ebrahimi and M. Rahmani, "Modeling chemical looping syngas production in a microreactor using perovskite oxygen carriers," *International Journal of Hydrogen Energy,* vol. 43, no. 10, pp. 5231-5248, 2018.

[52] Y. Zheng *et al.*, "Designed oxygen carriers from macroporous LaFeO3 supported CeO2 for chemical-looping reforming of methane," *Applied Catalysis B: Environmental,* vol. 202, pp. 51-63, 2017.

[53] F. He and F. Li, "Perovskite promoted iron oxide for hybrid water-splitting and syngas generation with exceptional conversion," *Energy & Environmental Science,* vol. 8, no. 2, pp. 535-539, 2015.

[54] J. Zhang, V. Haribal, and F. Li, "Perovskite nanocomposites as effective CO2-splitting agents in a cyclic redox scheme," *Science advances,* vol. 3, no. 8, p. e1701184, 2017.

[55] S. Bhavsar, M. Najera, R. Solunke, and G. Veser, "Chemical looping: To combustion and beyond," *Catalysis Today,* vol. 228, pp. 96-105, 2014.

[56] F. Donat, Y. Xu, and C. R. Müller, "Combined Partial Oxidation of Methane to Synthesis Gas and Production of Hydrogen or Carbon Monoxide in a Fluidized Bed using Lattice Oxygen," *Energy Technology,* 2019.

[57] F. Donat and C. R. Müller, "CO2-free conversion of CH4 to syngas using chemical looping," *Applied Catalysis B: Environmental,* p. 119328, 2020.

[58] C. Huang *et al.*, "In situ encapsulation of iron (0) for solar thermochemical syngas production over iron-based perovskite material," *Communications Chemistry,* vol. 1, no. 1, pp. 1-10, 2018.

[59] A. Evdou, V. Zaspalis, and L. Nalbandian, "La1− xSrxFeO3− δ perovskites as redox materials for application in a membrane reactor for simultaneous production of pure hydrogen and synthesis gas," *Fuel,* vol. 89, no. 6, pp. 1265-1273, 2010.

[60] A. Ugwu *et al.*, "Hydrogen production by water splitting using gas switching technology," *Powder Technology,* 2020.

[61] O. Mihai, D. Chen, and A. Holmen, "Chemical looping methane partial oxidation: the effect of the crystal size and O content of LaFeO3," *Journal of catalysis,* vol. 293, pp. 175-185, 2012.

[62] K. Zhao *et al.*, "Synergistic improvements in stability and performance of the double perovskite-type oxides La2− xSrxFeCoO6 for chemical looping steam methane reforming," *Applied energy,* vol. 197, pp. 393-404, 2017.

[63] C. Song and W. Pan, "Tri-reforming of methane: a novel concept for synthesis of industrially useful synthesis gas with desired H2/CO ratios using CO2 in flue gas of power plants without CO2 separation," *Prepr. Pap.-Am. Chem. Soc., Div. Fuel Chem,* vol. 49, no. 1, p. 128, 2004.

[64] Y. Zhu *et al.*, "Microstructure and reactivity evolution of LaFeAl oxygen carrier for syngas production via chemical looping CH4CO2 reforming," *International Journal of Hydrogen Energy,* vol. 42, no. 52, pp. 30509-30524, 2017.

[65] A. P. York, T. Xiao, and M. L. Green, "Brief overview of the partial oxidation of methane to synthesis gas," *Topics in Catalysis,* vol. 22, no. 3-4, pp. 345-358, 2003.

10 Conclusion and future work

10.1 The conclusion from the thesis

Four chemical looping processes (combustion, reforming, water splitting, and partial oxidation of methane) have been successfully demonstrated using the novel Gas Switching Technology. For the reforming demonstration, three iron-based oxygen carriers (Fe/Al_2O_3, $Fe-Ce/Al_2O_3$, and $Fe-Ni/Al_2O_3$) were first tested in a two-stage process for steam methane reforming at atmospheric pressure. Among the three oxygen carriers, $Fe-Ni/Al_2O_3$ performed best achieving about 75 – 80% CH_4 conversion to syngas in the reforming stage with the gas conversion improving as the temperature and H_2O/C ratio increase. Autothermal operation was also achieved with $Fe-Ni/Al_2O_3$ showing that the proposed gas switching reactor using fluidized bed reactor demonstrates good performance for the reforming of natural gas to syngas but an oxygen carrier with the good catalytic property is required. For health reasons, it is desired to eliminate toxic material such as Ni to achieve safe large-scale operation and commercialization of the GSR concept. However, at the end of the first reforming demonstration, Ni was only partially substituted and not eliminated. It is therefore important to put more effort towards developing non-toxic material with good catalytic properties for reforming reactions to actualize the full potential of the GSR process.

Following the successful demonstration of the first reforming campaign at atmospheric conditions, pressurized demonstration up to 5bar was completed with the oxygen carrier ($Fe-Ni/Al_2O_3$) that performed best. The second demonstration was designed through a four-stage (reduction, partial oxidation, reforming, and oxidation) process to comprehensively explore the behavior of the oxygen carrier towards syngas production. About 97.61% and 90% CH_4 conversion were achieved in the reduction stage and the reforming stages respectively. As expected from equilibrium, CH_4 conversion decreased in the reforming stage with the increase in pressure but remains insensitive to pressure at the partial oxidation stage. An increase in pressure changed the carbon deposition mechanism in the POX stage from methane cracking to Boudouard resulting in a decrease in carbon deposition with pressure. As the performance at the POX stage under pressurized conditions was better than the reforming stage in terms of CH4 conversion and reduced carbon of carbon deposition, eliminating the reforming stage by not feeding steam could be a viable option. It was concluded from this demonstration is that if a pressurized operation is desired, a three-stage (reduction, partial oxidation, and oxidation)

GSR process would be more suitable thus calling for future research to demonstrate the proposed three-stage GSR process at higher pressures above 5bar.

The third and fourth demonstrations focused on the utilization of CO_2 in dry reforming of methane to produce syngas for GTL applications using Ni-based oxygen. Autothermal and pressurized operations were achieved with the ability to control the syngas ratio (H_2:CO) by adjusting CO_2:CH_4 ratio and addition of steam. By varying the CO_2:CH_4 ratio from 0.25 – 2, the desired H_2/CO molar ratio between 1-3 was achieved with up to 90% syngas purity suitable for GTL processes. Although carbon deposition was significant for the cases with CO_2:CH_4 ratio less than 2, the activity and catalyst stability was not negatively affected since the cyclic nature of GSDR ensured that all the produced carbon was gasified/combusted in the preceding reforming and oxidation stages. It is also interesting to mention that when the CO_2:CH_4 ratio was increased beyond 2, carbon deposition was completely avoided. By co-feeding, steam, CO_2 and CH_4, the combined effects of steam methane reforming and dry methane reforming was achieved with the following benefits: i) desirable syngas quality (H_2/CO molar ratio) between 1 – 3 suitable for GTL processes, ii) reduced carbon deposition and iii) reduced cost by the elimination of air separation unit used in the conventional tri-reforming/autothermal reforming alternatives. The successful high-pressure demonstration has proven the viability of the GSDR integration to downstream pressurized GTL processes. Although other previous studies have shown no negative effect of pressure on the kinetics of the dry reforming reaction, the gas conversion to syngas of the GSDR process was affected negatively by pressure.

The experimental demonstration of Gas Switching Water Splitting (GSWS) was completed using two iron-based oxygen carriers. The 1st GSWS demonstration with 35 wt.% Fe_2O_3/Al_2O_3 showed good reactor performance with no agglomeration but with low H_2 purity (< 80%) was compromised due to gas mixing while switching between reactor stages. It was then proposed to increase the active content of the oxygen carrier to keep the stages longer and reduce the effect of mixing on H_2 purity. This promoted the development of Cu-doped $Mg(Fe_{0.9}Al_{0.1})_2O_4$ spinel OC with 74 wt.% active content for the 2nd GSWS demonstration. Although this oxygen carrier was very reactive, it exhibited a high degree of carbon deposition and agglomeration making it inoperable.

As mentioned earlier, it is necessary to develop a non-toxic (Ni-free) material for the scale-up of GST processes considering the health implication of handling a large quantity of toxic oxygen carriers. On this note, a lanthanum-based oxygen carrier was developed and tested under the Gas Switching Partial Oxidation conditions (GSPOX) for combined syngas and H_2

production. The experiments were performed at temperatures between 750 - 950 °C and pressures up to 5 bar. The results show that the oxygen carrier exhibits high selectivity to syngas production at the fuel stage with the process performance observed to improve with increasing temperature although carbon deposition could not be avoided. Co-feeding CO_2 with CH_4 at the fuel stage could reduce carbon deposition significantly and improve the purity of the H_2 produced at the steam stage but reduced the syngas H_2/CO molar ratio from 3.75 to 1 (at CO_2/CH_4 ratio of 1, 950 °C and 1 bar). Interestingly, the demonstration of CO_2 utilization at the fuel stage showed a stable syngas production over 12 h and maintained the H_2/CO ratio at almost unity, suggesting that the oxygen carrier was exposed to simultaneous partial oxidation of CH_4 with the lattice oxygen which is restored instantly by the incoming CO_2. There was no loss in activity of the oxygen carrier after the 12 h demonstration as similar trends of gas composition and temperature profile was recorded in the subsequent re-oxidation steps as observed when the fuel duration was less. The addition of steam could tune up the H_2/CO ratio up to a value of 4 without carbon deposition at H_2O/CH_4 ratio of 1, 950 °C and 1 bar; making the syngas from Gas Switching Partial Oxidation (GSPOX) suitable for any downstream process, e.g. gas-to-liquid (GTL) processes. The process was also demonstrated at higher pressures with over 70 % fuel conversion achieved at 5 bar and 950 °C.

For the combustion demonstration, a preliminary test was completed in a standalone lab-scale fluidized bed reactor using $CaMnO_{3-\delta}$-based oxygen carrier developed by EuroSupport. A pre-pilot 60kW_{th} cluster of three reactors was designed and commissioned for continuous operation of the pressurized gas switching technology. The demonstration of pressurized GSC was completed in this novel reactor cluster using $CaMnO_{3-\delta}$-based oxygen carrier at temperatures up to 1000 °C and pressures up to 15 bar.

10.2 Future work in the area

With the scope and the challenges encountered during the study, further research is still needed to ensure the commercialization of the proposed GST technology as outlined below:

- For the reforming demonstration, Ni was only partially substituted and not eliminated to achieve completely safe operation for scale-up and commercialization of the GSR concept. This calls for more research to develop non-toxic and affordable oxygen carriers to actualize the full GSR potential and ensure that human health would not put at risk during scale-up and commercialization. For the pressurized GSR demonstration, three stages (reduction, partial oxidation of methane, and oxidation of the OC) has been

recommended following. Further research is therefore important to optimize the three-stage GSR process at higher pressures. The demonstration of CO_2 utilization through Gas Switching Dry Reforming (GSDR) suggests that enormous benefits could be realized by integrating GSDR into GTL processes. It is therefore important to optimize the GSDR process and demonstrate further at higher pressures close to the target downstream GTL processes. There is also a need for the development of non-Nickel-based oxygen carriers for the GSDR process.

- The operation of GSWS is still not optimal due to excessive gas mixing with the 35 wt.% Fe_2O_3/Al_2O_3 in the 1st demonstration. The 2nd demonstration with 74 wt.% active content Cu-doped $Mg(Fe_{0.9}Al_{0.1})_2O_4$ spinel oxygen carrier created three operational challenges that should be addressed in future work to increase the attractiveness of the GSWS concept. Firstly, the degree of fuel utilization in the fuel stage was low, resulting in high fuel slippage. Although such slipped fuel can be productively integrated with a downstream process, it will certainly increase the attractiveness of the GSWS concept if fuel slip can be minimized. Secondly, the oxygen carrier started to agglomerate after about 34% of reduction. This issue does not allow the process to utilize even half of the oxygen-carrying capacity and will seriously hamper the CO_2 separation performance of the process. It is possible that this challenge can be overcome in a larger reactor where more vigorous fluidization is possible, but this needs to be confirmed in future experiments. Thirdly, the oxygen carrier showed significant carbon deposition, which contributes to the release of CO_2 and CO in the steam stage that contaminates the produced H_2. When the H_2-rich stream is combusted, this will result in CO_2 emissions of about 20 kg/GJ_{LHV} of H_2. Alternatively, a downstream pressure swing adsorption unit can be used to purify the H_2 before utilization.
- Although the GSPOX process was also demonstrated at high pressure with over 70% fuel conversion achieved at 5bar and 950°C, further demonstrations for continuous operation at higher pressures are required to improve the process efficiency and achieve an easy integration into downstream GTL processes which always operate a high pressure up from 30bar. This would create an opportunity for a good business case for subsequent scale-up and commercialization.
- A comprehensive reactor modeling, process modeling, and techno-economics are required for the GSWS, GSDR and GSPOX processes to provide a more fundamental explanation of the process behavior, ascertain the economic viability, and the possibility for scale-up. The proposed GST technology should be benchmarked with other similar

technologies (such as the gas switching chemical looping technology using a fixed bed reactor) to ascertain its comparative advantages.

- With the successful demonstrations of the cluster operation for a continuous GSC and GSR processes, a pilot-scale reactor is required to test all the process value chain for commercialization backed with good business case based on pilot demonstrations.

List of publications

1. Ugwu, A., F. Donat, A. Zaabout, C. Müller, K. Albertsen, S. Cloete, G. van Diest and S. Amini, *Hydrogen Production by Water Splitting using Gas Switching Technology*. Powder Technology, 2020. 370: p. 48 - 63
2. Ugwu, A., M. Osman, S. Cloete, A. Zaabout and S. Amini, *Novel Clean Energy Conversion Technologies with Integrated CO_2 capture.* in 2020 Spring Meeting & 16th Global Congress on Process Safety. 2020. AIChE.
3. Ugwu, A., A. Zaabout, and S. Amini, *An advancement in CO_2 utilization through novel gas switching dry reforming.* International Journal of Greenhouse Gas Control, 2019. 90: p. 102791.
4. Ugwu, A. Zaabout, JR. Tolchard, PI. Dahl and S. Amini, *Gas Switching reforming for syngas production with iron-based oxygen carrier-the performance under pressurized conditions.* International Journal of Hydrogen Energy, 2020. 45(2): p. 1267-1282.
5. Zaabout, A., PI. Dahl, A. Ugwu, JR. Tolchard, S. Cloete and S. Amini, *Gas Switching Reforming (GSR) for syngas production with integrated CO_2 capture using iron-based oxygen carriers*. International Journal of Greenhouse Gas Control, 2019. 81: p. 170-180.
6. Ugwu, A., A. Zaabout, SM. Nazir and S. Amini, Gas-to-liquid process for CO_2 utilization through gas switching dry reforming. *Chemical Engineering Journal*, 2020. Under review.
7. Ugwu, A., A. Zaabout, F. Donat, C. Müller, K. Albertsen, G. van Diest, S. Amini, Combined Syngas and Hydrogen Production using Gas Switching Technology. *Industrial & Engineering Chemistry*, 2020. Under review.

Conference contribution

1. Ugwu, A., A. Zaabout, F. Donat, C. Müller, K. Albertsen, G. van Diest, S. Amini, *The demonstration of pressurized Gas Switching Partial Oxidation (GSPOX) of methane using Lanthanum based oxygen carrier.* 2019, Trondheim CCS Conference (TCCS 10) Trondheim.
2. Zaabout, A., A. Ugwu, F. Donat, C. Müller, K. Albertsen, G. van Diest and S. Amini, *Pressurized Gas Switching Combustion in a pre-pilot scale reactor cluster.* 2019, Fluidization XVI Conference Guilin, China.
3. Ugwu, A., F. Donat, A. Zaabout, C. Müller, K. Albertsen, S. Cloete, G. van Diest and S. Amini, *Gas Switching Water Splitting (GSWS) for efficient hydrogen production.* 2019, Fluidization XVI Conference Guilin, China.
4. Ugwu, A., M. Osman, S. Cloete, A. Zaabout and S. Amini, *Gas Switching Reforming for syngas production with iron-based oxygen carrier- The performance under pressurized conditions.* 2019, PARTEC International Congress on Particle Technology, Germany.
5. Ugwu, A. Zaabout, JR. Tolchard, PI. Dahl and S. Amini, *Pressurized Gas Switching Reforming (GSR) for syngas production with iron-based oxygen carrier*. 2018, GHGT 14 International Conference Melbourne, Australia.
6. Ugwu, A., A. Zaabout, and S. Amini, *An advancement in CO2 utilization through novel Gas Switching Dry Reforming*. 2018, 5th International Conference on Chemical Looping Park City Utah, USA
7. Ugwu, A., A. Zaabout and S. Amini, *Demonstration of Gas Switching Technology for Accelerated Scale-up of Pressurized Chemical Looping Applications (GaSTech)*. 2018, 2018 Energy Conference organized by The Research Council of Norway, Oslo.
8. Ugwu, A., A. Zaabout, F. Donat, C. Müller, K. Albertsen, and S. Amini, *Gas Switching Water Splitting (GSWS) for high-efficiency Hydrogen Production*. 2018, 25th International Conference on Chemical Reaction Engineering, Florence, Italy.
9. Ugwu, A., A. Zaabout and S. Amini, *Gas Switching Water Splitting for Efficient Carbon-Free Hydrogen Production from Natural Gas: Heat Management*. 2018, International Hydrogen and Fuel Cell Conference Trondheim, Norway.